

**Characterisation of the Aqueous Corrosion Process in NdFeB
Melt Spun Ribbon and MQI Bonded Magnets**

By
Stephen McCain

**A thesis submitted to the
University of Birmingham
for the degree of
Doctor of Philosophy**

Department of Metallurgy and Materials
Faculty of Engineering
University of Birmingham
Birmingham
B15 2TT

September 2011

UNIVERSITY OF
BIRMINGHAM

University of Birmingham Research Archive

e-theses repository

This unpublished thesis/dissertation is copyright of the author and/or third parties. The intellectual property rights of the author or third parties in respect of this work are as defined by The Copyright Designs and Patents Act 1988 or as modified by any successor legislation.

Any use made of information contained in this thesis/dissertation must be in accordance with that legislation and must be properly acknowledged. Further distribution or reproduction in any format is prohibited without the permission of the copyright holder.

Acknowledgments

Firstly I would like to take this opportunity thank my supervisor Prof. I. R. Harris for being the driving force behind this project, and for the many useful discussions which helped to both resolve and create many interesting problems.

Special thanks also goes to Dr. Allan Walton who took on the unenviable task of completing paper work and organising examiners.

I also feel the need to extend thanks to my parents for their constant unfaltering support both emotionally and more importantly financially. Also to Leanne, without her understanding and constant nagging this process would not have been possible.

Last but not least I would like to thank my friends and colleagues of the AACG both past and present who have been the source of many inspirational conversations during the course of this work.

This PhD thesis is dedicated to the memory of Dr. Andy J. Williams (1967 – 2011).

Abstract

A major factor limiting the use and longevity of rare earth based magnetic materials is their susceptibility to aqueous corrosion and associated detrimental effects upon the magnetic properties of the material. This process was investigated through a combination of exposure to simulated environmental conditions and hydrogen absorption/desorption studies (HADS) in conjunction with magnetic characterisation. This study utilises NdFeB MQP-B melt-spun ribbon manufactured by Magnequench, in the form of MQI bonded magnets and also in its unbonded state as MQ powder.

Specifically, it was concerned with how effective a variety of bonding media (epoxy resin, PTFE, zinc) and surface coatings (PTFE, Qsil, zinc LPPS, Dex-Cool) were at limiting the impact of aqueous corrosion in MQI bonded magnets.

To characterise the effect of hydrogen absorption upon the magnetic properties of the MQP-B, hydrogen uptake was induced followed by a series of outgassing heat treatments with subsequent magnetic characterisation accompanied by HADS techniques performed after each outgas. This allowed comparisons to be made between the effects of aqueous corrosion process and hydrogen absorption upon the magnetic properties of the alloy.

This study has clearly demonstrated the link between the abundance of environmental moisture and rate of H_{ci} losses in MQI bonded magnets. In addition to this the key mechanism responsible for the degradation of magnetic properties has been identified.

These losses have been attributed to the absorption of hydrogen generated by the dissociation of water in the presence of NdFeB during the aqueous corrosion process.

It has been shown that the use of a bonding media that is impermeable to water can limit the effects of aqueous corrosion by limiting water access to the Magnequench particles

(MQP) and also the positive effects of the use of suitable surface coatings has been shown to be effective for the same reason.

Table of Contents

Chapter 1: Introduction	1
1.1 Introduction To Project	1
1.2 History Of Magnetism.....	3
1.3 The Origin Of Magnetism.....	7
1.4 Types of Magnetism.....	7
1.5 Magnetic Domains	12
1.6 Magnetic Hysteresis.....	15
1.7 Coercivity Control	18
1.8 Classification Of Magnetic Materials	19
1.8.1 Soft Magnetic Materials	19
1.8.2 Hard Magnetic Materials	20
Chapter 2: Literature Review	24
2.1 Rare Earth-Transition Metal (RE-TM) Permanent Magnets	24
2.1.1 SmCo Type Permanent Magnets	25
2.1.2 NdFeB Type Permanent Magnets.....	26
2.2 NdFeB Sintered Processing Route	29
2.3 NdFeB Melt Spinning Processing Route	31
2.4 Bonded Magnets	40
2.5 Hydrogen Decrepitation (HD) Process	42
2.5.1 The Hydrogen Decrepitation (HD) Process In NdFeB Type Alloys.....	45
2.5.2 The Hydrogen Decrepitation (HD) Process In SmCo Type Alloys	48
2.6 Hydrogen Disproportionation Desorption Recombination (HDDR) Process.....	50
2.7 Hydrogen Desorption	55
2.7.1 Hydrogen Desorption in SmCo Type Alloys	55
2.7.2 Hydrogen Desorption In NdFeB Type Alloys.....	56
2.8 Corrosion Of Rare Earth Based Alloys	57
2.9 Bonding Media	64
2.9.1 Epoxy Resin.....	66
2.9.2 Polytetrafluoroethylene (PTFE)	67
2.9.3 Zinc	69
2.9.4 Bonding Media Summary.....	71
2.10 Surface Coatings/Treatments	72
2.10.1 Low Pressure Pack Sublimation (LPPS) Zinc Coating	73
2.10.2 Dex-Cool/Ethylene Glycol (EG)	75
Chapter 3: Experimental Techniques.....	87
3.1 Magnetic Materials Employed	87

3.2 Bonding Media And Processing Techniques.....	91
3.2.1 Epoxy Resin (Polyepoxide)	91
3.2.1.1 Step-By-Step Production Method.....	92
3.2.2 PTFE (Polytetrafluoroethylene)	92
3.2.2.1 Step-By-Step Production Method.....	94
3.2.3 Zinc	94
3.2.3.1 Step-By-Step Production Method.....	95
3.3 Surface Coatings Employed.....	96
3.3.1 PTFE	96
3.3.2 QSil 12 (Two-part Silicone Potting Compound).....	96
3.3.2.1 Step-By-Step Production Method.....	97
3.3.3 Zinc Low Pressure Pack Sublimation (LPPS) Coating	98
3.3.3.1 Step-By-Step Production Method.....	99
3.4 Environmental Testing.....	100
3.4.1 Aqueous Environment	100
3.4.1.1 Dex-Cool (Antifreeze/Ethylene Glycol).....	101
3.4.2 Humid Environment	102
3.4.3 Dry Environment	102
3.5 Magnetic Hysteresis Measurements.....	103
3.5.1 Permeameter	103
3.5.2 Vibrating Sample Magnetometer (VSM)	105
3.6 Optical Characterisation.....	106
3.6.1 Surface Coating Characterisation	107
3.7 Mass Change Measurements	107
3.8 Density Measurements	108
3.9 Hydrogen Absorption/Desorption Studies (HADS).....	108
3.9.1 Step-By-Step Method	109
3.10 Thermogravimetric Analysis (TGA)/Mass Spectrometry (MS).....	110
 Chapter 4: Results and Discussion – Corrosion Behaviour of NdFeB Bonded Magnets	
.....	113
4.1 Project Introduction	113
4.2 NdFeB MQP-B in MQ-I Bonded Magnets	114
4.2.1 Aqueous Corrosion of NdFeB Magnequench Particles (MQP)	115
4.3 Aims	117
4.4 Epoxy Resin Binder Performance.....	118
4.4.1 Water Movement Through Epoxy Resin.....	118
4.5.2 Epoxy Resin: Water Ingress And Associated Effects	119
4.6 Alternate Bonding Media Performance	124
4.7 Sample Density and Aqueous Corrosion Performance.....	125
4.8 Optical Surface Characterisation.....	128

4.9 Alternate Bonding Media Aqueous Corrosion Performance	133
4.10 Dex-Cool (ethylene glycol (EG)) and Aqueous Corrosion Performance	139
4.10.1 Dex-Cool (EG) Aqueous Corrosion Inhibition Mechanisms	143
4.10.2 Ethylene Glycol/Water Hydrogen Bond Influence	145
4.10.3 Ethylene Glycol Mixing Schemes	148
4.10.4 Possible Ethylene Glycol Related Corrosion Prevention Mechanisms ..	151
4.11 Aqueous Corrosion Prevention Through Surface Coatings	155
4.11.1 High Humidity Environment Mass Measurements	155
4.11.2 High Humidity Environment Coercivity Measurements	159
4.11.3 Aqueous Environment Coercivity Measurements	165
4.12 Optical Evaluation Of Surface Coatings	170
4.12.1 PTFE Coating Application	171
4.13 Sample Surface Analysis of High Humidity Environmental Exposure..	180
4.14 Sample Surface Analysis of Aqueous Environmental Exposure.....	183
4.15 Surface Coatings in the Presence of Dex-Cool Additions	186
4.15.1 Optical Analysis of Samples Exposed to 50/50 (Dex-Cool/DI Water) Solution	189
4.16 Ethylene Glycol/Dex-Cool Summary	197
Chapter 5: Results and Discussion – Corrosion Behaviour of NdFeB Magnequench Particles (MQP)	202
5.1 Effect of Dex-Cool On Corrosion Behaviour of MQP.....	205
5.2 Hydrogen Absorption/Desorption Studies (HADS) of MQP	206
5.2.1 Hydrogen Absorption in MQP	207
5.3 Intrinsic Coercivity (H_{ci}) Loss Due To Hydrogen Ingress	210
5.4 Hydrogen Desorption and Effects Upon Magnetic Properties of MQP ...	211
5.4.1 Post Aqueous Corrosion Heat Treatment and Magnetic Properties	218
5.5 Influence of Dex-Cool On Hydrogen Absorption/Desorption Of MQP ...	223
Chapter 6: Conclusions	232
Chapter 7: Future Work.....	237

Chapter 1: Introduction

1.1 Introduction To Project

A major factor limiting the use and longevity of rare earth based magnetic materials is their vulnerability to aqueous corrosion and associated detrimental effects upon the magnetic properties of the material.

The driving force behind commissioning this study was an issue brought to our attention by Magnet Applications Ltd. They had a problem that had been presented to them by one of their end users. The end user required an NdFeB bonded magnet to operate within a permanent magnet water pump at approximately 80°C.

The epoxy bonded magnets supplied and fitted within a permanent magnet motor driven water pump had failed within a fraction of their expected service life through degradation of magnetic properties, resulting in a loss of drive without observed disintegration on a scale to warrant the loss of magnetic properties.

In order to understand the mechanism of this rapid loss, the process was investigated through a combination of exposure to simulated environmental conditions and hydrogen absorption/desorption studies (HADS) in conjunction with magnetic characterisation. This study utilises NdFeB MQP-B melt-spun ribbon manufactured by Magnequench, in the form of MQ-I bonded magnets and also in its unbonded state.

Specifically it was decided to investigate alternative bonding media and coatings in an attempt to mitigate against the problems of aqueous environments. In an attempt to limit the effects of the aqueous corrosion alternate bonding media (PTFE, zinc) and surface coatings (PTFE, Qsil, zinc LPPS, Dex-Cool) were investigated under the same conditions and compared to the standard MQ-I epoxy bonded magnets.

To characterise the effect of hydrogen absorption upon the magnetic properties of the MQP-B hydrogen uptake was induced followed by a series of outgassing heat treatments with subsequent magnetic characterisation accompanied by HADS techniques performed after each outgas. This allowed comparisons to be made between the effects of aqueous corrosion process and hydrogen absorption upon the magnetic properties of the alloy.

To summarise, the aims of this study are to establish the link between the abundance of moisture within a given operating environment and the degradation of magnetic properties. The mechanism(s) responsible for this observed degradation will be investigated, with the emphasis being geared towards preventing associated detrimental effects in terms of loss of magnetic properties through the application of novel bonding media and surface treatments.

1.2 History Of Magnetism

One of the earliest observations of magnetism can be traced back to Thales of Miletus who was a Greek philosopher in the 6th Century B.C. He studied primitive electrical and magnetic phenomena. Around 585 B.C he made the first definitive statement, saying lodestone attracts iron because it has a soul. The ancient Chinese scientist Shen Kuo (1031 – 1095) was the first person to write of the magnetic needle compass and that it improved the accuracy of navigation by employing the astronomical concept of true north. The loadstone compass was used for navigation in Europe and China by the 12th Century.

The modern understanding of magnetism didn't begin until 1600, when William Gilbert published "De Magnete, Magneticisque Corporibus, et de Magno Magnete Tellure" (On the Magnet and Magnetic Bodies, and on the Great Magnet the Earth). The experiments he conducted led him to the conclusion that the earth itself was a magnet and this was the reason compasses pointed north.

In 1819 Hans Christian Oersted inadvertently stumbled upon the relationship between electricity and magnetism. He observed that a current carrying wire could influence a compass needle. This became known as Oersteds Experiment. Others found links through further experiments, James Clerk Maxwell synthesised these insights into Maxwell's equations. Unifying electricity, magnetism and optics into the field of electromagnetism.

By 1821 Michael Faraday built two devices to produce what he called electromagnetic rotation; a continuous circular motion from the circular magnetic force around a wire and a wire extending into a pool of mercury with a magnet placed inside that would rotate around the magnet if supplied with current from a chemical battery. Faraday's breakthrough came when during an experiment he moved a magnet through a loop of wire,

an electric current flowed in the wire. The current also flowed if the loop was moved over a stationary magnet. These demonstrations established that a changing magnetic field produces an electric field. The relation was modelled mathematically by Maxwell as Faraday's law which subsequently became one of the four Maxwell equations. These in turn evolved into the generalisation known today as field theory. Faraday later used the principle to construct the electric dynamo, the ancestor of modern power generators.

This first electromagnet was invented by William Sturgeon in 1824. It was a horseshoe-shaped piece of iron, varnished to insulate it from the windings, wrapped with around 18 turns of bare copper wire.

In 1895 Pierre Curie discovered Curie's Law which states: In a paramagnetic material the magnetisation of the material is (approximately) directly proportional to an applied magnetic field. However, if the material is heated, this proportionality is reduced: for a fixed value of field, the magnetisation is approximately inversely proportional to temperature.

Paul Langevin proposed his theory of paramagnetism and diamagnetism in 1905. He devised the modern interpretation of this phenomenon in terms of spins of electrons within atoms.

In 1906 the theory of ferromagnetism was proposed by Pierre-Ernest Weiss. This is the basic mechanism by which certain materials (e.g. iron) form permanent magnets, or are attracted to magnets.

The physics of magnetism was developed by the 1920's, with theories involving electron spins and exchange interactions. These are the beginnings of quantum mechanics.

At the end of the 19th Century carbon steel magnets were discovered. It was found that with additions of tungsten and later chromium that materials with maximum energy products of 20 kJm^{-3} could be produced. The development of magnetic materials began during the early 20th Century with silicon steels used as the soft magnetic components of transformers. The properties of this material were optimised through processing, by Norman P. Goss in 1933. This became known as grain orientated steel, with magnetic flux density enhanced by 30% through this processing route alone.

The development of permanent magnetic materials, which had not significantly advanced since 1601 when Gilbert wrote of blacksmiths making steel compass needles, continued with the development of Alnico alloys in 1932 by Mishima. As the name suggests these alloys are based on aluminium, nickel, cobalt and iron, with energy products of 88 kJm^{-3} achieved. These magnets have the advantage of having a high Curie temperature ($\sim 850^\circ\text{C}$) which allows them to still be used today for high temperature applications or where thermal stability of magnetisation is required. For example in sensors such as speedometers, where changes in calibration due to temperature fluctuation must be avoided. The low intrinsic coercivity value of $\sim 80 \text{ kAm}^{-1}$ limits the application of these magnets such that they cannot be used for “power applications”, i.e. motors and generators.

The 1950's saw the discovery by Philips of hard hexagonal ferrites or ceramic magnets. These materials displayed far greater coercivity than had previously been seen, ($\sim 250 \text{ kAm}^{-1}$) although, when coupled with a low remanence this leads to an overall low maximum energy product. This high coercivity does allow the magnets to be made in thinner sections and also to be used in motors and generators where they will be exposed to ‘strong’ demagnetisation fields. The key to this high coercivity lies in the presence of uniaxial magnetic anisotropy. The barium and strontium hexaferrite have a hexagonal

crystal structure with uniaxial magnetocrystalline anisotropy, such that the crystals prefer to be magnetised in the c-axis of the crystal.

In the 1960's rare-earth (RE) transition metal (TM) compounds RECo_5 were discovered in the USA (Nesbitt et al., 1959). The combination of rare-earth and transition metal are complementary to one another. The rare-earth component provides the magnetic anisotropy to the phase, and the transition metal provides the high magnetisation and Curie temperature. The first RE-TM was polymer bonded with an energy product of $\sim 40 \text{ kJm}^{-3}$ (Coey, 1995). It was discovered that SmCo_5 magnets could be produced with an energy product of $\sim 160 \text{ kJm}^{-3}$ by sintering (Das, 1969). This was the first commercially available RE-TM permanent magnetic material. The success of these materials were limited due to the high costs associated with the raw materials and their production. These high costs were a driving force behind the discovery of NdFeB based magnetic materials.

In 1983, the search for an iron-based RE-TM produced a material based upon neodymium iron boron (NdFeB) ternary alloy. This was discovered simultaneously by General Motors (Croat et al., 1984b) and Sumitomo Special Metals, Japan (Sagawa et al., 1984a). Although both arrived at the same point through two totally different processing routes. The coercivity obtained from the NdFeB system was inferior to that found in SmCo type magnets, although it possessed a higher magnetic flux. The temperature stability and corrosion resistance of NdFeB is inferior to that of SmCo magnets. These inherent problems lead to increased production costs initially to produce magnets of similar specification to the then current SmCo based alloys. Through improvements in technology production costs have been reduced to the point where NdFeB type magnets are now cheaper than their SmCo counterparts.

1.3 The Origin Of Magnetism

To appreciate magnetism one must first appreciate the connection between electricity and magnetism. In an electromagnet a magnetic field is created in the coil while electricity flows through the wire. In an ordinary bar magnet the field created is associated with the motions and interactions of its electrons orbiting the nucleus.



Electricity is the movement of electrons. Each atom represents a tiny permanent magnet. The circulating electron produces its own magnetic moment. There is also a spin magnetic moment associated with the electron itself due to its spinning on its own axis. In most materials there are resultant magnetic moments, however some have no moment due to the electrons being grouped in pairs causing the electron spin moments to be cancelled out.

In certain magnetic materials, magnetic moments of a large proportion of the electrons align, producing a unified magnetic field. Any application of an externally applied field will cause the magnet to attempt to align itself with this field. Such forces are used to drive electric motors etc. The relationship between magnetism and electricity is essential to many modern devices used on a daily basis.

1.4 Types of Magnetism

All materials show some type of magnetic behaviour, which can be classified into five groups depending upon their bulk magnetic susceptibility. Two of the most common types of magnetism, often referred to as “non-magnetic” are diamagnetism and paramagnetism. These two types account for most of the periodic table of elements at room temperature, shown in Fig. 1.1.

1 **H** 2 He

 Ferromagnetic  Antiferromagnetic

3 Li 4 Be 5 B 6 C 7 N 8 O 9 F 10 Ne



11 Na 12 Mg 13 Al 14 Si 15 P 16 S 17 Cl 18 Ar

19 K 20 Ca 21 Sc 22 Ti 23 V 24 Cr 25 Mn 26 Fe 27 Co 28 Ni 29 Cu 30 Zn 31 Ga 32 Ge 33 As 34 Se 35 Br 36 Kr

37 Rb 38 Sr 39 Y 40 Zr 41 Nb 42 Mo 43 Tc 44 Ru 45 Rh 46 Pd 47 Ag 48 Cd 49 In 50 Sn 51 Sb 52 Te 53 I 54 Xe

55 Cs 56 Ba 57 La 72 Hf 73 Ta 74 W 75 Re 76 Os 77 Ir 78 Pt 79 Au 80 Hg 81 Tl 82 Pb 83 Bi 84 Po 85 At 86 Rn

87 Fr 88 Ra 89 Ac

 Paramagnetic  Diamagnetic

58 Ce 59 Pr 60 Nd 61 Pm 62 Sm 63 Eu 64 Gd 65 Tb 66 Dy 67 Ho 68 Er 69 Tm 70 Yb 71 Lu

Elements classified as ferromagnetic are more commonly known as magnetic materials. The only other type of magnetic behaviour exhibited by pure elements at room temperature is antiferromagnetism. Magnetic materials can also be classified as ferrimagnetic, this is not observed in pure elements, but can only be found in compounds, such as mixed oxides called ferrites, from which the name is devised. The magnetic susceptibility value falls into a particular range for each material. This is shown in Fig. 1.2.


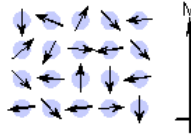
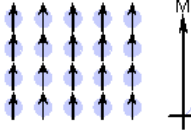
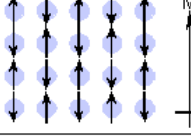
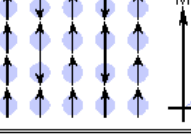
Type of Magnetism	Susceptibility	Atomic / Magnetic Behaviour		Example / Susceptibility	
Diamagnetism	Small & negative.	Atoms have no magnetic moment		Au Cu	-2.74×10^{-6} -0.77×10^{-6}
Paramagnetism	Small & positive.	Atoms have randomly oriented magnetic moments		β -Sn Pt Mn	0.19×10^{-6} 21.04×10^{-6} 66.10×10^{-6}
Ferromagnetism	Large & positive, function of applied field, microstructure dependent.	Atoms have parallel aligned magnetic moments		Fe	$\sim 100,000$
Antiferromagnetism	Small & positive.	Atoms have anti-parallel aligned magnetic moments		Cr	3.6×10^{-6}
Ferrimagnetism	Large & positive, function of applied field, microstructure dependent	Atoms have mixed parallel and anti-parallel aligned magnetic moments		Ba ferrite	~ 3

Fig. 1.2 A summary of different types of magnetic behaviour.

Primarily this study investigates Ferromagnetic materials. Ferromagnetism is only possible when atoms are arranged in a lattice and the atomic magnetic moments can interact to align parallel to one another. This effect is explained in classical theory through the presence of a molecular field within the ferromagnetic material. This was first suggested by Weiss in 1907.

The basis of the Weiss' molecular theory of ferromagnetism is that below the Curie temperature (T_c), a ferromagnet is composed of small, spontaneously magnetised regions called domains. The total magnetic moment of the material is the vector sum of the magnetic moments of the individual domains. Each domain is magnetised due to the strong magnetic interaction within the domain which tends to align the individual atomic

magnetic moments within. The movement of these domains determines how the material responds to a magnetic field and as a consequence the susceptibility is a function of applied magnetic field. Therefore, ferromagnetic materials are usually compared in terms of saturation magnetisation (magnetisation when all domains are aligned) rather than susceptibility. The spontaneous magnetisation below the T_c comes about from an internal magnetic field called the Weiss molecular field which is proportional to the magnetisation of the domain. Weiss theory states that ferromagnetism is caused by a molecular field which aligns the magnetic moments. He assumed that there was a field proportional to the magnetisation which tends to keep the magnetic moments of neighbouring atoms parallel. This hypothesis is good as it explains the principals of ferromagnetism. It predicts the variation of spontaneous magnetisation between absolute zero and T_c and the variation of paramagnetic susceptibility at $T > T_c$. Weiss was unable to explain the origin of this field; magnetic dipole-dipole interactions between magnetic moments are thousands of times too small. These days it is more appropriate to say that the exchange interactions cause the spins to be parallel.

The physical origin of the molecular field can only be understood using quantum mechanics. In 1929 Heisenberg attempted to explain ferromagnetism in terms of quantum mechanical exchange interactions. These interactions are dependant upon the relative orientation of the spins of two interacting electrons, this is known as exchange coupling.

These exchange interactions arise as a consequence of the Pauli exclusion principal. This states that two electrons can have the same momentum if they have opposing spins. If the spins are parallel they will stay apart. The coulomb electrostatic energy is modified by the orientation of the spin; the exchange interaction is thought to be largely electrostatic in origin.

To illustrate, consider two atoms, i and j having a spin angular momentum $S_i\hbar/2\pi$ and $S_j\hbar/2\pi$ respectively, then the exchange energy between them will be:

$$E_{ex} = -2J_{ex} S_i S_j = -2J_{ex} S_i S_j \cos\Phi$$

(equ 1.1)

where: J_{ex} is the exchange integral

Φ is the angle between the spins and S_i and S_j are vectors

When J_{ex} is positive, E_{ex} is a minimum where the spins are parallel ($\cos\Phi = 1$) and at a maximum when they are anti-parallel ($\cos\Phi = -1$). When J_{ex} is negative the situation arises where the lowest energy state is when the spins are antiparallel. Ferromagnetism occurs when the spin moments on adjacent atoms are aligned, then a positive value of the exchange integral is needed for ferromagnetism to occur.

The only elements that display ferromagnetic behaviour at and above room temperature are Iron (Fe), Cobalt (Co) and Nickel (Ni). Upon heating ferromagnetic materials the thermal agitation of the atoms means that the degree of alignment of the atomic magnetic moments decreases thus decreasing the saturation magnetisation. With continued heating the thermal agitation will become so great the material becomes paramagnetic; the temperature of this transition is the Curie temperature, T_c (Fe: $T_c = 770^\circ\text{C}$, Co: $T_c = 1131^\circ\text{C}$ and Ni: $T_c = 358^\circ\text{C}$). Above T_c then the susceptibility varies according to the Curie-Weiss law.

Ferrimagnetism is observed only in compounds. These have more complex crystal structures unlike that of pure elements. Within these materials exchange interactions lead to parallel alignment of atoms in some of the crystal sites and anti-parallel alignment in that of others. Whereas in an antiferromagnetic material the atomic moments cancel one another out. In a ferrimagnetic material there is an imbalance of parallel and anti-parallel

alignment resulting in an overall magnetic moment. The material breaks down into magnetic domains, just like a ferromagnetic material and the magnetic behaviour is also similar. Ferrimagnetic materials do usually have lower saturation magnetisations. For example in Barium ferrite ($\text{BaO} \cdot 6\text{Fe}_2\text{O}_3$) the unit cell contains 64 ions of which the barium and oxygen ions have no magnetic moment, 16 Fe^{3+} ions have moments aligned parallel and 8 Fe^{3+} aligned anti-parallel giving a net magnetisation parallel to the applied field, but with a relatively low magnitude as only $\frac{1}{8}$ of the ions contribute to the magnetisation of the material.

1.5 Magnetic Domains

A domain is a small volume of material that can be spontaneously magnetised in one direction. The bulk material is composed of many domains magnetised in different directions. A material is assumed to be demagnetised if these directions are at complete random and the net magnetisation is zero.

As mentioned previously, in order to explain the fact that ferromagnetic materials with spontaneous magnetisation could exist in the demagnetised state Weiss proposed the concept of magnetic domains. The findings revealed that within a domain large numbers of atomic moments are aligned (typically $10^{12} - 10^{18}$) The magnetisation within the domain is saturated and will always lie in the easy direction of magnetisation when there is no externally applied field. The direction of domain alignment across a volume of material is more or less random and hence the magnetisation of the specimen can be zero.

Domains exist in order to reduce the energy of a system. A uniformly magnetised sample has a large magnetostatic energy associated with it as a result of the presence of magnetic free poles at the material's surface generating a demagnetising field, H_d . The general

consensus adopted for the definition of the magnetic moment for a magnetic dipole, the magnetisation within the material points from South pole to North pole, while the direction of the magnetic field points from North to South. Therefore, the demagnetising field is in opposition to the magnetisation of the material. The magnitude of H_d is dependant upon the geometry and magnetisation of the specimen. Generally if the sample has a high length to diameter ratio (and is magnetised in the long axis) then the demagnetising field and magnetostatic energy will be low.

The break up of the magnetisation into two domains as illustrated in Fig. 1.3b reduces the magnetostatic energy by half. If the magnet breaks down into N domains then the magnetostatic energy is reduced by a factor of $1/N$ such that the material illustrated in Fig. 1.3c has a quarter of the magnetostatic energy of Fig. 1.3a. A closure domain structure can be seen in Fig. 1.3d where the magnetostatic energy is zero. This is only possible for materials that do not have a strong uniaxial anisotropy, as neighbouring domains are not at 180° to one another.

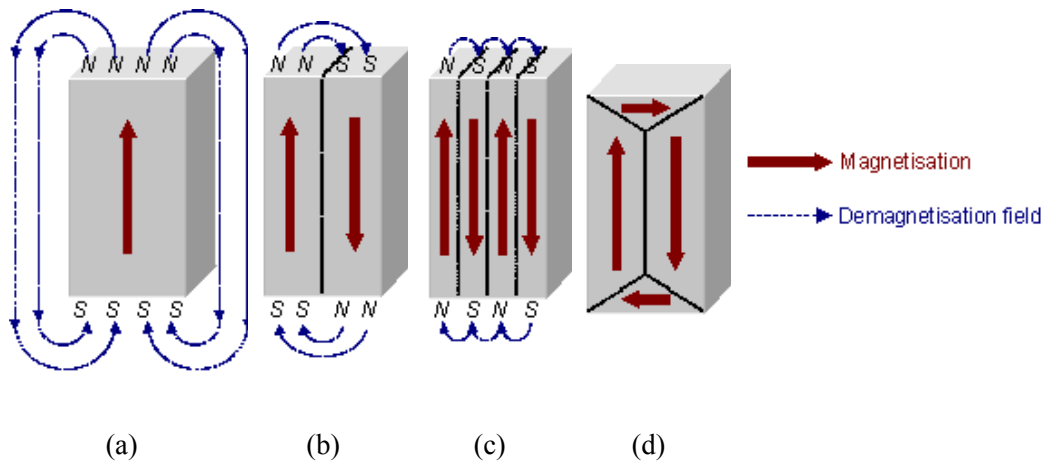


Fig. 1.3 A schematic illustration of the break up of magnetisation into domains (a) single domain, (b) two domains, (c) four domains and (d) closure domains.

However, the introduction of domains introduces domain wall energy to the system. Domains are separated by walls of a finite width, covering many atomic planes. The orientation of the electron spins change gradually through its width. Domain structure near the surface may be vastly different from that inside the material. Therefore the division into domains only continues while the reduction in magnetostatic energy is greater than the energy required to form the domain wall. The associated energy of a domain wall is proportional to its area. Fig. 1.4 illustrates that dipole moments of atoms within the wall are not pointing in the easy direction of magnetisation meaning they are in a higher energy state. These atomic dipoles within the wall are not at 180° to one another, so the exchange energy within the wall is also raised. The domain wall energy is an intrinsic property of a material, depending upon the strength of the exchange interaction between neighbouring atoms and the degree of magnetocrystalline anisotropy. These parameters will affect the thickness of the wall, strong magnetocrystalline anisotropy will favour a narrow wall, a strong exchange interaction will favour a wider wall.

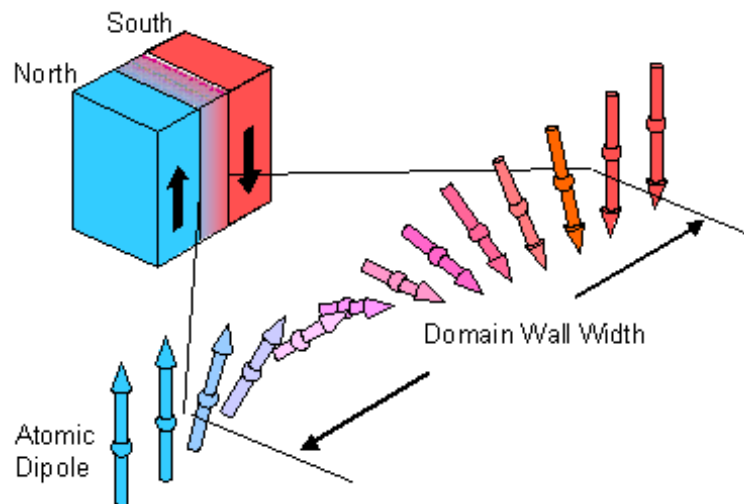


Fig. 1.4 A schematic representation of a 180° domain wall.

A specific number of domains within a material, can achieve a minimum energy. The number of domains will depend on the intrinsic magnetic properties of the material (effecting the magnetostatic energy and the domain wall energy) and the size and shape of the sample (this will effect the magnetostatic energy).

1.6 Magnetic Hysteresis

Ferromagnetic and Ferrimagnetic materials have non-linear initial magnetisation curves (i.e. dotted lines Fig. 1.5) due to the changing magnetisation with applied field causing a change in magnetic domain structure. These materials show hysteresis and the magnetisation does not return to zero after the application of the field. Fig. 1.5 shows a typical hysteresis loop; the two loops represent the same data, however, the red loop is the polarisation ($J = \mu_0 M = B - \mu_0 H$) and the blue loop the induction, both plotted against field.

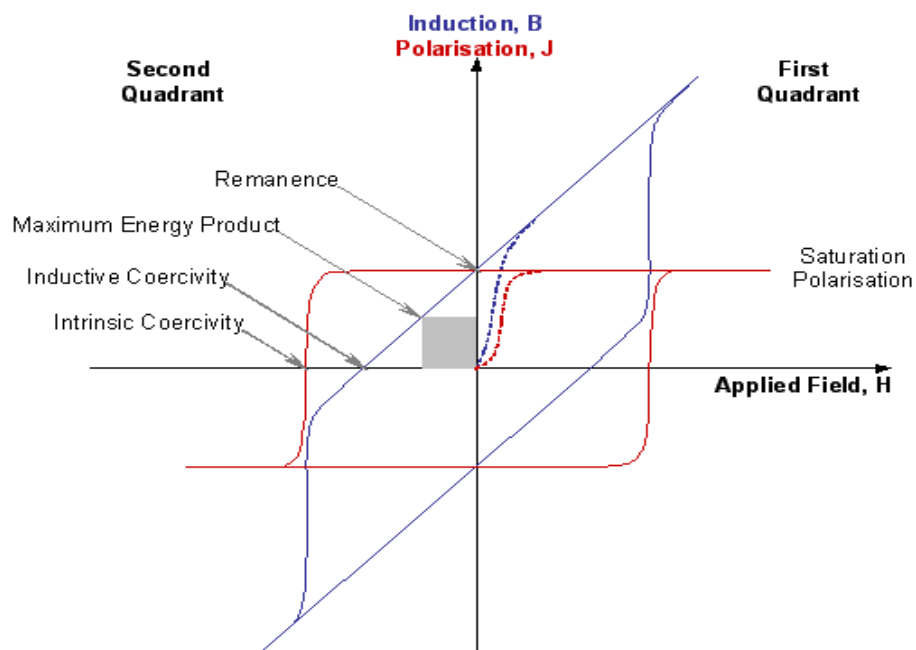


Fig. 1.5 A typical hysteresis loop for a ferro- or ferri- magnetic material.

In the first quadrant of the loop is the initial magnetisation curve (dotted line) that shows the increase in polarisation (and induction) as a field is applied to an unmagnetised sample. In the first quadrant the polarisation and applied field are both positive. Polarisation initially increases by the growth of favourably orientated domains. These will be magnetised in the easy direction of the crystal. When the polarisation cannot increase any further by domain growth, the direction of magnetisation of the domains then rotates away from the easy axis to align with the field. When all the domains have fully aligned with the applied field saturation is reached and the polarisation can increase no further.

If the field is removed the polarisation returns along the solid red line to the y-axis (i.e. $H=0$), the domains will then return to their easy direction of magnetisation, decreasing polarisation. In Fig. 1.5, the line from the saturation point to the y-axis is horizontal, this is representative of a well aligned material, where domains are magnetised in the easy direction of the crystal at the saturation point.

If the direction of applied field is reversed (i.e. into the negative direction) then polarisation will follow the redline into the second quadrant. The hysteresis means that polarisation lags behind the applied field and will not immediately switch direction into the third quadrant (i.e. negative polarisation). Polarisation will only decrease after a sufficiently high field is applied to:

- Nucleate and grow domains favourably orientated with respect to the applied field
- Rotate the direction of magnetisation of the domains towards the applied field.

After a field of sufficient strength is applied, saturation polarisation will be achieved in the negative direction. If the applied field is then decreased and again applied in the positive direction then the full hysteresis loop is plotted.

If the field is repeatedly switched from positive to negative directions in sufficient magnitude then the polarisation and induction will cycle around the hysteresis loop in an anti-clockwise direction. The area within the loop indicates the amount of energy absorbed by the material during each cycle of the hysteresis loop.

The hysteresis loop is a means of characterising magnetic materials. Various parameters can be determined from it. From the first quadrant the saturation polarisation, J_s and hence the saturation magnetisation, M_s can be measured. The most useful information can be derived from the second quadrant of the loop. For permanent magnets it is conventional to show only this quadrant. The field that is produced by the magnet after the magnetising field has been removed is called the remanence, B_r or J_r . The reverse field required to bring induction, B , to zero is called the inductive coercivity, ${}_bH_c$. The reverse field required to bring the magnetisation, M , or polarisation, J , to zero is called the intrinsic coercivity H_{ci} . The maximum value of the product of B and H is called the maximum energy product, $(BH)_{max}$ and is a measure of the maximum amount of useful work that can be performed by the magnet. This is also used as a figure of merit for permanent magnetic materials.

The shape of the initial magnetisation curve and the hysteresis loop can offer information regarding magnetic domain behaviour within the material. The squareness factor is a measure of how square the loop is. This is a dimensionless quantity between 0 and 1. This is defined by the ratio of the reverse field required to reduce J by 10% from the remanence to H_{ci} . A perfectly square loop corresponds to a value of 1. There are other methods to quantify the squareness of the loop, such as the ratio of J_r to J_s .

1.7 Coercivity Control

There are a number of ways to control the coercivity of magnetic materials, all of which involve controlling the magnetic domains within the material. For hard magnetic materials it is desirable for the domains not to be able to rotate its direction of magnetisation, with domain walls that do not move easily and/or nucleation of domains is difficult.

Easy rotation of domains in the material could be prevented by having strong uniaxial magnetocrystalline anisotropy. Shape anisotropy can occur in needle-like particles/grains where the magnetostatic energy is less when the magnetisation is in the long axis of the needle compared to the short axis.

If magnetic particle/grain size decreases there is a critical size below which the decrease in magnetostatic energy by splitting into two domains is less than the increase in energy due to the introduction of the domain wall. Particles below this size are known as “single domain particles”, and if they have sufficiently high anisotropy to prevent the easy rotation of the direction of magnetisation then the particles will be permanently magnetic. This type of coercivity mechanism can be observed in melt-spun NdFeB magnets where the crystal size is ~50nm, compared to the critical size for single domain particles of ~300nm.

Resistance to demagnetisation can also be achieved by pinning of the domain walls. In $\text{Sm}_2(\text{Co, Fe, Cu, Zr})_{17}$ type magnets this is achieved by the presence of a SmCo_5 based phase in which the domain wall energy is significantly lower than that of the majority $\text{Sm}_2\text{Co}_{17}$ based phase. The walls are therefore pinned within the SmCo_5 phase and both magnetisation and demagnetisation processes are difficult.

Permanent magnets can also achieve high coercivity by making the nucleation of new domains difficult. This mechanism can be found in sintered NdFeB permanent magnets

where non-magnetic grain boundary phases act to smooth the grain boundaries. This effectively removes domain nucleation sites. Nucleation controlled permanent magnets are easily magnetised as the initial state has several domains in each grain/crystal, but are difficult to demagnetise because this would require the nucleation of new reverse domains.

1.8 Classification Of Magnetic Materials

Classifications of magnetic materials are made according to the material's properties. Materials that are easily magnetised and demagnetised are referred to as soft magnetic materials. Materials that are difficult to demagnetise are referred to as hard or permanent magnetic materials. These two classifications of materials are also divided into subsets e.g. magnetostrictive and magnetoresistive materials.

1.8.1 Soft Magnetic Materials

These are easily magnetised and demagnetised. They usually have an intrinsic coercivity less than 1000 Am^{-1} . Primarily they are used to enhance and/or channel the flux produced by an electric current. The main parameters of interest are the relative permeability (μ_r , where $\mu_r = B/\mu_0 H$, this is a measure of how readily the material responds to the applied magnetic field), coercivity, saturation magnetisation and the electrical conductivity.

Applications for soft magnetic materials fall into two main categories: Alternating Current (AC) and Direct Current (DC). For DC applications the material is magnetised to perform an operation then demagnetised at the conclusion of the operation. For example an electromagnet on a crane at a scrap yard, it is switched on to attract the scrap steel, then switched off to drop. The main consideration for DC applications such as these is the permeability. Where the material is used to generate a magnetic field or to create a force then the saturation magnetisation may also be significant.

For AC applications the material will be continuously cycled from being magnetised in one direction to the other, throughout the period of operation. For example a power supply transformer. A high permeability is the primary desire of each of these applications but the significance of other properties vary. The most important consideration for AC applications is the energy lost in the system as the material is cycled around its hysteresis loop. Energy loss can originate from three different sources:

- Hysteresis loss – This is related to the area contained within the hysteresis loop.

Hysteresis losses can be minimised by the reduction of intrinsic coercivity. Consequently the area contained within the hysteresis loop will be reduced.

- Eddy current loss – This is related to the generation of electric currents in the magnetic material and associated resistive losses.

Eddy current losses can be reduced by decreasing the electrical conductivity of the material and by laminating. This has an influence on overall conductivity and is important due to skin effects at higher frequencies.

- Anomalous loss – This is related to the movement of domain walls within the material.

Anomalous losses can be reduced by having a completely homogenous material, within such materials there is no hindrance to the motion of the domain walls.

1.8.2 Hard Magnetic Materials

Hard magnetic materials also known as permanent magnets differ from soft magnetic materials as they retain their magnetism after being magnetised. This means that they possess an intrinsic coercivity greater than 10kAm^{-1} . Steel based permanent magnets retain their magnetism due to the pinning of domain walls by dislocations and inclusions.

Dislocation movement within the material is hindered by the same factors that affect the motion of domain walls, as a consequence these materials are mechanically hard. Hence the term hard magnets. There was shown to be a strong correlation between hardness and H_{ci} from a study carried out on hydrogen decrepitation (HD) production in $\text{Sm}_2\text{Co}_{17}$ based permanent magnets (Kianvash and Harris, 1985). Fig. 1.6 shows a summary of the B_r and H_{ci} plot of commercially available permanent magnets.

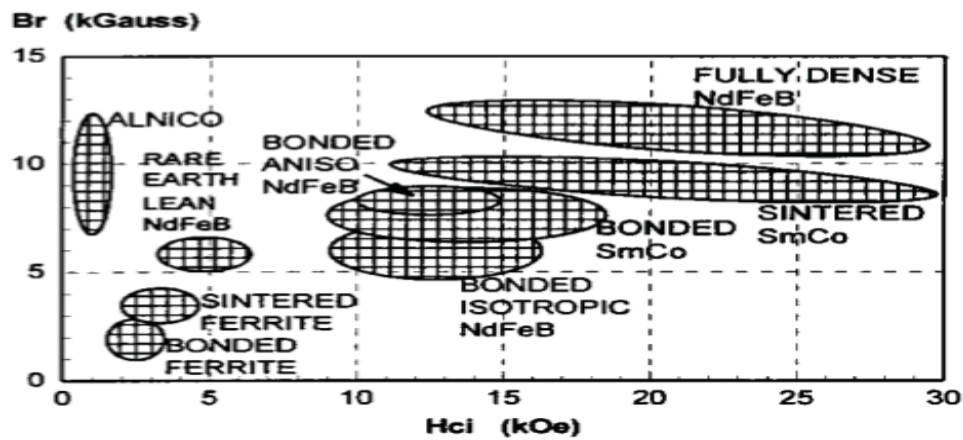


Fig. 1.6 The B_r and H_{ci} plot of commercially available permanent magnets (Ormerod and Constantinides, 1997a).

From Fig. 1.6 it can be seen that the properties of permanent magnetic materials are wide ranging and varied. This is due in part to the intrinsic properties of the material but are also derived as a result of the processing routes utilised during production. Due to the wide range of magnetic properties available it is possible to select a particular material to fit a particular application depending upon requirements such as cost, magnetic properties or operating temperature.

This thesis will investigate the corrosion behaviour of bonded isotropic NdFeB magnets. The investigation will be carried out with a view to prevent or limit the effects of aqueous

corrosion upon the magnetic properties of these components through the use of different bonding media, surface coatings and surface treatments.

References:

- COEY, J. M. D. 1995. Rare-earth magnets. *Endeavour*, 19, 146-151.
- CROAT, J. J., HERBST, J. F., LEE, R. W. & PINKERTON, F. E. 1984b. Pr-Fe and Nd-Fe-Based Materials - a New Class of High-Performance Permanent-Magnets. *Journal of Applied Physics*, 55, 2078-2082.
- DAS, D. 1969. Twenty million energy product samarium-cobalt magnet. *Magnetics, IEEE Transactions on*, 5, 214-216.
- KIANVASH, A. & HARRIS, I. R. 1985. Hydrogen decrepitation as a method of powder preparation of a 2:17-type, $\text{Sm}(\text{Co}, \text{Cu}, \text{Fe}, \text{Zr})_{8.92}$ magnetic alloy. *Journal of Materials Science*, 20, 682-688.
- NESBITT, E. A., WERNICK, J. H. & CORENZWIT, E. 1959. Magnetic Moments of Alloys and Compounds of Iron and Cobalt with Rare Earth Metal Additions. *Journal of Applied Physics*, 30, 365-367.
- ORMEROD, J. & CONSTANTINIDES, S. 1997a. Bonded permanent magnets: Current status and future opportunities (invited). *Journal of Applied Physics*, 81, 4816-4820.
- SAGAWA, M., FUJIMURA, S., TOGAWA, N., YAMAMOTO, H. & MATSUURA, Y. 1984a. New Material for Permanent-Magnets on a Base of Nd and Fe. *Journal of Applied Physics*, 55, 2083-2087.

Chapter 2: Literature Review

2.1 Rare Earth-Transition Metal (RE-TM) Permanent Magnets

Rare-earth permanent magnets are metallic magnets. Their magnetic components are alloys of 3d-transition metals with elements of the rare-earth (RE) group i.e. the 4f-elements. The “rare-earth permanent magnet” family has evolved over the last 50 years. Values for coercivity and maximum energy product of early SmCo based alloys were in the region of 5 – 10 times that of alnicos and ferrites (Strnat and Strnat, 1991).

Until the 1950's individual rare earths (RE) in metallic form were almost unavailable and of no industrial interest. The significance of the RE metals in nuclear fission caused the development of the technology required for their separation and reduction which made the elemental metals more readily available to interested research groups particularly in the mid-west area of the USA. This brought on a surge in scientific interest in RE alloys (Strnat and Strnat, 1991). From 1950 to 1965 systematic studies on RE-TM compounds were carried out by a number of groups in the mid-west region, in particular Ames Lab Iowa State University (Strnat et al., 1966), Bell Telephone Laboratories, New Jersey (Nesbitt et al., 1962), University of Pittsburgh (Nassau et al., 1960), US Naval Ordinance Lab, Maryland (Hubbard et al., 1960).

The realisation that the future of major advances in permanent magnetic materials would be achieved by shifting emphasis from shape anisotropy to crystal anisotropy in order to hinder magnetisation reversal (Ormerod, 1985). The discovery of the unusual crystal anisotropy properties of YCo₅ (Strnat and Hoffer, 1966) triggered further research into the RCo₅. The rare-earth permanent magnet family can be divided into two major subgroups:

- Rare-earth Co-based magnets (in particular SmCo)
- Rare-earth Fe-based magnets (NdFeB type)

2.1.1 SmCo Type Permanent Magnets

The beginning of the RE-Cobalt magnet era saw Strnat attempt to produce experimental SmCo resin bonded magnets by arc melting the components in the desired ratio under vacuum. Forming the alloy via a peritectic reaction usually as a single phase under the right cooling conditions (Strnat, 1970). Then ball milling the bulk alloy to near single crystal sizes and binding with resin. These “bonded” magnets were always prone to degradation of properties, for example by corrosion, or by time at elevated temperatures (Kirchmayr, 1996). This is due to the highly reactive nature of the rare-earth component in the alloy. The stability problems of SmCo₅ were solved by producing full density magnets through liquid phase sintering techniques. It was found that by sintering to a closed-pore structure, exposure to air at elevated temperatures lead to no reduction in magnetic properties (Benz and Martin, 1970). Samarium-Cobalt type magnets at their inception offered 2 – 3 times more energy per unit volume than previous Alnico type magnets, with 5 – 20 times their resistance to demagnetisation (Strnat, 1978). Since then SmCo₅ magnets have been produced with maximum energy products of 200 kJm⁻³ (Fidler, 2004). The dramatic increase in properties was attributed to the unique crystal lattice structure that was produced by alloying rare-earths with 3d-transition metals. The magnetic hardness of these materials is derived from their magnetocrystalline anisotropy and nucleation control of domains/domain wall pinning at the grain boundaries. The coercivity depends upon the state of the grain boundaries and in the case of the powders, on the state of the particle surface due to the presence of potential nucleation sites (Zijlstra, 1978).

Early in the search for RE-Co alloys it was realised that $\text{RE}_2\text{Co}_{17}$ phases displayed high curie temperatures coupled with high saturation magnetisation relative to RE-Co_5 phases. The preferred direction of magnetisation vector for some $\text{RE}_2\text{Co}_{17}$ within this system is perpendicular to the rhombohedral axis. This prevents coercivity development due to the free rotation of the magnetisation vector within the plane (Ormerod, 1985). However, the $\text{Sm}_2\text{Co}_{17}$ type magnets have uniaxial anisotropy and are closely related to their SmCo_5 counterparts. They are derived from a RE-TM₅ structure by a replacement of each third RE atom by a pair of TM atoms within the basal plane (Ostertag and Strnat, 1966).

The initial limiting factor associated with $\text{Sm}_2\text{Co}_{17}$ was the low coercivity. Although with the addition of some copper and an excess of samarium, this gives rise to a finely dispersed second phase that appears to inhibit domain wall movement, hence pinning them and, increasing coercivity, through precipitation hardening (Zijlstra, 1978).

2.1.2 NdFeB Type Permanent Magnets

NdFeB type magnets were discovered in 1984, simultaneously by General Motors (USA) (Croat et al., 1984a) and Sumitomo Special Metals (Japan) (Sagawa et al., 1984a). Both produced materials based on the magnetic phase $\text{Nd}_2\text{Fe}_{14}\text{B}$, although utilising different processing routes. The result of the different processing routes utilised by the two authors resulted in a material of roughly the same composition with vastly differing microstructures. These permanent magnets could be considered “third generation” magnetic materials. They utilise cheaper more abundant raw materials than their Sm-Co counterparts and also offer higher energy density at room temperature. However they do have greater problems with stability at both elevated and room temperature (Strnat and Strnat, 1991).

Within $\text{Nd}_{15}\text{Fe}_{77}\text{B}_8$ a complex multi-phase microstructure exists:

- The hard magnetic $\text{Nd}_2\text{Fe}_{14}\text{B}$ matrix (ϕ) Phase (85 vol%)
- Nd-rich grain boundary (ρ) Phase (12 vol%)
- B-rich $\text{Nd}_{1+x}\text{Fe}_4\text{B}_4$ (η) Phase (3 vol%)

The $\text{Nd}_2\text{Fe}_{14}\text{B}$ phase is responsible for the outstanding hard magnetic properties displayed by materials based on this system. The crystal lattice forms a tetragonal structure, with 68 atoms per unit cell and has the space group $\text{P4}_2/\text{mmn}$. Each unit cell contains four formula units. All of the Nd and B atoms and four of the 56 Fe atoms occupy $z = 0$ and $z = 0.5$ planes, and a further 5 non-equivalent Fe sites form folded, fully connected hexagonal nets. There are six crystallographically distinct iron sites, two different rare earth positions and one boron site (Herbst, 1991). This crystal lattice structure can be seen in Fig. 2.1.

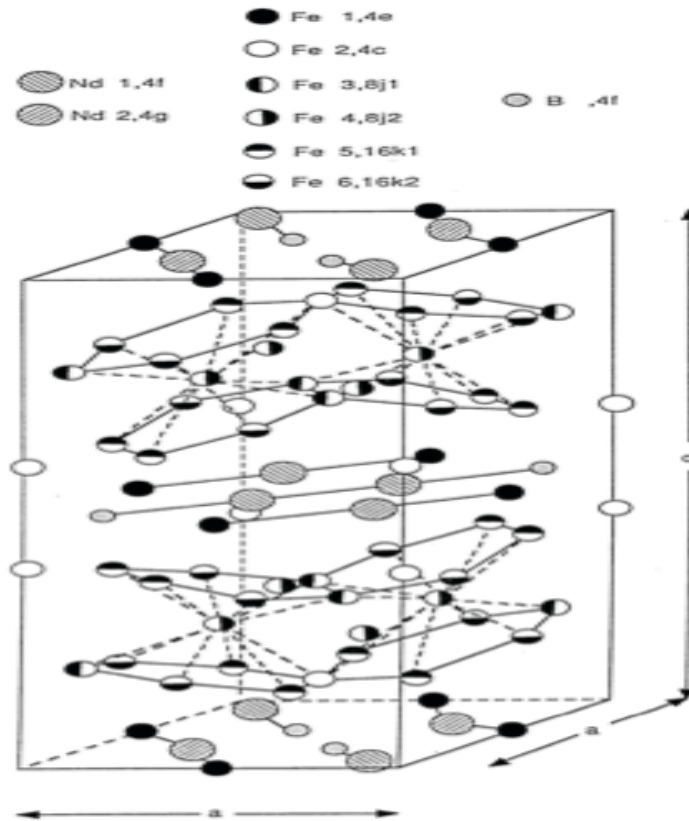


Fig. 2.1 Depicts the structure of tetragonal compound $\text{Nd}_2\text{Fe}_{14}\text{B}$: c-axis is the easy direction of magnetism (Herbst, 1991).

Differences in composition and processing routes between sintered ($\text{Nd}_{16}\text{Fe}_{76}\text{B}_8$) and melt-spun ($\text{Nd}_{15}\text{Fe}_{77}\text{B}_8$) materials lead to vastly different microstructures. Within the microstructure of the sintered material are irregular shaped grains of $\text{Nd}_2\text{Fe}_{14}\text{B}$ phase, around $10 - 20\mu\text{m}$ in size. The sintered material has an Nd-rich phase found along the grain boundaries of the $\text{Nd}_2\text{Fe}_{14}\text{B}$ matrix as a result of the off-stoichiometric composition with excess Nd. However, this excess Nd facilitates liquid phase sintering to improve density and magnetic properties. The melt-spun material possesses polyhedral shaped $\text{Nd}_2\text{Fe}_{14}\text{B}$ grain sizes in the region of $10 - 500\text{ nm}$, depending upon the velocity of the water cooled wheel. These $\text{Nd}_2\text{Fe}_{14}\text{B}$ grains are surrounded by a 2 nm thick layer of a $\text{Nd}_{0.7}\text{Fe}_{0.3}$ eutectic phase. The $\text{Nd}_2\text{Fe}_{14}\text{B}$ phase comprises around 95% of the bulk alloy.

2.2 NdFeB Sintered Processing Route

Sumitomo Special Metals developed a powder metallurgy processing route, through a chillcasting, annealing, grinding and powder sintering method. This produced the highest ever observed energy product, in excess of 300 kJm^{-3} (Sagawa et al., 1984b). Since then NdFeB based sintered permanent magnets have been produced with maximum energy products of 474 kJm^{-3} (Matsuura, 2006). This has been achieved by improved heat treatment, greater control of processing routes and the use of more iron rich compositions. The best commercially available NdFeB magnets possess energy products of around $405 \sim 437 \text{ kJm}^{-3}$ (Hatachi Metals Ltd, 2008)

The processing route for sintered NdFeB based magnets is shown in Fig. 2.2. Alloy ingots are prepared through an induction melting technique under an inert atmosphere, usually argon (Buschow, 1986b). The ingot in its as-cast state must be broken into a powder. This is achieved by exposing the ingot to hydrogen, which is absorbed at the surface. Hydrogen enters the material in spaces between the atoms, causing the material to expand. This differential expansion generates stress within the ingot causing it to break into a fine powder. This is known as the HD process and will be discussed in more detail within section 2.5 of this chapter. The HD powder is further broken up by jet milling. This reduces particle size from $20\mu\text{m}$ to around $5\mu\text{m}$. The size is critical to ensure each particle is a single domain. Before the discovery of the HD process the ingots were crushed roughly with a high energy hammer mill, then further by ball, attritor or jet milling.

After the powder has been broken down to a fine size, each particle is a single crystal which can be aligned within a magnetic field. The alignment can be held in place by pressing the powder into a green compact, approximately 60% dense. This green compact is then heated in a vacuum to around 1060°C for 1 hour. During heating hydrogen is

desorbed from the material and pumped away, sintering occurs and the compact densifies with the help of a liquid formed by the melting of the Nd-rich phase, this is commonly referred to as liquid phase sintering. After sintering the fully dense compact is quenched and heat treated to achieve the optimum magnetic properties. The magnet must then be machined to the final dimensions required for the intended application and coated to aid corrosion resistance.

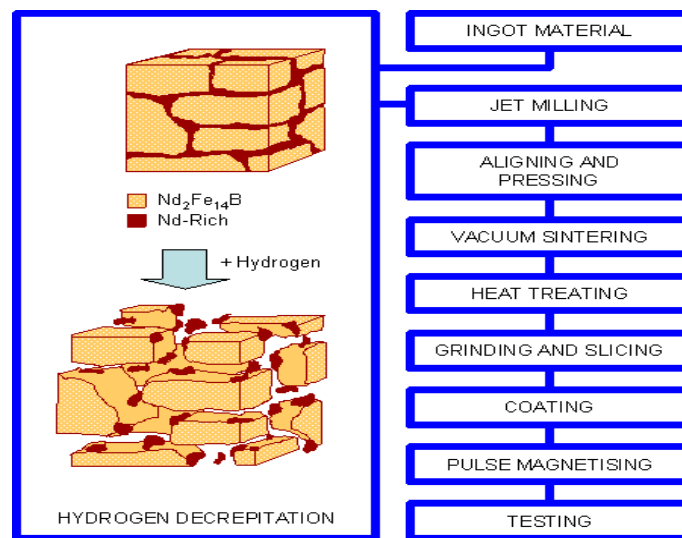


Fig. 2.2 Details the processing route for sintered NdFeB permanent magnets (Williams, 1994).

The starting alloys are an off-stoichiometric composition to prevent the formation of α -Fe which has a detrimental effect on the coercivity. Sintered NdFeB based magnets achieve their coercivity by virtue of an Nd-rich phase at the grain boundaries. This acts to produce liquid phase sintering, smoothing the boundaries and preventing the nucleation of reverse magnetic domains through domain wall pinning (Sagawa et al., 1984b).

Liquid phase sintering occurs due to the relatively low melting point of the Nd-rich phase present at the grain boundaries. It leads to densification without significant grain growth.

At the same time the liquid phase serves as an etching agent which removes damaged layers from the particles surfaces, leading to an enhanced coercive force (Buschow, 1986b). Smoothing the grain boundaries and reducing irregularities such as steps. It is also know that irregularities such as steps and sharp corners can act as nucleation sites for reverse domains. The Nd-rich grain boundary phase also prevents the nucleation of reverse domains by magnetically isolating each grain. (Harris, 1990). Other advantages of liquid phase sintering include enhanced resistance to oxidation, high magnetic flux density, the reduction in porosity also considerably increases the mechanical strength of the alloy (Buschow, 1986b).

2.3 NdFeB Melt Spinning Processing Route

The development of this process occurred at the same time as that of the powder metallurgy route reported by Sagawa (Sagawa et al., 1984a), discussed previously. This process relies on the rapid solidification (also know as rapid quenching or splat cooling) of a fine jet of molten alloy as it is ejected onto the surface of a rotating, water-cooled copper wheel. The whole process is carried out under the protection of an inert gas or vacuum to prevent oxidation during high temperature processing. Quench rates in the order of 10^6 K/s are produced. The jet of molten alloy feeds a pool of liquid alloy at its point of contact with the wheel, while the spinning wheel extracts the solidifying metal from the pool as a thin, rapidly quenched ribbon or flake. Ribbon fragments are typically in the region of 30-50 μm thick, 1-3 mm wide with lengths ranging from millimetres to centimetres, depending upon the surface velocity of the quench wheel.

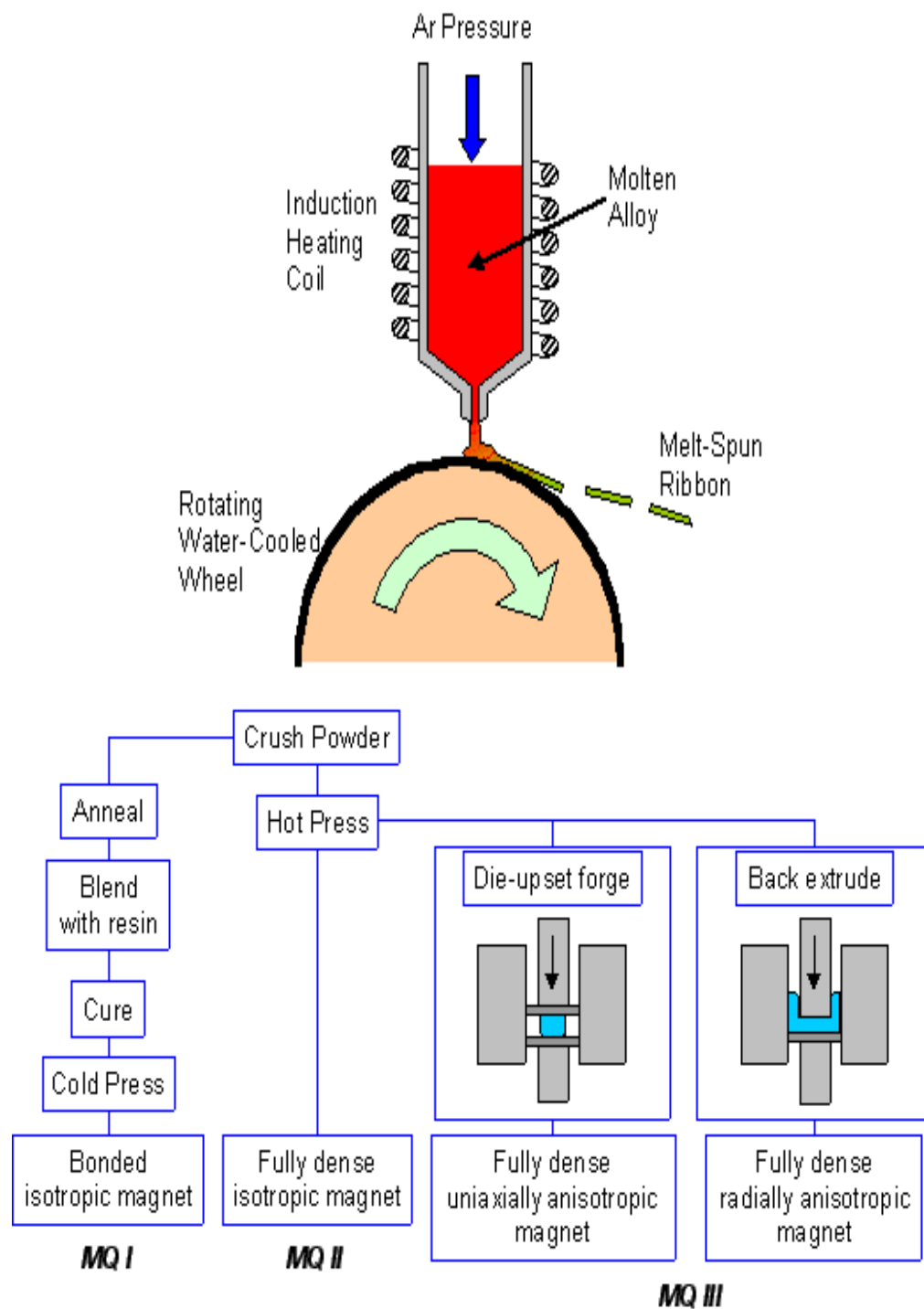


Figure 2.3 Depicts a schematic representation of the melt-spinning process and MQ magnet production (Williams, 1994).

The versatility of melt-spinning lies within the ability to control the microstructure of the ribbon by manipulating:

- Rotational velocity of the water cooled wheel.
- Speed at which the molten alloy is ejected onto the wheel.
- Temperature of the melt.

Higher wheel velocities lead to material with finer grains. Lower wheel velocities lead to the growth of larger grains within the alloy. Optimum magnetic properties occur when the microstructure consists of fine, polyhedral shaped $\text{Nd}_2\text{Fe}_{14}\text{B}$ grains approximately 30 nm in diameter, completely surrounded by a 2 nm thick layer of a $\text{Nd}_{0.7}\text{Fe}_{0.3}$ eutectic phase. The $\text{Nd}_2\text{Fe}_{14}\text{B}$ phase comprises approximately 95% of the volume (Herbst and Croat, 1991). These are single domain particles and thus have a high coercivity ($\sim 1000\text{kAm}^{-1}$). Due to the random orientation of grains within the ribbon the magnetic properties are isotropic (Croat, 1997).

The microstructure and magnetic properties of the NdFeB ribbons formed by melt-spinning are highly dependent upon the quench rate. The window to produce ribbons with optimal magnetic properties is very narrow, in terms of wheel velocity, the window is only a few m/s wide, hence optimally quenched material from the melt is difficult to produce. It is common practice in industry to over quench the molten alloy to an amorphous state and then to anneal the material allowing grains to grow to the desired size. This grain growth is very much time and temperature dependant but it is far easier to control through heat treatment rather than directly from the melt (Croat, 1997). Unfortunately, properties of the annealed material are worse than those with optimal microstructures as a direct result of quenching. High quench rates essentially produce amorphous ribbons with negligible intrinsic coercivity. This powder cannot be sintered to produce fully dense magnets

without destroying the magnetic properties. After the quenching and annealing process the flakes are ground down into a fine powder. The powder produced in this form is known as MQP.

There are a number of different grades of MQP. Each has been tailored to have slightly different magnetic properties. Some are designed for higher performance applications, others for lower cost requirements. The desired application, performance and cost of the magnet will strongly influence which grade is selected by the end user. Magnequench are the main manufacturer of NdFeB MQP, properties of the many grades produced can be seen from the scatter graph and chart in Fig. 2.4.

MQP™ Isotropic Powders	MELT SPUN ANNEALED CRUSHED RIBBON												
	Residual Induction, B _p mT (MG)	Energy Product, (BH) _{max} kJ/m ³ (MJ/De)	Intrinsic Coercivity, H _{ci} kA/m (kOe)	Coercive Force, H _c kA/m (kOe)	Magnetizing Field to >90% B _p (Oe)	Temperature Coefficient of B _p %/°C	Temperature Coefficient of H _c %/°C	Curie Temperature, T _c °C	Max Operating Temperature °C	Max Process Temperature °C	Density, ρ ₂₀ g/cm ³	Particle Size Distribution	
MQP-A													
10179-070	780 - 820 (7.80 - 8.20)	97 - 111 (12.2 - 14.0)	1030 - 1350 (13.0 - 17.0)	515 (6.40)	>2000 (>25)	-0.12	-0.4	305	120 - 160	200	7.61	Total > 40 Mesh (420 mm x 420µm opening) <0.1 wt. %	
MQP-B													
10184-070	860 - 895 (8.60 - 8.95)	111 - 126 (14.0 - 15.8)	640 - 800 (8.0 - 10.0)	500 (6.30)	>1600 (>20)	-0.11	-0.4	360	120 - 160	200	7.64		
20029-070	883 - 893 (8.83 - 8.93)	118 - 126 (14.8 - 15.8)	730 - 790 (9.2 - 9.9)	520 (6.50)	>1600 (>20)	-0.11	-0.4	330	120 - 160	200	7.63		
20052-070	885 - 885 (8.85 - 8.85)	116 - 124 (14.6 - 15.6)	800 - 860 (10.0 - 10.8)	520 (6.50)	>1600 (>20)	-0.13	-0.4	315	120 - 160	250	7.60		
20076-070	878 - 898 (8.78 - 8.98)	117 - 125 (14.7 - 15.7)	720 - 780 (9.1 - 9.8)	515 (6.50)	>1600 (>20)	-0.13	-0.4	313	120 - 150	250	7.61	Total >60 Mesh (250 mm x 250 µm opening) <25 wt. %	
MQP-B+													
10118-070	895 - 915 (8.95 - 9.15)	126 - 134 (15.8 - 16.8)	716 - 836 (9.0 - 10.5)	540 (6.80)	>1600 (>20)	-0.11	-0.4	360	120 - 160	200	7.64		
20056-70	893 - 901 (8.93 - 9.01)	122 - 128 (15.3 - 16.1)	750 - 810 (9.4 - 10.2)	530 (6.70)	>1600 (>20)	-0.11	-0.35	330	130 - 150	250	7.63	Total >270 Mesh (53 mm x 53 µm opening) <12 wt. %	
MQP-C													
20006-070	780 - 820 (7.80 - 8.20)	99 - 111 (12.5 - 14.0)	1230 - 1475 (15.5 - 18.5)	530 (6.70)	>2000 (>25)	-0.07	-0.4	470	120 - 160	200	7.72		
MQP-O													
20057-070	800 - 830 (8.00 - 8.30)	105 - 115 (13.2 - 14.5)	940 - 1070 (11.8 - 13.5)	525 (6.60)	>1600 (>20)	-0.13	-0.4	305	140 - 180	300	7.61		
MQP-14-12													
20000-070	820 - 850 (8.20 - 8.50)	107 - 120 (13.4 - 15.1)	940 - 1050 (11.8 - 13.2)	550 (6.90)	>1600 (>20)	-0.13	-0.4	305	140 - 180	250	7.62	Total > 40 Mesh (420 mm x 420µm opening) <0.1 wt. %	
MQP-15-7													
10271-070	900 - 930 (9.00 - 9.30)	115 - 123 (14.5 - 15.5)	510 - 640 (6.5 - 8.0)	440 (5.50)	>1600 (>20)	-0.11	-0.4	325	90 - 130	200	7.63		
20065-070	915 - 935 (9.15 - 9.35)	114 - 126 (14.3 - 15.8)	540 - 620 (6.8 - 7.8)	450 (5.70)	>1600 (>20)	-0.13	-0.43	309	80 - 120	200	7.61	Total >60 Mesh (250 mm x 250 µm opening) <25 wt. %	
MQP-13-9													
10533-070	790 - 820 (7.90 - 8.20)	97 - 105 (12.2 - 13.2)	640 - 800 (8.0 - 10.0)	470 (5.90)	>1600 (>20)	-0.12	-0.4	305	120 - 160	250	7.56		
20011-070	790 - 820 (7.90 - 8.20)	99 - 107 (12.4 - 13.4)	640 - 800 (8.0 - 10.0)	485 (6.10)	>1600 (>20)	-0.12	-0.4	293	125 - 170	250	7.47		
20063-070	795 - 825 (7.95 - 8.25)	100 - 112 (12.6 - 14.1)	720 - 800 (8.7 - 9.7)	505 (6.30)	>1600 (>20)	-0.14	-0.36	295	130 - 160	250	7.48	Total >270 Mesh (53 mm x 53 µm opening) <12 wt. %	
MQP-16-7													
11277-070	960 - 1000 (9.60 - 10.00)	124 - 140 (15.6 - 17.6)	520 - 600 (6.5 - 7.5)	460 (5.80)	>1600 (>20)	-0.08	-0.5	345	90 - 130	200	7.62		
20068-070	940 - 980 (9.40 - 9.80)	114 - 130 (14.3 - 16.3)	525 - 605 (6.6 - 7.6)	435 (5.50)	>1600 (>20)	-0.12	-0.52	291	80 - 120	250	7.61		

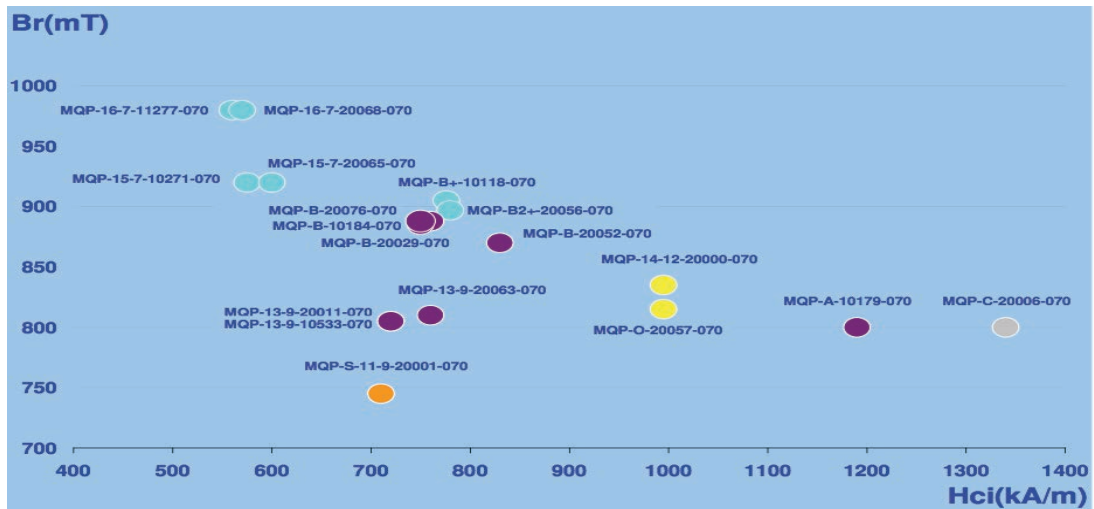


Fig. 2.4 Details properties of MQP powders produced by Magnequench accompanied by a graphical representation of properties (bottom) (Magnequench Inc, 2009g) (Magnequench Inc, 2009f).

There are three primary processes that utilise this powder to produce magnets. Therefore, there are three different types of magnet:

- MQI
- MQII
- MQIII

MQI type magnets are manufactured through a cold pressing technique whereby coarsely ground, optimally quenched or annealed over-quenched ribbons are blended with polymeric binder and compacted or injection moulded. The magnetic properties of the powders are not adversely affected by the grinding process due to the small grain size relative to the particle size.

The platelet like geometry of the particles allows them to “stack” in a highly uniform arrangement. Due to the stacking ability densities of approximately 85% can be achieved (Lee, 1985). Bonded magnets produced via the injection moulding route have lower loadings typically around 50-75 vol% (Ma et al., 2002) to prevent injection nozzle clogging. This study is primarily interested in this type of magnet produced from MQP-C powder supplied by Magnequench. The isotropic nature of this material limits the $(BH)_{\max}$ to $\sim 80 \text{ kJm}^{-3}$.

A limiting factor of MQI magnets is the stability of the bonding media at elevated temperatures. Exposure to elevated temperatures can cause softening/melting or decomposition of the binder, ultimately leading to disintegration of the magnet. As a consequence of the delamination, individual particles of MQP are exposed to the environment and moisture which can accelerate corrosion in the predominant $\text{Nd}_2\text{Fe}_{14}\text{B}$ magnetic phase. The corrosion process will be discussed in more detail later in this chapter.

Despite the disadvantages discussed above, bonded magnets do outperform their sintered counterparts in a number of ways. They can be created in a wider variety of shapes for a greater spectrum of appliances. A major advantage of the bonded process is the manufacturing to net shape. Bonded magnets will be discussed in greater detail later within section 2.4 of this chapter.

MQII type magnets are produced by a process known as hot pressing. At temperatures in the region of 700°C sufficient plasticity is developed in the alloy so that pressing at that temperature or higher transforms the cold press packing to a fully dense form (Lee, 1985). This plasticity is a result of the liquid, Nd-rich, grain boundary phase present above 670°C (Grunberger et al., 1997). The melt-spun ribbon is pressed around 750°C under an argon atmosphere. Pressures and temperatures are dependant upon the starting composition of the alloy. The best candidates in terms of starting material are over quenched ribbons. Through the hot pressing process a more favourable grain size is developed. This method can yield magnets that are fully dense using MQ powders. Although the MQ powders are isotropic the hot pressing process causes a degree of magnetic alignment, around 10%. The properties of these are not diluted by a non-magnetic material, such as resin. This gives a higher $(BH)_{\max}$ than MQI of 100-120 kJm⁻³. Due to the specialised nature of the hot pressing equipment and the exposure of the process there are currently no applications for MQII magnets.

MQIII type magnets are produced by die upset forging. This technique is a two stage method whereby, fully dense isotropic MQII magnets are subject to a further pressing process. During this second stage press the material is allowed to increase in dimension perpendicular to the direction of force applied.

The magnetic properties developed by this process show a strong correlation between composition and strain rate, working temperature and extent of deformation. The greatest magnetic properties were found to occur when the sample height was reduced by at least a factor of four during die upsetting. This additional working of the material produces grain alignment along the c-axis by plastic flow (Nozawa et al., 1988). This is thought to originate from a mixture of shear deformation in favourably oriented grains, grain boundary sliding, boundary migration and diffusion slip. The alignment produced by this method is purely crystallographic, no aligning field is required (Panchanathan, 1995). Mishra et al reported that a possible mechanism for grain alignment during die upsetting is that the grains rotate as they deform plastically so as to make the slip plane normal to the compressive stress axis, lubricated by the molten intergranular phase. So as all the aligned grains have their c-axis parallel to their stress axis. Also suggesting diffusion slip plays the decisive role in the deformation and alignment of this material and that the applied stress assists in preferential directional diffusion. Selective grain boundary migration under the applied stress then consumes the adjacent grains, which are unfavourably oriented. (Mishra, 1987). Li and Graham proposed a model for the development of crystallographic texture by hot-deformation. They believed that this alignment process occurs through liquid diffusion. The driving force for this was thought to be the concentration gradient of $\text{Nd}_2\text{Fe}_{14}\text{B}$ in the Nd-rich phase created by compressive stresses on differently oriented grains. The alignment process occurs when $\text{Nd}_2\text{Fe}_{14}\text{B}$ grains under a compressive strain connected by a liquid Nd-rich phase are each partially dissolved into the liquid Nd-rich phase at the solid liquid surfaces. If one grain is more preferentially aligned than another then more of the non-preferential grain will be dissolved into the Nd-rich liquid phase. As a consequence of this there is a concentration gradient in the liquid allowing atomic

diffusion in the Nd-rich phase (Li and Graham, 1992). The growth and stacking of these grains leads to good magnetic anisotropy. The properties of these MQ-III magnets can be further improved by a short anneal at 800°C.

These fully dense anisotropic magnets can also be ground to produce a stable anisotropic powder which can be used to make good anisotropic bonded magnets as reported by Tokunaga (Tokunaga et al., 1989). The stability of the anisotropic powder produced via the MQIII process appears to be greater than that of powder developed from grinding sintered magnets (Doser et al., 1991). Significant degradation of magnetic properties can be seen in milled and crushed sintered NdFeB powders upon exposure to air, which is not evident in powder produced from MQIII magnets. An alternative to grinding the MQIII material is to subject it to a hydrogen decrepitation process and degassing heat treatment. There is a need to modify this process due to the inherent inert nature of the rapidly solidified ribbons and also powder particles to produce bonded magnets are not required to be of a fine aggregate. Improved magnetic properties and stability for bonded magnets are obtained by having aggregates larger than 125 μm (Doser et al., 1991). Meisner and Panchanathan reported on the high dependence of the H_{ci} on the outgassing temperature, observing a full recovery of H_{ci} when hydrogen was completely desorbed from the $\text{Nd}_2\text{Fe}_{14}\text{B}$ phase at 240°C, with no increase in properties at higher temperatures. Due to there being no further increases in H_{ci} it is assumed that the remaining hydrogen is in the intergranular Nd-rich phase (Meisner and Panchanathan, 1993).

Due to a demand for higher energy product bonded magnets Magnequench now produce an anisotropic powder via Hydrogenation, Disproportionation, Desorption, Recombination (HDDR) processing. This process is used to manipulate the microstructure to produce a

finer grained structure. Grain sizes are in the region of 0.3 μm and are nearly spherical in shape. There is no second phase apparent inside the crystalline grains and the Nd-rich phase is only observed in some parts of the grain boundary regions. Uniform magnetic properties are displayed over a wide range of particle sizes (Panchanathan, 1995). This process will be discussed in greater detail within section 2.6 of this chapter.

2.4 Bonded Magnets

Bonded magnets are a mixture of permanent magnetic powder and a binder, as such, they can be thought of as a composite material. The magnetic properties of bonded magnets are highly sensitive to the intrinsic properties and volume fraction of the magnetic powder used, more so than their sintered fully dense counterparts. This is due to the dilution effect that the binder has upon the magnetic properties of the composite. This effect is summarised in equ 2.1:

$$B_r \text{ of polymer bonded magnet} = B_r \text{ of powder} \times \text{Volume fraction of powder}$$

(equ 2.1)

For this reason powders produced for bonded magnet production have fully optimised magnetic properties (e.g. high remanence) through processing. An example of such a powder would be Magnequench NdFeB isotropic melt spun ribbon which is used almost exclusively in bonded magnets (Ormerod and Constantinides, 1997b).

For bonded magnets, powder magnetic properties, loading factor, molding characteristics and density are important to obtain magnets with high energy product (BH_{max}) magnets. In general, powders of high BH_{max} are essential to achieve bonded magnets with a high BH_{max} . High loading of the NdFeB powder whilst still within molding capability, is also essential to obtain high BH_{max} magnets. In all cases, magnets would need to be molded

with a commercially available molding machine to achieve the desired shapes with proper magnetic and mechanical properties (Ma et al., 2002). The relationship between bonded magnet density and BH_{\max} is summarized by equ 2.2:

$$(BH)_{\max} \propto \left[(1 - V_{\text{non}}) \frac{d}{d_m} B_r(p) \right]^2 \quad (\text{equ 2.2})$$

where,

V_{non} is the volume fraction of non-magnetic phase

d is the density of the magnet

d_m is the theoretical density of ideal bonded NdFeB magnet

$B_r(p)$ is the remanence magnetization of the powder which is determined by the chemical composition and microstructure.

The effect of $B_r(p)$ on $(BH)_{\max}$ is assumed to be negligible if the powder composition is fixed. So the $(BH)_{\max}$ is mostly decided by the density and volume fraction of the non-magnetic phase which is determined by the processing (Li et al., 2006).

In addition to BH_{\max} ; the flux aging loss and thermal stability of magnets are important to applications where they may be exposed to elevated temperatures. Since there are various types of magnetic powder and polymer available for molding bonded magnets, it is important to establish the thermal characteristics of both powder and polymer to obtain high BH_{\max} bonded magnets with desired characteristics (Ma et al., 2002).

Bonded magnets are the most rapidly growing segment of the permanent magnet market. NdFeB bonded magnets can be used in a wide range of applications. The emergence of large developing economies, growth of the personal computer industry and related

technologies, and government regulation for efficiency in appliances and automobiles provide a tremendous growth opportunity for all NdFeB permanent magnets including bonded. Both powder and magnet producers need to constantly improve their products by introducing new powder grades or new manufacturing methods for the ever growing application opportunities.

Developments within the bonded magnet industry are centered on improvements in elevated temperature stability; this facilitates uses within the automotive industry. These ‘under the bonnet’ automotive applications are often subject to operating temperatures of 125 – 150°C. The requirement for powders that exhibit high resistance to corrosion under these harsh environments is constantly increasing due to the growing popularity of NdFeB type magnets for applications within cars, particularly as sensors. The bonding media used can play an important role in shielding the powder from its surrounding environment i.e. providing a barrier for moisture.

2.5 Hydrogen Decrepitation (HD) Process

The occlusion of hydrogen by metals of the rare earth group has been known since about 1900, when Matignon first noted that hydrogen was taken up by Ce, La, Pr, Nd and Sm to form solid products (Mulford and Holley, 1955). The most extensive work was carried out by Sieverts and co-workers who collected pressure-temperature-composition data for La, Ce, Nd and Pr during the 1920’s.

More recently the effect of hydrogen on the magnetic properties of RE compounds was reported by workers at the Philips Laboratories, Eindhoven who investigated the effect of hydrogen upon the magnetic properties of SmCo₅. It was found that the powdered alloy readily absorbed hydrogen at room temperature and pressure causing a dramatic drop in

coercivity. This drop in coercivity was thought to be due to the hydrogen distorting the crystal lattice structure from a hexagonal to an orthorhombic structure. It was found that a reduction in hydrogen pressure prompted a release of hydrogen and a recovery of the coercivity to its initial high value. This process was shown to be highly reversible (Zijlstra and Westendorp, 1969).

An early study into the absorption of hydrogen by intermetallic compounds found that powdered and crushed SmCo_5 at room-temperature under 100 atm hydrogen pressure needs about 48 hours to become fully saturated with hydrogen on the first cycle. It desorbs against 1 atm hydrogen in around 0.5 hours and without exposing the powder to air it may be reloaded in less than 1 minute under 50 atm hydrogen (van Vucht et al., 1970).

The beginnings of the HD process were observed by Buschow et al. (Buschow, 1976) who noted that during the uptake of hydrogen by the Y_6Fe_{23} alloy this caused a violent lattice expansion resulting in the breakdown of the original piece of metal into tiny powder particles. The decrepitation of the bulk material is usually associated with the formation of metal hydrides. This is the case for the brittle intermetallic compounds and the nature of the particulate material formed by this process depends on the fracture process or processes (Harris, 1987). A summary of the various hydrogen absorption induced fracture processes can be seen in Table 2.1:

Table 2.1 Summarises hydrogen absorption induced fracture processes

Type	Appearance
1) Intergranular fracture	Granular form might be equiaxed crystals, columnar or variations thereof. Smooth surface with grain boundary debris sticking to the surface.
2) Transgranular fracture:	
(i) Random	Irregular shapes with sharp features. Smooth surface if brittle failure. Regular crystallographic shapes. Smooth surfaces.
(ii) Cleavage planes	
(iii) Second phase interface	Depends on the nature of the interface, could result in needles, platelets etc.
3) Ductile failure	“Onion skin” effect. Flake-like particles with irregular surface. Poor reflectivity, high surface area.

Decrepitation is defined as “the separation of parts with a crackling sound”; this effect is achieved by introducing hydrogen into the system at pressures as low as 1 bar. The manufacture of RE-TM magnets by the HD route was first proposed in a 1978 patent by Harris et al (Harris et al., 1979). This referred mainly to SmCo based alloys but is generally applicable to any RE-TM alloy capable of absorbing significant quantities of hydrogen (Harris and McGuiness, 1991). Hydrogen was seen as an important processing tool with significant advantages over attritor or jet milling in the preparation of powdered RE-TM alloys for permanent magnet production. The main advantages according to Harris (Harris, 1987) are:

- Large ingots can be broken up readily into fine friable powder.
- Intergranular failure promotes the production of single-crystal particles.
- If controlled properly can negate the need for further attritor or jet milling.
- The HD process actively prevents the oxidation of the decrepitated powder.
- The HD particles have very clean surfaces suitable for subsequent sintering or bonding.

- Less strain was introduced in comparison to the normal milled material. Producing a better loop shape and H_{ci} when used to produce polymer bonded magnets.
- The desorption of high purity hydrogen during vacuum sintering produces a non-oxidising environment during the annealing process.

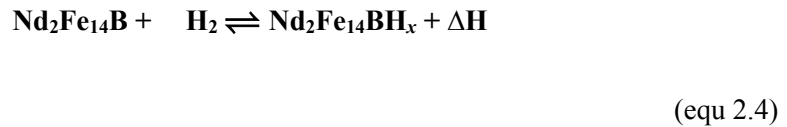
2.5.1 The Hydrogen Decrepitation (HD) Process In NdFeB Type Alloys

According to McGuiness et al. (McGuiness et al., 1986) HD in NdFeB type systems is a two stage process. Firstly the hydrogen reacts with the Nd-rich phase, situated at the grain boundaries causing intergranular cracking though a violent lattice expansion of 16.4% (Takeshita, 1995), and ultimately, intergranular failure. This reaction is represented by equ 2.3:



(where x depends on temperature and pressure; $x \sim 2.7$ for 1 bar at room temperature)

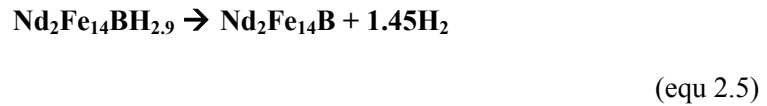
Due to the exothermic nature of the first stage reaction it allows the initiation of the second phase. Whereby the $\text{Nd}_2\text{Fe}_{14}\text{B}$ matrix is activated and readily absorbs hydrogen. It has been shown that the presence of the Nd-rich phase is essential for uptake of hydrogen by the $\text{Nd}_2\text{Fe}_{14}\text{B}$ phase at room temperature (Harris and McGuiness, 1991). The $\text{Nd}_2\text{Fe}_{14}\text{BH}$ phase is subject to a lattice expansion of 4.8% (Takeshita, 1995). The reaction is represented by equ 2.4:



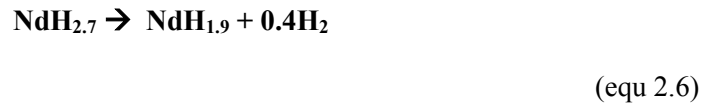
(where x depends on temperature and pressure; $x \sim 2.9$ for 1 bar at room temperature)

The lattice expansion generated by the interstitial uptake of hydrogen generates stresses leading to the decrepitation of the material, predominantly by intergranular fracture. The powder produced is more friable and readily milled than conventional powder (McGuinness et al., 1986). After milling, aligning and pressing the hydrided powders are sintered under vacuum and hydrogen is completely desorbed leading to the formation of a fully dense fine grain magnet. The desorption of hydrogen occurs in three stages (Williams et al., 1991):

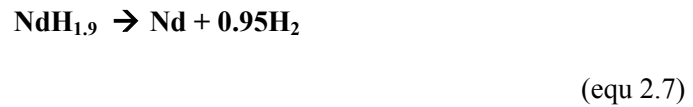
- Complete desorption from the ϕ Phase (occurs between room temperature to 300°C):



- Conversion of the Nd ‘trihydride’ ($\text{NdH}_{2.7}$) to Nd ‘dihydride’ ($\text{NdH}_{1.9}$) (occurs between 250°C to 400°C):



- Complete desorption of the Nd ‘dihydride’ (occurs between 550°C to 650°C):



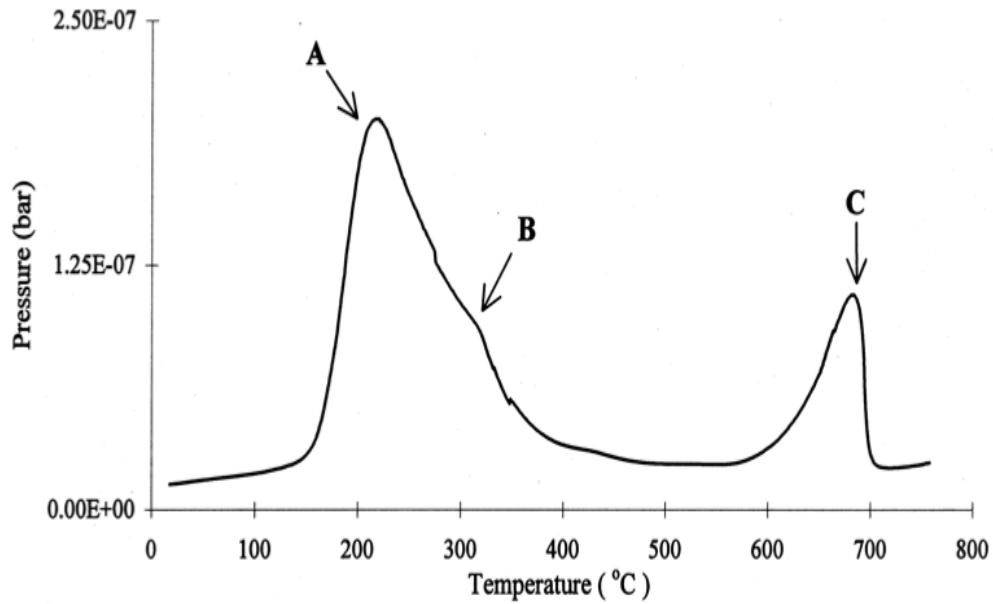


Fig. 2.5 Vacuum desorption of Nd₁₆Fe₇₆B₈ jet milled HD powder. Events A, B and C depict desorption stages from equ 2.5, 2.6 and 2.7 (Yan et al., 1999).

The complete desorption of hydrogen from the main Nd₂Fe₁₄B phase must occur in order to recover good magnetic properties before the sintering process continues at higher temperatures. Incomplete desorption of hydrogen can cause disproportionation whereby:



(equ 2.8)

(where NdH_x could be a mixture of hydrides.)

The disproportionation and the recombination processes will be discussed later within section 2.6 of this chapter.

2.5.2 The Hydrogen Decrepitation (HD) Process In SmCo Type Alloys

Magnetic studies on the $\text{SmCo}_5 - \text{H}_2$ system have showed that both H_{ci} and M_s are reduced by hydrogen additions and this reduction is particularly pronounced in the case of H_{ci} values. Harris et al. reported that the particles produced via this processing route displayed a probable fracture sequence of intergranular followed by transgranular cracking (Harris, 1987). The powder produced displays a sharp angular morphology compared to powder produced by conventional milling techniques. The powder also has smooth, clean fracture surfaces which is ideal for producing good sintered magnets (Harris et al., 1979).

It can be seen that the single crystal particles produced via HD processing are often scored with transcrystalline cracks. As a result of this the powder is very friable, passing the hydrided powder through a rotating vane or through other mechanical processing methods (attritator or jet milling) can see a further reduction in particle size in a relatively short time (Harris, 1987).

Early studies carried out on $\text{Sm}_2\text{Co}_{17}$ type alloys found that upon exposure of the bulk alloy to hydrogen at room temperature there is no absorption, even at high pressures. However, absorption does occur if the temperature is raised to around 200°C with a hydrogen pressure of around 200 bar although it is thought that such a high pressure is not required. Upon cooling and exposure to air the alloy remains in the hydrided condition unlike it's SmCo_5 counterparts (Harris, 1987), (Evans et al., 1985), (Kianvash and Harris, 1985).

However, more recent studies conducted have shown that hydrogen absorption can be achieved at room temperature with a hydrogen pressure of 10 bar. Although at this

temperature and pressure the reaction takes around 48 hours to reach saturation. The flake-like morphology of the material indicate that an “onion skin” type fracture process occurs, whereby thin layers are progressively removed from the magnet surface (Zakotnik et al., 2008), (Zakotnik et al., 2009). SmCo alloys display a high stability against disproportionation by hydrogen. Although it has been shown by Handstein et al. that the disproportionation of such stable compounds is successful when carried out under extreme conditions. Either by heating under high pressures of hydrogen (70 bar) or by reactive milling under a hydrogen atmosphere (Handstein et al., 1999).

The hydrogen desorption traces of SmCo_5 and $\text{Sm}_2\text{Co}_{17}$ shows two peaks; one located between 100 – 400°C which can be attributed to the desorption of δ hydrogen from $\text{SmH}_{2+\delta}$. The second peak between 450 and 625°C corresponds to the decomposition of SmH_2 , which is equivalent to the recombination of the SmCo_5 or $\text{Sm}_2\text{Co}_{17}$ phases (Gutfleisch et al., 1998).

Despite the reduction in coercivity due to the hydrogen absorption, the powder can still be uniaxially aligned and compacted in a magnetic field, indicating that c-axis anisotropy persists in the hydrided condition. Sintered metal SmCo magnets can be produced via HD processing as the hydrogen is removed during the vacuum sintering operation. If the powder is to be used for bonded magnets the hydrogen must be removed by vacuum degassing at around 200°C prior to the mixing and aligning stages (Harris, 1987). However, when HD powder is used to produce bonded magnets, a degradation of magnetic properties at room-temperature was observed and the bonded magnets were more susceptible to corrosion due to the highly reactive clean particle surfaces. The polymer

matrix was unable to provide protection against the oxidation of the particle surface (Harris, 1987).

2.6 Hydrogen Disproportionation Desorption Recombination (HDDR) Process

This is a high temperature hydrogen treatment used to manipulate the microstructure of the bulk alloy by inducing a reversible phase transformation. The process has been used to produce magnets of fine grained, homogeneous material from the coarse grained, non-homogeneous as cast alloy. The grain sizes and orientations together with the local elemental distribution all play a part in determining the bulk magnetic properties of the permanent magnet material (Thompson et al., 1999). Within this process the role of the interstitial hydrogen atoms are transient. The key to the process lies in the thermodynamic properties such as the enthalpy for formation of tertiary hydrides and activation energy for atomic motion. The hydrogen is removed once the desired microstructure modification has been achieved.

This process was first reported at the 10th International Workshop on Rare-Earth Magnets and their Application (Takeshita, 1989) followed by a further publication in 1991 (Nakayama et al., 1991) although the authors had recognised the process and its effects upon the material, they did not provide clear reasons for the improvement in magnetic properties.

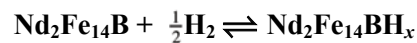
Researchers at Birmingham University followed up this study by relating the changes in microstructure observed to changes in magnetic properties recorded. It was reported that the hydrogen heat treatment results in the disproportionation of the two alloys into a finely divided mixture of iron, iron-boride and neodymium hydride. This occurs as a result of the greater stability of neodymium hydride relative to the stability of Nd₂Fe₁₄B hydride.

Disproportionation is observed at elevated temperatures due to the enhanced solid state diffusion of the metal atoms (McGuinness et al., 1990a). Studies on the disproportionation reaction in $\text{Nd}_{16}\text{Fe}_{76}\text{B}_8$ alloy have shown that the reaction begins at the Nd-rich grain boundary phase which acts as a fast diffusion path for the hydrogen, and then proceeds towards the centre of the original grains (Gutfleisch and Harris, 1996).

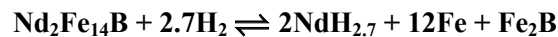
McGuinness et al also showed that with an appropriate vacuum annealing heat treatment the hydrogen could be removed from the alloy and subsequently allow the recombination of the iron, iron-boride and neodymium to form the original alloy. The process would be expected to proceed from many nucleation sites resulting in a fine, spherical type grain structure (McGuinness et al., 1990a).

The advantage of the HDDR process is that large coercivities can be obtained without the need for Nd-rich material at the grain boundaries (Nakayama and Takeshita, 1993). This allows alloys of closer stoichiometric composition to be used, driving down costs.

The HDDR process is comprised of two competing reactions:



(equ 2.9)



(equ 2.10)

The enthalpy of formation per mole for the second reaction is more negative than for the first, but a higher enthalpy of activation is needed for the second reaction to proceed. This

is due to the phase separation of $\text{Nd}_2\text{Fe}_{14}\text{B}$ into grains of $\text{NdH}_{2.7}$, Fe_2B and grains of Fe. At temperatures below 600°C long range diffusion is absent, which causes phase separation. This limited metal atom diffusion makes it possible to prepare R-3d-metal hydrides which are then metastable with respect to the R-H hydrides and 3d metal. This means that in $\text{Nd}_2\text{Fe}_{14}\text{B}$, the hydride will be formed at a higher temperature along with Fe_2B and Fe, or if the $\text{Nd}_2\text{Fe}_{14}\text{B}$ alloy is heated for extended periods under a hydrogen atmosphere. This disproportionation process occurs at approximately 600°C .

The events of the HDDR process are summarised schematically in Fig. 2.6. Initially hydrogen decrepitation occurs at room-temperature, leading to production of a friable powder. Upon heating under hydrogen the $\text{Nd}_2\text{Fe}_{14}\text{B}$ disproportionates to a fine mixture of Fe, Fe_2B , and Nd hydride. The hydrogen is then desorbed allowing recombination to occur with the nucleation of fine ($\sim 0.3\mu\text{m}$) randomly oriented grains of $\text{Nd}_2\text{Fe}_{14}\text{B}$. The Nd-rich grain boundary phase is left unaffected by this process. It has been shown that coercive powder can be produced from near stoichiometric ($\text{Nd}_{2.1}\text{Fe}_{14}\text{B}$) alloy via HDDR processing (Zhang et al., 1991).

Researchers have shown that the HD reaction can be avoided altogether by introducing the hydrogen at elevated temperatures. This results in disproportionation with the absence of cracking known as ‘solid HDDR processing’ (Gutfleisch and Harris, 1996).

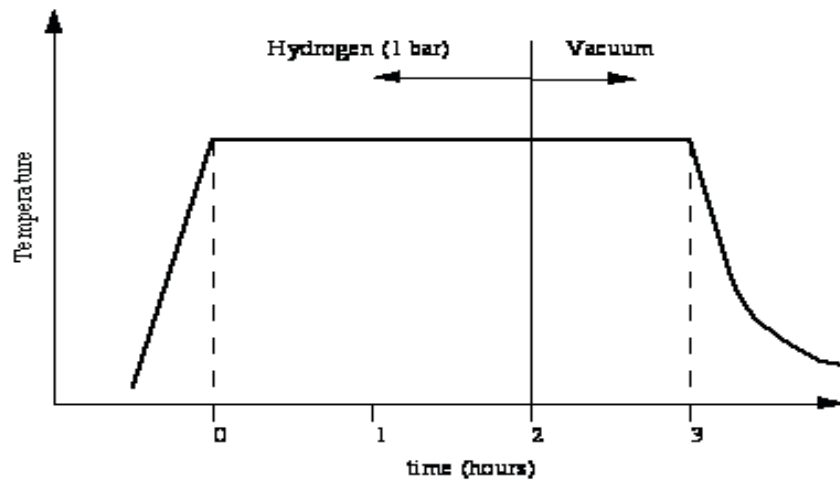


Fig. 2.6 Processing conditions for production of HDDR powder (Williams, 1993).

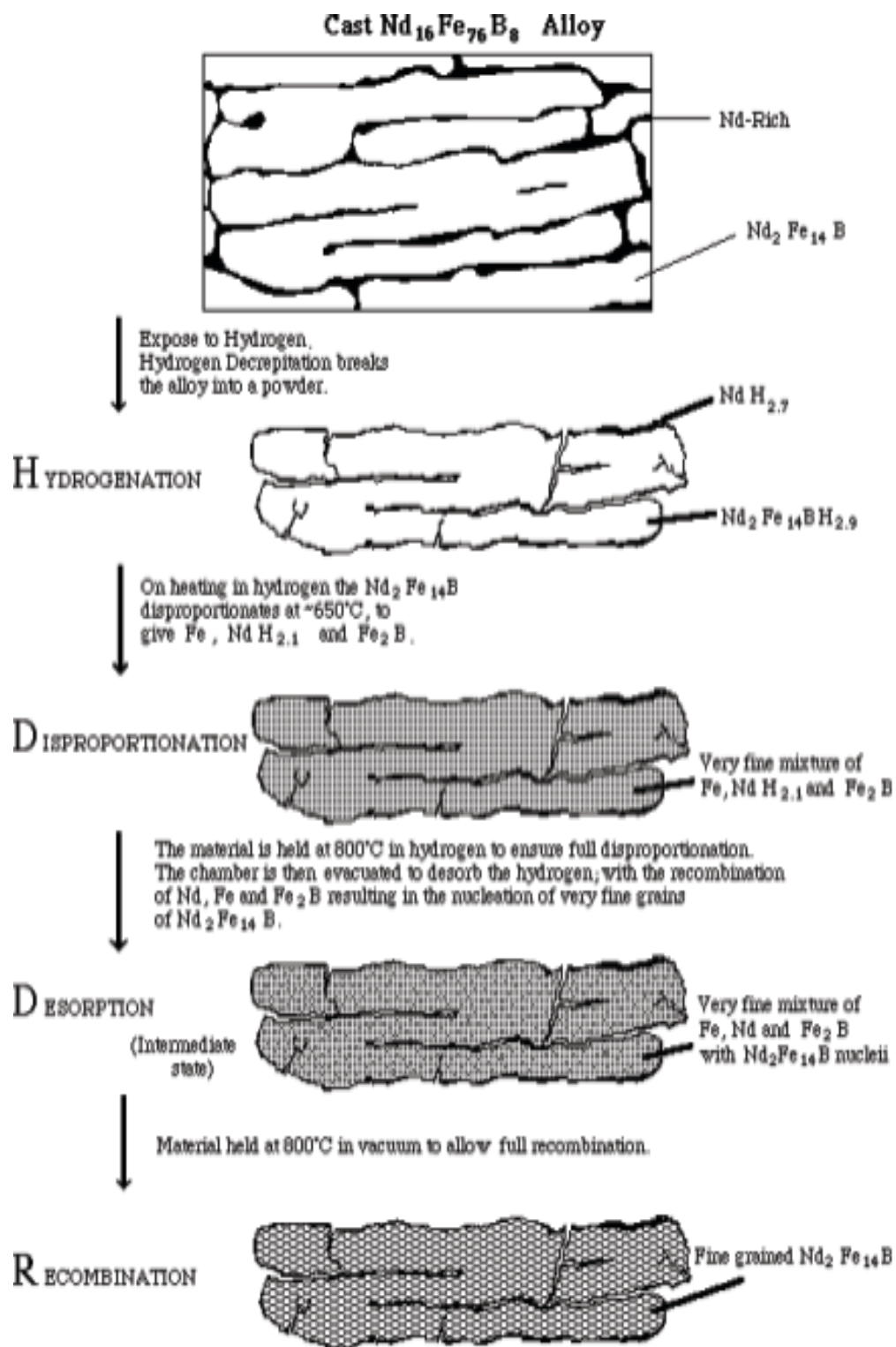


Fig. 2.7 Illustration of the various stages of HDDR processing (Williams, 1993)

2.7 Hydrogen Desorption

The desorption of hydrogen can be achieved via two methods; either by increasing the temperature of the system or by reducing the hydrogen pressure in the system. During the manufacture of RE-TM magnets from powders produced via the HD process, this relies upon the temperature increase during the sintering process to liberate absorbed hydrogen from the alloy.

2.7.1 Hydrogen Desorption in SmCo Type Alloys

Hydrogen desorption traces of SmCo type alloys, seen in Fig. 2.8 after being subject to reactive milling, show two clear peaks. The first peak of the two curves between 100 – 400°C can be attributed to the desorption of δ hydrogen from SmH_{2+x} . With the second peak evident between 450 – 625°C corresponding to the decomposition of SmH_2 which depending upon the conditions of hydrogen uptake (i.e. reactive milling) can also correspond to the recombination SmCo_5 or $\text{Sm}_2\text{Co}_{17}$ (Gutfleisch et al., 1998).

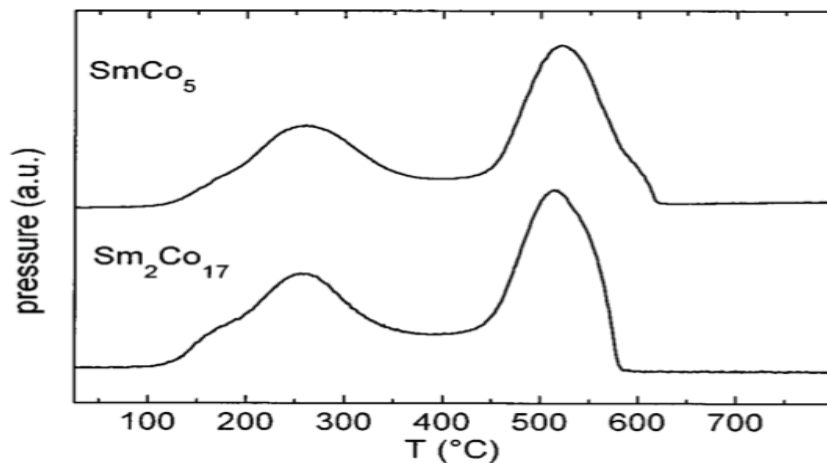


Fig. 2.8 Hydrogen Desorption trace of SmCo type alloys after reactive milling under hydrogen (Gutfleisch et al., 1998)

2.7.2 Hydrogen Desorption In NdFeB Type Alloys

In NdFeB type alloys hydrogen desorption was first reported to occur in either one or two stages depending upon the composition of the alloy and thus phases present in the bulk material. The majority of the hydrogen is desorbed in the region of 150-260°C, with a smaller amount desorbed over the 350-650°C. This two stage desorption was attributed to it's desorption from two different phases. The first lower temperature desorption corresponds to hydrogen lost from the Nd₂Fe₁₄B matrix phase. The higher temperature desorption corresponds to hydrogen lost from the Nd-rich grain boundary phase (Cadogan and Coey, 1986), (Harris et al., 1987).

More recent work carried out at Birmingham University has shown that this absorption actually occurs in three stages. The desorption has been reported to occur in the following order: Firstly hydrogen is desorbed from the Nd₂Fe₁₄B matrix phase. The second stage is the partial desorption of hydrogen from the Nd-rich material, where Nd 'trihydride' is converted to Nd 'dihydride'. The third and final stage is the complete desorption of hydrogen from the Nd-rich material (Williams et al., 1991). The desorption traces of Nd₂Fe₁₄B matrix material (Fig. 2.9a) and Nd_{15.5}Fe_{77.5}B₇ (Fig. 2.9b) can be seen below. It is worth noting that in the absence of any Nd-rich material there is no evidence of second or third stages of hydrogen desorption as discussed above.

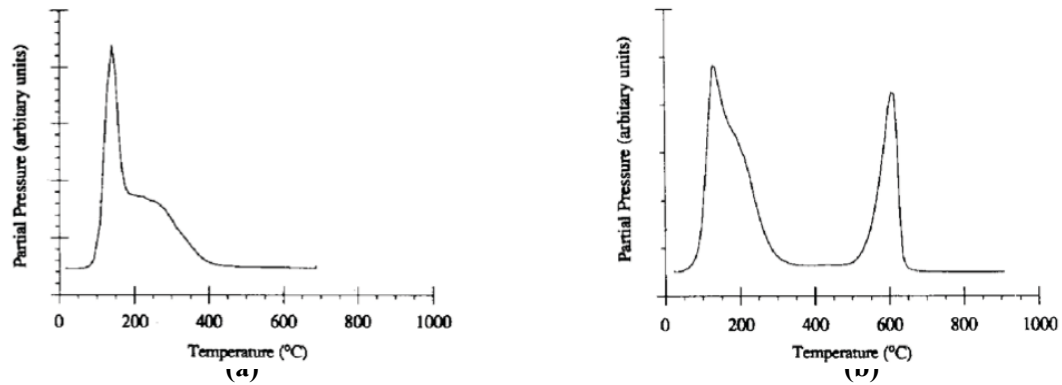


Fig. 2.9 Mass spectrometer hydrogen desorption trace of (Williams et al., 1991):
(a) $\text{Nd}_2\text{Fe}_{14}\text{B}$ phase
(b) $\text{Nd}_{15.5}\text{Fe}_{77.5}\text{B}_7$ alloy

Removal or desorption of hydrogen results in the intimate mixture of iron, iron-boride and neodymium to become thermodynamically unstable, causing it to revert to the more stable original $\text{Nd}_2\text{Fe}_{14}\text{B}$ alloy (Ragg et al., 1997). This process would proceed from many different nucleation sites and result in a very fine, spherical-type grain structure, with excess Nd distributed at the grain boundaries. The recombination process is highly sensitive to temperature. If the temperature is too low the alloy will not fully recombine leaving dendrites of free iron. If the temperature is too high then excessive grain growth will occur. Both extremes result in a reduction in coercivity with most favourable properties being achieved with the removal of all free iron and establishment of an optimal grain size (McGuinness et al., 1990a).

2.8 Corrosion Of Rare Earth Based Alloys

Within the permanent magnet market rare earth based alloys are heavily utilised due to their high maximum energy products relative to other available permanent magnet materials. NdFeB based alloys are most attractive as they have high maximum energy

products coupled with relatively low cost when compared with other RE-TM magnets such as SmCo types.

The issue that prevents increasingly widespread use, especially with those materials from the Nd-Fe based family, is its inherent poor corrosion resistance upon exposure to humid environments (Willman and Narasimhan, 1987). This poor resistance to corrosion is due in part to the highly reactive rare earth element upon which the alloys are based and an electrochemical coupling between two phases present in the bulk alloy. This problem can limit the life span of the component or even prevent it from being used for certain applications altogether. For situations where NdFeB magnets are unsuitable, but high energy products are still required, designers would have to turn to the more stable SmCo based counterparts, driving up costs significantly.

If a suitable solution can be found to combat the poor corrosion resistance displayed by the NdFeB type alloys this will facilitate more universal use regardless of environment. If this was to be the case, devices operating under these conditions would benefit greatly from the higher maximum energy products, lower production costs and further miniaturisation that NdFeB based magnets can offer.

Papers published on the subject of humid corrosion in NdFeB based alloys differ greatly in a number of key experimental variables. Many studies for example utilise different alloy compositions coupled with a variety of corrosion tests. There are also many factors that affect the corrosion mechanisms and rates. These factors include:

- Starting composition of alloy.

- Microstructure – Volume and dispersion of grain boundary material, surface oxides formed.
- Surface preparation – roughness, cleanliness, oxide layer, fresh surface.
- Conditions of the corrosion test – Temperature, humidity, pressure, fluid composition.
- Monitoring method of corrosion rate during testing.

The large number of variables and difference in experimental techniques makes it very difficult to compare and contrast results obtained by different authors.

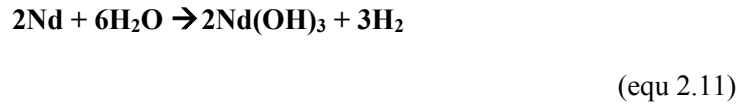
NdFeB based permanent magnets are less stable than their SmCo counterparts, both in terms of environmental degradation and thermal stability at moderate to high temperatures (T_c). They are particularly susceptible to aqueous corrosion and oxidation. Although the greatest cause of irreversible losses in terms of magnetic properties are due to the interactions of the alloy with water, and by-products of the decomposition of water i.e. hydrogen.

As discussed previously in the Hydrogen Decrepitation (HD) section Nd based magnets react readily with hydrogen, mostly due to the presence of the Nd-rich grain boundary phase. This paramagnetic Nd-rich phase responsible for isolating the $Nd_2Fe_{14}B$ grains to produce high coercivities is also the Achilles heel of the alloy. It is highly susceptible to aqueous corrosion and readily reacts with the hydrogen that is liberated as a result of this aqueous corrosion.

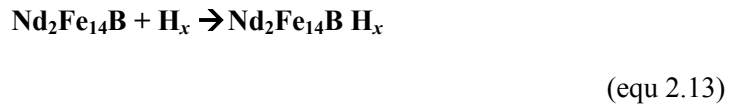
Workers from Birmingham University were among the first to report the similarities between the results of aqueous corrosion upon exposure to humid environments and

hydrogen decrepitation behaviour in sintered NdFeB type magnets (McGuinness et al., 1994). Similarities between the corrosion caused by exposure to aqueous environments and exposure to hydrogen gas infers a common corrosion mechanism (Kim et al., 1996).

It is possible that hydrogen is generated by the disassociation of water by the Nd-rich phase according to equ 2.11:



The hydrogen liberated from the decomposition of water proceeds to diffuse into the Nd-rich grain boundary phase and Nd₂Fe₁₄B matrix phase as follows:



Upon adsorption of the hydrogen by susceptible phases the lattice expansion associated with hydrogen uptake by rare earth based alloys causes layers of the Nd-rich grain boundary phase to peel away in an “onion skin” type decrepitation. The removal of grain boundary material in this way causes a progressive loosening of Nd₂Fe₁₄B grains of the matrix phase as seen in Fig. 2.10. The action of time and the continual loosening and removal of grain boundary phase provides fresh Nd-rich surface for attack.

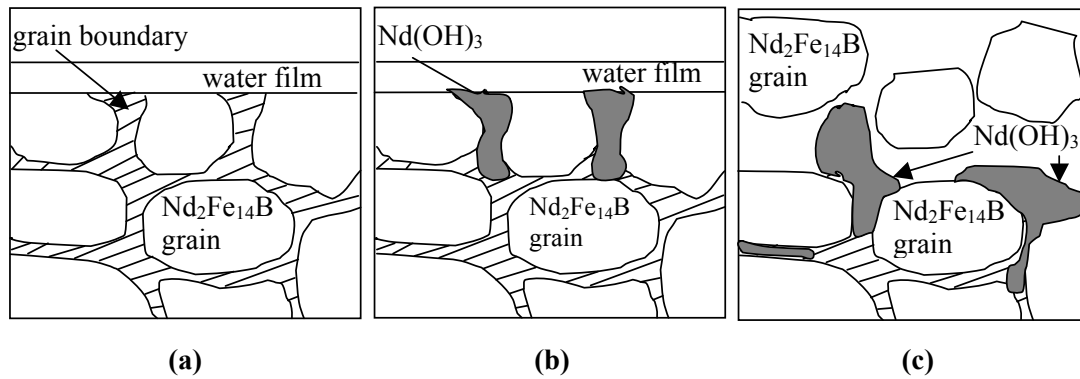


Fig. 2.10 Depicts a schematic representation of a sintered NdFeB magnet cross sections at (a) the initial contact with an autoclave environment, (b) the onset of grain boundary corrosion, (c) Nd₂Fe₁₄B grain "pull out" from the surface of the magnet (Walton, 2001).

It has been reported that the disintegration of metal magnets in a humid environment proceeds as follows: The Nd-rich phase reacts anodically with water forming Nd(OH)₃ possibly with some iron corrosion products; meanwhile water is reduced cathodically on the Nd₂Fe₁₄B matrix phase. Part of the resulting hydrogen is absorbed by Nd₂Fe₁₄B and the Nd-rich phase to form Nd₂Fe₁₄BH_x and NdH_{2+x}. The combined effect of the lattice expansion of the Nd₂Fe₁₄B–H phase, the formation of NdH_{2+x} and the volume expansion on formation of Nd(OH)₃, leads to the disintegration of the magnets (Yan et al., 1999).

Standard Nd₁₆Fe₇₆B₈ sintered magnets are composed of three phases: 85 vol% Nd₂Fe₁₄B (ϕ), 12 vol% Nd-rich (ρ), and 3 vol% Nd_{1+x}Fe₄B₄ (η). The relative electronegativity of these phases leads to the formation of an electrochemical couple with the η and ρ phases being anodic relative to the ϕ phase, and hence the preferential corrosion/oxidation of the η and ρ phases. As a result of corrosion these phases expand, causing a disintegration of the surface and a breaking away of corrosion products and ϕ grains from the bulk magnet (Yan et al., 1999).

NdFeB alloys prepared via the melt spinning process have an advantage over their HD and HDDR powder counterparts due to the starting composition of the alloy. The rapid quenching technique and the near stoichiometric starting composition of the material ($\text{Nd}_4\text{Fe}_{78}\text{B}_{18}$) enable the ribbon produced to be predominately composed of $\text{Nd}_2\text{Fe}_{14}\text{B}$ grains with a significant reduction in volume of the highly reactive Nd-rich grain boundary phase. As a result melt spun ribbon is far less susceptible to aqueous corrosion and oxidation. Although hydrogen absorption by the $\text{Nd}_2\text{Fe}_{14}\text{B}$ phase will still occur, usually requiring elevated temperatures or pressures (Harris et al., 1987). Decrepitation type behaviour as a result of hydrogen absorption displayed by the Nd-rich phase is not observed in the $\text{Nd}_2\text{Fe}_{14}\text{B}$ phase. Although detrimental effects upon coercivity are observed as a result of expansion of the crystal lattice structure. It has been reported that the decrease in H_{ci} as a result of hydrogen absorption is due to the decrease of the uniaxial anisotropy field. This is caused by a reduction in Nd-Fe exchange brought about by a change in Nd to Fe bond lengths (Oesterreicher and Oesterreicher, 1984). It has been demonstrated through the application of HADS techniques that these losses in terms of H_{ci} are mostly reversible.

It has been determined (Isnard et al., 1995) that the insertion of hydrogen into the $\text{Nd}_2\text{Fe}_{14}\text{B}$ crystal structure does not effect the lattice symmetry, the space group remains at $P4_2/mnm$. However, the insertion of hydrogen does lead to a significant increase in the unit cell volume. The lattice expansion has been found to be approximately 2.7\AA^3 per hydrogen atom, up to three hydrogen atoms per formula unit. For higher hydrogen contents it is much lower $\approx 2.2\text{\AA}^3$ per hydrogen atom. The lowering of the cell expansion rate denotes a saturation of the interstitial site. It has been shown that hydrogen insertion into the $\text{Nd}_2\text{Fe}_{14}\text{B}$ crystal involves four interstitial sites having Nd_3Fe and Nd_2Fe_2 coordinations.

Four inequivalent interstitial sites have been found to be occupied by H atoms all of which are pseudotetrahedral: H(1) in site 8j (Wyckoff notation) with three Nd atoms and one iron at the corners, this is the most attractive site and fills first, likely due to the Nd-rich environment and its large size. H(2) in site 16k is surrounded by two Nd and two iron, this is next to fill. The filling of the H(2) site corresponds with decreased occupancy of H(1) due to significant modification of the H(1) environment as a result of the two sites sharing an edge. H(3) in site 16k with two iron and two Nd atoms at the corners; in this site larger Fe-H distances are observed producing weaker Fe-H repulsion than on the H(4) site. H(4) in site 4e with two Nd and two iron as closest neighbors, due to its small size occupancy remains low, even at relatively high hydrogen content. (Isnard et al., 1995), (Chaboy et al., 2002), (Ferreira et al., 1985). The crystal structure of $\text{Nd}_2\text{Fe}_{14}\text{B}$ showing the interstitial sites occupied by hydrogen can be seen in Fig. 2.11.

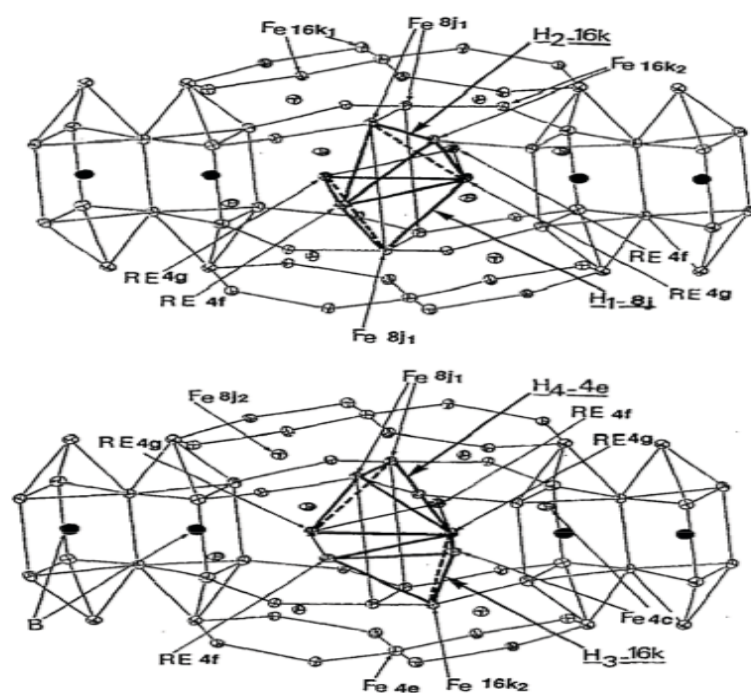


Fig. 2.11 Depicts the crystal structure of $\text{Nd}_2\text{Fe}_{14}\text{B}$ showing the interstitial sites occupied by hydrogen (Isnard et al., 1995).

The inherent stability of the melt spun ribbon is evident when compared to NdFeB powders produced via HD and HDDR methods. MQ particles can be readily exposed to air without any significant reduction in magnetic properties, whereas powders produced via HD and HDDR will oxidise if they are not contained within an inert atmosphere.

The current niche market for the bonded magnets that this study is focused on would see uses in the automotive industry with “under the bonnet” type applications. The under bonnet environment has a detrimental effect upon the life span of NdFeB based magnets due to the elevated temperature coupled with high humidity. For this reason an ideal test to simulate the rigours of the under bonnet environment is the environmental chamber where temperature and relative humidity can be adjusted accordingly. A survey of related literature has shown that tests using the environmental chamber use conditions in the region of 85°C with 80-90% relative humidity (RH) (Yan et al., 1999) (Tokuhara and Hirose, 1991) (Yan et al., 2009).

2.9 Bonding Media

Unlike metal magnets made through the traditional powder metallurgy/sintering route, bonded magnets call for a binder to act as “a glue” to hold the magnetic particles together in the desired shape. Bonding media are required to provide sufficient strength to hold the magnetic component of the bonded magnet together and to maintain the designed shape to specification up to the intended operation temperature, and to sustain that operation temperature without softening deforming or breaking (Guschl and Campbell, 2005).

Apart from providing structural integrity the binder also serves another crucial role in preserving the longevity of the magnetic component. This protection is provided by a barrier between the magnetic particles and the environment in which the bonded

component is operating. If the binder is permeable to water/moisture then the bonded magnet can be thought of as a very low density sintered magnet providing maximum surface area for environmental attack. Studies carried out by workers at Birmingham University into the effect of metal magnet density on corrosion resistance showed that lower density magnets were far more susceptible to corrosion than their higher density counterparts due to increased surface area availability for attack (Yan et al., 1999).

Since the discovery of NdFeB in the early 1980's the problem of poor corrosion resistance has been approached from several different directions:

Some studies have concentrated on investigating the effect of additions to the NdFeB microstructure to stabilise grain boundary phases (El-Moneim et al., 2002) (Yu et al., 2004) (Camp and Kim, 1991). Although these alloying additions usually have a detrimental effect upon the magnetic properties of the material. For use within the bonded magnet sector this method would be of little use as powders are required to be optimised in terms of magnetic properties to compensate for the lower volume fraction of magnetic material in these composites. As previously mentioned bonded magnets can be composed of as little as 80 vol% magnetic material.

Other studies have investigated the use of metallic or polymer coatings (Saliba-Silva et al., 2004) (Mitchell, 1990) (Walton et al., 2000). These methods of protection are primarily aimed at the sintered magnet market again. Which as mentioned before are more suited to magnetic components with higher maximum energy products, as the coating itself will cause a decrease in remanence of the magnet due to the increased volume of non-ferromagnetic material on the surface of the magnet, with magnetic flux decreasing with the square of the distance from the magnet. It has been shown that a Zinc coating of 25 μm

decreased remanence by approximately 8% (Cheng et al., 1997). In commercially available magnets 10-30 μ m layers are most commonly observed on coated NdFeB magnets this would appear to be the compromise which has been reached. This illustrates the trade off between corrosion protection and performance in terms of magnetic properties.

Although coatings are aimed more towards the sintered magnet market the results of these corrosion resistance studies can still be used to give an indication of which materials may have properties that could translate into a useful barrier against corrosion when used as a matrix material.

Within the scope of this study a number of different bonding media were utilised. These will now be introduced:

2.9.1 Epoxy Resin

This is a thermoset polymer with permanent cross links after curing. It is most commonly used for compression molded bonded magnets. The excellent compatibility is mostly attributed to the high polarity of the epoxy and the metal surfaces. However, in practice the wettability and the compatibility can be greatly reduced as a result of the chemical heterogeneity and/or the physical roughness of the metal surfaces. This in turn will result in imperfect couplings which form voids in the bonded magnet (Chen et al., 1999).

The molecule of epoxy resin consists of a hydroxy group, an aether bond, and an epoxy group. This can be seen in Fig. 2.12. These functional groups can join with a close molecule of epoxy resin and a magnetic powder interface. Particularly, the epoxy group can be polymerised into a sizeable molecule of three-dimensional net by the effect of a curing agent, which causes high strength among the bonded magnets (Zhang et al., 2009).

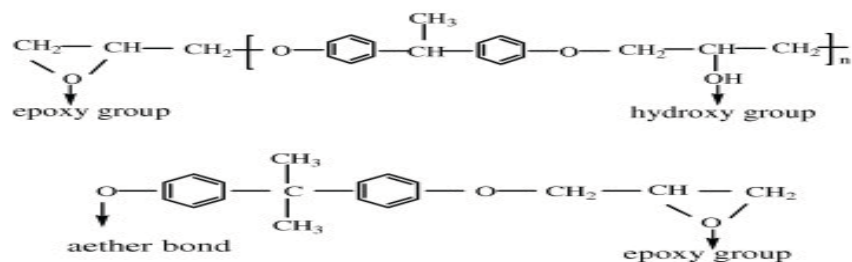


Fig. 2.12 Chemical representation of an epoxy resin molecule structure (Zhang et al., 2009).

An advantage of using epoxy resin as a binder is that the loading, in terms of magnetic material, can be as high as 80 vol%. Manufacturing of bonded magnets via the compression molding route is almost net shape, thus minimizing secondary machining operations.

A study conducted into the corrosion resistance of epoxy coated sintered $\text{Nd}_{15}\text{Fe}_{78}\text{B}_7$ magnets showed that flaking of the epoxy film after a 300 hour humidity test (80°C 90% RH) was not due to the epoxy coating losing adhesion with the $\text{Nd}_2\text{Fe}_{14}\text{B}$ grains at the interface. SEM observations showed that these grains were still attached to the inner side of the epoxy flakes. This suggests that the flaking epoxy coating was in fact caused by intergranular corrosion causing the grains of $\text{Nd}_2\text{Fe}_{14}\text{B}$ to lose contact with the surface of the bulk material (Tokuhara and Hirosawa, 1991). This study clearly demonstrates that epoxy resin as a surface coating does not provide an effective barrier against water to prevent aqueous corrosion in humid environments. From this it can be concluded that if it were to be used as a binder in bonded magnets the same would be true.

2.9.2 Polytetrafluoroethylene (PTFE)

There have been very few studies conducted using PTFE as a binder. Although, it has been found to perform very effectively for MQI type bonded magnets. It was first used as an

additive during rotary forging to enhance the flow of MQP flakes. It was utilised due to its low coefficient of friction. It was through this application that its potential as a binder was first noticed (Tattam et al., 1994).

Researchers at Birmingham University have found that PTFE content can be increased without the loss of any MQP component of the bonded magnet. This happens as the PTFE binder displaces the porosity within the composite. Densities of up to 98% of the theoretical fully dense composite can be achieved. In terms of corrosion resistance any decrease in porosity within the bonded magnet is an attractive prospect. Decreased porosity restricts the movement/diffusion of moisture within the composite via the network of pores, thus reducing the surface area of the magnetic component accessible to moisture. Restricted movement of moisture within the bonded magnets restricts the corrosion process to the unprotected MQP at the surface (Tattam et al., 1996a).

A problem encountered when using PTFE as a binder was the lack of mechanical strength displayed by the polymer. A follow-up study to the above mentioned work (Tattam et al., 1994) found that PTFE bonded magnets subjected to a post-forge heat treatment under a vacuum of 10^{-1} or better at 370°C for 5 minutes displayed an increase in mechanical strength by a factor greater than two. SEM analysis of the fracture surfaces of heat treated and non heat treated samples showed that this heat treatment process caused a layer of PTFE to adhere to the surface of the MQP flakes. This suggests that a form of bonding has taken place between the MQP flake and PTFE during the heat treatment process. It is believed that the substantial increase in mechanical strength can be attributed to this bonding between the PTFE and MQ flakes (Tattam et al., 1996b).

The bonding observed between the PTFE binder and MQP flake at the interface as a result of the heat treatment process not only holds benefits for the mechanical strength of the bonded magnet but also improves the corrosion resistance properties. Due to the intimate bonding at the MQP-PTFE interface there is no way moisture can permeate along the interface as the MQP is completely encompassed by an adherent layer of PTFE. As PTFE is impermeable to water this provides an effective barrier to moisture (Tattam et al., 1996a).

2.9.3 Zinc

Soft metals such as zinc have been the focus of many studies investigating its use as a binder and the effect it had upon magnetic properties, density and corrosion resistance of the bonded magnet. Metal binders were investigated primarily in response to the poor thermal stability of polymer based binders when used in SmCo bonded magnets. SmCo magnets possess a relatively high T_c and thus require a binder that is appropriately matched in terms of thermal tolerances if they are to be used at elevated temperatures.

Soft metal binders have been found to be very useful at preventing flux losses at elevated temperatures over extended periods of time. A study found that a lead/tin solder bonded $\text{Sm}_2\text{Co}_{17}$ magnet produced a nearly identical demagnetisation curve after 3000 hours of aging at 125°C. In contrast the other polymer based binders investigated performed relatively poorly, suffering either a loss of structural integrity or extremely high flux losses in the region of 50% after only 1000 hours (Strnat et al., 1982). The potential of soft metal binders in terms of thermal stability at elevated temperatures was exploited when designing a prototype travelling wave tube utilising SmCo bonded magnets to focus an electron beam in an evacuated tube. These bonded magnets were required to operate at

temperatures in the region of 150°C (Strnat et al., 1987). At these temperatures polymer binders are subject to degradation resulting in loss of structural integrity. Another problem associated with polymer binders is their low thermal conductivity, in contrast metal-matrix bonded magnets have a high thermal conductivity promoting easy heat removal. This is important for applications within electrical machines and microwave tubes (Ji and Chao, 2002).

A problem associated with using zinc as a matrix material for bonded magnets is the degree of porosity incorporated into the composite upon the formation of a “green compact”. Studies have shown that the density of zinc bonded magnets is very low, with “green compacts” only achieving around 80% of the maximum theoretical density (Chin et al., 1995). As previously discussed porosity has a negative effect upon corrosion resistance of bonded magnets and it is desirable to have densities as close to the maximum theoretical density as possible. The low densities achieved through the use of zinc as a binder is due to the high viscosity of the metal, relative to polymer binders such as PTFE, during uniaxial pressing. This restricts the plastic flow of the metal matrix around the magnetic component preventing the displacement of porosity.

It is important to mention that zinc does provide an effective barrier to moisture, as it is impervious to water. In previously conducted corrosion studies involving zinc bonded magnets it has been found that the initial corrosion rate is relatively high, similar to that of bonded magnets utilising PTFE. This has been attributed to the corrosion process acting on the surface of the magnet where there is an abundance of exposed NdFeB particle surfaces. It is worth noting that although this process is limited to the surface of the bonded magnet to begin with, as this process continues to remove Nd₂Fe₁₄B grains from the bulk material

this exposes fresh surfaces vulnerable to attack. It is also possible that through the action of grain/material removal this could provide access to the network of porosity present in the matrix increasing the surface area of particles exposed to moisture.

There are also conflicting reports on the sacrificial nature of zinc in comparison to NdFeB substrates. A white corrosion product on the surface of zinc coated magnets found to be hydrated zinc oxide, suggest that zinc is a sacrificial anode (Ji and Chao, 2002). Although the zinc may be sacrificial compared to Nd₂Fe₁₄B grains it seems unlikely that it will protect the Nd rich grain boundary phase against humid exposure (Walton, 2001).

2.9.4 Bonding Media Summary

In terms of corrosion resistance PTFE bonding in MQI magnets outperformed other more traditionally used binders such as epoxy resin and zinc. In the corrosion resistance studies conducted at Birmingham University the epoxy resin for bonded MQI magnets resisted the onset of corrosion for the longest period. This was attributed to the method by which the epoxy component was applied. The epoxy resin coats each MQP individually, although it is permeable to water, before any corrosive attack can occur the moisture requires time to reach the surface of the MQP, even for particles located at the surface of the bonded magnet. In contrast due to the MQP for the PTFE and zinc bonded magnets only being “mixed” with their respective binders, MQP at the surface of the bonded magnets had no barrier to prevent contact with moisture. For this reason corrosion of PTFE and zinc bonded magnets was fairly rapid from the onset but after all of the available MQP at the surface of the bonded magnet have reacted with moisture from the air the rate of corrosion declines. This rate of decline is more pronounced for PTFE than it is for its zinc bonded counterparts due to the greater degree of porosity present in the zinc bonded magnet.

2.10 Surface Coatings/Treatments

It is apparent from studies conducted into bonding media that even if the ideal binder is utilised with minimal porosity incorporated into the structure upon pressing, magnetic particles exposed to moisture at the surface are still vulnerable to corrosive attack. This in turn provides more 'fresh' surfaces for reactions with moisture. There would appear to be two different routes to combat this problematic surface corrosion. The success of these routes is dependant upon a suitable binder/barrier material being selected for the task.

One route would involve coating or encapsulating each individual particle in a similar method to that of the epoxy resin bonded magnets. It has been observed in work carried out at Birmingham University that the epoxy coating applied to sintered NdFeB magnets delayed the onset of corrosion by 1-2 days during exposure to a humid environment, the onset was only delayed as the epoxy resin is in fact permeable to water (Walton, 2001). The use of epoxy resin was originally intended to decrease the volume fraction of binder within the magnet, so as to reduce the diluting effect on the magnetic properties. The consequence of this was to create a vast interlinked network of porosity. If the same coating method i.e. individual particle encapsulation could be adapted to apply a non-permeable barrier to water corrosion resistance could be dramatically improved.

Studies focussed on encapsulating individual particles to enhance corrosion resistance have been conducted. Some have focused on the application of a thin film to the surface of individual particles via sol-gel processing. Sol-gel processing is a low temperature, wet chemical route for the production of oxide glasses and ceramics. This process involves the hydrolysis and polymerisation/condensation reactions of an appropriate metal alkoxide precursor normally in an alcohol solution. The most common alkoxide precursor is

tetraethylorthosilicate (TEOS). The authors have also used this technique to produce a surface coating to encapsulate an entire polymer bonded magnet (Hodgson et al., 1999).

The application of submicron sol-gel coatings has been found not to significantly affect the magnetic properties of magnetic powders. From the results shown it is claimed that the coating does have a positive effect upon corrosion resistance (Hodgson et al., 1999). Although, this is difficult to quantify as the rate of corrosion has only been measured in terms of mass change during exposure. Had the magnetic properties been monitored a more accurate conclusion could have been drawn regarding corrosion resistance based upon coercivity and remanence measurements. Another important factor to consider when evaluating thin-film coatings such as these is their durability. For example, if individual particles were coated and then pressed into a bonded magnet, how much damage would the coating sustain, and how would this effect the level of protection offered by the coating? Could this problem be overcome by applying a second coating after pressing is complete?

Much of the work investigating the effects of surface coatings on NdFeB magnets have been focussed on the protection of sintered metal magnets. It is of great importance to provide a suitable barrier to protect the surface of these sintered magnets. Although they maybe fully dense there is an interconnected lattice of highly reactive, Nd-rich, grain boundary phase running throughout the bulk material. The high susceptibility of the Nd-rich phase from attack by moisture and the nature of the reaction means any flaws in the coating could lead to the corrosion propagating throughout the bulk material.

2.10.1 Low Pressure Pack Sublimation (LPPS) Zinc Coating

Studies carried out at Birmingham University have focused on zinc surface coatings as a method of protection for NdFeB sintered magnets. Low Pressure Pack Sublimation (LPPS)

is based upon a form a sherardizing where the component to be coated is placed in a rotating chamber at 390°C in a mixture of sand and zinc dust. However, during the LPPS process, a moderate vacuum is applied and the chamber is not rotated (Walton et al., 2000).

Characterisation of the LPPS zinc layers deposited on sintered NdFeB magnets revealed intergranular diffusion of zinc up to a depth of 10µm at 390°C hence the zinc-substrate interface is not well defined. Analysis of the Zn-NdFeB interface showed the intergranular areas to be zinc rich, with fragmentation of the surface grains are attributed to the expansion of grain boundary phases on reaction with zinc (Walton et al., 2000).

LPPS deposition of zinc produced an adherent surface coating which when placed in a corrosive environment, displayed superior performance in terms of weight loss and reduction in magnetic properties compared to those exhibited by the commercially electroplated zinc, nickel and ion vapour deposition (IVD) aluminium magnets. Although the LPPS process produced a small reduction in remenance and coercivity, approximately 10% and 5% respectively by changing the surface conditions of the magnets. When exposed to a corrosive environment LPPS coated magnets developed a white corrosion product which was revealed to be ZnO and showed little change in mass during autoclave testing. The formation of ZnO would suggest that the zinc film is acting at least partially as a sacrificial anode (Walton et al., 2000).

A more recent study conducted into improving corrosion resistance of NdFeB sintered magnets involved a combination of two previously mentioned techniques. A zinc coating was applied via electroplating followed by coating the whole surface with a silane sol. The authors claim that the corrosion resistance properties were excellent although this was only measured by means of electrochemical testing (Yang et al., 2010). It is difficult to translate

results from electrochemical testing into how the component as a whole would perform under a simulated corrosive environment.

2.10.2 Dex-Cool/Ethylene Glycol (EG)

Dex-cool is primarily utilised within the automotive industry as an engine coolant that is resistant to freezing, boiling and also prevents corrosion within the cooling system. The active components are listed in Table. 2.2.

Table 2.2 Components of Dex-cool according to the material safety data sheet (Chevron Texaco Global Lubricants, 2002)

COMPONENTS	CAS NUMBER	AMOUNT
Ethylene Glycol	107-21-1	80 – 96.99 %weight
Diethylene Glycol	111-46-6	1 – 4.99 %weight
Potassium 2-ethylhexanoate	3164-85-0	1 – 4.99 %weight
Water	7732-18-5	1 – 2.99 %weight

Commercial information provided describes the benefits of Dex-cool as:

- Low alkalinity
- Contains no silicates
- Is nitrite-, borate-, phosphate-, nitrate-, amine-free.
- 100% biodegradable in its pure unused condition.
- Longer lasting (It has been shown to remain above 95% of its original concentration after 150,000 miles in automobiles)

From Table 2.2, it can be seen the active compound in Dex-cool is ethylene glycol (EG) and has the chemical formula $(\text{CH}_2\text{OH})_2$. This is used within coolant systems for the effect it has when dissolved in water. When mixed in water at a 1:1 ratio, the melting point of the solution is lowered to $\sim -34^\circ\text{C}$ and the boiling point is increased to $\sim 107^\circ\text{C}$. Ideal for

protecting the radiator from freezing and also well suited to effective heat transfer without the build up of excess pressure through boiling.

EG is described as a polar organic solvent. This type of solvent is characterised by a high dielectric constant, high cohesive energy, and considerable hydrogen bonding abilities. It has one of the lowest ratios among alcohols of weakly polar methylene (or methyl) groups to polar hydroxyl groups, which means that its properties will be strongly influenced by hydrogen-bonding interactions (Zhang et al., 2008). The effect of mixing Ethylene Glycol with water on the physical properties of the solution can be explained by the presence of the O-H groups at either end of the carbon chain and their interaction with hydrogen atoms from water. These O-H groups participate in hydrogen bonding within the network of H₂O, because of this EG can be said to demonstrate hydrophilic tendencies. The dipole-dipole forces between O-H groups in EG and H from H₂O facilitate hydrogen bonding (Kao et al., 2005). Both inter- and intramolecular hydrogen bonds are formed in ethylene glycol, although they are not as strong as those formed in water. (Javadian et al., 2010).

Within the EG molecule is one pair of O-H groups, these are responsible for hydrogen bonding. Each O-H group consists of a hydrogen (H) atom covalently bonded to an oxygen (O) atom. The oxygen atom possesses a stronger electro-negativity, hence it will attract the electron cloud of the hydrogen nucleus and, by decentralising the cloud, leaves the hydrogen atom with a partial positive charge. Hence the O-H^+ group could be described as polarised. Due to the small size of hydrogen relative to the other atoms, the resulting charge, though only partial, represents a large charge density. A hydrogen bond occurs when this strong positive charge density attracts a lone pair of electrons from another atom, this atom becomes the hydrogen bond acceptor (Kao et al., 2005). One molecule of EG

contains two hydrogen bond donor sites and four hydrogen bond acceptor sites (Rodnikova et al., 2006).

The hydrogen bonding that occurs between EG and water is thought to involve both; oxygen atoms from water and hydrogen atoms of the O-H group in EG, and, hydrogen atoms from water and oxygen atoms of the O-H group in EG. This may form the structure $R'CH_2OH \cdots OH(H) \cdots$ (Where R' represents $-CH_2OH$) (Zhang et al., 2008). The structure of EG and the hydrogen bonding with water molecules can be seen in Fig. 2.13.

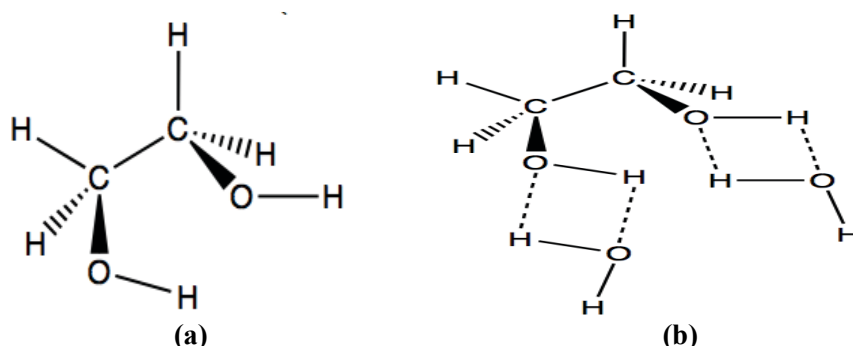


Fig. 2.13 (a) Shows the 3D structure of Ethylene Glycol (EG) (b) Shows the 3D structure of Ethylene Glycol and Hydrogen Bonds formed with water (depicted by - - - - -).

A factor which may affect the ability of EG to inhibit corrosion within the scope of this study is the degradation due to thermal oxidation over a period of time. This process can lead to the formation of organic acids which would decrease the PH of the solution, this could accelerate the corrosion process of metallic components within the system. The major acidic degradation products from the thermal oxidation of EG have been identified as oxalic, glycolic and formic acids. The thermal oxidative degradation of glycols is a complex process involving a free radical mechanism. The three major steps involve radical initiation, propagation and termination. The thermal oxidation reaction is dependant upon temperature and availability of oxygen (Rossiter Jr et al., 1985).

It does not appear that any research has been conducted into the use of EG to enhance corrosion resistance in NdFeB based magnets as a surface treatment or an environmental modification. A limited amount of published research has been carried out into the effects of EG on the corrosion rates of aluminium (Wong et al., 1979) and magnesium engine blocks (Song and StJohn, 2004) with a view to use ethylene glycol within the automotive industry as an engine coolant. Interestingly (Song and StJohn, 2004) found that adsorption of ethylene glycol occurs at the surface of magnesium. This competitive adsorption between ethylene glycol and contaminants contained within water (NaCl, NaHCO₃, Na₂SO₄) results in differences in corrosivity of the ethylene glycol solutions.

A recent unpublished study conducted at Birmingham University investigated the use of EG as a surface treatment with a view to prevent hydrogen absorption by NdFeB MQP. This did show some promise although this work is yet to be published pending further investigations into “hydrogen blocking” mechanisms. This work is best discussed in the results and discussions section with the support of relevant data in the context of corrosion. This along with any mechanisms responsible for the enhancement of corrosion prevention will be discussed and related to experimental evidence gathered.

References:

- BENZ, M. G. & MARTIN, D. L. 1970. Cobalt-samarium permanent magnets prepared by liquid phase sintering. *Applied Physics Letters*, 17, 176-177.
- BUSCHOW, K. H. J. 1976. Hydrogen absorption and its effect on the magnetic properties of rare-earth iron intermetallics. *Solid State Communications*, 19, 421-423.
- BUSCHOW, K. H. J. 1986b. New permanent magnet materials. *Materials Science Reports*, 1, 1-63.
- CADOGAN, J. M. & COEY, J. M. D. 1986. Hydrogen absorption and desorption in $\text{Nd}_2\text{Fe}_{14}\text{B}$. *Applied Physics Letters*, 48, 442-444.
- CAMP, F. E. & KIM, A. S. 1991. Effect of microstructure on the corrosion behavior of NdFeB and NdFeCoAlB magnets. *Journal of Applied Physics*, 70, 6348-6350.
- CHABOY, J., UACUTE & PIQUER, C. 2002. Modification of the magnetic properties of the $\text{R}_2\text{Fe}_{14}\text{B}$ series (R=rare earth) driven by hydrogen absorption. *Physical Review B*, 66, 104433.
- CHEN, Q., ASUNCION, J., LANDI, J. & MA, B. M. 1999. The effect of the coupling agent on the packing density and corrosion behavior of NdFeB and SmCo bonded magnets. *Journal of Applied Physics*, 85, 5684-5686.
- CHENG, C. W., MAN, H. C. & CHENG, F. T. 1997. Magnetic and corrosion characteristics of Nd-Fe-B magnet with various surface coatings. *Magnetics, IEEE Transactions on*, 33, 3910-3912.
- CHEVRON TEXACO GLOBAL LUBRICANTS. 2002. *Dex-Cool Material Safety Data Sheet* [Online]. San Ramon, CA: Chevron Texaco Global Lubricants. Available: www.havoline.com [Accessed 25/11/2010 2010].
- CHIN, T. S., CHENG, K. H. & YAO, J. M. 1995. Magnetic properties of $(\text{LR}_x\text{Sm}_{1-x})_2(\text{FeCo})_{17}\text{N}_2 - \text{6 Zn}$ bonded magnets ($\text{LR} \equiv \text{La, Ce}$). *Journal of Alloys and Compounds*, 222, 148-152.
- CROAT, J. J. Year. Current status and future outlook for bonded neodymium permanent magnets (invited). *In*, 1997 Atlanta, Georgia (USA). AIP, 4804-4809.
- CROAT, J. J., HERBST, J. F., LEE, R. W. & PINKERTON, F. E. 1984a. High-energy product Nd-Fe-B permanent magnets. *Applied Physics Letters*, 44, 148-149.
- DOSER, M., PANCHANATHAN, V. & MISHRA, R. K. Year. Pulverizing anisotropic rapidly solidified Nd-Fe-B materials for bonded magnets. *In*, 1991 Pittsburgh, Pennsylvania (USA). AIP, 6603-6605.

- EL-MONEIM, A. A., GEBERT, A., UHLEMANN, M., GUTFLEISCH, O. & SCHULTZ, L. 2002. The influence of Co and Ga additions on the corrosion behavior of nanocrystalline NdFeB magnets. *Corrosion Science*, 44, 1857-1874.
- EVANS, J., KING, C. E. & HARRIS, I. R. 1985. The hydrogenation behaviour of the phases $\text{Sm}_2\text{Co}_{17}$ and $\text{Pr}_2\text{Co}_{17}$. *Journal of Materials Science*, 20, 817-820.
- FERREIRA, L. P., GUILLEN, R., VULLIET, P., YAOUANC, A., FRUCHART, D., WOLFERS, P., L'HERITIER, P. & FRUCHART, R. 1985. Magnetization, ^{57}Fe and ^{161}Dy Mössbauer study of $\text{Dy}_2\text{Fe}_{14}\text{B}_x$ with $0 \leq x \leq 4.7$. *Journal of Magnetism and Magnetic Materials*, 53, 145-152.
- FIDLER, J. 2004. Recent developments in hard magnetic bulk materials. *Journal of Physics: Condensed Matter*, 16, S455.
- GRUNBERGER, W., HINZ, D., KIRCHNER, A., MÜLLER, K. H. & SCHULTZ, L. 1997. Hot deformation of nanocrystalline Nd-Fe-B alloys. *Journal of Alloys and Compounds*, 257, 293-301.
- GUSCHL, P. C. & CAMPBELL, P. 2005. Rare-Earth Fe-B powder coating for improvements in corrosion resistance, flux aging loss, and mechanical strength of bonded magnets. *Magnetics, IEEE Transactions on*, 41, 3859-3861.
- GUTFLEISCH, O. & HARRIS, I. R. 1996. Fundamental and practical aspects of the hydrogenation, disproportionation, desorption and recombination process. *Journal of Physics D: Applied Physics*, 29, 2255.
- GUTFLEISCH, O., KUBIS, M., HANDSTEIN, A., MÜLLER, K. H. & SCHULTZ, L. 1998. Hydrogenation disproportionation desorption recombination in Sm-Co alloys by means of reactive milling. *Applied Physics Letters*, 73, 3001-3003.
- HANDSTEIN, A., KUBIS, M., GUTFLEISCH, O., GEBEL, B. & MÜLLER, K. H. 1999. HDDR of Sm-Co alloys using high hydrogen pressures. *Journal of Magnetism and Magnetic Materials*, 192, 73-76.
- HARRIS, I. R. 1987. The potential of hydrogen in permanent magnet production. *Journal of the Less Common Metals*, 131, 245-262.
- HARRIS, I. R. 1990. Hard magnets. *Materials Science and Technology*, 6, 962-966.
- HARRIS, I. R., EVANS, J. & NYHOLM, P. S. 1979. U.K. Patent 1554384. U.K. patent application 1554384.
- HARRIS, I. R. & MCGUINNESS, P. J. 1991. Hydrogen: its use in the processing of NdFeB-type magnets. *Journal of the Less Common Metals*, 172-174, 1273-1284.
- HARRIS, I. R., MCGUINNESS, P. J., JONES, D. G. R. & ABELL, J. S. 1987. Nd-Fe-B Permanent Magnets: Hydrogen Absorption/Desorption Studies (HADS) on $\text{Nd}_{16}\text{Fe}_{76}\text{B}_8$ and $\text{Nd}_2\text{Fe}_{14}\text{B}$. *Physica Scripta*, 1987, 435.

- HATACHI METALS LTD. 2008. *NEOMAX Magnet* [Online]. Tokyo. Available: <https://www.hitachi-metals.co.jp/e/eh2009/data/NEOMAXCatalog2.pdf> [Accessed 25/11/2010 2010].
- HERBST, J. F. 1991. $R_2Fe_{14}B$ materials: Intrinsic properties and technological aspects. *Reviews of Modern Physics*, 63, 819.
- HERBST, J. F. & CROAT, J. J. 1991. Neodymium-iron-boron permanent magnets. *Journal of Magnetism and Magnetic Materials*, 100, 57-78.
- HODGSON, S. N. B., HOGGARTH, C. G., DAVIES, H. A. & BUCKLEY, R. A. 1999. Protection of NdFeB magnets by ultra-thin sol-gel derived films. *Journal of Materials Processing Technology*, 92-93, 518-524.
- HUBBARD, W. M., ADAMS, E. & GILFRICH, J. V. 1960. Magnetic Moments of Alloys of Gadolinium with Some of the Transition Elements. *Journal of Applied Physics*, 31, S368-S369.
- ISNARD, O., YELON, W. B., MIRAGLIA, S. & FRUCHART, D. 1995. Neutron-diffraction study of the insertion scheme of hydrogen in $Nd_2Fe_{14}B$. *Journal of Applied Physics*, 78, 1892-1898.
- JAVADIAN, S., GHARIBI, H. & FALLAH, H. T. 2010. Adsorption and Micellar Properties of Binary Ionic/Nonionic Surfactant Mixtures in Ethylene Glycol + Water. *Journal of Chemical & Engineering Data*, 55, 1122-1130.
- JI, J.-F. & CHAO, C. 2002. A novel technique for manufacturing metal-bonded Nd-Fe-B magnets by squeeze casting. *Metallurgical and Materials Transactions A*, 33, 637-646.
- KAO, M. J., TIEN, D. C., JWO, C. S. & AND TSUNG, T. T. 2005. The study of hydrophilic characteristics of ethylene glycol. *Journal of Physics: Conference Series*, 13, 442.
- KIANVASH, A. & HARRIS, I. R. 1985. Hydrogen decrepitation as a method of powder preparation of a 2:17-type, $Sm(Co, Cu, Fe, Zr)_{8.92}$ magnetic alloy. *Journal of Materials Science*, 20, 682-688.
- KIM, A. S., CAMP, F. E. & LIZZI, T. 1996. Hydrogen induced corrosion mechanism in NdFeB magnets. *Journal of Applied Physics*, 79, 4840-4842.
- KIRCHMAYR, H. R. 1996. Permanent magnets and hard magnetic materials. *Journal of Physics D: Applied Physics*, 29, 2763.
- LEE, R. W. 1985. Hot-pressed neodymium-iron-boron magnets. *Applied Physics Letters*, 46, 790-791.
- LI, J., LIU, Y., GAO, S. J., LI, M., WANG, Y. Q. & TU, M. J. 2006. Effect of process on the magnetic properties of bonded NdFeB magnet. *Journal of Magnetism and Magnetic Materials*, 299, 195-204.

- LI, L. & GRAHAM, C. D., JR. 1992. The origin of crystallographic texture produced during hot deformation in rapidly-quenched NdFeB permanent magnets. *Magnetism, IEEE Transactions on*, 28, 2130-2132.
- MA, B. M., HERCHENROEDER, J. W., SMITH, B., SUDA, M., BROWN, D. N. & CHEN, Z. 2002. Recent development in bonded NdFeB magnets. *Journal of Magnetism and Magnetic Materials*, 239, 418-423.
- MAGNEQUENCH INC. 2009f. *MQP Isotropic Powder Properties* [Online]. Ontario, Canada: Neomaterial Technologies Ltd., Available: http://www.magnequench.com/assets/download/MQP_Isotropic_Chart_v2.6.pdf [Accessed 25/11/2010 2010].
- MAGNEQUENCH INC. 2009g. *MQP Powder Properties Chart* [Online]. Ontario, Canada: Neomaterial Technologies Ltd. Available: http://www.magnequench.com/assets/download/Powder_Properties_Chart_30Jan09.pdf [Accessed 25/11/2010 2010].
- MATSUURA, Y. 2006. Recent development of Nd-Fe-B sintered magnets and their applications. *Journal of Magnetism and Magnetic Materials*, 303, 344-347.
- MCGUINESS, P., HARRIS, I., ROZENDAAL, E., ORMEROD, J. & WARD, M. 1986. The production of a Nd-Fe-B permanent magnet by a hydrogen decrepitation/attritor milling route. *Journal of Materials Science*, 21, 4107-4110.
- MCGUINESS, P. J., FITZPATRICK, L., YARTYS, V. A. & HARRIS, I. R. 1994. Anisotropic hydrogen decrepitation and corrosion behaviour in NdFeB magnets. *Journal of Alloys and Compounds*, 206, L7-L10.
- MCGUINESS, P. J., ZHANG, X. J., YIN, X. J. & HARRIS, I. R. 1990a. Hydrogenation, disproportionation and desorption (HDD): An effective processing route for Nd-Fe-B-type magnets. *Journal of the Less Common Metals*, 158, 359-365.
- MEISNER, G. P. & PANCHANATHAN, V. Year. Hydrogen decrepitated anisotropic Nd-Fe-B powder: Hydrogen desorption and magnetic properties. In, 1993 Houston, Texas (USA). AIP, 6482-6484.
- MISHRA, R. K. 1987. Microstructure of hot-pressed and die-upset NdFeB magnets. *Journal of Applied Physics*, 62, 967-971.
- MITCHELL, P. 1990. Corrosion protection of NdFeB magnets. *Magnetism, IEEE Transactions on*, 26, 1933-1935.
- MULFORD, R. N. R. & HOLLEY, C. E. 1955. Pressure-Temperature-Composition of Rare Earth-Hydrogen Systems. *The Journal of Physical Chemistry*, 59, 1222-1226.
- NAKAYAMA, R. & TAKESHITA, T. 1993. Nd-Fe-B anisotropic magnet powders produced by the HDDR process. *Journal of Alloys and Compounds*, 193, 259-261.

- NAKAYAMA, R., TAKESHITA, T., ITAKURA, M., KUWANO, N. & OKI, K. 1991. Magnetic properties and microstructures of the Nd-Fe-B magnet powder produced by hydrogen treatment. *Journal of Applied Physics*, 70, 3770-3774.
- NASSAU, K., CHERRY, L. V. & WALLACE, W. E. 1960. Intermetallic compounds between lanthanons and transition metals of the first long period: I-Preparation, existence and structural studies. *Journal of Physics and Chemistry of Solids*, 16, 123-130.
- NESBITT, E. A., WILLIAMS, H. J., WERNICK, J. H. & SHERWOOD, R. C. 1962. Magnetic Moments of Intermetallic Compounds of Transition and Rare-Earth Elements. *Journal of Applied Physics*, 33, 1674-1678.
- NOZAWA, Y., IWASAKI, K., TANIGAWA, S., TOKUNAGA, M. & HARADA, H. 1988. Nd-Fe-B die-upset and anisotropic bonded magnets (invited). *Journal of Applied Physics*, 64, 5285-5289.
- OESTERREICHER, K. & OESTERREICHER, H. 1984. Structure and Magnetic Properties of $\text{Nd}_2\text{Fe}_{14}\text{BH}_{2.7}$. *physica status solidi (a)*, 85, K61-K64.
- ORMEROD, J. 1985. The physical metallurgy and processing of sintered rare earth permanent magnets. *Journal of the Less Common Metals*, 111, 49-69.
- ORMEROD, J. & CONSTANTINIDES, S. Year. Bonded permanent magnets: Current status and future opportunities (invited). In, 1997b Atlanta, Georgia (USA). AIP, 4816-4820.
- OSTERTAG, W. & STRNAT, K. J. 1966. Rare Earth-Cobalt Compounds with the A_2B_{17} Structure. *Acta Crystallographica*, 21, 560-565.
- PANCHANATHAN, V. 1995. Magnequench magnets status overview. *Journal of Materials Engineering and Performance*, 4, 423-429.
- RAGG, O. M., KEEGAN, G., NAGEL, H. & HARRIS, I. R. 1997. The HD and HDDR processes in the production of Nd-Fe-B permanent magnets. *International Journal of Hydrogen Energy*, 22, 333-342.
- RODNIKOVA, M., CHUMAEVSKII, N., TROITSKII, V. & KAYUMOVA, D. 2006. Structure of liquid ethylene glycol. *Russian Journal of Physical Chemistry A, Focus on Chemistry*, 80, 826-830.
- ROSSITER JR, W. J., GODETTE, M., BROWN, P. W. & GALUK, K. G. 1985. An investigation of the degradation of aqueous ethylene glycol and propylene glycol solutions using ion chromatography. *Solar Energy Materials*, 11, 455-467.
- SAGAWA, M., FUJIMURA, S., TOGAWA, N., YAMAMOTO, H. & MATSUURA, Y. 1984a. New Material for Permanent-Magnets on a Base of Nd and Fe. *Journal of Applied Physics*, 55, 2083-2087.

- SAGAWA, M., FUJIMURA, S., YAMAMOTO, H., MATSUURA, Y. & HIRAGA, K. 1984b. Permanent-Magnet Materials Based on the Rare Earth-Iron-Boron Tetragonal Compounds. *Ieee Transactions on Magnetism*, 20, 1584-1589.
- SALIBA-SILVA, A., FARIA, R. N., BAKER, M. A. & COSTA, I. 2004. Improving the corrosion resistance of NdFeB magnets: an electrochemical and surface analytical study. *Surface and Coatings Technology*, 185, 321-328.
- SONG, G. & STJOHN, D. 2004. Corrosion behaviour of magnesium in ethylene glycol. *Corrosion Science*, 46, 1381-1399.
- STRNAT, K. 1970. The recent development of permanent magnet materials containing rare earth metals. *Magnetism, IEEE Transactions on*, 6, 182-190.
- STRNAT, K., HOFFER, G., OSTERTAG, W. & OLSON, J. C. 1966. Ferrimagnetism of the Rare-Earth-Cobalt Intermetallic Compounds R_2Co_{17} . *Journal of Applied Physics*, 37, 1252-1253.
- STRNAT, K. J. 1978. Rare-earth magnets in present production and development. *Journal of Magnetism and Magnetic Materials*, 7, 351-360.
- STRNAT, K. J. & HOFFER, G. I. 1966. YCo_5 A Promising New Permanent Magnet Material. *National Technical Information Service, Springfield, VA 221161*.
- STRNAT, K. J. & STRNAT, R. M. W. 1991. Rare earth-cobalt permanent magnets. *Journal of Magnetism and Magnetic Materials*, 100, 38-56.
- STRNAT, R. M. W., CLARKE, J. P., LEUPOLD, H. A. & TAUBER, A. 1987. Metal-matrix magnets for new TWT applications. *Journal of Applied Physics*, 61, 3463-3465.
- STRNAT, R. M. W., LIU, S. & STRNAT, K. J. 1982. Thermal stability and temperature coefficients of four rare-earth-cobalt matrix magnets heated in dry air. *Journal of Applied Physics*, 53, 2380-2382.
- TAKESHITA, T. 1995. Some applications of hydrogenation-decomposition-desorption-recombination (HDDR) and hydrogen-decrepitation (HD) in metals processing. *Journal of Alloys and Compounds*, 231, 51-59.
- TAKESHITA, T. A. N., R. 1989. Proc. 10th Int. Workshop on Rare-Earth Magnets and their Application, Kyoto.
- TATTAM, C., WILLIAMS, A. J., HAY, J. N., HARRIS, I. R., TEDSTONE, S. F. & ASHRAF, M. M. 1994. The use of polytetrafluoroethylene in the production of high-density bonded Nd-Fe-B magnets. *Journal of Applied Physics*, 76, 6831-6833.
- TATTAM, C., WILLIAMS, A. J., HAY, J. N., HARRIS, I. R., TEDSTONE, S. F. & ASHRAF, M. M. 1996a. The corrosion behaviour of uncoated bonded Nd-Fe-B magnets in humid environments. *Journal of Magnetism and Magnetic Materials*, 152, L275-L278.

- TATTAM, C., WILLIAMS, A. J., HAY, J. N., HARRIS, I. R., TEDSTONE, S. F. & ASHRAF, M. M. 1996b. Improvement in the mechanical properties of PTFE bonded Nd-Fe-B magnets by heat treatment. *Journal of Magnetism and Magnetic Materials*, 154, 328-332.
- THOMPSON, P., GUTFLEISCH, O., CHAPMAN, J. N. & HARRIS, I. R. 1999. A comparison of the micromagnetic and microstructural properties of four NdFeB-type materials processed by the HDDR route. *Journal of Magnetism and Magnetic Materials*, 202, 53-61.
- TOKUHARA, K. & HIROSAWA, S. 1991. Corrosion resistance of Nd-Fe-B sintered magnets. *Journal of Applied Physics*, 69, 5521-5523.
- TOKUNAGA, M., NOZAWA, Y., IWASAKI, K., TANIGAWA, S. & HARADA, H. 1989. Magnetic properties of isotropic and anisotropic Nd-Fe-B bonded magnets. *Journal of Magnetism and Magnetic Materials*, 80, 80-87.
- VAN VUCHT, J. H. N., KUIJPERS, F. A. & BRUNING, H. C. A. M. 1970. Reversible Room-Temperature Absorption Of Large Quantities Of Hydrogen By Intermetallic Compounds. *Philips Research Reports*, 25, 133 - 140.
- WALTON, A. 2001. *Low Pressure Pack Sublimation (LPPS): A Zinc Coating Process for NdFeB Magnets*. Doctor of Philosophy PhD Thesis, University of Birmingham.
- WALTON, A., SPEIGHT, J. D., WILLIAMS, A. J. & HARRIS, I. R. 2000. A zinc coating method for Nd-Fe-B magnets. *Journal of Alloys and Compounds*, 306, 253-261.
- WILLIAMS, A. J. 1993. Materials Science and Engineering PhD, University Of Birmingham.
- WILLIAMS, A. J. 1994. *Hydrogen absorption and desorption studies on NdFeB type alloys used for the production of permanent magnets*. Materials Science and Engineering PhD, University Of Birmingham.
- WILLIAMS, A. J., MCGUINNESS, P. J. & HARRIS, I. R. 1991. Mass spectrometer hydrogen desorption studies on some hydrided NdFeB-type alloys. *Journal of the Less Common Metals*, 171, 149-155.
- WILLMAN, C. J. & NARASIMHAN, K. S. V. L. 1987. Corrosion characteristics of RE-Fe-B permanent magnets. *Journal of Applied Physics*, 61, 3766-3768.
- WONG, D., SWETTE, L. & COCKS, F. H. 1979. Aluminum Corrosion in Uninhibited Ethylene Glycol-Water Solutions. *Journal of The Electrochemical Society*, 126, 11-15.
- YAN, G., MCGUINNESS, P. J., FARR, J. P. G. & HARRIS, I. R. 2009. Environmental degradation of NdFeB magnets. *Journal of Alloys and Compounds*, 478, 188-192.

- YAN, G., WILLIAMS, A. J., FARR, J. P. G. & HARRIS, I. R. 1999. The effect of density on the corrosion of NdFeB magnets. *Journal of Alloys and Compounds*, 292, 266-274.
- YANG, X., LI, Q., ZHANG, S., LIU, F., WANG, S. & ZHANG, H. 2010. Microstructure characteristic and excellent corrosion protection properties of sealed Zn-TiO₂ composite coating for sintered NdFeB magnet. *Journal of Alloys and Compounds*, 495, 189-195.
- YU, L. Q., WEN, Y. H. & YAN, M. 2004. Effects of Dy and Nb on the magnetic properties and corrosion resistance of sintered NdFeB. *Journal of Magnetism and Magnetic Materials*, 283, 353-356.
- ZAKOTNIK, M., PROSPERI, D. & WILLIAMS, A. J. 2009. Kinetic studies of hydrogen desorption in SmCo 2/17-type sintered magnets. *Thermochimica Acta*, 486, 41-45.
- ZAKOTNIK, M., WILLIAMS, A. J., MARTINEK, G. & HARRIS, I. R. 2008. Hydrogen decrepitation of a 2/17 sintered magnet at room temperature. *Journal of Alloys and Compounds*, 450, L1-L3.
- ZHANG, J., ZHANG, P., MA, K., HAN, F., CHEN, G. & WEI, X. 2008. Hydrogen bonding interactions between ethylene glycol and water: density, excess molar volume, and spectral study. *Science in China Series B: Chemistry*, 51, 420-426.
- ZHANG, X. H., XIONG, W. H., LI, Y. F. & SONG, N. 2009. Effect of process on the magnetic and mechanical properties of Nd-Fe-B bonded magnets. *Materials & Design*, 30, 1386-1390.
- ZHANG, X. J., MCGUINNESS, P. J. & HARRIS, I. R. 1991. The production of high coercivity cast magnets using the HDD process. *Journal of Applied Physics*, 69, 5838-5840.
- ZIJLSTRA, H. 1978. Trends in permanent magnet material development. *Magnetics, IEEE Transactions on*, 14, 661-664.
- ZIJLSTRA, H. & WESTENDORP, F. F. 1969. Influence of hydrogen on the magnetic properties of SmCo₅. *Solid State Communications*, 7, 857-859.

Chapter 3: Experimental Techniques

The following chapter will describe the materials used within the scope of this study, sample preparation methodology, simulated environmental testing conditions, hydrogen adsorption/desorption studies (HADS) and materials characterisation techniques.

3.1 Magnetic Materials Employed

NdFeB MQP isotropic melt spun ribbon grade B (Batch – 10184-070) was supplied by Magnequench. The material is an Nd-Fe-Co-B based alloy with the approximate composition of $\text{Nd}_{12.3}\text{Fe}_{65.1}\text{Co}_{16.6}\text{B}_6$. The particles are in the form of flakes approximately 1mm in length and 50 μm thick with sub micron grains ($\sim 50\text{nm}$). The material properties for a range of grades according to the data sheet supplied by Magnequench can be seen in Table 3.1:

Table 3.1 Properties of various grades of MQP isotropic powder supplied by Magnequench (Magnequench Inc, 2009a), (Magnequench Inc, 2009b), (Magnequench Inc, 2009c), (Magnequench Inc, 2009d), (Magnequench Inc, 2009e).

Magnetic Characteristics	MQP-A	MQP-B	MQP-B+	MQP-C	MQP-14-12
Residual Induction, B_r (mT)	780-820	860-895	895-915	780-820	820-850
Energy Product $(BH)_{\max}$ (kJ/m ³)	97-111	111-126	126-134	99-111	107-120
Intrinsic Coercivity, H_{ci} (kA/m)	1030-1350	640-800	716-836	1230-1474	940-1050
Coercive Force, H_c (kA/m)	515	500	540	520	550
Magnetising Field to >95% Saturation (min), H_s (kA/m)	≥2000	≥1600	≥1600	≥2000	≥1600
Temperature Coefficient of B_r , α , to 100°C (%/°C)	-0.12	-0.11	-0.11	-0.07	-0.13
Temperature Coefficient of H_{ci} , β , to 100°C (%/°C)	-0.4	-0.4	-0.4	-0.4	-0.4
Curie Temperature, T_c (°C)	305	360	360	470	305
Maximum Operating Temperature (°C)	120-160	120-160	120-160	120-160	140-180
Maximum Process Temperature (°C)	200	200	200	200	250

From Table 3.1 it can be seen that there are differences in various properties between the various grades of MQP. The properties of powders are easily tailored to particular applications via small additions such as cobalt and or variations in processing conditions (i.e. temperature and duration of the post rapid solidification heat treatment and wheel velocity) which alter the microstructure of the alloy (Pollard et al., 1988).

MQP-A is based on the Nd-Fe-B alloy and was the first powder grade commercialised by Magnequench. Typically, it is used for applications requiring high coercivity where costs are also an important factor (Magnequench Inc, 2009a).

MQP-B powder is a general all purpose grade which is used when there are no specific environmental requirements placed upon the component e.g. elevated temperature uses (Magnequench Inc, 2009b).

MQP-B+ is the highest performing grade of powder based upon the Nd-Fe-Co-B alloy. Due to its high coercivity and $(BH)_{\max}$, this grade lends itself to automotive applications (Magnequench Inc, 2009c).

MQP-C was produced to meet the needs of components requiring both flux and demagnetisation protection for elevated temperature applications. It is based on the Nd-Fe-Co-B alloy and boasts a high curie temperature and high coercivity (Magnequench Inc, 2009d).

MQP-14-12 is designed specifically for high magnetic flux and high temperature applications, such as under the hood automotive motors and sensors (Magnequench Inc, 2009e). It is based upon a patented Nd-Fe-Nb-B alloy (Ref for patent put all in?)

This study required a powder that had not been engineered specifically to resist the effects of elevated temperatures or exposure to moisture so that the properties of the binder/coating would be more critical to performance. The resultant effects from exposure to various environments would not be masked through powder design. For this reason MQP-B was chosen and it is the most common grade used.

The second quadrant demagnetisation curve of the MQP-B in powder form can be seen in Fig. 3.1 illustrating magnetic performance of the powder at various temperatures. The second quadrant demagnetisation curve of a bonded magnet produced with the MQP-B powder can be seen in Fig. 3.2.

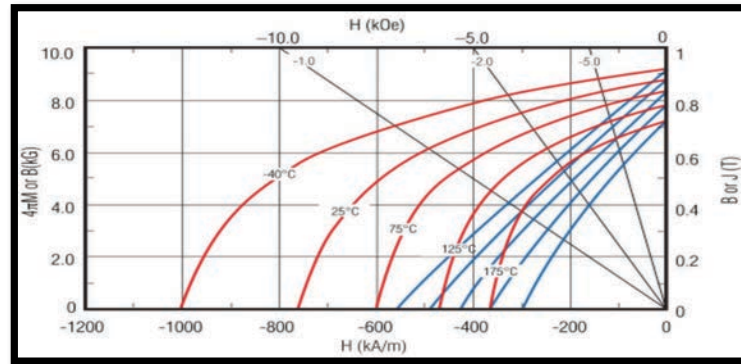


Fig 3.1 The second quadrant demagnetisation curve of MQP-B powder at various temperatures (Magnequench Inc, 2009b).

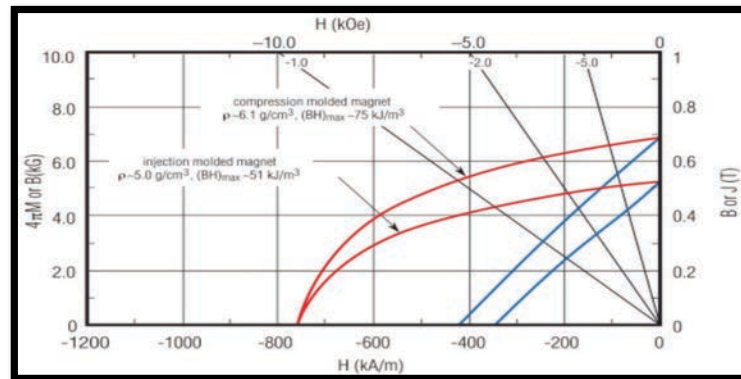


Fig 3.2 The second quadrant demagnetisation curve of a bonded magnet produced using MQP-B powder at 25°C (Magnequench Inc, 2009b).

This material was used in two different configurations during the study:

- In the form of a bonded magnet.
- In the ‘as received’ loose powder form.

Both forms employed within the scope of this study will be discussed in greater detail in the sample preparation section of this chapter.

3.2 Bonding Media And Processing Techniques

3.2.1 Epoxy Resin (Polyepoxide)

Epoxy resin coated MQP-B powder was supplied by Magnet Applications. The application of this epoxy resin coating is a multiphase process. The epoxy resin consists of two parts, Part A and Part B, both of which are white crystalline powders. Part A is the thermosetting polymer, Part B is the catalysing agent or “hardener” which is added to facilitate the polymerisation and formation of crosslinks upon “curing”. The two parts are mixed in a ratio of 10:1 (Part A:Part B) and dissolved in acetone. The magnetic powder to be coated, in this case MQP-B, is added to this solution and the mixture is agitated in a large Z blade mixer, to ensure even coating. As the mixture is agitated the acetone evaporates leaving a thin uniform epoxy coating on the surface of the magnetic powder. This process is known as the liquid coating technique. The application of the epoxy coating ensures each individual powder particle is encapsulated. This method of blending allows relatively low volume fractions of binding agent to be used, thus avoiding unnecessary dilution of magnetic properties. Although the use of a low volume fraction of bonding media has its advantages in terms of magnetic properties, it does however lead to the incorporation of a large network of porosity into the composite.

The epoxy resin liquefies under the pressures generated during uniaxial pressing and thus has a very low viscosity and excellent flow properties. It is cured at temperatures in the region of 100°C – 120°C for approximately 1 hour (Tattam, 1996). During this time the low molecular weight resins are converted into 3D crosslinked polymers. The epoxy resin produces fairly robust bonded magnets. Some typical properties of epoxy resin compounds can be seen in Table 3.2

Table 3.2 Properties of Epoxy resin compounds (Tattam, 1996)

Property	
Density (g/cm ³)	1.8
Tensile Strength (Nm ⁻²)	40
Service Temperature (°C)	
Short Term	180
Long Term	130
Volume Resistivity (Ωcm)	10 ¹⁴
Water Absorption (mg/cm ³ /day)	7.5
Fully Saturated (% weight gain)	7 – 8.5

3.2.1.1 Step-By-Step Production Method

- 1) The required mass of epoxy coated NdFeB powder was weighed.
- 2) The epoxy coated NdFeB was loaded into the die cavity and the punches inserted.
- 3) The die was located between the hydraulic rams of a manual 30 Ton press.
- 4) The pressure between the rams was increased to approximately 3 Ton/cm².
- 5) The epoxy bonded NdFeB magnet was ejected from the die.
- 6) The epoxy bonded magnet was then cured in an oven using the following heat treatment 120°C → 60 minute dwell.

3.2.2 PTFE (Polytetrafluoroethylene)

PTFE grade G163 is around 94% crystalline with a mean particle size of 25µm according to the manufacturer data, it was supplied by ICI Fluoropolymers. PTFE is unique in that it has an unusually high glass transition temperature (T_g), approximately 340°C. It also displays good flow properties during uniaxial pressing which is attributed to its low coefficient of friction (<0.01) especially under high loads. It has demonstrated good stability and is unreactive with most materials (Asahi Glass Co Ltd, 1996). These

properties coupled with a good resistance to chemicals and useful mechanical properties make PTFE an attractive bonding medium.

The method best suited to production of bonded magnets utilising PTFE is very similar to that of powder metallurgy routes for sintered magnets i.e. compacting and sintering. Through this processing route PTFE has displayed excellent barrier properties, as the PTFE is sintered into a continuous matrix surrounding magnetic particles with minimal porosity.

Sintering PTFE at 360°C for 5 minutes causes a decrease in the level of crystallinity from a starting point of around 94%, to approximately 55-70%. This drop in crystallinity increases with increased time at temperature and leads to an increase in mechanical strength. Sintering times of around 6 minutes have been found to produce the greatest mechanical strength gains (Tattam et al., 1996b).

Some physical properties of interest for PTFE are listed in Table 3.3:

Table 3.3 Properties of PTFE (Asahi Glass Co Ltd, 1996)

Property	
Density (g/cm ³)	2.2
Tensile Strength (Nm ⁻²)	30
Service Temperature (°C)	
Short Term	300
Long Term	250
Volume Resistivity (Ωcm)	>10 ¹⁸
Water Absorption (mg/cm ² /day)	0

3.2.2.1 Step-By-Step Production Method

- 1) The required mass of NdFeB powder was weighed.
- 2) The required mass of crystalline PTFE was weighed.
- 3) The NdFeB powder and crystalline PTFE were blended together in a container with 10 × 5mm diameter stainless steel ball bearings using a rotary powder blender for 30 minutes.
- 4) The composite blend was loaded into the die cavity and the punches inserted.
- 5) The die was located between the hydraulic rams of a manual 30 Ton press.
- 6) The pressure between the rams was increased to approximately 3 Ton/cm².
- 7) The PTFE bonded NdFeB material was ejected from the die.
- 8) The NdFeB bonded magnet was then sintered in a vacuum furnace using the following heat treatment cycle 50°C/min Ramp → 370°C → 6 minute dwell → Furnace roll off to cool (Tattam et al., 1996b).

3.2.3 Zinc

Zinc was used in the form of a powder with a particle size of approximately 60µm as a bonding material. Again this medium relies on a powder metallurgy type route whereby the matrix material and magnetic material are blended together in a predetermined ratio, pressed, and then sintered to densify the composite.

This soft metal possesses excellent barrier properties, although, as it is a metal it displays fairly poor flow characteristics during pressing. The poor flow properties are a direct result of its hardness, making it relatively non-malleable when compared with other binders such as PTFE or epoxy. This leads to a high degree of porosity being incorporated into the bulk

material, and thus a low density composite. The sintering process aids densification and thus improves corrosion resistance (Tattam, 1996).

From a corrosion resistance perspective it is thought that zinc can act sacrificially to protect the $\text{Nd}_2\text{Fe}_{14}\text{B}$ component of the bonded magnets (Attanasio and Latanision, 1995). However, it is unlikely that it would protect the highly reactive Nd-rich phase from attack from aqueous corrosion.

3.2.3.1 Step-By-Step Production Method

- 1) The required mass of NdFeB powder was weighed.
- 2) The required mass of zinc powder was weighed.
- 3) The NdFeB and zinc powder were blended together in a container with $10 \times 5\text{mm}$ diameter stainless steel ball bearings using a rotary powder blender for 30 minutes.
- 4) The composite blend was loaded into the die cavity and the punches inserted.
- 5) The die was located between the hydraulic rams of a manual 30 Ton press.
- 6) The pressure between the rams was increased to approximately 3 Ton/cm^2 .
- 7) The bonded magnet was ejected from the die.
- 8) The zinc bonded magnet was then subject to the LPPS surface coating technique (described in section 3.3.3).
- 9) The zinc bonded magnet was subject to sintering during the LPPS coating technique in a vacuum furnace using the following heat treatment cycle 50°C/min Ramp $\rightarrow 390^\circ\text{C} \rightarrow 90 \text{ minute dwell} \rightarrow \text{Furnace roll off to cool}$.

3.3 Surface Coatings Employed

3.3.1 PTFE

Within this study PTFE was also employed as a surface coating for PTFE bonded magnets. It was supplied in the form of an aerosol from RS Components and is described as a dry film lubricant. It consists of inert particles of PTFE in a suspension medium. After application, the suspension medium, serving as the delivery method, evaporates leaving a thin PTFE coating on the surface of the magnet. The coating was built-up through the application of a number of thin layers, allowing time for evaporation of the suspension medium between coatings. After the PTFE coating had been applied it was subject to the same sintering treatment described in section 3.2.2.1. The aim of sintering was two-fold; to produce an adhesive surface coating on powder particles, and to fill any voids at the magnet surface which were incorporated during uniaxial pressing.

3.3.2 QSil 12 (Two-part Silicone Potting Compound)

This is a clear, transparent, low viscosity, 2-component liquid silicone material which cures at room temperature and is primarily intended for potting applications. This material is typically mixed at a 100:5 ratio. Once mixed, the material is self-leveling and will have a useful work-life of approximately 2 hours. The material will be fully cured after 24 – 48 hours at room temperature. This material can also be vulcanized at elevated temperatures (up to 70°C) to increase the cure speed.

Table 3.4 Properties of QSil 12 (Quantum Silicones LLC, 2009)

Colour	Clear/Slight Haze
Consistency	Low Viscosity
Viscosity Base Component cps	1400
Specific Gravity (g/cm ³)	1.00
Work Life (minutes)	160 – 180
Useful Temperature Range	-60 – 240°C
Durometer, ShoreA, 72 Hour	18

Due to the requirements upon the material during use as a surface coating a mixing ratio of 10:1 was utilised to significantly reduce the work life and increase the viscosity of the compound. This facilitated vastly decreased cure times and allowed the surface coating to cure upon the surface of the bonded magnet assisted by the elevated temperature environment of the oven (Quantum Silicones LLC, 2009).

3.3.2.1 Step-By-Step Production Method

- 1) Part A and Part B of the compound were thoroughly mixed in a 10:1 ratio (A:B).
- 2) The bonded magnet was completely encapsulated in the QSil manually with a spatula.
- 3) The bonded magnet was then placed in an oven at 70°C for 30 minutes to reduce the cure time.
- 4) The coated magnet was then allowed to cure at room temperature for a further 72 hours.

3.3.3 Zinc Low Pressure Pack Sublimation (LPPS) Coating

Low pressure Pack Sublimation (LPPS) was developed from the process of sheradizing. The techniques vary in that LPPS is carried out in a low vacuum ($\sim 10^{-2}$ Torr) without chamber rotation. Full details of this technique can be found here (Walton et al., 2000).

The materials utilised to produce the LPPS zinc coating on the surface of the zinc bonded magnets were zinc dust with a particle size of 6 - 8 μ m and silica sand with a average particle size of around 300 μ m. These two components were mixed in a ratio of 1:2 respectively by weight. Magnets were placed within this mixture to perform the coating procedure. The LPPS apparatus and schematic diagram of the process can be seen in Fig. 3.4 and Fig. 3.5 respectively.

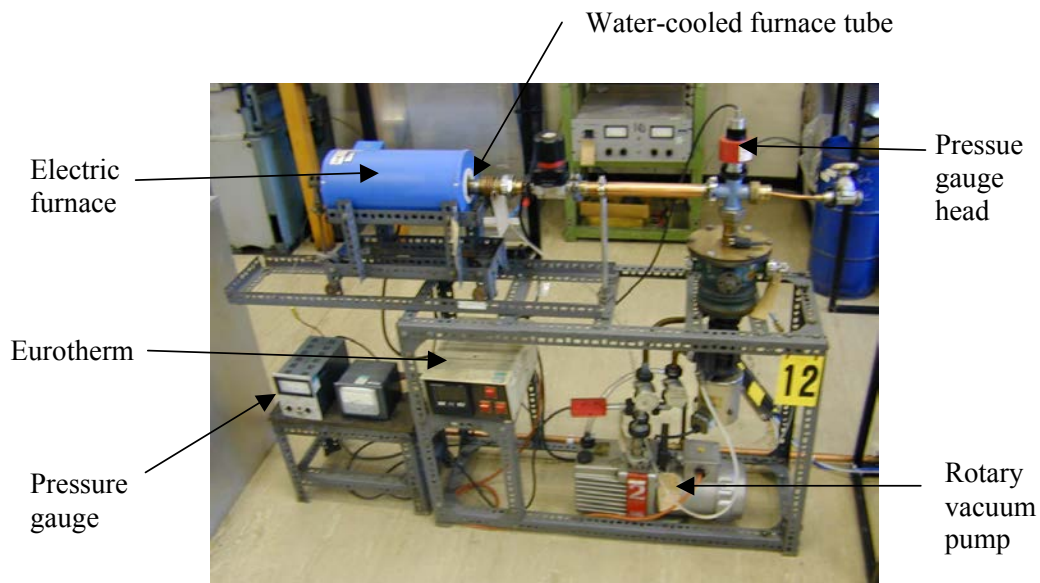


Fig. 3.4 Image of LPPS coating rig (Walton, 2001).

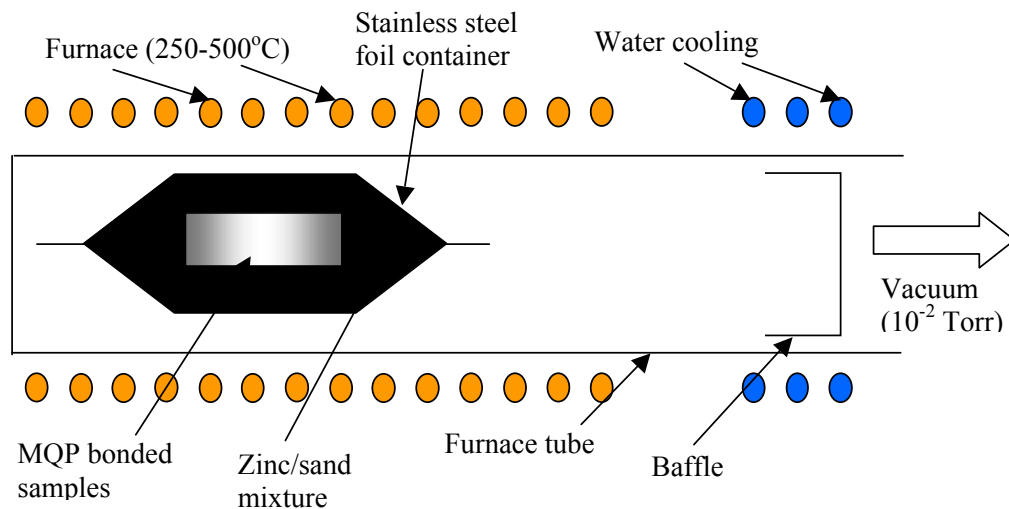


Fig 3.5 Schematic diagram of the LPPS coating process (Walton, 2001)

3.3.3.1 Step-By-Step Production Method

- 1) Zinc bonded magnets were washed in methylated spirits and then dried.
- 2) A stainless steel foil container was formed around a wooden mandrill and closed at one end.
- 3) The container was filled with 1/3 zinc dust (6-8 μm) and silica sand (300 μm) in a 1:2 ratio (weight) respectively.
- 4) The zinc bonded magnets were placed into the mix.
- 5) The capsule was subsequently filled to the top and sealed.
- 6) The container was then slid into the vacuum tube and evacuated to 10^{-2} Torr.
- 7) A resistively heated electric furnace was rolled over the vacuum tube. A k-type thermocouple positioned adjacent to the sample was used in conjunction with a Eurotherm to monitor and control furnace temperature. This was to ensure that the zinc did not melt as overheating is more common with the standard system of a control thermocouple incorporated into the furnace.

- 8) The vacuum furnace was set to apply the following heat treatment cycle 50°C/min
Ramp → 390°C → 90 minute dwell → Furnace roll off to cool.

3.4 Environmental Testing

The aims of this section of the study were threefold:

- To document the effects of moisture exposure on the magnetic properties MQP-B powder in various aqueous environments.
- To assess the level of corrosion protection offered to MQP-B material by various bonding media and surface coatings in bonded magnets.
- To determine the effect that varying concentrations of antifreeze (Dex-cool) has on corrosion behaviour of both bonded MQP-B and 'loose' MQP-B powder.

Within this study MQP-B bonded magnets and 'loose' unbonded powder was subject to a variety of simulated elevated temperature (80°C) environmental conditions over a period of 2016 hours. These conditions ranged from a completely aqueous environment (water bath), to a high humidity environment (environmental chamber) to a zero humidity environment (oven). These simulated environments will be described below:

3.4.1 Aqueous Environment

Samples were exposed to a simulated aqueous environment at elevated temperatures over 2016 hour period. This simulated aqueous environment entailed samples being fully submerged in a variety of solutions at 80°C. These solutions were:

- Deionised (DI) water
- A solution of 50%vol Dex-cool and 50%vol DI water (50/50)
- 100% Dex-cool.



Fig 3.6 Image of MQP samples in water bath setup.

In the case of the bonded magnets, monitoring the magnetic properties at regular intervals (every 168 hours) allowed bonding media and surface coatings to be evaluated for effectiveness in protecting the magnetic component from aqueous corrosion. In addition to this, the effect of varying concentrations of Dex-cool upon the rate of corrosion could also be monitored as these experiments were run side-by-side. Details of Dex-cool can be found in 3.4.1.1.:

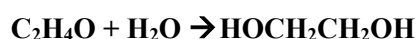
3.4.1.1 Dex-Cool (Antifreeze/Ethylene Glycol)

Dex-Cool is commonly used as a heat transfer fluid and antifreeze, it is composed primarily of Ethylene Glycol (EG). All of the components and relative quantities by %weight can be seen in Table 3.5

Table 3.5 Components of Dex-cool according to the material safety data sheet (Chevron Texaco Global Lubricants, 2002)

COMPONENTS	CAS NUMBER	AMOUNT
Ethylene Glycol	107-21-1	80 – 96.99 %weight
Diethylene Glycol	111-46-6	1 – 4.99 %weight
Potassium 2-ethylhexanoate	3164-85-0	1 – 4.99 %weight
Water	7732-18-5	1 – 2.99 %weight

EG is produced from ethylene via the intermediate ethylene oxide. Ethylene oxide reacts with water to produce EG according to the chemical equation:



(equ 3.1)

3.4.2 Humid Environment

For the simulated high humidity environment samples of both bonded MQP-B material and ‘loose’ MQP-B were placed into individual soda glass viles and loaded into a Sanyo MTH-4100 environmental chamber. The chamber was set to produce conditions of 85% humidity at 80°C. Samples were subject to these conditions for 2016 hours with magnetic measurements being taken every 168 hours. As with the simulated aqueous environment monitoring of magnetic properties allowed the effectiveness of bonding media and surface coatings in preventing aqueous corrosion to be assessed. The susceptibility of MQP-B powder to corrosion in a high humidity environment could also be measured.

3.4.3 Dry Environment

For the simulated dry environment, which, for the purpose of this study will act as the control group. Samples were placed into individual soda glass viles and loaded into a (blagh blagh) oven set to 80°C. Samples were subject to this condition for a period of 2016 hours, with the magnetic properties being measured at 168 hour intervals. The

measurement of these samples served as a comparison between dry and wet environments and illustrates the effect of water.

3.5 Magnetic Hysteresis Measurements

In this section of the study bonded samples were characterised magnetically with a permeameter which was constructed in-house using Hirst fluxmeters. MQP-B powder samples were characterised magnetically using a LakeShore (model 7300) vibrating sample magnetometer (VSM).

3.5.1 Permeameter

Bonded samples were removed from their environment and allowed to cool to room temperature before being pulse magnetised in a 6 Tesla field. Samples were then located between the pole-tips within the fluxmeter coils and hysteresis measurements were performed to determine the magnetic behaviour.

The permeameter is a technique utilised primarily for characterisation of bulk samples. Unlike the VSM, the poles of the electromagnet are in contact with, or in very close proximity to the sample. This reduces the de-magnetisation factors to negligible levels. The strength of the applied field and, the magnetic moment of the sample are detected through a set of pickup coils surrounding the sample.

From Faraday the voltage induced in the detection coil depends on the rate of change of magnetic flux through the sample, as per the equation 3.2:

$$E = -N \frac{d\Phi}{dt}$$

(equ 3.2)

Where,

E is the voltage

N is the number of turns in the detection coil

dΦ is the change in flux

dt is change in time

Therefore to obtain a value for the total flux the voltage is integrated with respect to time.

$$\int_0^t E dt = -N \int_{\Phi_2}^{\Phi_1} d\Phi = -N[\Phi_1 - \Phi_2]$$

(equ 3.3)

The detection coils were sourced from Stringover and are five concentric coils designed in such a way that any change in flux caused by ramping of the applied field is not picked up in the measurement of the magnetisation of the sample. The applied flux and flux of sample detected from the coils is integrated by two Hirst integrating fluxmeter (model IF02), linked to a PC through an Analogue-Digital converter (ADC).

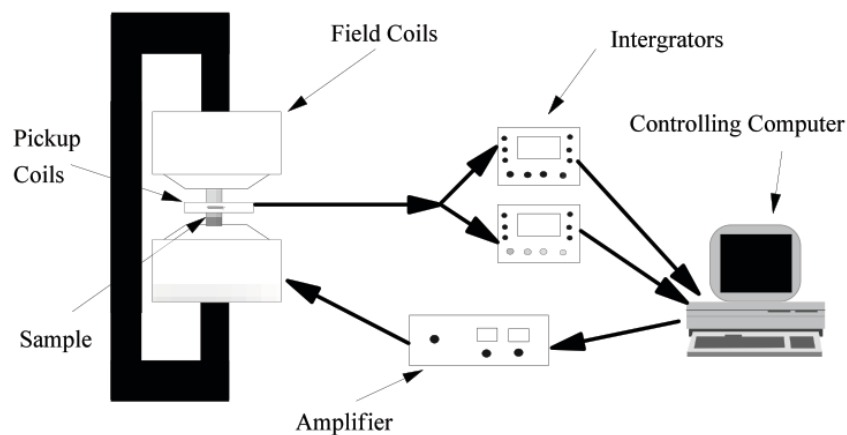


Fig. 3.9 Schematic of the permeameter system constructed in-house (Walton, 2001).

3.5.2 Vibrating Sample Magnetometer (VSM)

MQP-B powdered material samples were removed from their environment and allowed to cool to room temperature. Approximately 50mg of powder was added to a LakeShore cylindrical sample holder (3mm internal diameter \times 3mm high) with a quantity of candle wax to act as a binder. The powder and wax were sealed inside and placed into a beaker of boiling water in order to melt the wax and form a coherent matrix. Upon cooling the wax holds the powder in place preventing movement of particles during the hysteresis measurement. The sample holder was then attached to the stem of the VSM head and a hysteresis measurement was performed. From this magnetic properties can be derived.

The VSM technique lends itself to the hysteresis measurement of powders as the sample is suspended and vibrated between the poles of an electromagnet. Sensing coils are attached to the poles of the electromagnet, which detect the magnetic moment from the sample as the field lines of the sample cut the detection coils in a uniform magnetic field (produced by the electromagnet). The AC voltage on the detection coils is read through a lock-in amplifier which is in phase with the sample vibration.

The limiting factor of VSM measurements is the result of separation between the sample and detection coils. This results in sample demagnetisation factors becoming involved, i.e. sample flux will loop back around into the sample. However, it is possible to correct for this if the geometry of the sample is known.

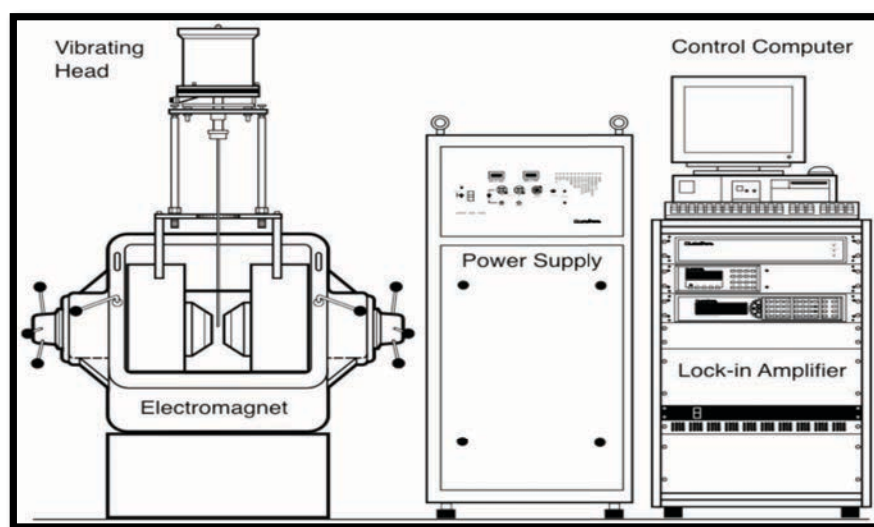


Fig. 3.10 Schematic of LakeShore VSM (7300 series) system (after LakeShore 7300 Series user manual)

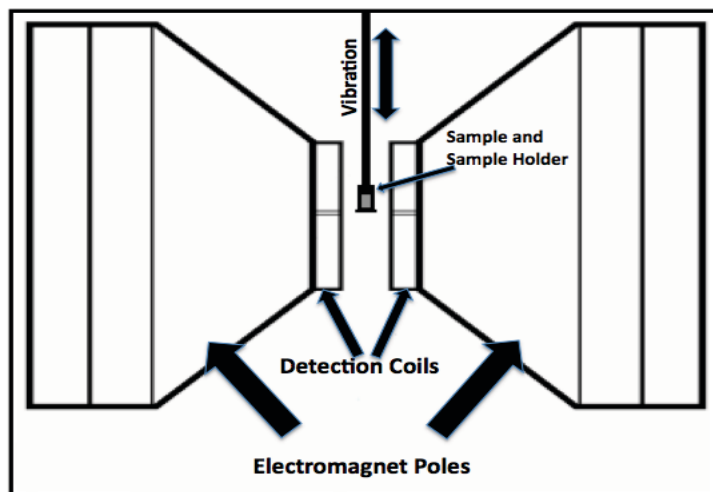


Fig. 3.11 Schematic of LakeShore VSM (after LakeShore 7300 Series user manual)

3.6 Optical Characterisation

To document general surface changes i.e. colour of corrosion products, brought about by the corrosion process through environmental exposure. Samples were removed from their respective environments and allowed to dry in an oven at 80°C for 10 minutes. Macro images of bonded samples were taken at 168 hour intervals for the duration of the study using a digital camera.

3.6.1 Surface Coating Characterisation

Sample surfaces were analysed at 168 hour intervals using an Olympus LEXT OLS3100 mounted on a TableStable anti-vibration table. The microscope uses a 408 nm class II ultraviolet laser source and has a plane resolution (X and Y) of 120 nm and a space pattern (z resolution) of 10 nm. This allows accurate measurements of surface roughness, pore depth and pore volume to be performed.

Surface morphology data is calculated from a series of 'stacked' confocal images along the z-axis. As the laser is reflected by the surface it passes back through the objective and converges at a second focal point, which is optically conjugate to the first. A circular pinhole positioned within this confocal plane ensures that only light from the focal plane is detected, with light reflected from other regions rejected. This information is used to generate an optical section of the sample. The sample is then moved along the z-axis in 5-100nm increments and another optical section is created at a higher/lower focal plane. As the position of the z-axis progresses, a 3D stack of images is generated. It contains the intensity levels for each individual point defined by the laser focus co-ordinates. Using this data, a single composite image is generated, from which accurate surface morphology measurements can be made.

3.7 Mass Change Measurements

To document water absorption and compositional changes induced i.e. formation of corrosion products, as a result of exposure to simulated environmental conditions. Samples were removed from their respective environments and allowed to dry in an oven at 80°C for 20 minutes. Mass measurements of samples were then taken using a (blagh blagh) balance measuring grams accurate to 3 decimal places at 168 hour intervals.

3.8 Density Measurements

This involved weighing the sample in both air and under a liquid of known density. Density measurements performed were based on the Archimedes' principal and were calculated using the following equation:

$$\rho_{Sample} = \frac{W_{air} \times \rho_{liq}}{W_{air} - W_{liq}}$$

(equ 3.4)

Where,

W_{air} = weight of sample in air

W_{liq} = weight of sample submerged in liquid

ρ_{liq} = density of liquid

ρ_{sample} = density of sample

The liquid used was diethyl-phthlate as it has a high thermal stability with a measured density of 1.1135g/cm⁻³ at 20°C (Calculated using a copper standard)

3.9 Hydrogen Absorption/Desorption Studies (HADS)

To examine the links between corrosion, hydrogen ingress and the effects that these processes have upon on the magnetic properties of the materials. MQP-B and magnets were exposed to a hydrogen environment to ascertain if, as a result of hydrogen absorption, magnetic properties were affected in a similar way to samples exposed to moisture. The literature suggests that hydrogen absorption by one or more phases present in the bulk material affects the magnetic properties (Zijlstra and Westendorp, 1969). The degree of hydrogen uptake and phases of the bulk material involved were to be identified through materials characterisation techniques.

‘As received’ MQP-B powder was exposed to a hydrogen atmosphere in a rig designed to perform the hydrogen decrepitation (HD) process. The system incorporates a vacuum furnace and computer controlled mass flow controllers, coupled with a low pressure source of hydrogen. The computer programme monitored and recorded hydrogen pressures and furnace temperatures at 1 second intervals for the duration of exposure.

3.9.1 Step-By-Step Method

- 1) Approximately 5g of MQP-B powder was sealed in metal foil and loaded into the vacuum tube.
- 2) The vacuum system was then evacuated to a level of 10^{-4} Tor.
- 3) The furnace controller was set to ramp and maintain a temperature of 200°C throughout.
- 4) The computer interface was used to instruct the mass flow controllers to fill and maintain a hydrogen pressure of 1 bar in the furnace tube for the duration of exposure.
- 5) After 2 hours the furnace was rolled off allowing the MQP-B powder to cool under a hydrogen atmosphere.

The hydrided MQP-B were subject to a series of outgassing heat treatments at various temperatures ranging from 200-700°C in a vacuum furnace (Fig. 3.4) Hysteresis measurements and HADS were performed after subsequent heat treatments to document changes in magnetic properties and gases evolved upon heating.

Magnetic characterisation was performed using a LakeShore VSM (model 7300) and HADS was conducted with a thermogravimetric analyser (TGA) produced by Netzsch in conjunction with a Hiden mass spectrometer.

3.10 Thermogravimetric Analysis (TGA)/Mass Spectrometry (MS)

This equipment has been installed in an Argon atmosphere glovebox. Approximately 50mg of sample was loaded into an alumina crucible and placed on the heating stage. The sample was heated at a predetermined rate in an argon flow at 1 bar pressure. During heating the sample mass is monitored, with exhausted gas being flowed through the mass spectrometer for analysis. This enables changes in mass of sample to be related to the type of gas evolved. This data can also be used in conjunction with literature to identify the phases involved in the absorption/desorption, giving a more detailed picture of the process.

References:

- ASAHI GLASS CO LTD. 1996. *PTFE G163 Material Data* [Online]. Tokyo, Japan: AGC-Group. [Accessed 25/11/2010 2010].
- ATTANASIO, S. A. & LATANISION, R. M. 1995. Corrosion of rapidly solidified neodymium-iron-boron (Nd---Fe---B) permanent magnets and protection via sacrificial zinc coatings. *Materials Science and Engineering A*, 198, 25-34.
- CHEVRON TEXACO GLOBAL LUBRICANTS. 2002. *Dex-Cool Material Safety Data Sheet* [Online]. San Ramon, CA: Chevron Texaco Global Lubricants. Available: www.havoline.com [Accessed 25/11/2010 2010].
- MAGNEQUENCH INC. 2009a. *MQP-A-10179-070 Isotropic Powder* [Online]. Ontario, Canada: Neomaterial Technologies Ltd,. [Accessed 25/11/2010 2010].
- MAGNEQUENCH INC. 2009b. *MQP-B-20076-070 Isotropic Powder* [Online]. Ontario, Canada: Neomaterial Technologies Ltd,. [Accessed 25/11/2010 2010].
- MAGNEQUENCH INC. 2009c. *MQP-B+-20056-070 Isotropic Powder (Former name MQP-B2+)* [Online]. Ontario, Canada: Neomaterial Technologies Ltd,. Available: http://www.magnequench.com/assets/download/MQP-Bplus-20056-070_v2.3.pdf [Accessed 25/11/2010 2010].
- MAGNEQUENCH INC. 2009d. *MQP-C-20006-070 Isotropic Powder* [Online]. Ontario, Canada: Neomaterial Technologies Ltd,. [Accessed 25/11/2010 2010].
- MAGNEQUENCH INC. 2009e. *MQP-14-12-20000-070 Isotropic Powder* [Online]. Ontario, Canada: Neomaterial Technologies Ltd,. [Accessed 25/11/2010 2010].
- POLLARD, R. J., PARKER, S. F. H. & GRUNDY, P. J. 1988. The effect of quench rate on the microstructure and coercivity of some Nd-Fe-B based ribbons. *Journal of Magnetism and Magnetic Materials*, 75, 239-242.
- QUANTUM SILICONES LLC. 2009. *Qsil 12 Technical Data Sheet* [Online]. Richmond, VA: Quantum Silicones LLC. Available: www.quantumsilicones.com [Accessed 25/11/2010 2010].
- TATTAM, C. 1996. *The Processing and Properties of Bonded Nd-Fe-B Magnets*. Doctor of Philosophy PhD Thesis, University of Birmingham.
- TATTAM, C., WILLIAMS, A. J., HAY, J. N., HARRIS, I. R., TEDSTONE, S. F. & ASHRAF, M. M. 1996b. Improvement in the mechanical properties of PTFE bonded Nd-Fe-B magnets by heat treatment. *Journal of Magnetism and Magnetic Materials*, 154, 328-332.
- WALTON, A. 2001. *Low Pressure Pack Sublimation (LPPS): A Zinc Coating Process for NdFeB Magnets*. Doctor of Philosophy PhD Thesis, University of Birmingham.

WALTON, A., SPEIGHT, J. D., WILLIAMS, A. J. & HARRIS, I. R. 2000. A zinc coating method for Nd-Fe-B magnets. *Journal of Alloys and Compounds*, 306, 253-261.

ZIJLSTRA, H. & WESTENDORP, F. F. 1969. Influence of hydrogen on the magnetic properties of SmCo₅. *Solid State Communications*, 7, 857-859.

Chapter 4: Results and Discussion:

Corrosion Behaviour of NdFeB Bonded Magnets

4.1 Project Introduction

The driving force behind commissioning this study was an issue brought to our attention by Magnet Applications Ltd. They came to us with a problem that had been presented to them by one of their end users. The end user required an NdFeB bonded magnet to operate within a permanent magnet water pump at approximately 80°C. The user also required information regarding the affect of Dex-Cool (antifreeze/ethylene glycol) used within the system upon the performance of the magnetic components. Epoxy bonded magnets previously supplied had failed within a fraction of their expected service life without observed disintegration on a scale to warrant the loss of magnetic properties.

The magnetic drive pump is energy efficient and requires no seals or lubricants for operation. In this case the pump was circulating water at 80°C. The main components are a rotating impeller, with an array of magnets attached to the shaft. It is located in an enclosed housing and is powered by a rotating magnetic field produced by the motor coils and stator. The rotation of the magnets attached to the impeller produces a centrifugal force that drives liquid through and outside of the pumps housing.

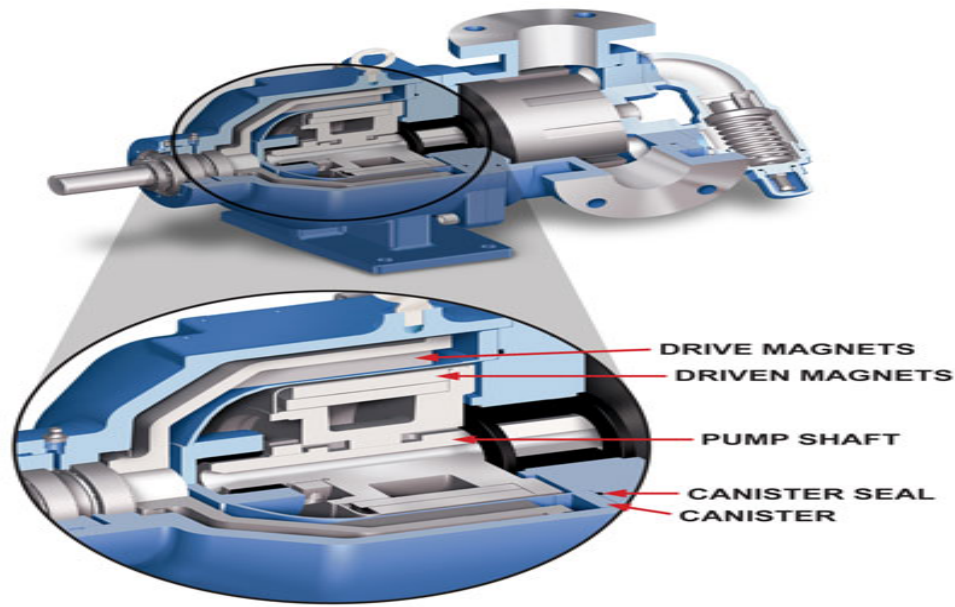


Fig 4.1 Exploded diagram of a magnetic drive pump (Viking Pump Inc., 2011)

4.2 NdFeB MQP-B in MQ-I Bonded Magnets

The components supplied by Magnet Applications were NdFeB MQI epoxy bonded magnets produced using MQP-B melt quenched ribbon manufactured by Magnequench. Sintered NdFeB magnets are responsible for some of the highest recorded maximum energy products, circa 474 kJ/m^{-3} (Matsuura, 2006).

However, bonded magnets also have remanence and thus $(BH)_{\max}$ is diluted through the addition of a binder used to form the composite. In addition, the MQP is isotropic which limits the $(BH)_{\max}$ of these bonded magnets to $\sim 80 \text{ kJm}^{-3}$. It is important that the materials utilised in these specialised bonded magnet applications are optimised magnetically. The effect of binder addition in terms of remanence is summarised by the following equation:

$$B_r \text{ of polymer bonded magnet} = B_r \text{ of powder} \times \text{Volume fraction of powder}$$

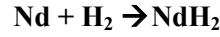
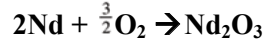
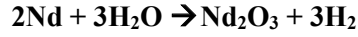
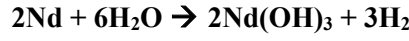
(equ 4.1)

It is worth noting that melt spun ribbon produced by Magnequench is used almost exclusively within the bonded magnet market as a result of the excellent intrinsic powder properties and highly “stackable” flake morphology for high loadings, relative to HD and HDDR manufactured powder. Also processing routes and methods employed in MQP production result in powder particles with sub-micron size grains with a low sensitivity to oxidation upon exposure to air. In contrast powders produced via HD and HDDR routes are more sensitive to oxidising atmospheres, due to larger grain size and partly due to the fresh fracture surfaces exposed by the HD processing, and thus must be handled inertly to prevent detrimental effects for intrinsic magnetic properties.

4.2.1 Aqueous Corrosion of NdFeB Magnequench Particles (MQP)

Despite the positive attributes associated with NdFeB based alloys, its uses however, are restricted as a result of its inherent weaknesses. The alloy has a relatively low T_c , and thus, a relatively low maximum operating temperature (160 – 180°C) when compared with SmCo based alloys (350 – 550°C). Although, arguably the greatest limiting factor in terms of use is the susceptibility of the alloy to corrosion and oxidation. The most vulnerable phase present is the Nd-rich phase, which reacts readily with both oxygen and water from the surrounding atmosphere. Although, in MQP the composition of the starting alloy is very close to the stoichiometry of the predominant $Nd_2Fe_{14}B$ phase which means that there is only a very small volume of the highly reactive Nd-rich phase present within the structure, compared to sintered magnets.

The anodic reaction of water with the Nd-rich phase leads to the disassociation of water into hydrogen and oxygen leading to the formation of $Nd(OH)_3$ (neodymium hydroxide) and Nd_2O_3 (neodymium oxide) as per the following equations (Kim et al., 1996):



(equ 4.2)

It was found by Camp et al. 1991 that NdO_x and the more stable Nd_2O_3 were formed at triple junctions and on the grain boundaries of sintered NdFeB magnets upon contact with air at elevated temperatures (Jacobson and Kim, 1987) (Camp and Kim, 1991). It is safe to assume that this oxidation process will also occur within humid environments fuelled by oxygen formed by the disassociation of water. On the other hand it has also been suggested that oxidation of the Nd-rich phase can be beneficial, improving corrosion resistance by reducing the available Nd-rich grain boundary available (Camp and Kim, 1991).

As previously stated, the main phase present within MQP is the relatively stable $\text{Nd}_2\text{Fe}_{14}\text{B}$ phase. Although this phase is less reactive than the Nd-rich phase it will still absorb hydrogen at elevated temperatures or pressures (Harris et al., 1987). Hydrogen liberated via the disassociation of water through reaction with the Nd-rich phase has a negative effect upon the H_{ci} of the $\text{Nd}_2\text{Fe}_{14}\text{B}$ phase upon absorption.

The decrease in H_{ci} as a result of hydrogen uptake is caused by an expansion of the crystal lattice, mostly along the a-axis (basal plane) caused by the movement of hydrogen into interstitial sites of the crystal. This causes an overall increase in the interatomic Fe-Fe distances leading to local negative exchange interactions also resulting in an increase in T_c .

There is also a strong effect observed on the Nd-B interatomic distances which is thought to be the main reason for the drop of the uniaxial magnetic anisotropy whereby hydrogen insertion pushes B atoms closer to the Nd atoms. All Nd-Fe interatomic distances are increased except for the shortest one which remains unaffected (Isnard et al., 1995).

A feasible solution to prevent the aqueous corrosion process and associated effects occurring upon contact with the magnetic component is to use a binder that acts as an impermeable barrier to water limiting contact. By limiting or preventing contact between moisture and MQP this would prevent the disassociation of water and hence the uptake of hydrogen and oxygen by the Nd₂Fe₁₄B phase.

4.3 Aims

This section of the study aims to characterise the performance of MQI bonded magnets before, during and after exposure to a spectrum of moisture containing environments. Environmental conditions range from dry to an aqueous environment, where the sample is fully submerged, each condition is maintained at 80°C. These environments are designed to simulate accelerated use within real world applications i.e. “under the bonnet” type applications. Details of the environmental conditions are as follows:

- Oven – Set to maintain a temperature of 80°C (Dry Heat)
- Environmental Chamber – Set to maintain a temperature of 80°C with a relative humidity (RH) of 85%.
- Aqueous Environment – Samples are fully submerged within various solutions (Dex-Cool, DI Water, or 50/50 (DI Water/Dex-Cool mix)) with a constant 80°C temperature maintained by a water bath.

This initial investigation is specifically focussed upon assessing the performance of the single current commercially available bonding media, epoxy resin. The performance of epoxy resin will then be compared with other potential bonding media candidates when exposed to the same environmental conditions detailed above.

The bonding media will be assessed primarily by measuring the H_{ci} of bulk samples on a weekly basis (every 168 hours). This will provide evidence relating to the level of protection offered against moisture ingress and subsequent corrosion of MQP during environmental exposure. Other techniques employed will provide density measurements and mass of samples thus enabling an approximation of water absorption to be made. With further characterisation through optical techniques such as laser confocal microscopy and macro images.

4.4 Epoxy Resin Binder Performance

At present the only commercially available NdFeB bonded magnets utilise epoxy resin as a binder. Epoxy resin does little to prevent the ingress of water and therefore, does little to prevent the attack of MQP by aqueous corrosion. The material properties of epoxy resin show that it absorbs 7.5 mg/cm^2 of water per day (Tattam, 1996). To allow water ingress on this scale the epoxy resin structure must be highly porous, making it an ineffective barrier material in moisture rich environments.

4.4.1 Water Movement Through Epoxy Resin

A study conducted by (Soles and Yee, 2000) has produced a model depicting the movement of water molecules through the structure of epoxy resin. It shows the movement of water through nanopores that are themselves similar in size to that of the water molecules. The mechanism that they attributed to regulation of water flow through these

nanopores is the dominance and availability of free polar groups. If, at a crosslink junction where a polar group is exposed to a nanopore in a disrupted state then a water molecule will be attracted to form a hydrogen bond with the amine and the hydroxyl polar group. This in turn would momentarily block the nanopore hindering the transport of other water molecules through that nanopore (Fig. 4.2a). However, if a polar group located at a nanopore had already formed a hydrogen bond, intramolecularly or otherwise this would prevent a water molecule from associating with either polar group. As water molecules cannot associate with shielded polar sites then they can easily traverse the nanopores (Fig. 4.2b). This is depicted in Fig. 4.2.

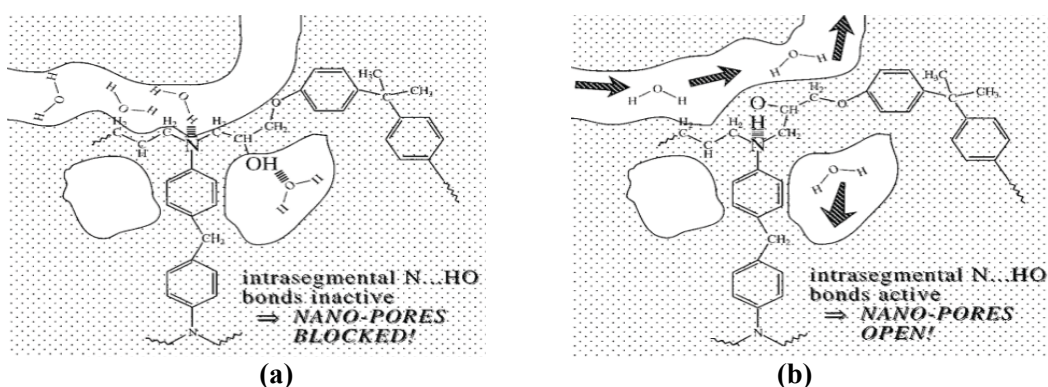


Fig. 4.2 A plausible picture of moisture diffusion through the nanopores of an amine-containing epoxy resin where specific interactions between the water and the polar hydroxyls and amines regulate transport. (a) Shows polar groups in a disrupted state. (b) Show polar groups in an associated state (Soles and Yee, 2000).

4.5.2 Epoxy Resin: Water Ingress And Associated Effects

Measurements of how effective a binder is in terms of preventing water ingress can be performed via two different routes; through recording changes brought about in the intrinsic properties of magnetic component as a result of exposure to moisture, in particular

H_{ci} , and through recording changes in the mass of the composite. These two measurements will vary as a result of reactions with moisture.

Changes in mass and H_{ci} of epoxy bonded samples as a result of exposure to a high humidity (85%) environment are shown in Fig. 4.3. It can be seen that after 1848 hours of exposure the sample mass had increased steadily to nearly 2% as a result of water ingress and corrosion products formed. During this mass increase the sample also suffered H_{ci} losses with them beginning to plateau after around 1512 hours to approximately 93% of their initial value. This figure provides evidence supporting the fact that epoxy resin absorbs water and there may be a relationship between water ingress and decrease in H_{ci} of epoxy bonded samples.

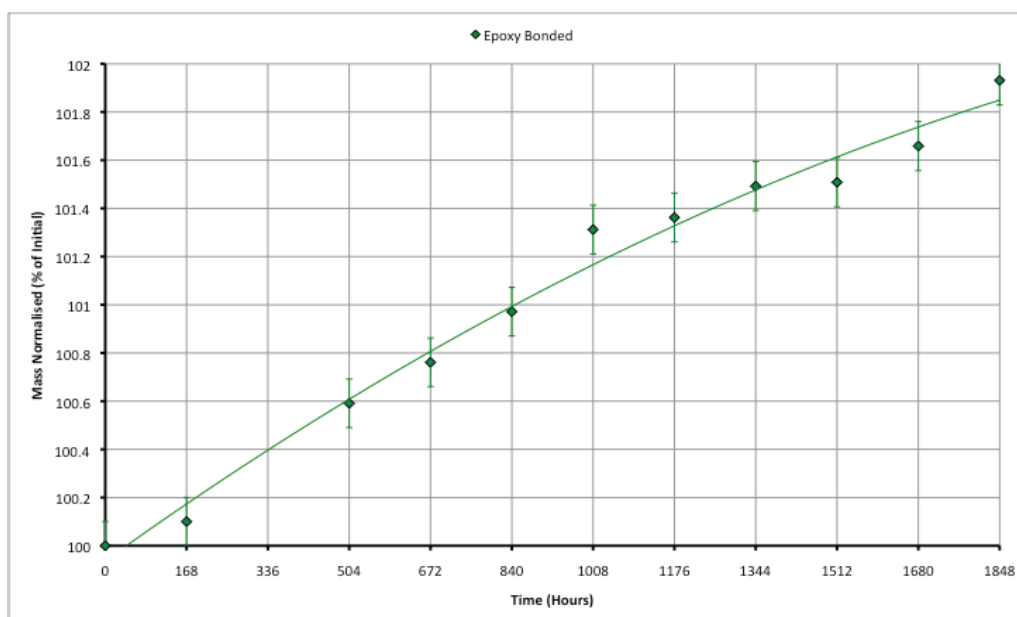


Fig. 4.3 Depicts normalised mass (%) against time for an MQ-I epoxy bonded sample exposed to 80°C at 85% humidity.

The strong correlation between water ingress and reduction in H_{ci} can be demonstrated by producing a plot of normalised mass against normalised H_{ci} of the same epoxy bonded sample shown in Fig. 4.3. This can be seen in Fig.4.4.

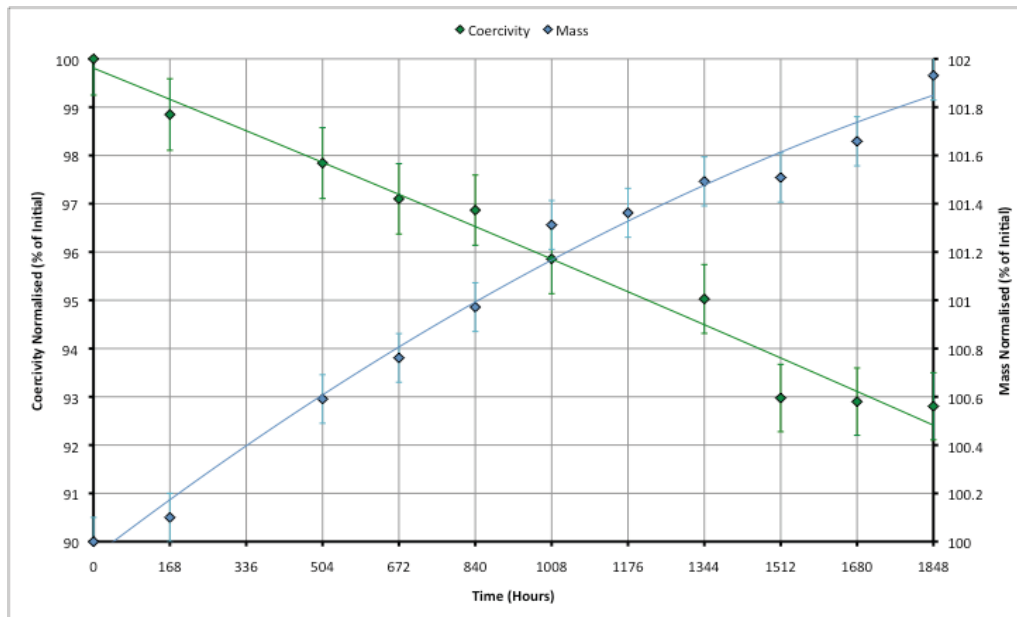


Fig. 4.4 Depicts the correlation between normalised mass (%) against normalised coercivity (%) with time for an MQ-I epoxy bonded sample exposed to 80°C at 85% humidity.

The positive correlation between the two sets of data points from Fig. 4.4 give a clear indication that there is a relationship between water ingress into the epoxy sample and H_{ci} losses. From the plot produced it can be seen that as mass due to water absorption increases steadily, H_{ci} decreases steadily. It can be stated with confidence that the ingress of moisture into the bulk material, and subsequent MQP exposure to said moisture, is responsible for the observed decreases in H_{ci} .

To emphasise the correlation between moisture ingress and H_{ci} losses in epoxy bonded samples, a plot was produced using the same data from Fig. 4.4 whereby H_{ci} was measured against sample mass. This chart can be seen in Fig. 4.5

From Fig. 4.5 it can be seen that the rate of moisture ingress is very closely related to H_{ci} losses. Where moisture ingress is rapid H_{ci} losses are at their greatest and when moisture ingress begins to plateau H_{ci} losses follow suit.

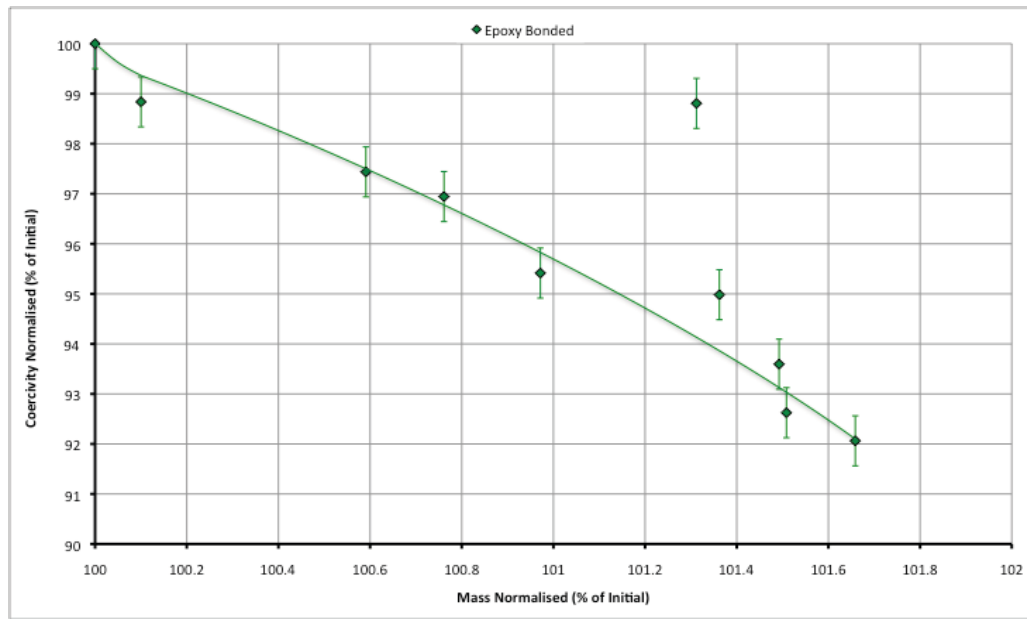


Fig. 4.5 Depicts the correlation between normalised coercivity (%) against normalised mass (%) for an MQ-I epoxy bonded sample exposed to 80°C at 85% humidity.

Further evidence to support the link between water ingress and H_{ci} losses can be seen in Fig. 4.6 where, the effect of varying moisture concentrations in the environment has upon the magnetic properties of epoxy bonded samples. This data is provided by hysteresis measurements taken from samples exposed to the spectrum of simulated environmental conditions. To effectively illustrate changes brought about due to water ingress, H_{ci} measurements were recorded from the second quadrant demagnetisation curves taken at 168 hour intervals.

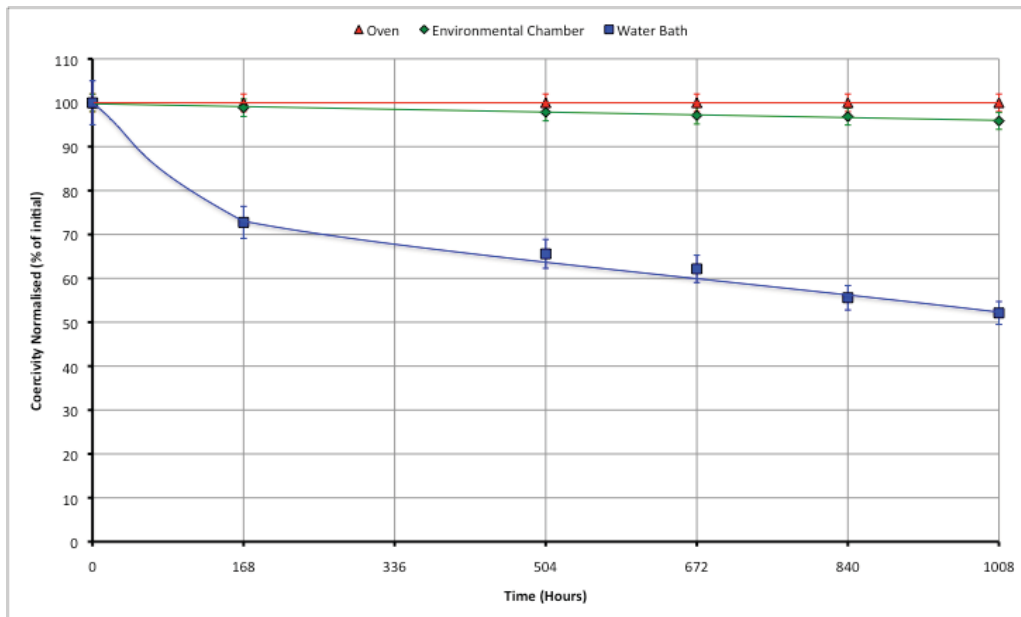


Fig. 4.6 Depicts normalised coercivity (%) against time for MQ-I epoxy bonded samples exposed to a spectrum of moisture containing environments. (Oven samples expose to dry circulating air at 80°C, Environmental Chamber samples exposed to 80°C at 85% humidity, Water Bath samples fully submerged in DI Water at 80°C)

From Fig. 4.6 it can be seen that the abundance of water within a given environment is directly proportional to the size and time taken before significant reductions in H_{ci} occur. Epoxy bonded samples fully submerged in DI water show the greatest and most rapid losses in terms of H_{ci} . A decrease of approximately 50% of the initial value was observed after 1008 hours. By contrast epoxy bonded samples exposed to 85% humidity suffered losses in the region of 5% over the duration of the testing. Samples exposed to the simulated dry environment of the oven exhibited no noticeable deterioration in H_{ci} .

This gives a clear indication that H_{ci} losses observed as a result of exposure to simulated environmental conditions are closely related to the availability of moisture within a given operating environment. The greater the moisture content of the environment, the more rapid and pronounced the onset of H_{ci} losses. This supports the initial logic behind the

commissioning of this study i.e. epoxy resin does little to protect MQP within a bonded magnet against moisture ingress from the surrounding environment and associated detrimental effects on performance.

4.6 Alternate Bonding Media Performance

It was deemed that a comprehensive investigation into the performance of currently utilised epoxy resin and associated problems could help identify other more suitable candidates. These candidates should provide better barrier properties thus vastly improving the longevity and performance of magnetic components operating in environments where the bonded magnet may come into contact with moisture.

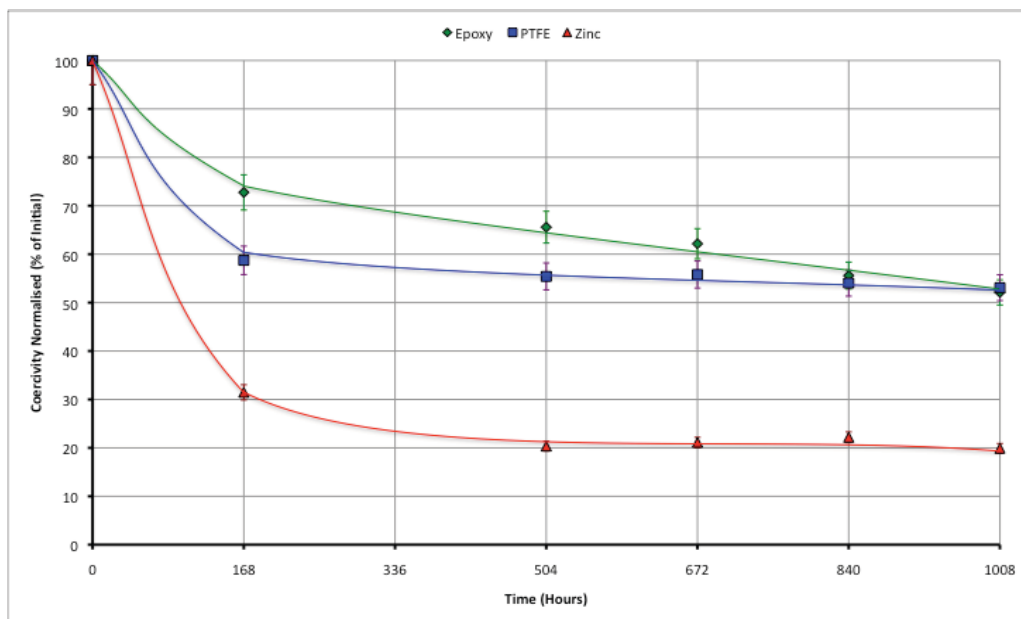


Fig. 4.7 Depicts normalised coercivity (%) against time for MQ-I samples bonded with different media. Samples were fully submerged in DI water at 80°C.

Fig. 4.7, shows the data from the initial investigation into the performance of bonding media in terms of their capacity to preserve magnetic properties of MQP against moisture

ingress from an aqueous environment, and related coercivity losses. As before, the data has been normalised and is expressed as a percentage of the initial coercivity.

Data gathered from initial trials of this study showed that the majority of H_{ci} losses occurred over the initial 168 hour period with relatively small changes occurring between the 168 to 336 hour time frame. As a result of these initial trials it was deemed unnecessary to perform an H_{ci} measurement after 336 hours. For the sake of continuity this trend has been continued throughout the experimental data collection within this study.

It can be seen that the onset of H_{ci} loss is by far the most pronounced and rapid in zinc bonded LPPS samples, where a reduction to approximately 30% of the original value had occurred within 168 hours. Zinc being a metal possesses excellent barrier properties as it is totally impermeable to water. Thus, the poor performance of the zinc as a binder must therefore be attributed to another factor that would allow moisture easy access to a large surface area of MQP contained within the sample.

4.7 Sample Density and Aqueous Corrosion Performance

Previous studies have found that the corrosion behaviour of NdFeB sintered magnets (Yan et al., 1999) and bonded magnets (Tattam et al., 1996a) is highly dependent upon the density of the magnet. The density, usually expressed as a percentage of the theoretical maximum, is a critical factor in determining corrosion resistance, as any magnet that is less than fully dense will have a corresponding degree of porosity incorporated into the structure. Any incorporation of porosity can provide an easy pathway for the ingress of elements from the surrounding environment through the interconnected network of empty voids.

The theoretical maximum density of the composite is calculated using the following equation:

$$T_{MAX\rho} = (V_{MQP} \times \rho_{MQP}) + (V_{BIND} \times \rho_{BIND})$$

Where,

$T_{MAX\rho}$ is the theoretical maximum density of the composite

V_{MQP} is the volume fraction of MQP

ρ_{MQP} is the density of MQP

V_{BIND} is the volume fraction of the binder

ρ_{BIND} is the density of the binder

(equ 4.3)

The measured density of samples can then be compared to the theoretical maximum to give the volume of porosity incorporated into the composite as follows:

$$\% \text{ Vol porosity} = \frac{M\rho}{T\rho}$$

where,

$M\rho$ is the measured density

$T\rho$ is the theoretical density

(equ 4.4)

Samples with a low density, relative to the theoretical maximum, will as a consequence be composed of a large network of porosity. Porosity plays a significant role in facilitating the aqueous corrosion process in that; the network of pores provides access to a larger surface area of MQP that are not necessarily located at or in close proximity to the surface. These pathways will inevitably lead to increased accessibility and attack of MQP by moisture. As

a result, exposure to environmental conditions is not solely limited to particles located at or near the surface of the bonded magnet.

Density measurements of bonded magnets taken before testing support the findings of previous works (Tattam, 1996) (Mokal, 1998) (Yan et al., 1999) in that samples with a low density, relative to the theoretical maximum, display poor resistance to aqueous corrosion when monitored through H_{ci} losses. Samples with fewer pores incorporated into the structure would afford much greater protection to MQP within the bonded magnet. The physical characteristics of samples in terms of density can be seen in Table 4.1:

Table 4.1 Physical characteristics of samples in terms of density

Sample	Volume Fraction MQP-C (%)	Volume Fraction Binder (%)	Volume Fraction Porosity (%)	H_{ci} Losses After 1008 Hours DI Water Exposure (%)
Epoxy Bonded	77.9	15	7.1	47
PTFE Bonded	76.4	15	8.6	48
Zinc Bonded	69.7	15	15.3	80.0

Upon comparison of the data in Table 4.1 it can be seen that there is a positive correlation between the degree of porosity incorporated into a sample and its susceptibility to the aqueous corrosion process. It should be noted that the zinc bonded sample displays the largest and most rapid decrease in H_{ci} but also possesses the most porous structure (15.3%). By contrast both the epoxy resin and PTFE bonded samples both have a much smaller volume of porosity incorporated into their structures, 7.1% and 8.6% respectively, and they suffer from H_{ci} losses on a much smaller scale as a result of this.

4.8 Optical Surface Characterisation

In an attempt to relate porosity data extrapolated from density measurements to a visual representation of sample surface morphology a series of images were generated using an Olympus LEXT OLS3100 laser confocal microscope. Using this piece of equipment it is possible to produce a single 3D image from a composite of stacked confocal images along the Z axis. It is also possible to overlay this 3D image with the 2D real colour image.

Two images of the epoxy bonded sample surface can be seen in Fig. 4.8.

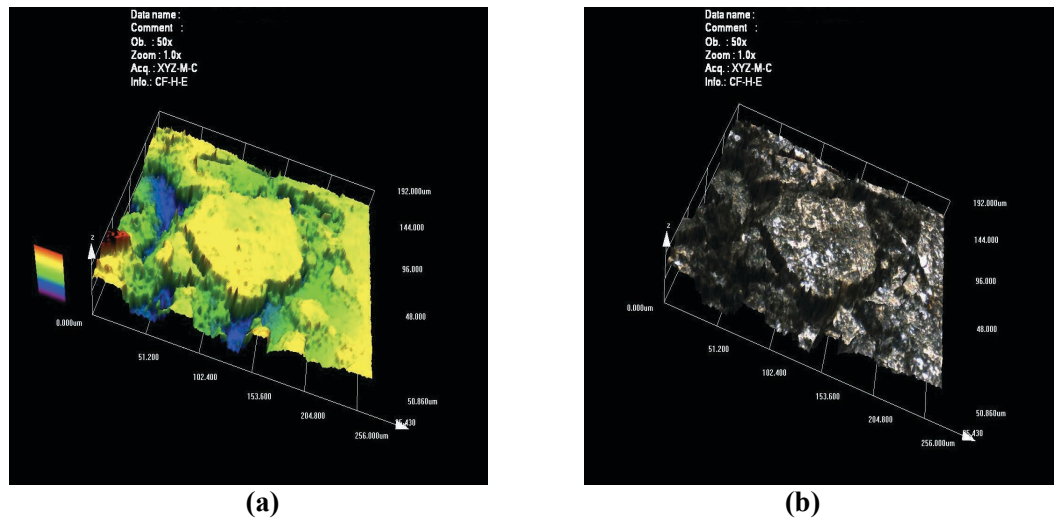


Fig. 4.8 Depicts the surface morphology of an epoxy bonded sample (a) shows a 3D stacked composite image (b) shows the 3D stacked composite with 2D real colour image overlaid.

From the image of the epoxy bonded sample surface (Fig. 4.8a), it can be seen that the surface is largely heterogeneous. An MQP can be clearly identified (depicted in yellow) surrounded by some large deep pores (depicted in blue/green), which exceeded the depth of the scan in the z plane. It would be expected that pores such as these would lead deep into the structure of the bonded sample with smaller pores branching off. When fully submerged these pores would provide easy access for water to the inner structure. From the

real colour image (Fig. 4.8b & 4.11a) it can be seen that the majority of the MQP located at the surface of the sample is covered by epoxy resin (depicted as dark areas). There are also a few small areas where the shiny metallic surface of the MQP is visible. It is likely that during the pressing process the complete particle encapsulation epoxy coating was damaged by a combination of contact with the punches from the die and the forces involved. This may lead to a slightly accelerated corrosion rate at the surface negating the need for water to percolate through the nanopores in the epoxy surrounding each particle. Although in the presence of Dex-Cool this “clean” surface may be beneficial, this will be discussed later within section 4.10.4

By contrast the PTFE bonded sample, seen in Fig. 4.9 and 4.11b, has a largely homogenous surface. This can be attributed to the highly favourable flow properties of the polymer during pressing.

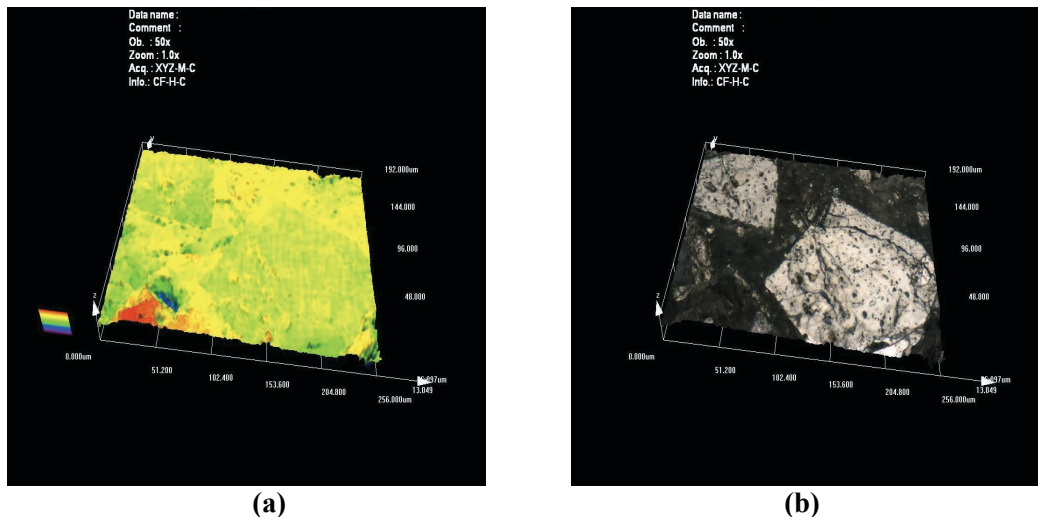


Fig. 4.9 Depicts the surface morphology of a PTFE bonded sample (a) shows a 3D stacked composite image (b) shows the 3D stacked composite with 2D real colour image overlaid.

In fact, the PTFE matrix (depicted in yellow) is actually raised above the level of the MQP (depicted in green). This is probably as a result of excess PTFE being “squeezed” out between the MQP during the pressing process. This means that once the PTFE bonded sample has been heat treated it should be almost impermeable to water. However, it can clearly be seen from the real colour image (Fig. 4.9b) that any particles located at the surface of the sample (depicted as shiny metallic) due to the method of blending MQP with the binder these surface particles are totally exposed and vulnerable to attack by aqueous corrosion. Although the uncoated configuration of surface MQP appears to aid corrosion resistance in the presence of Dex-Cool. As stated before this will be discussed within section 4.10.4

To aid a complete comparison between sample porosity measurements and surface morphology, two images of the zinc bonded LPPS coated sample can be seen in Fig. 4.10

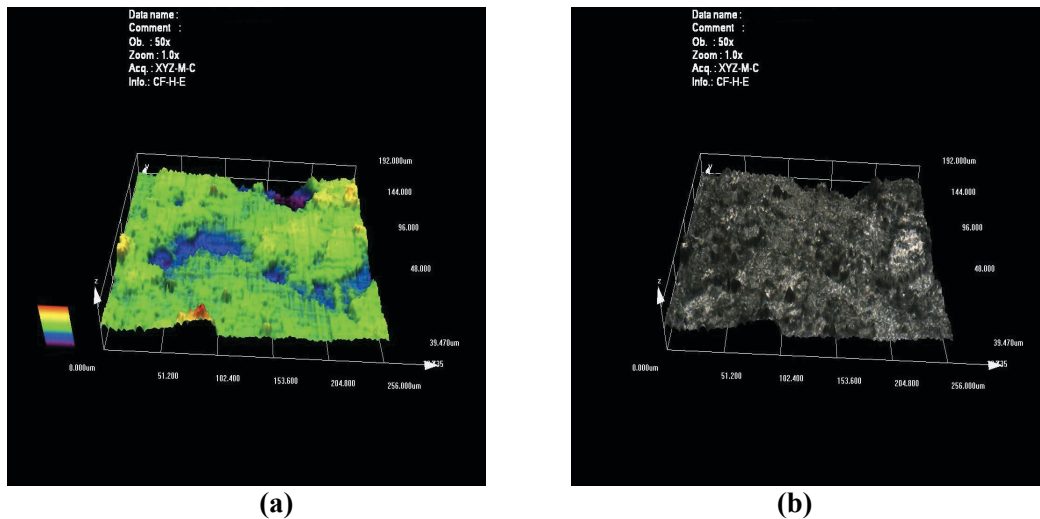
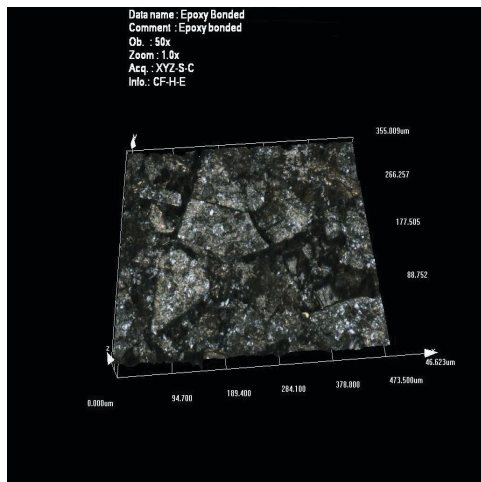


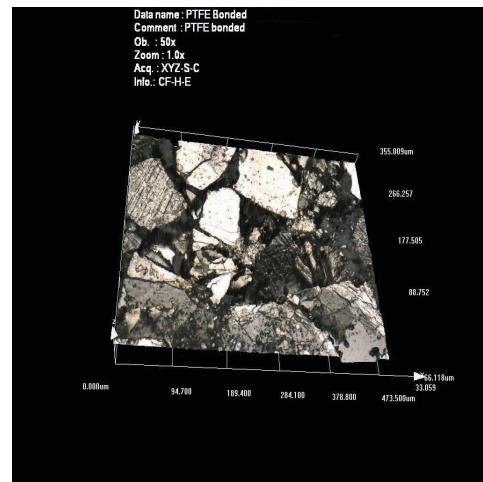
Fig. 4.10 Depicts the surface morphology of a zinc bonded LPPS coated sample (a) shows a 3D stacked composite image (b) shows the 3D stacked image with 2D real colour image overlaid.

From the images above it can be seen that within the zinc bonded samples there is clear evidence to support the incorporation of porosity during production (depicted by the blue/purple/black areas) from surface morphology. As with the epoxy bonded sample it is expected that this surface porosity would provide access to the network of porosity running through the entire structure. It can be seen that the surface of the MQP (depicted in green) is much rougher than those seen in the epoxy and PTFE bonded samples, this can be attributed to the LPPS zinc coating applied to the sample. From the real colour image (Fig. 4.10b) it can be seen that the LPPS coating applied to the surface of the zinc bonded sample is not composed of a single smooth coherent layer, but instead it appears to be made up of clusters of zinc globules. This effect can be attributed to the nature of the coating process whereby zinc vapour is deposited indiscriminately upon the surface of the sample. To produce a continuous protective coating the layer of zinc would have to be much thicker, but as a consequence the magnetic properties would suffer as a result of this dilution effect. It should be noted that the LPPS coating technique has not been optimised for this application. Previous applications have seen it used as a surface coating for NdFeB sintered magnets (Walton et al., 2000).

It should also be noted that there is a marked difference between the surfaces of the epoxy and PTFE bonded samples in terms of MQP exposure. This evidence will be used to support the corrosion behaviour hypothesis within a variety of aqueous solutions (DI water, Dex-Cool/DI water, Dex-Cool).



(a)



(b)

Fig. 4.11 Depicts the surface morphology through a real colour image of (a) epoxy bonded sample. (b) PTFE bonded sample.

From Fig. 4.11a it can be seen that the appearance of the epoxy bonded sample surface is noticeably duller than that of the PTFE bonded sample. This can be attributed to the thin layer of epoxy resin that is applied to every MQP during the single particle encapsulation process. By contrast the surface of the PTFE bonded sample is relatively shiny on the most part, indicating that there is a large surface area of MQP that is directly exposed to environmental conditions. This surface appearance can again be attributed to the bonding media and blending process. As there is no intimate bonding between PTFE and MQP, during the blending process PTFE will not adhere to the surface of the MQP unlike the epoxy resin. This leaves MQP at the sample surface relatively unmodified and exposed. The MQP only becomes integrated into the structure of the PTFE matrix upon sintering whereby the individual PTFE particles form a continuous matrix around the MQP forming a water proof barrier. Any particles outside this impermeable barrier i.e. particles located at the surface will be vulnerable to attack by environmental moisture.

The corrosion behaviour of both epoxy and PTFE bonded samples is dictated by the bonding media and its application to/interaction with the MQP surface. The single particle encapsulation technique utilised in epoxy bonded sample production and the relatively large surface area of uncoated MQP at the surface in PTFE bonded samples due to PTFE/MQP interactions during blending will shape how these composites perform under various environmental conditions. This will be discussed in greater detail within section 4.9 of this chapter.

4.9 Alternate Bonding Media Aqueous Corrosion Performance

The bonding media that initially performs the best from Fig. 4.7 in terms of H_{ci} losses is the epoxy resin. Initial losses are relatively small compared to those for the PTFE and zinc bonded samples. This indicates that there are factors at work within the epoxy resin structure that only serve to slow the rate of water ingress towards the MQP without preventing water uptake completely. Although initial losses were small the decrease in coercivity was steady. After 1008 hours of exposure to DI water the coercivity of the epoxy bonded sample had decreased to approximately 52% of the initial value.

It can be seen from the gradient of the epoxy curve that if the aqueous environmental exposure test were to be continued over a longer period of time, further losses of H_{ci} would occur. It is safe to assume that given enough time the losses in terms of H_{ci} would reach similar levels to that of the zinc bonded sample and maybe beyond. This behaviour could be attributed to the permeability of the epoxy resin structure to water.

It is highly likely that these small and steady losses in coercivity could be attributed to a combination of the liquid coating technique employed to apply the epoxy resin to the MQP and the entangled polymer network/chains of the resin that would hinder the movement of

water through these nanopores. This method of liquid coating ensures that each individual particle is completely encapsulated meaning water would have to filter through a layer of epoxy resin approximately 10µm thick before reaching the surface of any MQP. This applies in particular to MQP located at the surface of the sample, which if produced utilising different binders, that did not benefit from the liquid coating technique, the surface MQP would not be afforded the same protection. During uniaxial pressing the forces required to produce a bonded magnet cause the epoxy resin to become liquid and flow between the MQP producing uniform coverage and entangling the polymer chains from neighbouring resin encapsulated MQP.

Although particles are completely encapsulated by this epoxy resin coating it does not prove to be an impermeable waterproof barrier. It can be seen from Fig. 4.3 that epoxy resin is in fact permeable to water; this is supported by the increase in mass observed during exposure to a humid environment. Total submersion in water is likely to produce much greater changes in mass; this is supported by the fact that much larger coercivity losses are observed during exposure to the DI aqueous environment. It could be said that initially the PTFE binder performs poorly over the initial 168 hours, although only when compared with that of epoxy resin bonded samples. The initial rapid rate of decline in H_{ci} accompanied by a relatively small increase in mass is likely to be attributed to the easily accessible unmodified MQP at the surface of the sample and a certain degree of MQP exposed surfaces due to interconnected porosity. Unlike their epoxy bonded counterparts PTFE bonded MQP do not have the benefit of individual particle encapsulation through the liquid coating technique. This means any MQP located at the surface of the sample are immediately exposed to the surrounding environment. After the initial rapid loss of H_{ci} over the first 168 hours of exposure the gradient of the curve flattens to a plateau. The

gradient of this curve provides strong evidence that the PTFE binder is performing well at shielding the MQP within the bulk material from environmental effects taking into account initial surface MQP attack. The continuing minor decreases in H_{ci} could possibly be due to the volume of porosity incorporated into the structure of the sample (8.6%), allowing access to a limited surface area of MQP within the bulk of the sample. Evidence to support this hypothesis is provided in the form of Fig. 4.12, which shows the results of exposure in the environmental chamber.

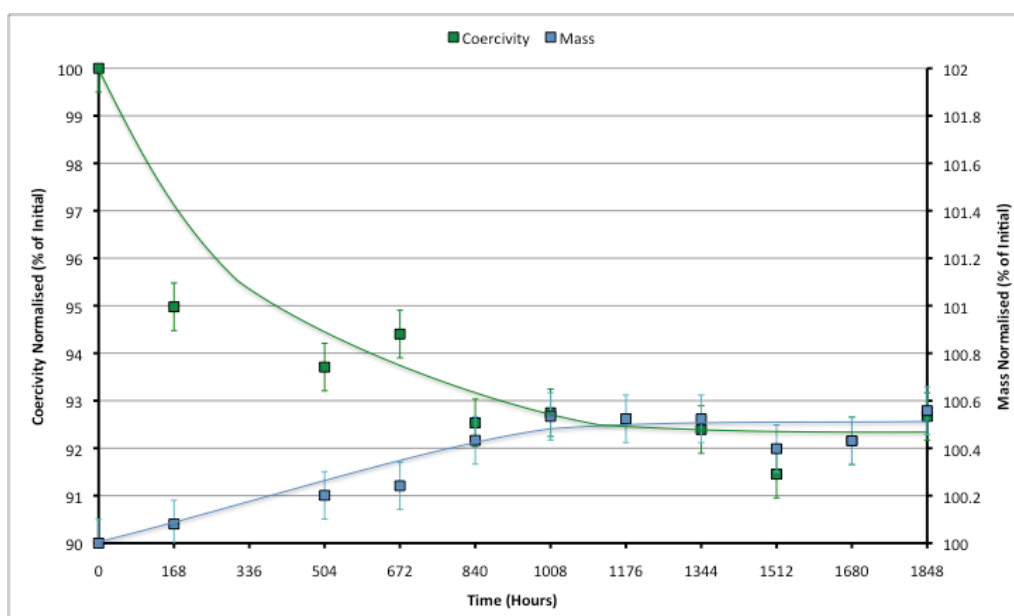


Fig. 4.12 Depicts the correlation between normalised mass (%) against normalised coercivity (%) with time for an MQ-I PTFE bonded sample exposed to 80°C at 85% humidity.

From Fig. 4.12 a plot of normalised H_{ci} against normalised mass with time, for a PTFE bonded sample can be seen. At first glance it is clear that for a relatively large decrease in H_{ci} only a small change in mass was required. For the PTFE bonded sample to suffer H_{ci} losses of approximately 95% of the initial value, a mass increase of only 0.1% of the initial

mass is required. This evidence suggests that the H_{ci} losses are initially occurring as a result of attack of unprotected surface MQP.

To highlight the stark contrast between the corrosion behaviour displayed by both epoxy and PTFE bonded samples a plot of normalised H_{ci} against normalised mass was produced using the same data as that for Fig. 4.4 and Fig. 4.5 This can be seen in Fig. 4.13

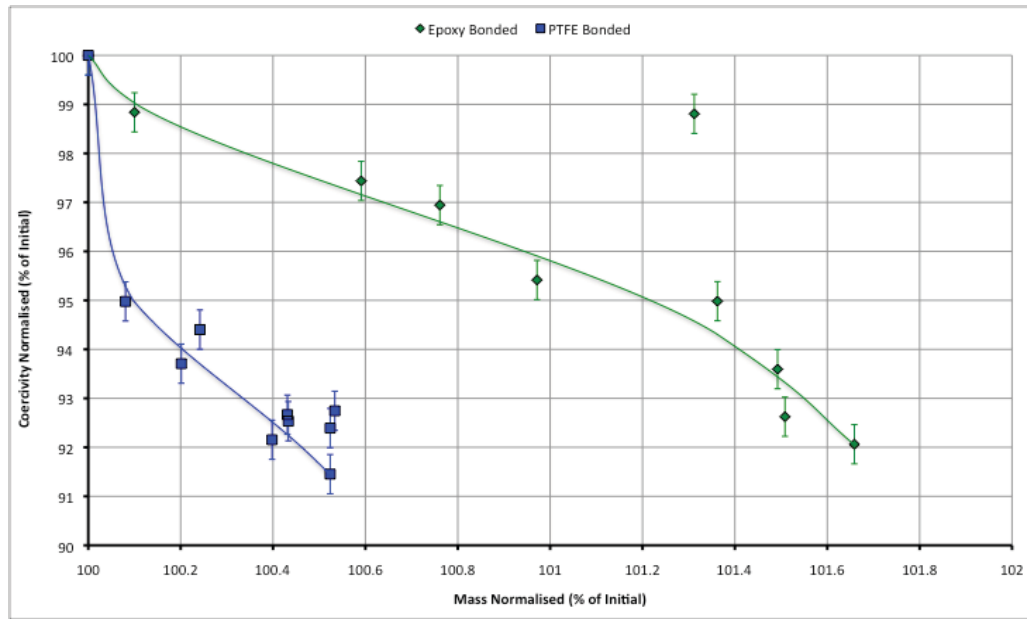


Fig. 4.13 Depicts the correlation between normalised coercivity (%) against normalised mass (%) for an MQ-I epoxy bonded sample (green) and a PTFE bonded sample (blue) exposed to 80°C at 85% humidity.

Fig. 4.13 further demonstrates the relationship between mass increase i.e. water ingress and H_{ci} of epoxy and PTFE bonded samples. From this it can be seen that the PTFE sample only requires a mass increase of approximately 0.1% to invoke a 5% decrease in H_{ci} . Whereas the epoxy bonded sample requires a mass increase of approximately 1.4% to invoke the same 5% decrease in H_{ci} . The small mass increase of the PTFE bonded sample relative to its epoxy bonded counterpart can be attributed to the impermeable nature of the PTFE binder. As a result, any mass increases observed for the PTFE bonded sample will

be predominantly due to the formation of corrosion products, rather than as a result of water ingress/absorption by the matrix. In contrast the mass increase of the epoxy bonded sample can predominantly be attributed to the absorption of water by the epoxy resin. This relatively large increase in mass is accompanied by a relatively small decrease in H_{ci} . This data supports the hypothesis in that the relatively high H_{ci} losses associated with such a small mass increase in the PTFE bonded samples this indicates that the majority of these losses can be attributed to attack of exposed surface MQP.

Fig. 4.14 shows normalised coercivity (%) against time for PTFE bonded samples in the water bath and environmental chamber. To aid comparison the results obtained for the equivalent epoxy bonded samples have been overlaid using a dashed line. The epoxy bonded samples can be identified by the corresponding colour dashed line.

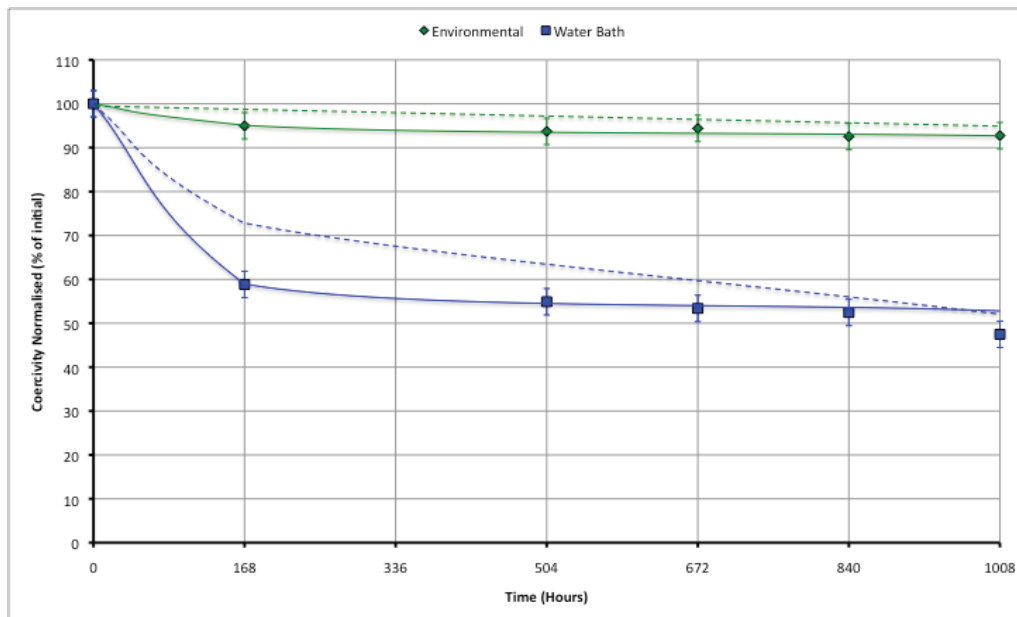


Fig. 4.14 Depicts normalised coercivity (%) against time for MQ-I PTFE bonded samples exposed to a spectrum of moisture containing environments. Overlaid onto the chart are the corresponding epoxy bonded curves (---) (Environmental Chamber samples exposed to 80°C at 85% humidity, Water Bath samples fully submerged in DI Water at 80°C)

From the results displayed in Fig. 4.14 it can be seen that the epoxy bonded samples (represented by ---), consistently outperform the equivalent PTFE bonded samples in terms of preventing H_{ci} losses upon exposure to moisture. Although this may be true over the 1008 hour period in which this testing took place, the gradient of curves representing the epoxy bonded samples would suggest that the H_{ci} would continue to decline had exposure been continued. On the other hand it would appear that the PTFE bonded samples had suffered the vast majority of their H_{ci} losses within the first 168 hours. As previously discussed this was thought to be a result of the exposure of unprotected surface MQP to environmental moisture. When comparing the curve gradients of the PTFE to the epoxy bonded samples after 168 hours exposure the PTFE sample curves are almost flat suggesting either no, or rather small H_{ci} losses.

4.10 Dex-Cool (ethylene glycol (EG)) and Aqueous Corrosion Performance

Due to the requirement for information regarding the influence of Dex-Cool within the aqueous environment on the corrosion resistance properties of bonded magnets it seemed prudent to run this study along side the initial investigation into the performance of alternate bonding media (section 4.6) in aqueous environments. This will allow the effect of differing concentrations of Dex-Cool on performance of bonding media from the preliminary investigation to be compared and contrasted. Within this section of the study two different concentrations of Dex-Cool were utilised:

- 100% Dex-Cool in the as received “pure” form (100% Dex-Cool).
- Dex-Cool and DI water in a 1:1 ratio to give a 50/50 mix.

Fig. 4.15 shows the effect that varying concentrations of Dex-Cool has upon the corrosion behaviour of epoxy bonded samples.

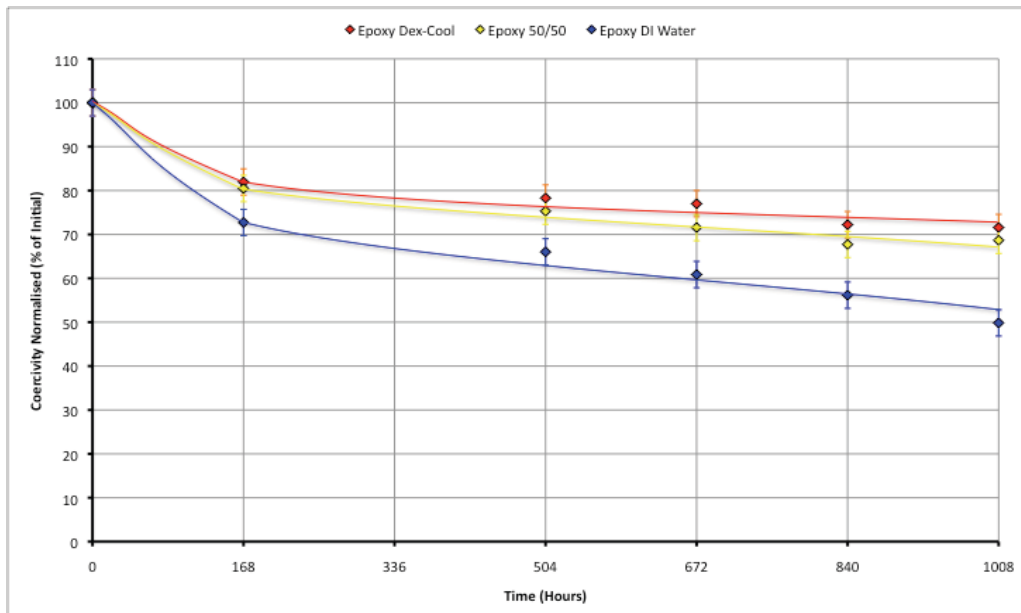


Fig. 4.15 Depicts normalised coercivity (%) against time for MQ-I epoxy bonded samples fully submerged in a spectrum of Dex-Cool/DI water environments at 80°C.

From Fig. 4.15 the effect of Dex-Cool addition upon the corrosion process in terms of H_{ci} losses can be clearly seen. Over the same time period both the 50/50 solution of Dex-Cool and DI water, and the “pure” Dex-Cool managed to preserve approximately 20% of the initial H_{ci} when compared to the performance of the same epoxy resin in DI water. This is a significant improvement. It is worth noting that the performance of the 50/50 and “pure” Dex-Cool are not too dissimilar, despite there being only half the volume of Dex-Cool in the 50/50 solution. This would suggest that the decrease in H_{ci} losses should not simply be attributed to the presence of a decreased availability of water molecules, otherwise one would expect the curve for 50/50 solution to lay equidistant from the “pure” Dex-Cool and DI water curves. It can be said with certainty that this phenomenon is not due to rogue data as or a set of erroneous results. Fig. 4.16 lends support to the positive effects observed through the addition of Dex-Cool on H_{ci} losses over time.

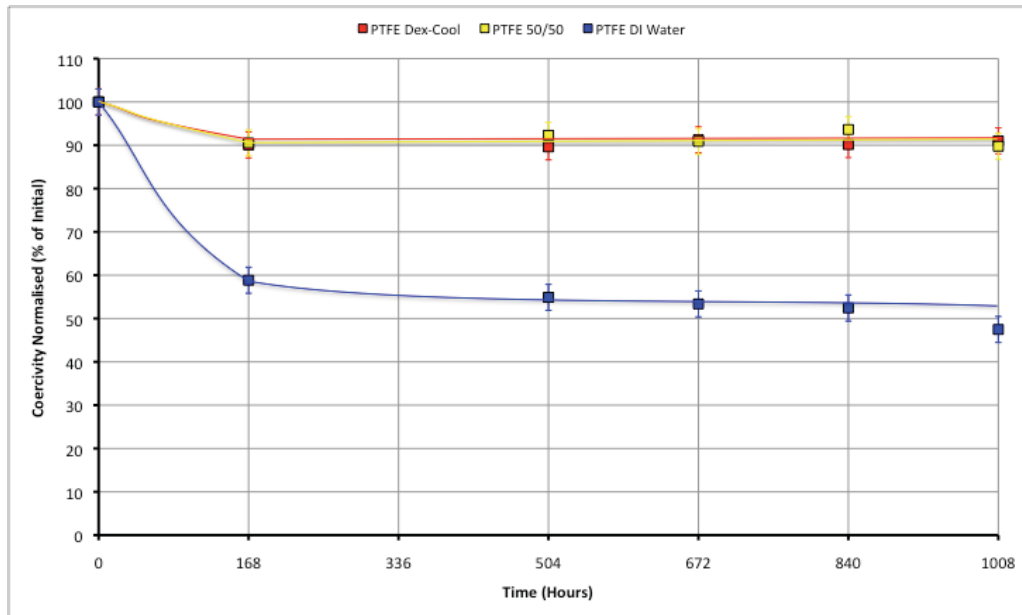


Fig. 4.16 Depicts normalised coercivity (%) against time for MQ-I PTFE bonded samples fully submerged in a spectrum of Dex-Cool/DI water environments at 80°C.

The plot seen in Fig. 4.16 depicts the corrosion behaviour of PTFE bonded samples in the presence of Dex-Cool additions. It is apparent that the two samples in the Dex-Cool containing solutions have retained over 90% of the initial H_{ci} after exposure to the aqueous environment at 80°C for 1008 hours. This is in stark contrast to the samples exposed to DI water for the same duration, which after only 168 hours had suffered H_{ci} losses in the region of 40% of the initial value. After 1008 hours the H_{ci} of the sample exposed to DI water was around 50% of the initial value.

Fig. 4.17 shows a plot conveying the performance of the zinc binder within the Dex-Cool modified aqueous environment.

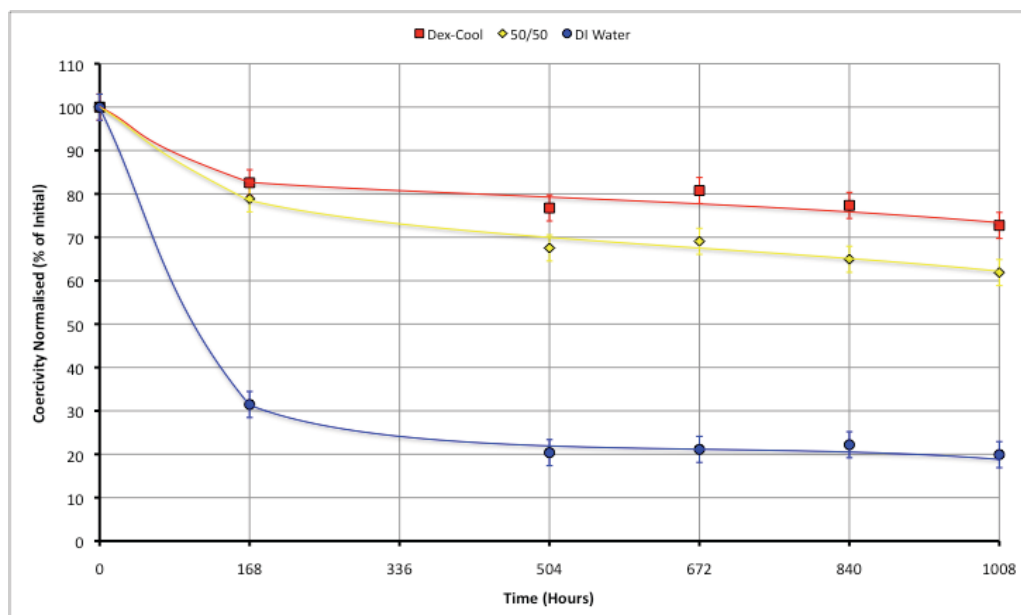


Fig. 4.17 Depicts normalised coercivity (%) against time for MQ-I zinc bonded samples fully submerged in a spectrum of Dex-Cool/DI water environments at 80°C.

From Fig. 4.17 it can be seen that the same positive effects associated with Dex-Cool additions from the epoxy and PTFE bonded samples is also true for that of the zinc bonded samples. The introduction of Dex-Cool has facilitated the retention of approximately 70%

and 60% of the initial H_{ci} values for “pure” Dex-Cool and 50/50 Dex-Cool solutions respectively. Again this is a significant improvement upon the 20% H_{ci} value for the sample exposed to DI water for 1008 hours. The zinc binder has been the poorest performer in terms of providing protection against H_{ci} losses throughout the testing thus far so it is promising to see the much-improved retention of H_{ci} through the addition of Dex-Cool. Although, as a result of the consistently poor performance of the zinc over the duration of testing, it was deemed that further investigation was not warranted within the scope of this study. Efforts would be concentrated on binding materials displaying more promise in terms of retaining H_{ci} values closer to pre moisture exposure levels.

To aid in the comparison of the data from Fig. 4.15 and Fig. 4.16 it has been presented on the same chart. This plot can be seen in Fig. 4.18, it shows the results of exposure to the spectrum of Dex-Cool solutions for epoxy and PTFE bonded samples. The curve for epoxy bonded samples can be identified through the use of a dashed line with corresponding colours.

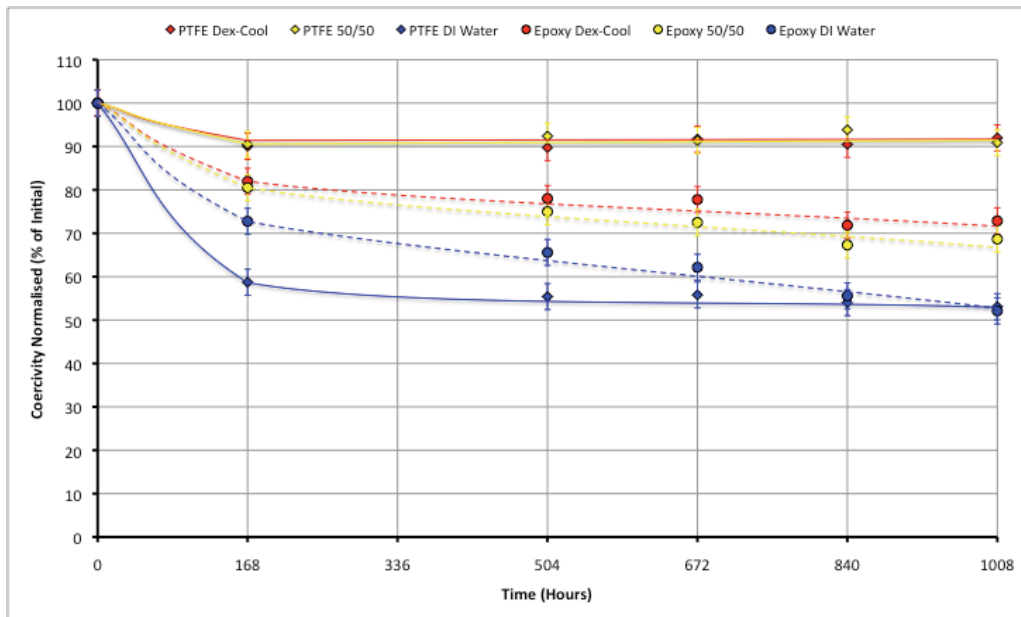


Fig. 4.18 Depicts normalised coercivity (%) against time for MQ-I PTFE bonded and epoxy bonded (---) samples fully submerged in a spectrum of Dex-Cool/DI water environments at 80°C.

Fig. 4.18 provides clear evidence that the addition of Dex-Cool to a system in which bonded magnets are operating greatly reduces H_{ci} losses suffered by the MQP. The same phenomenon is also observed in samples with what would be considered a high degree of porosity incorporated i.e. zinc bonded MQP. Understanding the mechanism that provides protection to the MQP from the process or the effects of aqueous corrosion could facilitate the use of Dex-Cool within other areas of the life cycle of magnetic materials, rather than solely during operation.

4.10.1 Dex-Cool (EG) Aqueous Corrosion Inhibition Mechanisms

Determining the actual mechanism by which Dex-Cool prevents H_{ci} losses through experimental research is beyond the scope of this study due to constraints upon time. It is possible however to offer a plausible explanation through a survey of literature in conjunction with interpretation of experimental data.

When considering possible mechanisms for the improved corrosion resistance of MQP in the presence of Dex-Cool the most obvious factor to jump out initially would be, within the Dex-Cool containing solutions the volume of water available to react with the submerged MQP is at best reduced by half (for 50/50 solution). For samples exposed to “pure” Dex-Cool one would expect the effects of corrosion on H_{ci} to be near zero as there is no or very little water available within the solution for the aqueous corrosion process to play out. The data sheet for Dex-Cool details the water content to be anywhere between 1-3.99% by weight. Another factor worth considering is, EG will actively absorb moisture from the atmosphere, trapping this moisture through hydrogen bonding. This will cause the water content of Dex-Cool to rise steadily through the course of these investigations. This will affect the molar concentration of the EG/water solution and may alter the mixing scheme.

Logic dictates that if around half of the molecules contained within the solution are water molecules then the probability of a water molecule making contact with an MQP and disassociating are greatly reduced. Although from experimental evidence this would appear not to be the case. If this were the only factor at work then the values of H_{ci} losses for samples exposed to 50/50 solutions should lay equidistant from the DI water sample curve and the Dex-Cool curve. This would mean that H_{ci} losses due to corrosion would be directly proportional to the volume of water available within the solution. From experimental evidence gathered and illustrated by plots in Fig. 4.15, Fig. 4.16, Fig. 4.17 it can be seen that in each case the rates of H_{ci} losses for both Dex-Cool and 50/50 solutions display a maximum difference of approximately 10% for zinc bonded samples. It can be seen from Fig. 4.15 and Fig. 4.16 that the difference between Dex-Cool and 50/50 solutions for epoxy and PTFE bonded samples are much closer in terms of H_{ci}

preservation. This indicates there must be one or more factors at work influencing the interactions of water and MQP.

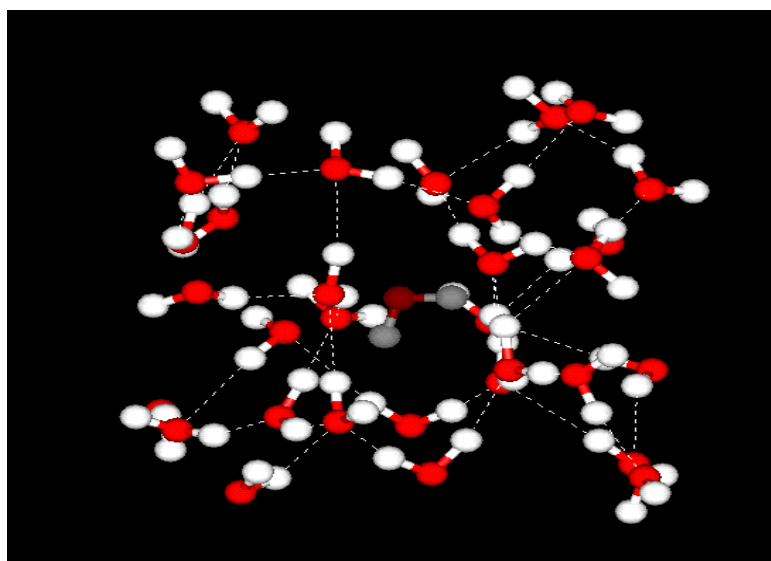
4.10.2 Ethylene Glycol/Water Hydrogen Bond Influence

Within the array of related literature surveyed it is indicated that the chemical structure/make-up of ethylene glycol (EG) is the key to interactions with itself and with water. EG is composed of weakly polar methyl groups and polar hydroxyl groups. It has one of the lowest ratios of methyl groups to hydroxyl groups among alcohols, this means that its behaviour in solution will be strongly influenced by hydrogen bonding interactions (Zhang et al., 2008). The tendency toward hydrogen bonding can be explained through the presence of these O-H groups at either end of the carbon chain and their interactions with hydrogen atoms from water molecules. The O-H groups participate in hydrogen bonding within the network of H₂O, driven by the hydrophilic tendencies of EG. Hydrogen bonding occurs as a result of the dipole-dipole interaction forces between O-H groups in EG and hydrogen (H) from H₂O (Kao et al., 2005). Both inter- and intramolecular hydrogen bonds are formed in ethylene glycol, although they are not as strong as those formed in water (Javadian et al., 2010).

Each O-H group consists of a hydrogen (H) atom covalently bonded to an oxygen (O) atom. The oxygen atom possesses a stronger electro-negativity, hence it will attract the electron cloud of the hydrogen nucleus and, by decentralising the cloud, leaves the hydrogen atom with a partial positive charge. Hence the $^-\text{O}-\text{H}^+$ group could be described as polarised. Due to the small size of hydrogen relative to the other atoms, the resulting charge, though only partial, represents a large charge density. A hydrogen bond occurs when this strong positive charge density attracts a lone pair of electrons from another atom, this atom becomes the hydrogen bond acceptor (Kao et al., 2005). One molecule of EG

contains two hydrogen bond donor sites and four hydrogen bond acceptor sites (Rodnikova et al., 2006).

Each water molecule can form four hydrogen bonds with other water molecules around it to form a continuous “net”, as would be found within the DI water aqueous environment. Many properties of liquid water can be attributed to its hydrogen bonding, for example water's affinity for itself i.e. the desire of its molecules to stick together. As a result of this it is liquid over a relatively large temperature range compared to other molecules of its size. It also possesses good solvent properties, being particularly good at dissolving ionic/polar substances. A representation of a partially ordered dynamic ‘net’ of water due to hydrogen bonding can be seen in Fig. 4.19.



**Fig. 4.19 Depicts hydrogen bonding amongst water molecules.
(Where hydrogen atoms are represented by white spheres
and oxygen atoms are represented by red spheres) (New York University, 2009)**

It is thought that additions of Dex-Cool (EG) alter the behaviour of water by disrupting the partially ordered, hydrogen-bonded, almost tetrahedral “net” that it forms with itself. The net in “pure” water is in constant flux with hydrogen bonds being broken and formed

constantly. The structure of EG and possible EG-water hydrogen bonding interactions can be seen in Fig. 4.20 whereby water bonds to the functional OH groups leaving the hydrophobic C-C backbone free.

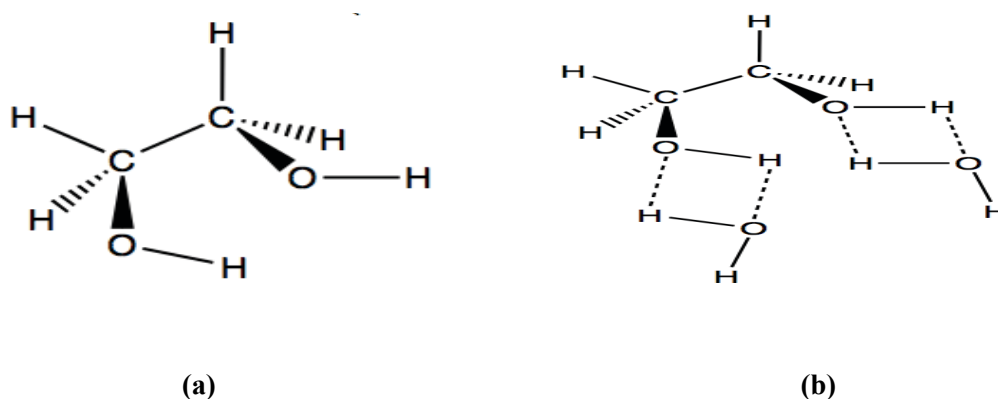


Fig. 4.20 Shows (a) The structure of ethylene glycol $\text{CH}_2\text{OH}-\text{CH}_2\text{OH}$ molecule. (b) Possible hydrogen bonding interactions between ethylene glycol and water (Zhang et al., 2008).

Results from a study carried out by (Zhang et al., 2008) has suggested that a complex of three EG molecules are required to bond with four water molecules at the maximum excess molar volume. The configuration of hydrogen bonding within this EG/water solution can be seen in Fig. 4.21. However (Saiz et al., 2001) believe that EG is capable of forming four hydrogen bonds with neighbouring molecules. Although this behaviour is difficult to accurately predict as the molecule exists in a number of trans and gauche configurations due to flexing of the C-C backbone, with some forms eliciting intramolecular hydrogen bonding.

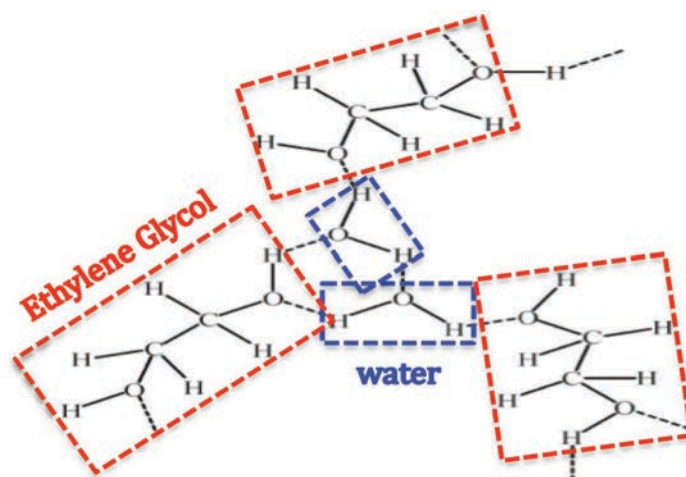


Fig. 4.21 Depicts possible hydrogen bonding interactions between ethylene glycol and water molecules of unknown concentration. Water molecules highlighted with red box. after(Zhang et al., 2008).

It can be seen from Fig. 4.21 that dissolving EG into water causes a considerable change to the previous largely uniform hydrogen bonded structure of water molecules seen in Fig. 4.19. The hydrogen bonding interactions in water no longer form an almost tetrahedral “net” due to the hydrophobic carbon-carbon backbone of the EG molecule (Koga, 2003). These molecules of EG are unable to conform to the tetrahedral “net” of hydrogen bonding in water due to its molecular geometry and presence of the methylene groups, neighbouring EG molecules have a tendency to orient their molecular dipoles parallel (Saiz et al., 2001). This is the type of change that maybe elicited through the addition of Dex-Cool in the 50/50 (Dex-Cool/DI water) solution.

4.10.3 Ethylene Glycol Mixing Schemes

A study conducted by (Koga, 2003) has found that in EG-water binary systems there are three distinct mixing schemes which are dependent upon solute (EG) concentration. These mixing schemes are important to our understanding if the corrosion inhibition mechanism

was determined to be related to the mobility of water molecules as a result of Dex-Cool additions. The conditions and mixing schemes are listed below:

- An H₂O-rich region – Mixing Scheme I: is a progressive modification of liquid H₂O by the solute, but the basic characteristics of liquid water are still retained. In particular, the bond percolation of the hydrogen bond network is still intact.
- An intermediate region consisting of two kinds of clusters, each rich in solute and H₂O respectively – Mixing Scheme II: the bond percolation nature of the hydrogen bond network of liquid H₂O is lost.
- A solute-rich region – Mixing Scheme III: The solute molecules are in a similar situation as in the pure state, most likely in clusters of its own kind.

We can speculate that if the concentration of solute were only sufficient to illicit mixing scheme I at the lower end of the EG concentration spectrum then there would likely be limited evidence of improved H_{ci} losses during aqueous exposure. Due to the water-rich nature of the solution initially there would likely be limited if any modification of the hydrogen bonding interactions until nearer the mixing scheme II threshold (Koga, 2003).

Within mixing scheme I OH groups in EG would participate in hydrogen bonding to the network of H₂O. As EG lacks symmetry in terms of the H donor/acceptor pair, the degree of hydrogen bond fluctuation inherent in water is retarded. The global average of the hydrogen bond probability is also reduced progressively as EG concentration increases. When the hydrogen bond probability reaches the bond-percolation threshold, the hydrogen bond network of H₂O is no longer connected throughout and mixing scheme II sets in. However, near the threshold of mixing scheme II the semi hydrophobic nature of EG, attributed to its C-C backbone causes the formation of “icebergs” with a concomitant reduction of the hydrogen bond probability of bulk H₂O away from solute. The reduction

in probability for the latter is also responsible for the loss of bond percolation resulting in the system undergoing a conversion to mixing scheme II (Koga, 2003).

Within mixing scheme III, which we can be certain is governing the behaviour in that of the “pure” Dex-Cool solution. Molecules of EG cluster together and interact with water molecules without forming a hydrogen bond network. The improved aqueous corrosion resistance in the presence of this solution was to be expected due to the lack of water in the environment. A graphical representation depicting mixing scheme thresholds with varying molar concentrations for the enthalpic interaction of EG within the EG-H₂O binary system can be seen in Fig. 4.22.

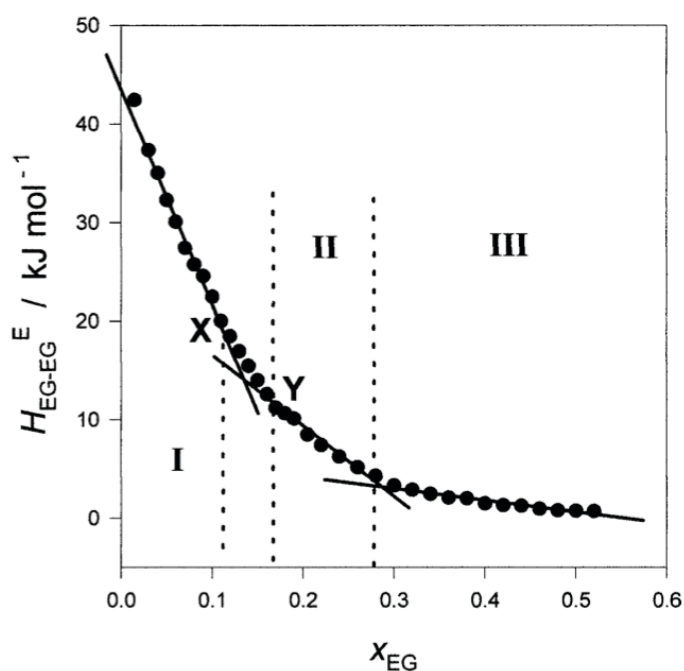


Fig. 4.22 Depicts enthalpic interaction between EG, H_{EG-EG}^E , in EG-H₂O at 25°C (Koga, 2003).

4.10.4 Possible Ethylene Glycol Related Corrosion Prevention Mechanisms

Calculations performed to establish the molar concentration of the 50/50 (EG/water) solution have indicated that the X_{EG} is approximately 0.28-0.3. It is likely that the concentration of EG in water utilised for the 50/50 (Dex-Cool/water) solution would be sufficient to induce mixing scheme II near the upper epsilons. As a result of this there will likely be a disruption in hydrogen bonding behaviour of water as previously discussed. At this concentration we are likely to witness the effects of hydrogen bond disruption. Koga suggested that in order to minimise interactions between the water molecules and the non-polar hydrophobic backbone, EG may form “icebergs” with itself, whereby the hydrophobic backbone will lie in the centre of the “iceberg” to avoid interaction with H_2O . As this occurs “shells” of water will form around the EG cluster as the system seeks to maximise the number of hydrogen bonds. Thus, through the clustering of EG molecules the overall entropy of the system is increased (Koga, 2003). It is possible to believe that these “icebergs” could interact with the porosity present within the structure of the bonded magnet in some form to hinder water mobility.

Other possible interactions with EG and water which may retard the corrosion behaviour of MQP within the aqueous environment could be the formation of an EG bilayer as a result of “iceberging”. It is also feasible that if the EG is forced to form “icebergs” with itself in solutions at molar concentrations sufficient to elicit mixing scheme II. Then, there may also be a situation in which the hydrophobic C-C backbone of EG molecules would be driven by the force of hydrogen bonding to attach to the surfaces of the submerged sample in order to increase the overall entropy of the system. In this case the sample would simply provide sites i.e. rough surfaces for the C-C backbone to attach itself, away from water

molecules, thus achieving exclusion from hydrogen bonding interactions within the EG/water solution and maximizing the entropy of the system.

It is still largely unknown if this protective film bilayer would form on any surface present within the solution or if the layer formed is specifically attracted to the surface of the MQP as it is with a magnesium electrode in a study conducted by (Song and StJohn, 2004). This study was conducted into the corrosion resistance of magnesium engine blocks in the presence of EG/water solutions. It found, from capacitance measurements that EG was being adsorbed onto the surface of a magnesium electrode. The greater the concentration of EG within the solution, the thicker the EG layer and the more complete the coverage of the magnesium surface. This layer of EG at the surface of magnesium decreases surface access to the water, thus preventing the occurrence of the corrosion process (Song and StJohn, 2004).

If it were the case that the mechanism responsible for preventing surface access to water was through the formation of an EG bilayer, it is possible that low concentrations of EG could be equally as effective at improving the corrosion resistance behaviour of MQP within a submerged aqueous environment. The investigation of a larger range of EG concentrations was outside the scope of this study but is a definite candidate worthy of further investigation.

If, like in the (Song and StJohn, 2004) study, EG is attracted to the surface of the MQP as it is with magnesium, then this could explain why the Dex-Cool is much more effective at preserving the H_{ci} of PTFE bonded samples than that of their epoxy bonded counterparts. The key difference between the epoxy and PTFE bonded samples lies with the surface of the MQP. The surface of epoxy bonded MQP is heavily modified through the single particle encapsulation technique utilised to apply the epoxy coating. It is possible that this

large surface area provided by the network of cross linked polymer chains provides a suitable place for the C-C backbone of EG to seek refuge from hydrogen bonding water molecules. However, due to the structure of the epoxy resin coating and the size of the EG molecule in comparison to water molecules, it is feasible that EG will form an “iceberg” on the surface of the epoxy resin rather than on the surface of the MQP. This is because the network of cross-linked polymer chains will limit access of the EG molecules to the MQP surface as they are too large to slip through these nanopores, however, it will still be possible for the smaller water molecules to percolate through these tiny voids leading to disassociation at the surface of the MQP (Soles and Yee, 2000).

By comparison the exposed MQP surfaces of the PTFE bonded samples are much cleaner in that there is no intimate bonding between the surface of the MQP and the PTFE even upon sintering under vacuum. The heat treatment performed causes a softening of the PTFE polymer chains and upon cooling these chains will solidify upon the surface of neighbouring MQP. Due to processing differences this adhesion will only involve a very thin web of PTFE that is closest to the MQP flake. Whereas, epoxy resin during uniaxial pressing will become liquid and flow between MQP to produce an evenly distributed uniform epoxy interconnected web between MQP.

It is likely that EG is improving corrosion resistance primarily by acting upon the unprotected surface MQP within the PTFE bonded samples. This seems to be the case as the initial large decrease of approximately 40% H_{ci} that was apparent in PTFE bonded samples exposed to DI water for only 168 hours was reduced to around 10% H_{ci} losses for samples in a 50/50 (Dex-Cool/water) solution for an equal duration. It is also worth noting that the most pronounced effect produced by the addition of Dex-Cool was seen in the zinc bonded sample. Here the H_{ci} losses experienced by zinc in DI water were around 20% of

the initial value after 1008 hours. For zinc bonded samples exposed to the 50/50 solution over the same period of time H_{ci} losses were limited to approximately 62% of the initial value. The effect of Dex-Cool on epoxy bonded samples was far less pronounced, approximately an 8% improvement in H_{ci} losses over the initial 168 hours, possibly due to the individual particle encapsulation method employed to coat the MQP before bonding. Due to the size of the nanopores present in the epoxy resin structure it would be difficult for a molecule the size of EG to reach the MQP surface to form a protective coating to prevent the disassociation of water.

Despite the dramatically improved corrosion resistance, in terms of H_{ci} losses, during exposure to the 50/50 (Dex-Cool/water) solution at 80°C, especially for zinc and PTFE bonded samples. The mechanism that preserves the H_{ci} of samples remains largely unclear. Although the evidence gathered at the moment is showing that the greatest protection is offered to samples with the most easily accessible MQP component i.e. the zinc bonded sample which is composed of 15.3% porosity.

Logically the EG mechanism could prevent the degradation of H_{ci} at one of two points; either the Dex-Cool performs a “hydrogen blocking” role, a water dissociation prevention role, or a combination of both. Further investigations will be carried out on the same MQP-B material utilising HADS techniques to determine which is the case.

The discussion generated from the results of Dex-Cool additions it appears that this body of work has provided a solid base on which future work can be based. It has found that additions of Dex-Cool dramatically improve the corrosion resistance of bonded magnets submerged in aqueous environments where access to the MQP surface is uninhibited. The area of work centred on Dex-Cool probably warrants an investigation in its own right due to the promising results shown. This would provide an understanding of much greater

depth into the mechanisms at work, the interactions between EG and water and possible interactions of EG with MQP. As it stands, from the current experimental evidence gathered within the scope of this study we can only speculate as to why we are seeing these dramatic improvements in H_{ci} losses in the presence of Dex-Cool supplemented with the published work of others from unrelated studies. It would be highly beneficial if the mechanisms at work could be fully understood.

4.11 Aqueous Corrosion Prevention Through Surface Coatings

The aims of this section of the study were to build upon previously gathered data from the initial corrosion investigation into binder performance. Due to the poor performance of the zinc bonded LPPS coated samples, these were omitted from this section. This batch of testing was to include:

- Extended exposure times up to 1848 hours.
- The use of Dex-Cool in a 50/50 (Dex-Cool/DI Water) solution.
- The application of PTFE coatings to samples due to its outstanding performance as a barrier to water.
- The application of a Qsil (silicone) coating.
- Repetition of uncoated PTFE and epoxy bonded samples as per the initial investigation, run in parallel with PTFE coatings over the extended testing period, in an attempt to determine the reproducibility of previous results gathered.

4.11.1 High Humidity Environment Mass Measurements

As with the initial investigation changes in mass can be an important tool to aid in the prediction of corrosion resistance levels offered by bonding media during exposure to moisture. More importantly, significant changes in mass would indicate that moisture is

penetrating the structure in some way, this penetration will generally lead to the degradation of magnetic properties namely H_{ci} . Measuring changes in mass is particularly important for this section of the study as it is a primary indicator of how effective the surface coating is at providing a barrier to prevent the water ingress. To allow accurate comparisons to be made between coated and non-coated samples all lines of best fit will be shown on the same plot.

Fig. 4.23 shows a plot of the change in mass experienced by epoxy bonded samples, both coated and uncoated, exposed to 85% humidity at 80°C.

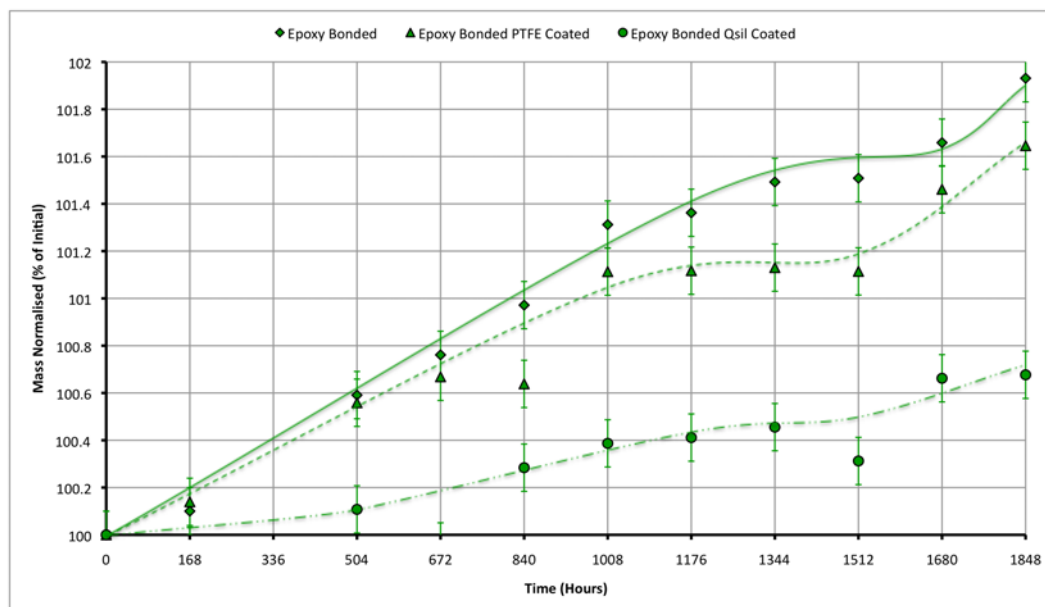


Fig. 4.23 Depicts normalised mass (%) against time for coated and uncoated epoxy bonded samples exposed to 80°C at 85% humidity.

From Fig. 4.23 it can be seen that the application of PTFE and Qsil coatings onto the surface of the epoxy bonded samples appear to retard levels of water ingress compared to those of the uncoated samples. The Qsil coating in particular seems to perform exceptionally well with a mass increase of approximately 0.7% over the duration of the test. The PTFE coating performed marginally better than the uncoated sample in

preventing water ingress, with a mass increase in the region of 1.6% compared with that of the uncoated sample at 1.9%.

At this juncture it is worth pointing out that although PTFE has previously performed well as a bonding medium, during those tests the sample had been subject to high forces during uniaxial pressing and a sintering heat treatment. This causes the polymer to densify and form a single coherent layer trapping the MQP within the matrix. Due to the temperature tolerances of the epoxy resin these samples could not be subject to the heat treatment at 370°C so the PTFE coating remained as more of a loose powdery layer with no adhesion to the surface of the bonded sample. Even if the epoxy resin had been able to withstand these relatively high sintering temperatures it is unlikely that the PTFE surface coating would have formed any kind of bonds with the epoxy resin due to the inert nature of PTFE.

Fig. 4.24 shows a plot of the same test for the batch of PTFE bonded samples both coated and uncoated for comparison. It should be noted that the y axis is not scaled the same as previous plots produced due to the range of data.

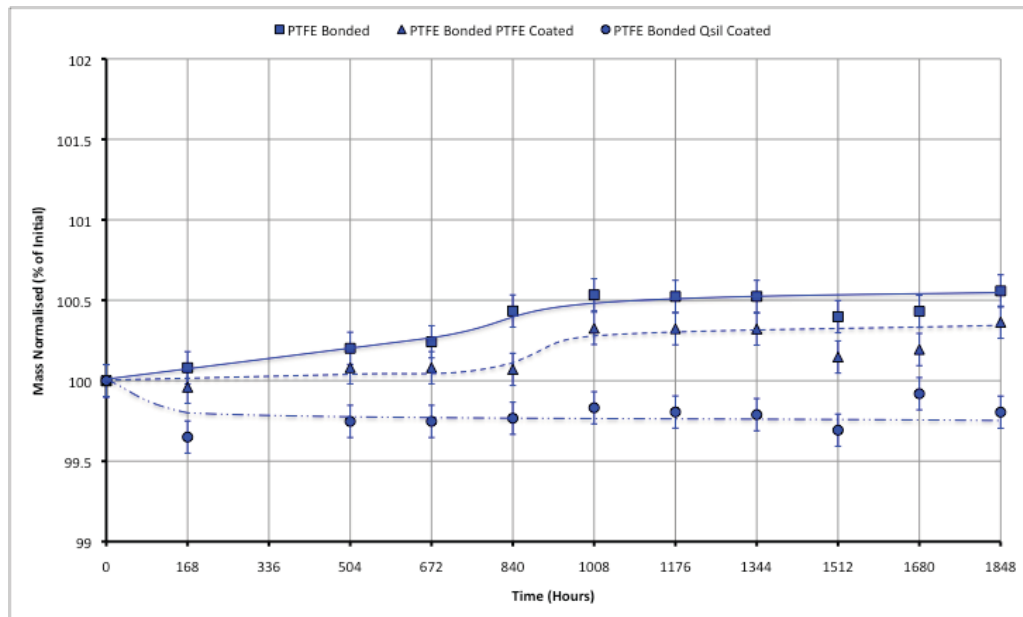


Fig. 4.24 Depicts normalised mass (%) against time for coated and uncoated PTFE bonded samples exposed to 80°C at 85% humidity.

Fig. 4.24 shows that through the application of a PTFE coating mass increases associated with moisture ingress and corrosion products are slightly decreased by around 0.2% when compared to the uncoated PTFE bonded sample. It is interesting to note that the Qsil coated sample has exhibited a decrease in mass of around 0.3%.

Qsil rubber is formed during a two part cross-linking reaction. Within the Qsil coating there may be some unreacted monomers still in their volatile state if the mixing ratio was not perfect or the two parts were not combined thoroughly. As a result of this it is possible that the Qsil rubber is slowly degrading during its exposure to the 80°C heat through the evaporation of these monomers. It may also be possible that it is not providing the water resistant barrier that was hoped for as if the Qsil is degrading at a constant rate then there is another factor at work here in both the epoxy resin and PTFE bonded samples. In the case of the Qsil coated epoxy resin, overall the sample mass is increasing masking the

degradation effects of the Qsil and then some, this mass change could likely to be attributed to water absorption by the epoxy resin and/or the formation of corrosion products. This may indicate that Qsil is not such a suitable barrier coating although this will be determined through H_{ci} measurements. In the case of the Qsil coated PTFE bonded sample there is an initial small decrease in mass of approximately 0.2% and then it appears to remain relatively constant. It is possible that the formation of corrosion product is counteracting the mass decrease through degradation of the Qsil coating. Again showing that it is likely that aqueous corrosion is occurring beneath the surface coating.

It would appear that the addition of surface coatings has made the mass change data less reliable in terms of the ability to monitor water absorption and thus predicting corrosion behaviour. Extra variables like the degradation of coatings upon exposure to heat play a part in the overall mass change, as with the Qsil coating. Also there may be issues with fragile coatings, such as the PTFE coating on the epoxy bonded sample. If small fragments of the coating break away during handling or as a result of stresses induced through corrosion product formation this may have a significant impact on how data is interpreted.

4.11.2 High Humidity Environment Coercivity Measurements

To gather data on the effects of aqueous corrosion upon bonded magnet samples treated with PTFE or Qsil surface coatings this section of the study will rely primarily upon H_{ci} measurements taken from hysteresis loops of samples at 168 hour intervals. This will allow an accurate profile of magnetic properties to be built up in relation to exposure time to a particular environment.

Fig. 4.25 shows a plot of H_{ci} values for epoxy bonded samples with and without coatings upon exposure to the high humidity environment. This will allow an accurate comparison to be made between coated and uncoated corrosion performance.

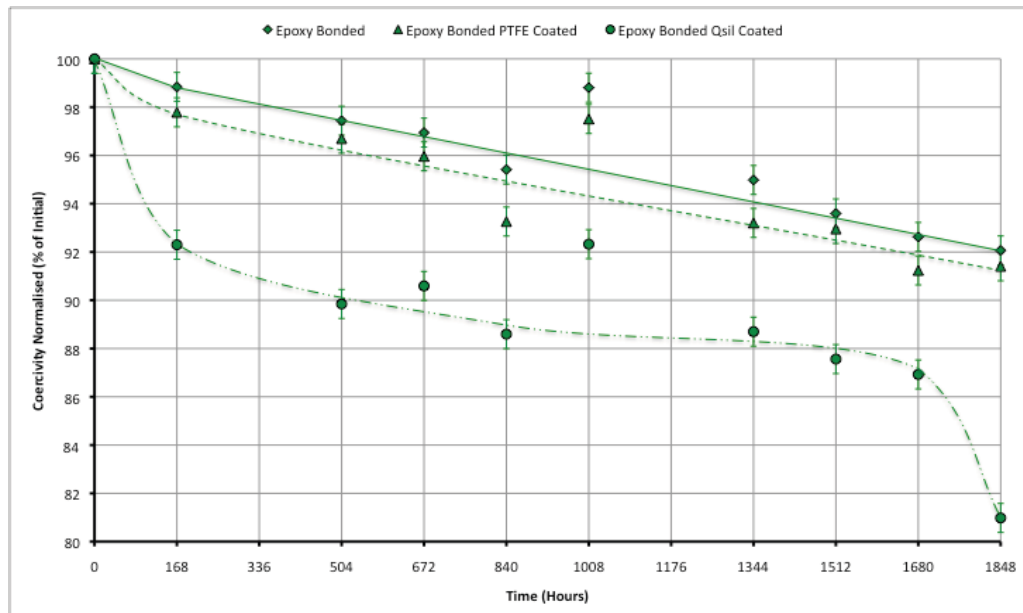


Fig. 4.25 Depicts the change in normalised coercivity (%) with time for MQ-I epoxy bonded samples with and without surface coatings exposed to 80°C at 85% humidity.

From Fig. 4.25 above it can be seen that the application of surface coatings to the epoxy bonded samples did not produce the desired positive effect on corrosion behaviour upon exposure to the high humidity environment. The PTFE coating displayed very little effect in preventing aqueous corrosion, although as previously pointed out significant improvements were not really expected due to the absence of the sintering process required to solidify the small particles of PTFE into a coherent layer. It can also be seen that the Qsil surface coating significantly affected the performance of the epoxy bonded sample with H_{ci} losses in the region of 81% of the initial value. It should be noted that this sample failed catastrophically after 1680 hours with a large crack propagating most of the way

through the bulk material. This is likely to have occurred while the magnetic measurement was being performed with the sample located between the pole tips of the electromagnet.

It seems that with the PTFE and Qsil surface coatings applied, as with any surface coating, it is only as strong as its weakest point. Any small pinhole in the coating as a result of a less than perfectly flat sample surface may result in water bypassing the coating and gaining access to the sample surface through the “back door”. This is likely to be the case with the PTFE coated epoxy bonded sample. At this point it is worth pointing out that, as a coating, even if the Qsil had performed well it would have been impractical to use due to the overall thickness ($\sim 1\text{mm}$). The detrimental effect which this extra material would have had upon the magnetic properties would have been unacceptable. As yet the mechanism by which the Qsil coating has increased the rate of H_{ci} decline is still unclear.

In Fig. 4.26 the same plot has been produced for coated and uncoated PTFE bonded samples.

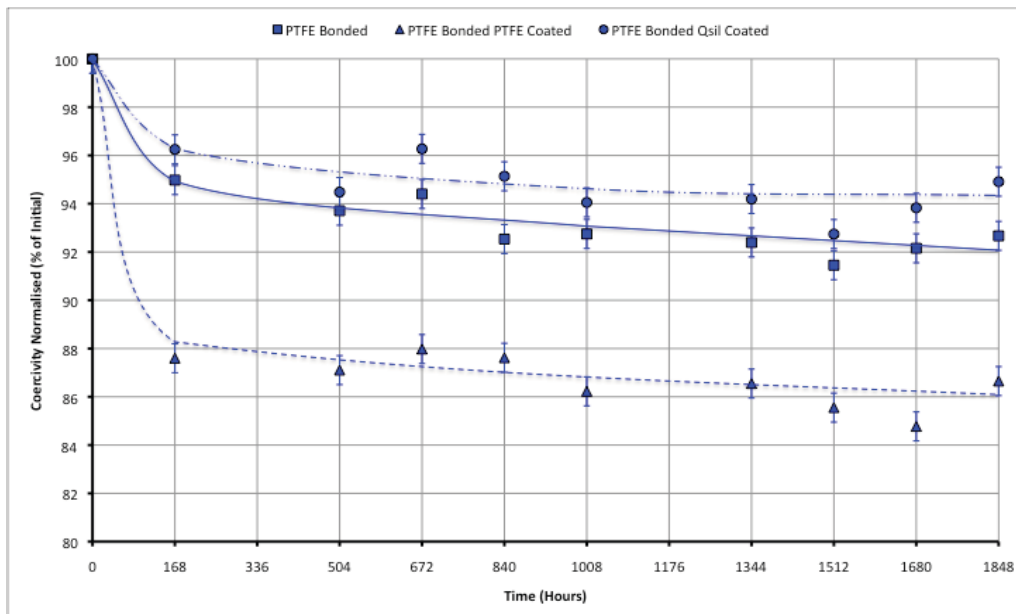


Fig. 4.26 Depicts the change in normalised coercivity (%) with time for MQ-I PTFE bonded samples with and without surface coatings exposed to 80°C at 85% humidity.

From Fig. 4.26 it can be seen that the Qsil coating offers improved corrosion resistance properties for the PTFE bonded sample. The degradation of the H_{ci} appears to plateau at approximately 94% of the initial value. This is a slight improvement on the performance of the uncoated sample, which from the gradient of the curve would appear that H_{ci} losses would continue after the measured 1848 hours came to an end. The coating that provided the least protection for the magnetic component of the PTFE bonded sample was the PTFE coating. After 1848 hours the H_{ci} had dropped to around 86% of the initial value. This is significantly worse than that of the Qsil coated or even the uncoated sample. This is surprising as the PTFE performed so well as a binder, yet this performance didn't translate into a protective coating. This phenomenon could possibly be attributed to the method of coating application.

From previous studies conducted into corrosion behaviour (Tattam et al., 1994), (Tattam et al., 1996a), (Tattam et al., 1996b), (Mokal, 1998) using PTFE as a binder for MQP. These studies also established a clear link between the porosity of samples and the rate/extent of aqueous corrosion damage. The studies utilised the rotary forging process (Penny and Slater, 1979) which is a novel powder compaction method whereby a floating die tool arrangement capable of applying a higher load to the compact is employed. Through this process it was possible to produce samples with much less porosity incorporated compared to conventional uniaxial pressing route. A schematic diagram of the rotary forging tool can be seen in Fig. 4.27

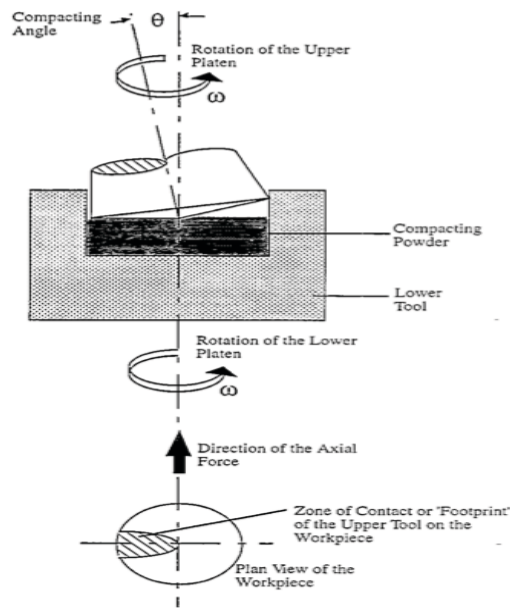


Fig. 4.27 Depicts a schematic diagram of the rotary forging process (Willey et al., 1997).

This rotary forging process produced PTFE bonded samples that were less susceptible to aqueous corrosion than their uniaxial pressed counterparts through the incorporation of less porosity into the sample. By applying the same logic it could be said that the spray on PTFE coating was not as effective at providing protection as the binding medium subject to uniaxial pressing due to the incorporation of porosity within the coating. This is possibly due to there being no compaction to densify and adhere the coating to the sample surface after application. It is likely that it would be largely covered by nano or micron sized pores possibly allowing the absorption of water in a similar fashion to that of the epoxy bonded samples. It is still unclear as to why the PTFE coating significantly worsened the corrosion behaviour compared to that of the uncoated PTFE bonded sample.

It is possible that the highly porous structure of the PTFE surface coating actively encourages the corrosion process by channelling the water vapour from the high humidity environment through the surface coating to any exposed MQP at the sample surface. The

nanopores incorporated into the PTFE surface coating would provide an ideal site for water vapour to condense and be transported to the underlying surface MQP via capillary action.

This is a suitable juncture to bring to the attention of the reader that a duplicate coated sample was produced to replicate each experimental configuration. This sample would only be subject to one magnetic measurement which would take place after 1848 hours. This was to allow comparisons to be made between samples that were measured on a weekly basis to ascertain if this frequent measurement caused significant damage to the surface coatings thus leading to an increased rate of aqueous corrosion.

From Table 4.2 it can be seen that samples with surface coatings which were subject to magnetic characterisation measurements on a weekly basis did experience detrimental effects as a result of the process. The effect of these measurements were particularly pronounced in the epoxy bonded Qsil coated sample and the PTFE bonded PTFE coated sample, with discrepancies between results of 12.76% and 11.37% respectively. It is likely that the damage to the sample coating occurred during the positioning of the samples between the pole tips of the permeameter. This simple comparison has highlighted a few important points. Firstly how ineffective the PTFE coating was when applied to the epoxy bonded sample due to the consistency of the results (<2%). Secondly the potential of the PTFE surface coating when applied to a PTFE bonded sample. Thirdly the frailties of both the PTFE and Qsil coatings, as irreparable damage had been caused during magnetic characterisation measurements while actively taking every precaution to not damage the coatings.

Table 4.2 Depicts the difference in recorded H_{ci} values (%) of coated samples exposed to the high humidity environment magnetically characterised every 168 hours versus one measurement after 1848 hours.

Sample Configuration	H_{ci} Value (%) Weekly Measurement Sample (after 1848 hours)	H_{ci} Value (%) Single Measurement Sample (after 1848 hours)	Difference in H_{ci} Value (%) due to coating damage
Epoxy Bonded PTFE Coated	92.16	94.10	1.94
Epoxy Bonded Qsil Coated	81.85	94.61	12.76
PTFE Bonded PTFE Coated	86.80	98.17	11.37
PTFE Bonded Qsil Coated	94.97	97.18	2.21

4.11.3 Aqueous Environment Coercivity Measurements

Primarily this branch of the investigation will be focussed on the effect of PTFE and Qsil surface coatings upon the corrosion behaviour of fully submerged epoxy and PTFE bonded samples. Repetition of tests run with duplicate samples will also enable accurate comparisons to be drawn from the initial full submersion testing performed over an extended period. This will also determine how reproducible results gathered from the initial investigation were whilst providing a glimpse of corrosion behaviour over a greater time period.

The plot seen in Fig. 4.28 shows the coated and uncoated corrosion behaviour of epoxy bonded samples exposed to a fully submerged environment at 80°C.

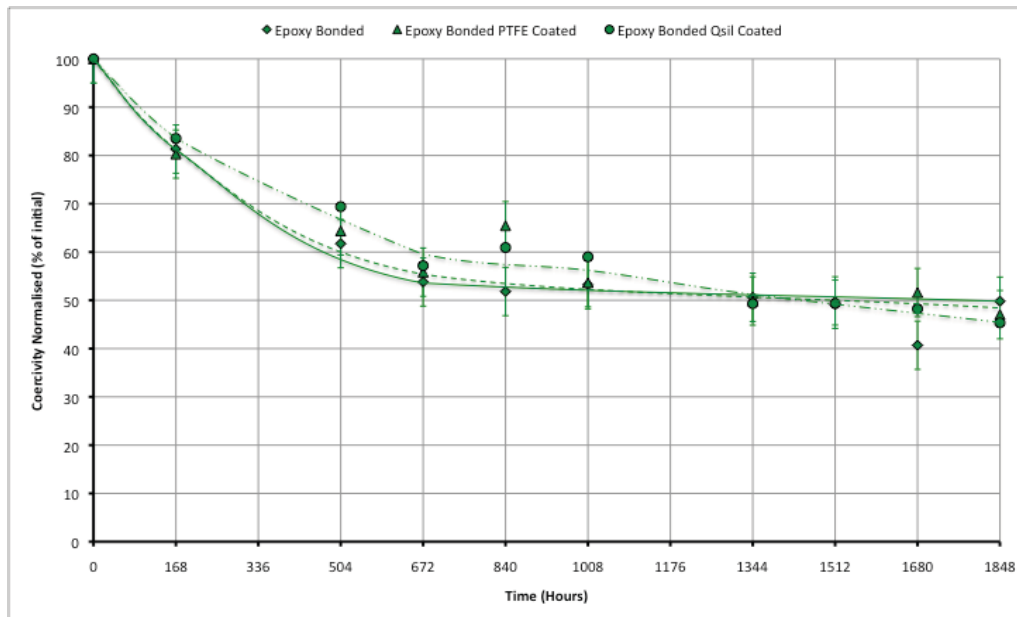


Fig. 4.28 Depicts normalised coercivity (%) against time for MQ-I epoxy bonded samples with and without surface coatings, fully submerged in DI Water at 80°C (Water Bath).

From Fig. 4.28 it can be seen that the Qsil and PTFE surface coatings had very little effect upon the corrosion resistance of the epoxy bonded samples. It could be said that the Qsil coating slightly delayed the onset of H_{ci} losses although this difference was not really significant. This poor coating performance as discussed previously would only require a single small pinhole to allow moisture in through the “back door” effectively bypassing the coating.

Most importantly from this plot it can be seen that after 1008 hours of exposure to the DI water the uncoated epoxy bonded sample retained approximately 52% of the initial H_{ci} value. This figure is in strong agreement with earlier testing performed when comparing this with an identical sample from Fig. 4.7. Previous predictions had suggested that the decline in H_{ci} would continue after the initial 1008 hours judging by the gradient of the curve in Fig. 4.7, which it did, although not as much as first thought.

The same plot was produced to show the fully submerged corrosion behaviour of coated and uncoated PTFE bonded samples. This can be seen in Fig. 4.29.

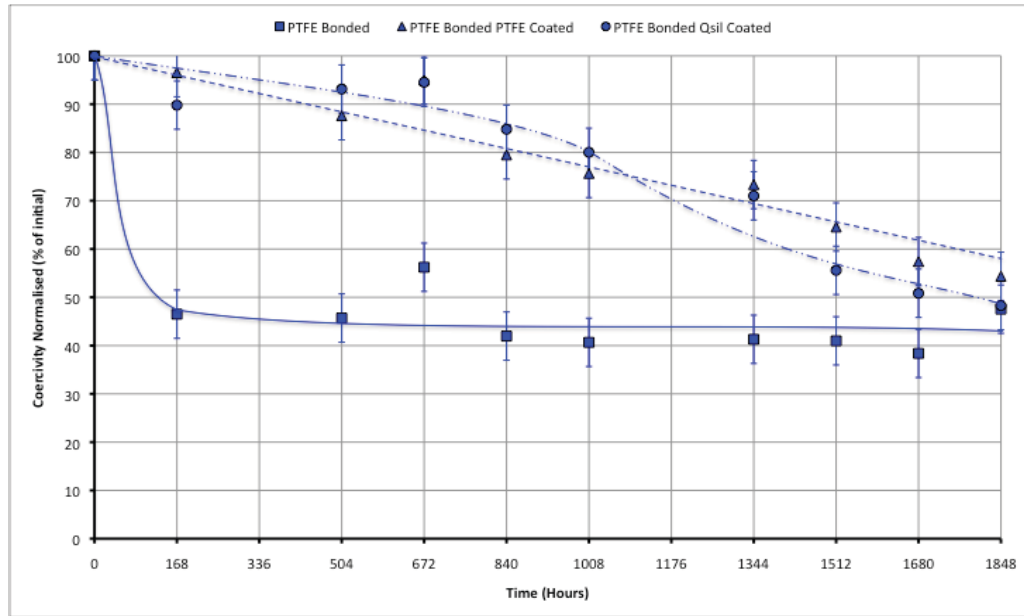


Fig. 4.29 Depicts normalised coercivity (%) against time for MQ-I epoxy bonded samples with and without surface coatings, fully submerged in DI Water at 80°C (Water Bath).

Fig. 4.29 shows that both the PTFE and Qsil surface coatings decrease the severity of initial H_{ci} losses suffered by uncoated PTFE samples. From the initial investigation this sharp drop off in H_{ci} was attributed to unprotected MQP located at the surface of the samples. The two coatings are obviously providing a certain degree of protection for MQP located at the surface, slowing corrosion of these surface particles. Although, it is likely that the integrity of the coatings will have been compromised from the application process through a number of tiny pinholes.

It can be seen that when comparing like-for-like results from Fig. 4.7 and Fig. 4.29 the uncoated PTFE bonded samples display similar aqueous corrosion behaviour characterised by a steep initial drop in H_{ci} , which has been attributed to unprotected MQP located at the

sample surface, followed by a plateau possibly due to the protection afforded by the impermeable PTFE binder to MQP within the bulk sample. There is a slight discrepancy in the H_{ci} values of approximately 8% although this may be due to sample variation i.e. MQP distribution within the sample and the surface area of unprotected MQP available for aqueous corrosion attack at the sample surface.

Upon comparison of this data with data gathered from the initial investigation (Fig. 4.7) it can be seen that both data sets are in agreement over H_{ci} losses over the 1008 hour exposure period.

As before with the samples exposed to the high humidity environment a duplicate coated sample was produced to replicate each experimental configuration. This sample would only be subject to one magnetic measurement which would take place after 1848 hours. This was to allow a comparison to be made between samples that were measured on a weekly basis to ascertain if this frequent measurement caused significant damage to the surface coatings thus leading to an increased rate of aqueous corrosion.

From Table 4.3 it can be seen that samples with surface coatings which were subject to magnetic characterisation measurements on a weekly basis did experience detrimental effects as a result of the process. The effect of these measurements were particularly pronounced in; the epoxy bonded PTFE coated sample exposed to DI water, the epoxy bonded Qsil coated sample exposed to DI water, the PTFE bonded PTFE coated sample exposed to DI water, and the PTFE bonded PTFE coated sample exposed to DI water, with discrepancies between results of 12.76%, 14.53%, 20.21% and 32.48% respectively. As before it is likely that the damage to the sample coating occurred during the positioning of the samples between the pole tips of the permeameter. Again this simple comparison has highlighted a few important points. Firstly how ineffective the PTFE coating was when

applied to the epoxy bonded sample due to the relative consistency of the results ($\sim 12\%$). Secondly the potential of the PTFE and Qsil surface coatings to provide protection if they remain intact. Thirdly the frailties of both the PTFE and Qsil coatings, as irreparable damage had been caused during magnetic characterisation measurements while actively taking every precaution to not damage the coatings.

It is also interesting that the samples exposed to the 50/50 (Dex-Cool/DI water) aqueous environment showed very small discrepancies in data collected, with PTFE bonded samples suffering relatively small H_{ci} losses. This could highlight the capacity of Dex-Cool additions to provide protection to the clean surfaces of the MQP. It is possible that as the surface coating was damaged exposing the clean surface of the MQP, Dex-Cool was able to gain access and “attach” preventing water disassociation.

Table 4.3 Depicts the difference in recorded H_{ci} values (%) of coated samples exposed to the aqueous environment including Dex-Cool additions magnetically characterised every 168 hours versus one measurement after 1848 hours.

Sample Configuration	H_{ci} Value (%) Weekly Measurement Sample (after 1848 hours)	H_{ci} Value (%) Single Measurement Sample (after 1848 hours)	Difference in H_{ci} Value (%) due to coating damage
Epoxy Bonded PTFE Coated (DI water)	44.25	57.01	12.76
Epoxy Bonded Qsil Coated (DI water)	42.47	57.00	14.53
Epoxy Bonded PTFE Coated (50/50)	42.12	44.61	2.49
Epoxy Bonded Qsil Coated (50/50)	41.93	45.61	3.68
PTFE Bonded PTFE Coated (DI water)	44.92	65.13	20.21
PTFE Bonded Qsil Coated (DI water)	38.52	71.00	32.48
PTFE Bonded PTFE Coated (50/50)	87.54	89.60	2.06
PTFE Bonded Qsil Coated (50/50)	66.53	71.05	4.52

4.12 Optical Evaluation Of Surface Coatings

The surface coatings applied to the epoxy and PTFE bonded samples have been evaluated optically through the use of confocal laser microscope images. This data will be used in conjunction with H_{ci} measurements to evaluate the effectiveness of surface coatings applied.

Macro images were utilised to document changes in sample surfaces throughout the duration of corrosion testing. Points of interest arising from captured images will be discussed during this section.

4.12.1 PTFE Coating Application

In Fig. 4.30 (3D surface plots) and Fig. 4.31 (real colour images) the step-by-step process of building up a PTFE coating on the epoxy bonded sample can be seen. The images were taken at varying intervals in this case, the sample surface before, and after, 30, 50, 70 and 100 passes with PTFE containing aerosol. One pass was defined as a left to right or right to left sweep (alternated) with the aerosol nozzle depressed at a distance of approximately 10cm from the sample surface.

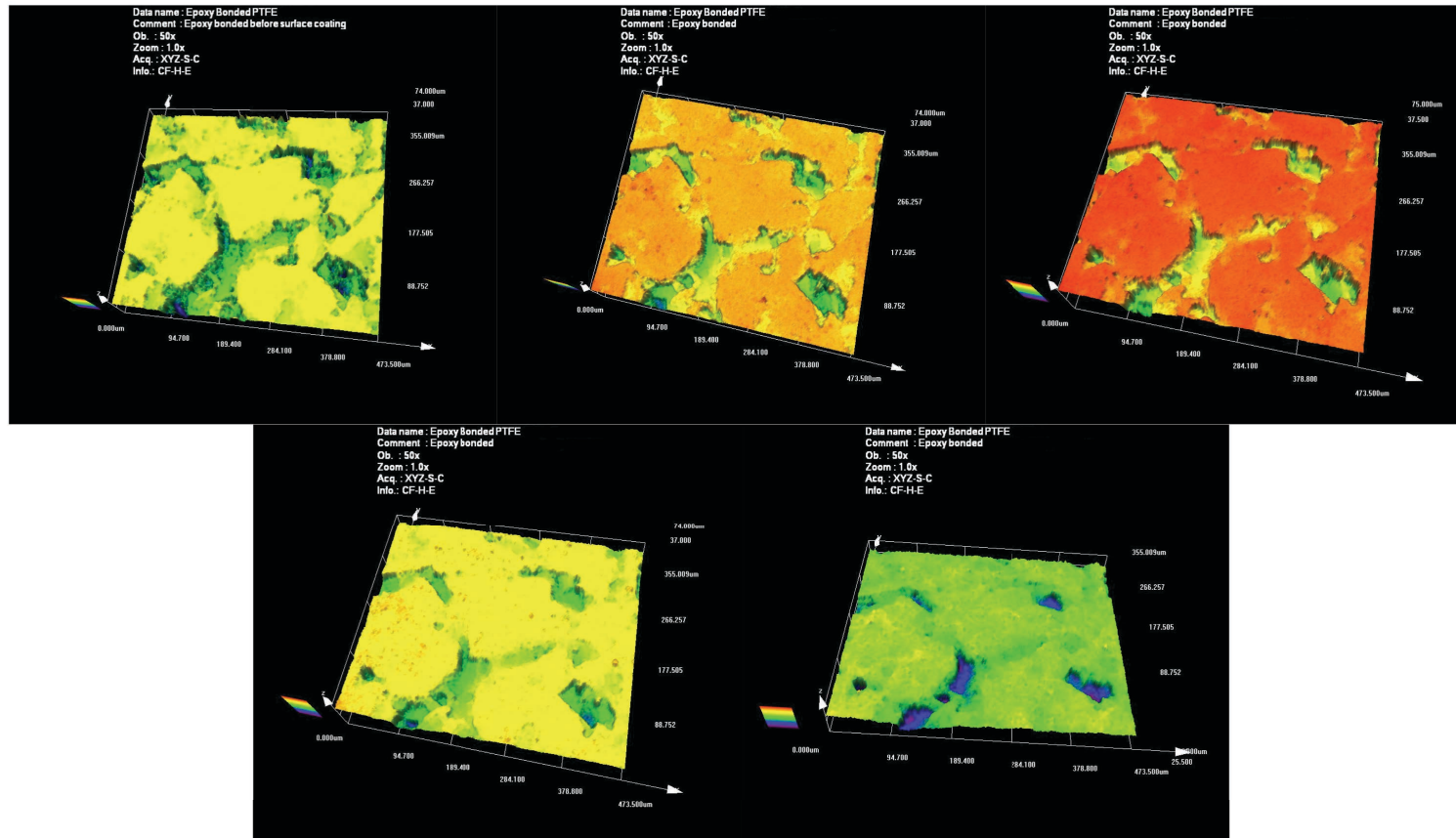


Fig. 4.30 Depicts a 3D image of the epoxy bonded sample surface before and during the PTFE coating application process on (From top left to bottom right: Before, 30 passes, 50 passes, 70 passes and 100 passes)

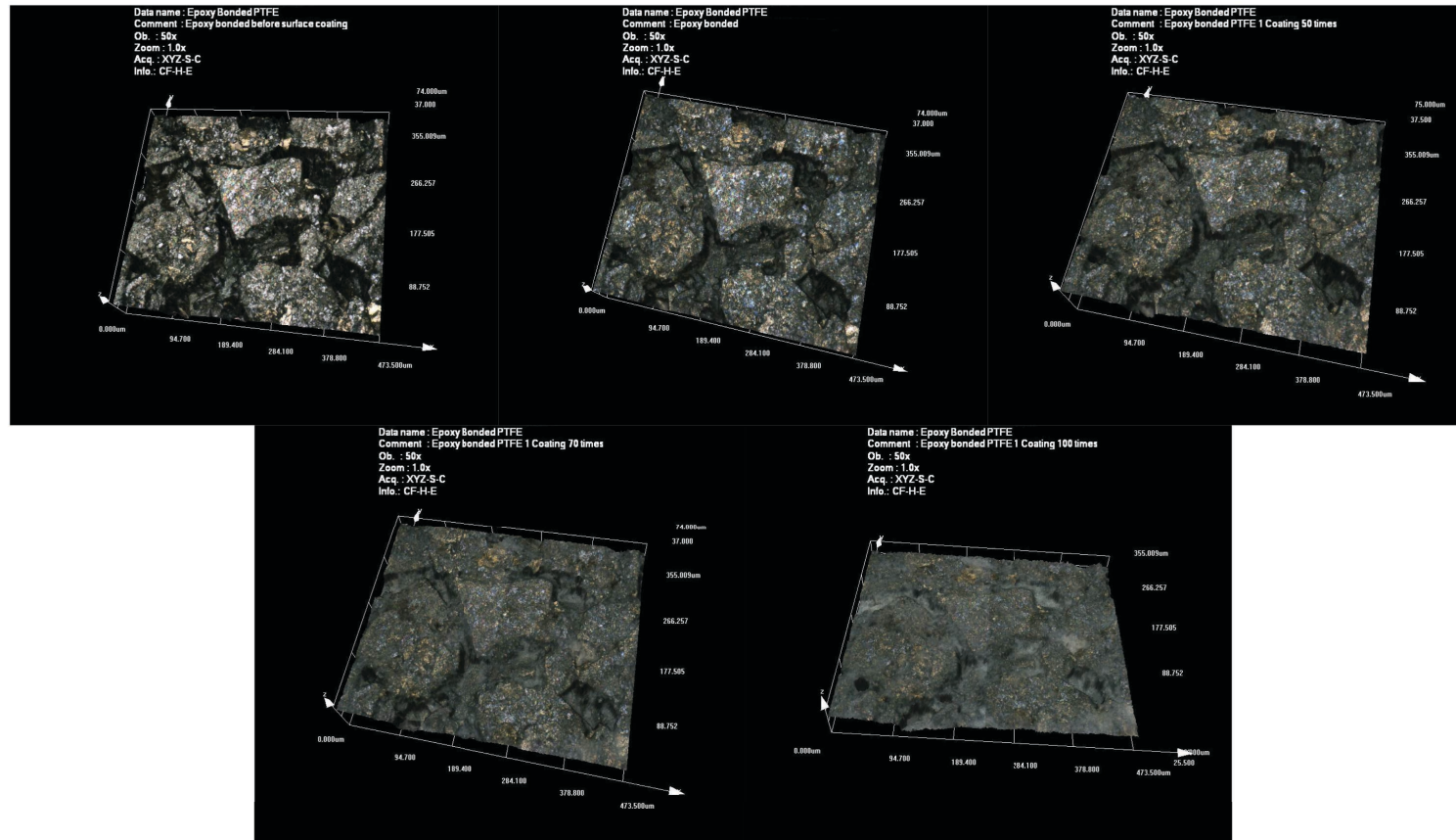


Fig. 4.31 Depicts the real colour image of the epoxy bonded sample surface before and during the PTFE coating application process on (From top left to bottom right: Before, 30 passes, 50 passes, 70 passes and 100 passes)

The first point of interest to note is the relatively heterogeneous surface of the epoxy bonded sample before the coating process. In the 3D surface image, areas marked with blue/green are lower lying and should be treated as surface porosity many of these pores will lead deep into the bulk sample far beyond the depth of the scan. The next picture shows a clear build up of PTFE on the surface of the sample, indicated by a change of the yellow areas to orange and the green areas to yellow. This progressive build up continues with each application. In the final image it can be seen that the surface is largely homogenous although such is the extent of the porosity on the surface of the epoxy bonded sample that the PTFE applied did not manage to level these areas. The real colour images give a clear picture of the progressive build up and distribution of PTFE on the sample surface.

The downfall of coating epoxy resin with PTFE is the issue of being unable to subject the PTFE to a sintering treatment at 370°C due to the thermal tolerances of the epoxy resin. As a result of the absence of the required heat treatment the PTFE coating remains as a powdery layer with no real adhesion to the surface of the epoxy resin or itself. As a result the PTFE coating readily flakes off upon handling and also upon contact with moisture.

Even after the application of the coating there are still some large pores which could provide moisture with easy access to the interior of the sample. The optical evaluation of this coating is in strong agreement with the findings of the H_{ci} measurements taken during the corrosion testing i.e. the PTFE coating did little to protect the sample from the effects of aqueous corrosion.

Fig. 4.32 shows the step-by-step process of building up a PTFE coating on the PTFE bonded sample can be seen. The images were taken at various stages, in this case; the sample surface before, and after, 20, 40, 60, 80 and 100 passes with PTFE containing aerosol.

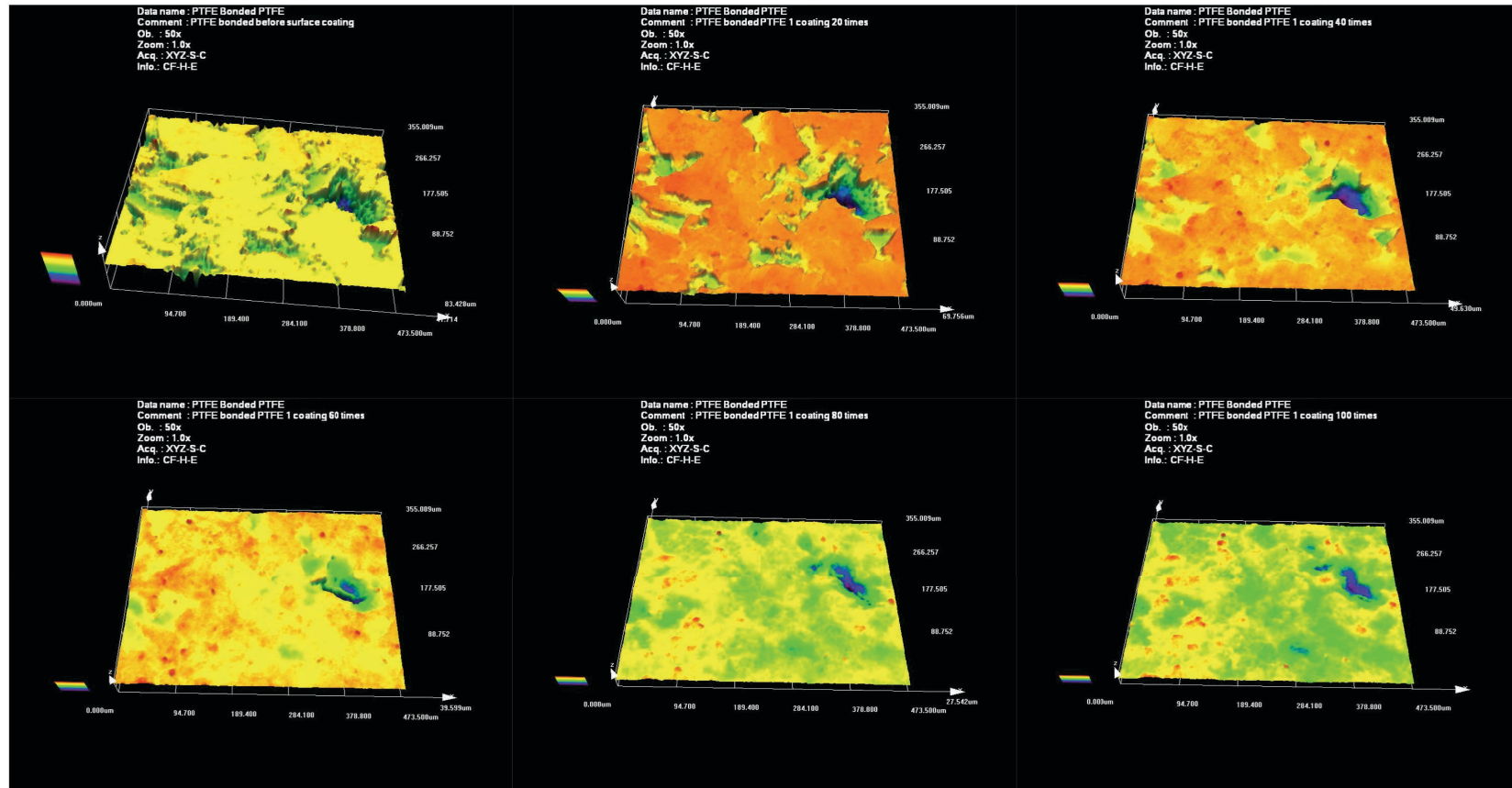


Fig. 4.32 Depicts a 3D image of the PTFE bonded sample surface before and during the PTFE coating application process on (From top left to bottom right: Before, 20 passes, 40 passes, 60 passes, 80 passes and 100 passes)

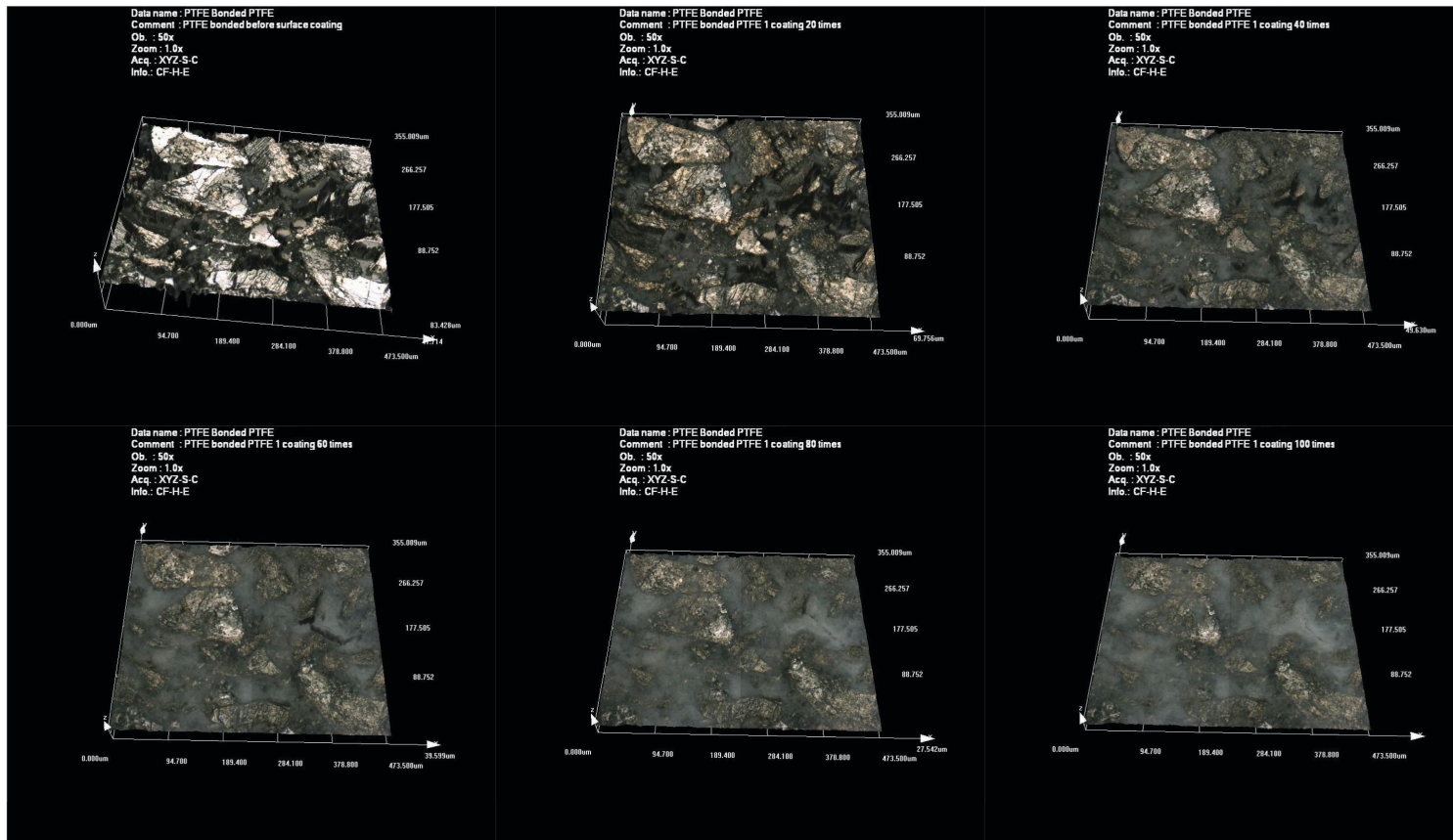


Fig. 4.33 Depicts the real colour image of the epoxy bonded sample surface before and during the PTFE coating application process on (From top left to bottom right: Before, 20 passes, 40 passes, 60 passes, 80 passes and 100 passes)

Fig. 4.32 and Fig. 4.33, show the 3D surface image and the overlaid real colour image respectively. It can be seen from the 3D image of the pre coated sample that a particularly heterogeneous area, relative to other areas of the PTFE sample surface, was chosen to image. This was in an attempt to ascertain how well the coating would perform when applied under less than favourable conditions. Also the real colour image of the pre coated surface shows a large surface area of exposed MQP at the sample surface that would potentially be vulnerable upon exposure of the sample to moisture. As previously discussed it is thought that aqueous corrosion of these surface MQP are responsible for the majority of the H_{ci} losses displayed within the first 168 hours, due to the ease of access for moisture. If a surface coating could be applied that would prevent this surface corrosion then PTFE would instantly become more attractive as a binder.

It can be seen from the 3D surface images in Fig. 4.32 that the PTFE coating produced a relatively homogenous surface after 100 passes with the aerosol. Although it probably would have been beneficial to have built up a slightly thicker layer to afford the surface MQP more protection.

It can be seen from the real colour images that there are still some surface MQP which are not fully encapsulated by the coating. It was hoped that upon sintering the PTFE coating would densify and adhere to the PTFE bonding media and extend the matrix of the PTFE over the surface MQP (Tattam, 1996). MQP within the bulk material do not display any form of intimate bonding with the PTFE binder, however the relatively large forces required to press the samples simply squash the PTFE particles into the MQP. Upon sintering the PTFE softens and the polymer chains reorder themselves, upon cooling the PTFE solidifies upon the surface of the MQP.

Without the application of pressure to induce flow of the PTFE particles around the MQP and force out porosity, it is unlikely the PTFE surface coating will display the same impermeable barrier properties as that of the PTFE binder in the bulk material. It is likely that this PTFE coating will be relatively porous with the pore sizes being in the region of microns rather than pores on the nano scale as seen in the structure of the epoxy resin.

Although the PTFE coating is far from perfect and as completely uniform as it appears with the naked eye, it can be said that it is an improvement upon an uncoated surface. This statement is clearly backed by the results of the aqueous corrosion testing which can be seen in Fig. 4.29 This showed that the rate of H_{ci} losses due to aqueous corrosion were greatly reduced in the presence of both the PTFE and Qsil coatings.

Fig. 4.34 shows the 3D surface and real colour images of a PTFE bonded and coated sample surface post sintering heat treatment.

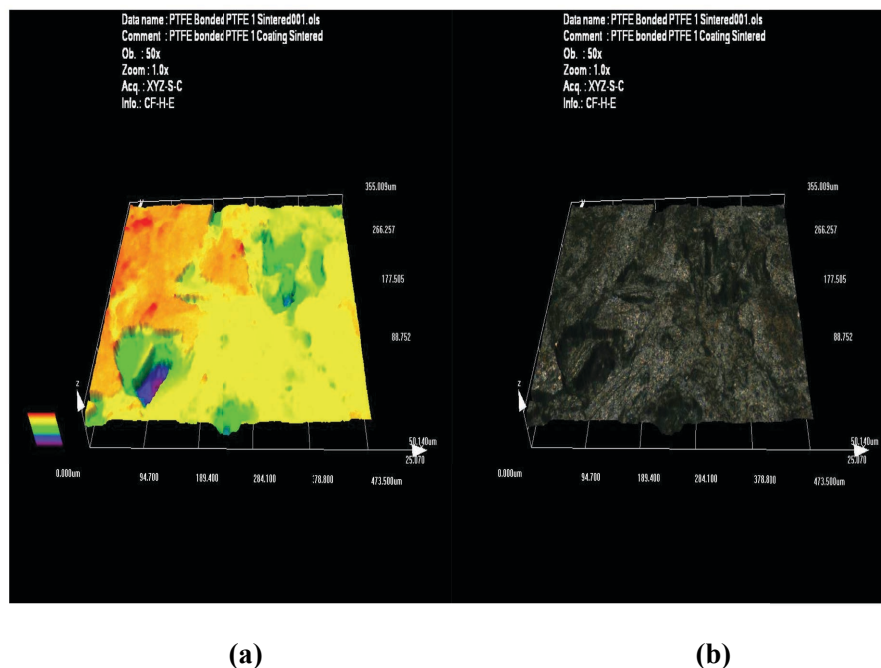


Fig. 4.34 Depicts the 3D surface image (a) and real colour image overlaid (b) of a PTFE bonded and coated sample surface post sintering heat treatment at 370°C.

The real colour images in Fig. 4.34 depicts the PTFE bonded PTFE coated sample surface post sinter, this indicates that there appears to be a relatively uniform surface coating which seems to encapsulate the entire sample surface. Although upon viewing the 3D surface image this paints a different picture. It appears that the heat treatment has caused the spray on PTFE coating to densify. This is apparent as the contours of the sample surface are now evident when compared with the 3D surface images taken of the same sample surface before sintering (Fig. 4.32 bottom right) it can be seen that the morphology of the surface is relatively flat.

There is also clear evidence of particles breaking lose from the sample surface. These particle shaped holes can be seen indicated by the blue/green areas. Upon heating, magnetic materials progressively lose magnetisation up to the Curie temperature, which leads to a reduction in the magnetic repulsion between the neighbouring magnetic atoms. In NdFeB the contraction due to loss of magnetic repulsion is greater than the conventional thermal expansion caused by increased atomic thermal vibration. This overall contraction of the MQP coupled with the conventional thermal expansion of the PTFE matrix during the heat treatment may lead to a loosening of the MQP within the PTFE matrix allowing the MQP to fall from the surface of the magnet (Buschow, 1986a). Regardless of how it happened this is clearly a much larger problem than the pinholes or nanopores that were originally thought to be responsible for the lack of coating integrity. It is likely that these particle size holes are responsible for the slow and steady decline of H_{ci} due to aqueous corrosion.

It should not really be surprising that MQP located at the sample surface of PTFE bonded samples are prone to breaking loose when considering that, as previously mentioned, there is no intimate bonding between the PTFE and MQP surface. Any MQP breaking away

from the sample surface could potentially provide easy access to interconnected porosity for moisture to penetrate into the bulk material, possibly exposing previously inaccessible MQP lying below the sample surface. The application of a slightly thicker coating of PTFE may not only prevent aqueous corrosion of surface MQP, but it may also improve sample integrity. Ideally if a thin PTFE rich layer could be introduced to the sample surface during the pressing process this may eliminate the need for a separate PTFE coating and prevent MQP from breaking away during the sintering, greatly enhancing the integrity of the sample structure. This would also prevent aqueous corrosion of surface MQP that appears to be responsible for the rapid and large H_{ci} losses within the initial 168 hours of exposure.

Unfortunately due to the transparent nature of the Qsil coating the confocal microscope was unable to image the surface of the coating but instead produced a slightly distorted view of the original bonded sample surface. The Qsil coating will be discussed in the context of macro images taken during exposure to the aqueous environments.

4.13 Sample Surface Analysis of High Humidity Environmental Exposure

To document surface changes induced in epoxy and PTFE bonded samples, in both coated and uncoated configurations, during exposure to the high humidity environment, macro images were taken at various intervals when it was deemed that surface changes had occurred that required documenting.

The following images were taken; after the application of the coating/before exposure to the high humidity environment, then after, 168 hours exposure, 504 hours exposure, 672 hours exposure, 1344 hours exposure and finally after 1680 hours exposure.

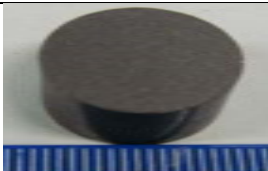
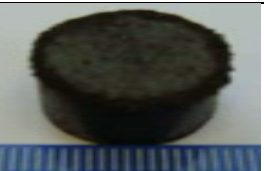

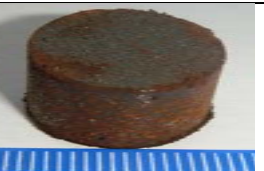


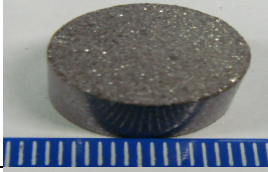





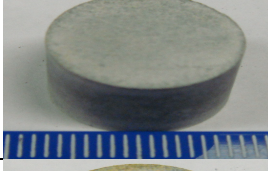





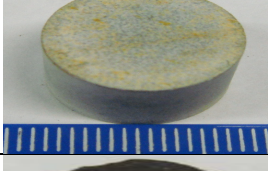


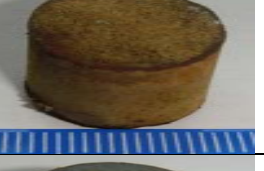



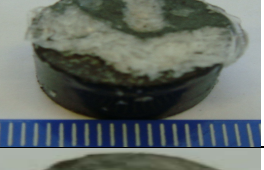




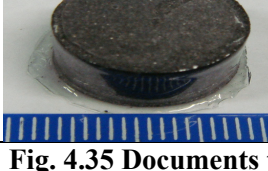





Sample	Before	168 Hours	504 Hours	672 Hours	1344 Hours	1680 Hours
Epoxy Bonded						
PTFE Bonded						
Epoxy Bonded PTFE Coated						
PTFE Bonded PTFE Coated						
Epoxy Bonded Qsil Coated						
PTFE Bonded Qsil Coated						

Fig. 4.35 Documents the surface changes experienced by epoxy and PTFE bonded samples in both coated and uncoated configurations exposed to the high humidity environment.

From Fig. 4.35 it can be seen that exposure to the high humidity environment brought about surface changes in every sample configuration without exception. Suffice to say that none of the coatings prevented the ingress of moisture. The first sample to show the telltale signs of aqueous corrosion attack was the epoxy bonded sample which displayed significant “furring” at the north pole after the initial 168 hours. A similar build up of rusty corrosion product was observed in the PTFE bonded sample, although significantly less “furring” occurred throughout the testing duration relative to its epoxy bonded counterpart.

A similar action was observed in the epoxy bonded PTFE coated sample which was showing signs of a rusty corrosion product through the coating after only 168 hours. This would suggest that the coating has not prevented the aqueous corrosion process but merely masked it. It should be noted that by 168 hours exposure small pieces of the PTFE coating have broken away and continued to do so throughout the investigation.

The PTFE bonded PTFE coated sample showed signs of a rusty corrosion product from below the surface at 168 hours exposure, again indicating moisture ingress. However the coating remained almost intact until approximately 672 hours exposure. After this time the coating began to flake away from the sample in chunks often with MQP still imbedded within it. These pieces then progressively migrated towards the north pole to form “furring”. The “furring” observed in the PTFE bonded and PTFE coated sample was not on the same scale as that observed in the epoxy bonded PTFE coated sample.

Both samples treated with the Qsil coating showed very little resistance to moisture ingress. This was due in part to the Qsil coating not being able to stand up to the rigours of testing within the permeameter. The effects of which can be seen from the crazing observed on the epoxy bonded Qsil coated sample after 168 hours. Exposure to the high humidity environment at 80°C seemed to make the Qsil much more brittle than before

exposure. Consequently it broke away and flaked off more freely. It is also important to point out that the application of the Qsil coating appeared to embrittle the PTFE binder. As a result after 504 hours exposure the sample experienced catastrophic failure during magnetic measurement with the crack clearly apparent in the 672 hour image.

4.14 Sample Surface Analysis of Aqueous Environmental Exposure

To document surface changes induced in epoxy and PTFE bonded samples, in both coated and uncoated configurations, during exposure to the aqueous environment, macro images were taken at various intervals when it was deemed that surface changes had occurred that required documenting.

The following images were taken; after the application of the coating/before exposure to the aqueous environment, then after, 168 hours exposure, 504 hours exposure, 672 hours exposure, 1344 hours exposure and finally after 1680 hours exposure.

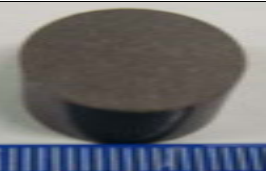
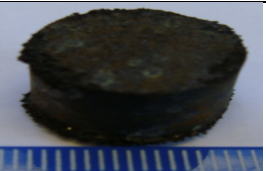





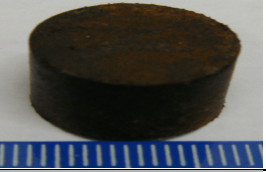
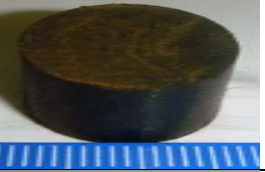



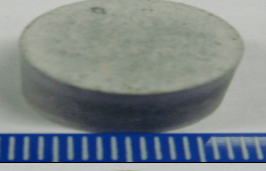





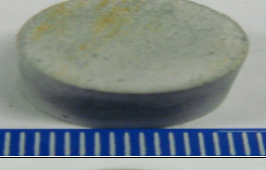
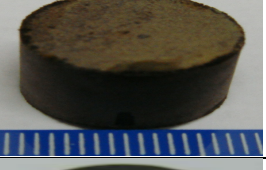





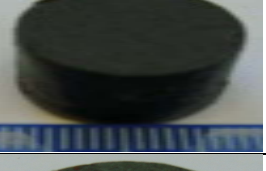

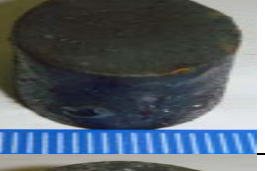


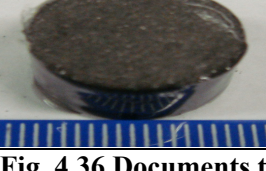
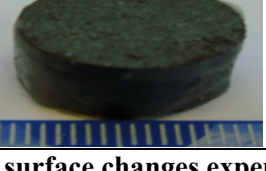




Sample	Before	168 Hours	504 Hours	672 Hours	1344 Hours	1512 Hours
Epoxy Bonded						
PTFE Bonded						
Epoxy Bonded PTFE Coated						
PTFE Bonded PTFE Coated						
Epoxy Bonded Qsil Coated						
PTFE Bonded Qsil Coated						

Fig. 4.36 Documents the surface changes experienced by epoxy and PTFE bonded samples in both coated and uncoated configurations exposed to the aqueous environment.

From Fig. 4.36 it can be seen that as with exposure to the high humidity environment the epoxy bonded sample shows the first signs of aqueous corrosion attack after only 168 hours exposure. However, compared with the corresponding epoxy bonded sample exposed to the high humidity environmental there appears to be a greater loss of structural integrity. This is particularly pronounced at the poles with clear evidence of “furring”. There are also patches of a white corrosion product evident which suggests the formation of $\text{Nd}(\text{OH})_3$ from the disassociation of water.

The PTFE bonded sample exhibits a rust coloured corrosion product on the surface although the structure seems to survive the aqueous corrosion attack better than its epoxy counterpart, this is indicated by the well defined edges even after 1344 hours exposure. This suggests the damage done is limited to the outer edges of the sample.

The epoxy bonded PTFE coated sample behaves in a similar way to the high humidity environmental exposure. The sample displays flaking of the PTFE coating with clear evidence of “furring” at the poles. The furring is composed of rust coloured particles.

The PTFE bonded PTFE coated sample displays good resistance to the aqueous environment with the coating maintaining structural integrity until approximately 1008 hours. Although, after only 168 hours exposure there is evidence of underlying corrosion from the rust colour leaching through the coating.

Both the epoxy and PTFE bonded Qsil coated samples show little evidence of corrosion product on the samples surface below the coating initially. There are a few small patches of a rust coloured product. However, at this point the coating still appears to be structurally intact so it is likely that the corrosion is caused by moisture trapped beneath the coating from before or during application. In both samples there is clear evidence of degradation of

the Qsil coat, which is characterised by “thinning”. This would account for the mass loss shown by these samples. After 1512 hours there appears to be very little of the previously thick coating remaining. Both sample surfaces are largely covered by a rust coloured corrosion product at this point. There is nothing to suggest that this coating survived particularly well.

From optical analysis it would appear that the PTFE bonded sample and the PTFE bonded PTFE coated sample performed the best.

4.15 Surface Coatings in the Presence of Dex-Cool Additions

To complete this section of the investigation into PTFE and Qsil surface coatings, building upon previously gathered data it seemed prudent to assess the effect of Dex-Cool additions for both coated and uncoated samples. Repetition of tests run with duplicate samples will enable, as before, accurate comparisons to be drawn from the initial full submersion testing performed over an extended period. This will again determine how reproducible results gathered from the initial investigation were, whilst providing a glimpse of corrosion behaviour over an extended period.

This particular branch of the study will concentrate upon Dex-Cool additions in the form of a 50/50 (Dex-Cool/Water) solution as previous findings had indicated that this particular concentration had performed comparably to Dex-Cool in its “pure” form.

The plot seen in Fig. 4.37 shows the coated and uncoated corrosion behaviour of epoxy bonded samples exposed to a fully submerged 50/50 (Dex-Cool/Water) solution environment at 80°C. To aid comparison between aqueous corrosion behaviour of samples in DI water those curves from Fig. 4.28 are depicted by the corresponding green lines.

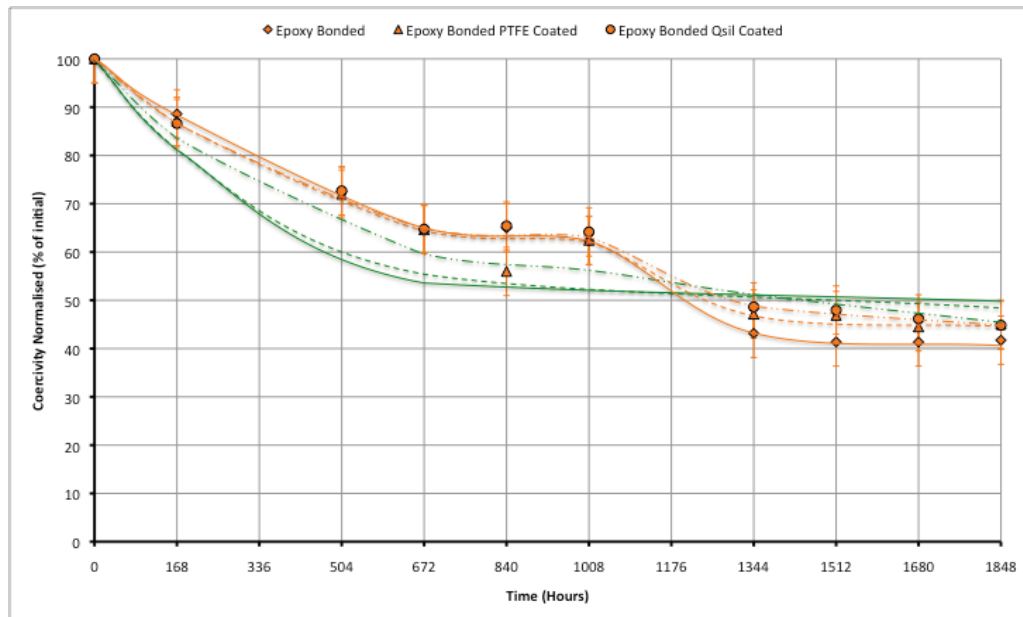


Fig. 4.37 Depicts normalised coercivity (%) against time for MQ-I epoxy bonded samples with and without surface coatings, fully submerged in 50/50 (DI water/Dex-Cool) at 80°C (Water Bath). The corresponding green lines indicate aqueous corrosion behaviour of samples in DI water (from Fig. 4.28)

Fig. 4.37 gives a clear indication that the behaviour of both coated and uncoated epoxy bonded samples in the presence of 50/50 (DI water/Dex-Cool) solution is very similar to that of the identical samples when exposed to DI water over the same period of time.

As previously discussed this behaviour has been attributed to the complete particle encapsulation method used to apply the epoxy coating to the MQP, and also the physical structure of the epoxy resin. Whereby, the pores are on the nano size scale and thus are far too small for large molecules such as EG to penetrate and gain access to the surface of the MQP. Some form of surface interaction between EG and the MQP surface appears to be required to provide protection against aqueous corrosion. This seems to have been the case with PTFE bonded samples with clean MQP at the sample surface.

Fig. 4.38 shows the coated and uncoated corrosion behaviour of PTFE bonded samples fully submerged in a 50/50 (Dex-Cool/Water) solution at 80°C. To enable comparisons to be made easily between aqueous corrosion behaviour in a 50/50 solution and those in DI water, the curves for DI water are depicted by the corresponding blue lines.

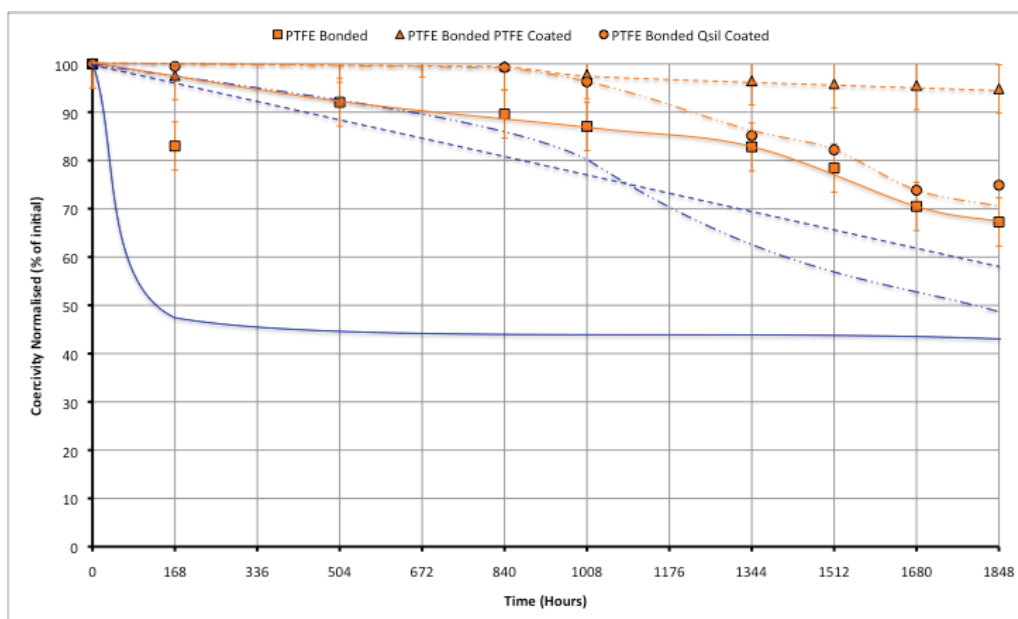


Fig. 4.38 Depicts normalised coercivity (%) against time for MQ-I epoxy bonded samples with and without surface coatings, fully submerged in 50/50 (DI water/Dex-Cool) at 80°C (Water Bath). The corresponding blue lines indicate aqueous corrosion behaviour of samples in DI water (from Fig. 4.29)

From Fig. 4.38 it can be seen that PTFE bonded samples, both coated and uncoated displayed significantly improved aqueous corrosion behaviour during exposure to the 50/50 (Dex-Cool/DI water) solution. Even the uncoated PTFE bonded sample displayed a significantly reduced rate of H_{ci} loss over the duration of exposure. The sample exposed to DI water showed H_{ci} losses of approximately 50% after only 168 hours exposure, whereas an identical sample exposed to the 50/50 (Dex-Cool/DI water) experienced a reduction in H_{ci} to approximately 70% of the initial value. The best performer during testing was the PTFE bonded and PTFE coated sample exposed to the 50/50 solution. This sample only

showed H_{ci} losses in the region of 5% after 1848 hours, compared to losses in the region of 40% for the same sample configuration exposed to DI water. The Qsil coated sample also saw a reduced rate although it could be seen that the addition of Dex-Cool had a detrimental effect upon the integrity of the coating. The Dex-Cool appeared to actively hasten the dissolution of the Qsil coating. This will be discussed later with the aid of macro images.

The plots contained within Fig. 4.38 provide definitive evidence of the dramatic improvement in the performance life of MQP when bonded/coated with PTFE and exposed to an aqueous environment treated with Dex-Cool additions. Over the 1848 hours exposure the Dex-Cool additions have managed to preserve around 95% of the initial H_{ci} compared to the 42% for an identical sample exposed to DI water.

4.15.1 Optical Analysis of Samples Exposed to 50/50 (Dex-Cool/DI Water) Solution

As before surface changes induced in both coated and uncoated epoxy and PTFE bonded samples, during exposure to DI water and the 50/50 (Dex-Cool/DI water) solution, were recorded through macro images. These images were taken at various intervals when it was deemed that surface changes had occurred that required documenting.

The following images were taken; after the application of the coating/before exposure to the high humidity environment, then after, 168 hours exposure, 504 hours exposure, 672 hours exposure, 840 hours exposure, 1008 hours exposure, 1344 hours exposure and finally after 1512 hours exposure. To aid comparison each sample configuration is displayed with the corresponding 50/50 (Dex-Cool/DI water) solution shown directly below the DI water exposed sample.




























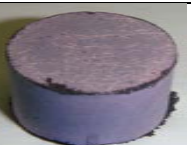




















Sample	Before	168 Hours	504 Hours	672 Hours	840 Hours	1008 Hours	1344 Hours	1512 Hours
Epoxy Bonded DI Water								
Epoxy Bonded Dex-Cool								
Epoxy Bonded PTFE Coated DI Water								
Epoxy Bonded PTFE Coated Dex-Cool								
Epoxy Bonded Qsil Coated DI Water								
Epoxy Bonded Qsil Coated Dex-Cool								

Fig. 4.39 Documents the surface changes experienced by epoxy bonded samples in both coated and uncoated configurations exposed to the aqueous environment.

From Fig. 4.39 it can be seen that generally there is very little, if any features to distinguish between the appearance of the epoxy bonded samples exposed to DI water and the appearance of identical samples exposed to the 50/50 (Dex-Cool/DI water) solution. It can be said with certainty from optical observations that Dex-Cool additions had very little effect upon the aqueous corrosion behaviour of epoxy bonded samples.

Interestingly in the epoxy bonded samples exposed to the 50/50 (Dex-Cool/DI water) environment there does seem to be an absence of the white patches of corrosion product seen on the corresponding DI water exposed epoxy bonded sample after only 168 hours.

The epoxy bonded PTFE coated samples again exhibited relatively similar behaviour to one another. The sample exposed to the 50/50 (Dex-Cool/DI water) solution exhibited less “furring” during the early stages of exposure. By the end of exposure the two looked very similar apart from the pink staining that had leached out of the Dex-Cool into the PTFE coating.

The epoxy bonded Qsil coated samples again behaved in a similar manner to one another. The primary difference in corrosion related behaviour appeared to be the more rapid thinning of the Qsil coating evident in the 50/50 (Dex-Cool/DI water) solution sample.

Fig. 4.40 shows surface changes induced in PTFE bonded samples exposed to DI water and 50/50 (Dex-Cool/DI water) solution. As before these changes were documented through macro images captured on the same time scale as the epoxy bonded samples to aid comparisons.
















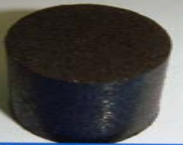
































Sample	Before	168 Hours	504 Hours	672 Hours	840 Hours	1008 Hours	1344 Hours	1512 Hours
PTFE Bonded DI Water								
PTFE Bonded Dex-Cool								
PTFE Bonded PTFE Coated DI Water								
PTFE Bonded PTFE Coated Dex-Cool								
PTFE Bonded Qsil Coated DI Water								
PTFE Bonded Qsil Coated Dex-Cool								

Fig. 4.40 Documents the surface changes experienced by PTFE bonded samples in both coated and uncoated configurations exposed to the aqueous environment.

From Fig. 4.40 it can be seen that the addition of Dex-Cool has a marked effect upon the surface of the PTFE bonded sample. The sample exposed to DI water is covered in a rust-coloured corrosion product as early as 168 hours with no shiny surfaces visible due to the build up of corrosion product. By contrast the PTFE bonded sample exposed to the 50/50 (Dex-Cool/DI water) solution shows no evidence of the rust coloured corrosion product even after 1512 hours exposure. Incredibly there are still shiny surfaces evident on the MQP when testing was concluded. This gives a clear indication of what is likely to be occurring below the surface coating of the samples exposed to the 50/50 (Dex-Cool/DI water) solution, if the PTFE coating integrity is compromised.

Both PTFE bonded and coated samples show little change on the surface apart from a colour change. The coating was initially white, both samples exhibited a rust coloured staining leaching through the PTFE coating. The sample exposed to the 50/50 (Dex-Cool/DI water) solution displayed as a slight staining from the Dex-Cool addition and the surface coating retained its integrity slightly better than that of the sample in DI water. This sample also showed a slight roughening of the surface coating, it is likely that this coating simply masked much of the aqueous corrosion occurring below the surface.

The PTFE bonded Qsil coated samples followed suit in their aqueous corrosion behaviour. The noticeable difference between the samples being the enhanced thinning of the Qsil coating for the sample exposed to the 50/50 (Dex-Cool/DI water) solution. After 1344 hours exposure when the coating had clearly lost integrity there was some rust coloured staining but the source of this is unclear and may be due to staining from the Dex-Cool additions. The sample exposed to DI water displayed a clear build up of corrosion product beneath the Qsil coating surface with some evidence of surface roughening.

Overall, from observations alone it is clear that there is a marked difference between the corrosion process in the presence of Dex-Cool compared to that of DI water. It is interesting that there is an absence of the rust-coloured corrosion build up, which you would associate with the oxidation of iron, in the presence of Dex-Cool. It could be possible that the Dex-Cool is being adsorbed onto the surface and is actively preventing the disassociation of water.

A survey of literature was conducted into studies involving EG and metals to see if any evidence could be found to support the hypothesis that EG forms a thin coating on the surface of the MQP. There is evidence to suggest that EG is actively adsorbed onto the surface of transition metal oxides (Vodyankina et al., 1998), alkaline earth oxides (Calatayud, 2010) and aluminium oxide (Zaharieva et al., 2009). These metals involved are primarily used as catalysts, in a reaction involving EG or other alcohols which are adsorbed onto the metal surface and upon the application of heat yield products such as aldehydes or ketones (Bowker and Madix, 1982).

(Bayman and Hansma, 1980) conducted a study utilising inelastic electron tunnelling spectroscopy which was used to reveal the vibrational spectrum of organic molecules on the oxide of a metal-oxide-metal junction. This study found that during the adsorption of EG both OH groups react with the aluminium oxide surface. The workers also found that there were no peaks in the tunnelling spectra where the O–H and O–D vibrations for EG should occur. This shows that the EG molecule must lose protons from both OH groups during bonding to the aluminium oxide surface (Bayman and Hansma, 1980) (Vodyankina et al., 1998).

This investigation provides evidence to support the affinity EG has for metal oxide surfaces. As a result of production methods and the highly reactive nature of the Nd-rich

phase present in the bulk alloy, MQP should have neodymium oxide surfaces in abundance on all particles. Despite evidence to suggest that there is an attraction between EG and metal oxide surfaces, these studies were conducted using vapour deposition techniques which may induce differences in the behaviour of EG compared to aqueous solution. This hypothesis relies upon EG retaining this affinity for metal oxide surfaces when it forms 50% of an EG-water solution. Although the increased mobility of EG molecules within the solution would not hinder this attraction.

A study was conducted by (Capote and Madix, 1989) using temperature-programmed reaction spectroscopy (TPRS) into EG adsorption behaviour onto a clean silver surface versus a silver oxide surface. It showed that EG is reversibly adsorbed onto the clean surface, upon heating it is desorbed by 260K. However, on the oxidised surface of the silver catalyst, EG reacts with atomic oxygen to yield adsorbed water and ethylenedioxy. The ethylenedioxy species is stable up to a temperature of 350K where C–H bond breaking and reformation occur leading to the evolution of CH_2OH_2 at 365K, glyoxal at 380K and H_2 at both temperatures (Capote and Madix, 1989).

This shows that the attraction of EG to the MQP surface may lie within the atomic oxygen present in the surface oxide layer rather than the underlying metal. If this was the case whereby hydrophilic OH groups were bound to the metal oxide surface of the MQP through hydrogen bonding then this would leave the EG hydrophobic backbone exposed to the network of hydrogen bonded water molecules. As previously discussed this would increase the overall entropy of the system. To combat these unfavourable interactions between the hydrophobic C–C backbone and hydrogen bonding water molecules interactions must be reduced through the formation of clusters or ‘icebergs’ within the solution. Although within this configuration lies a key difference, instead of the EG

'icebergs' being free floating within the solution as previously discussed, in this case the basis of the EG cluster is anchored to the metal oxide surface of the MQP through hydrogen bonding. In theory the formation of a secondary layer of EG would reduce unfavourable interactions with the hydrophobic C–C backbone of EG bound to the metal oxide surface, with any hydrogen bonding water molecules in close proximity. The secondary EG layer could potentially form in a similar configuration to the free floating 'iceberg' previously discussed within mixing scheme II of the EG-water solution (Koga, 2003), whereby hydrophobic C–C groups of the EG molecule would cluster together back-to-back, creating what Parker and Claesson term a solvophobic cavity (Parker and Claesson, 1992). These EG layers could be thought of as an anchored 'iceberg' through the hydrogen bonding action of EG with the metal oxide surface layer. The hydrophilic OH groups of the secondary EG layer could then be actively involved in forming hydrogen bonds with any water molecules in close proximity. A configuration such as this would maximise the number of hydrogen bonds within the system, in the same way that the 'iceberging' in mixing scheme II did. Maximising hydrogen bonds is ultimately the driving force behind the system order in this case. This could actively form a barrier preventing water molecules from gaining access to the surface of the MQP within the bonded magnets hence preventing the disassociation of water. A simplified schematic representation of the possible configuration of the EG layer can be seen in Fig. 4.41

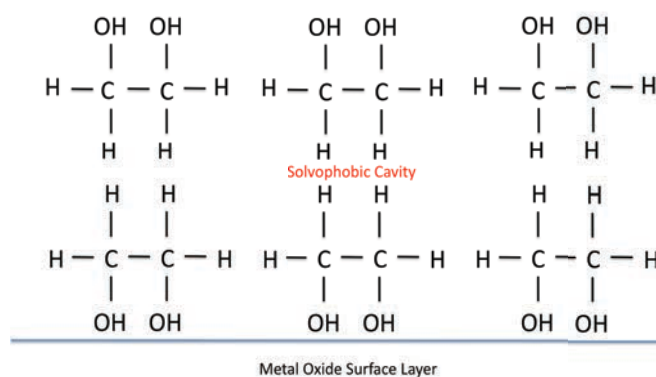


Fig. 4.41 Depicts a simplified representation of ethylene glycol layers forming a solvophobic cavity induced by hydrogen bonding with the metal oxide surface.

4.16 Ethylene Glycol/Dex-Cool Summary

To summarise the body of work involving EG/Dex-Cool, it is clear from the experimental evidence gathered that EG shows great potential as an additive/surface coating for industrial applications as a corrosion inhibitor for NdFeB type alloys within aqueous environments. From experimental evidence gathered during this study it has shown to preserve approximately 30% more of the initial H_{ci} over 1848 hour period for uncoated PTFE bonded samples. The performance when coupled with a PTFE surface coating has shown to preserve approximately 95% of the initial H_{ci} value over the 1848 hours. Experimental evidence has also shown that the use of Dex-Cool additives has little effect upon H_{ci} losses experienced by epoxy bonded samples. The potential of this organic compound is clear unfortunately at present from work carried out within this study the mechanisms are not. At the moment much of the discussion involving Dex-Cool and the methods of protection are centred around speculation based upon unrelated literature and the application of adapted theories. To fully optimise the gains in performance offered in terms of extended service life of NdFeB type alloys a large body of further work is required to reveal the mechanisms involved and how it is best employed i.e. surface

coating or aqueous environment additive. Further details of the work required will be provided within the future work section.

References:

- BAYMAN, A. & HANSMA, P. K. 1980. Inelastic electron tunnelling spectroscopic study of lubrication. *Nature*, 285, 97-99.
- BOWKER, M. & MADIX, R. J. 1982. XPS, UPS and thermal desorption studies of alcohol adsorption on Cu(110): II. Higher alcohols. *Surface Science*, 116, 549-572.
- BUSCHOW, K. H. J. 1986a. Invar effect in R₂Fe₁₄B compounds (R = La, Ce, Nd, Sm, Gd, Er). *Journal of the Less Common Metals*, 118, 349-353.
- CALATAYUD, M. 2010. Ethylene glycol interaction on alkaline earth oxides: A periodic DFT study. *Catalysis Today*, 152, 88-92.
- CAMP, F. E. & KIM, A. S. 1991. Effect of microstructure on the corrosion behavior of NdFeB and NdFeCoAlB magnets. *Journal of Applied Physics*, 70, 6348-6350.
- CAPOTE, A. J. & MADIX, R. J. 1989. Oxygen-hydrogen and carbon-hydrogen bond activation in ethylene glycol by atomic oxygen on silver(110): heterometallacycle formation and selective dehydrogenation to glyoxal. *Journal of the American Chemical Society*, 111, 3570-3577.
- HARRIS, I. R. & ET AL. 1987. Nd-Fe-B Permanent Magnets: Hydrogen Absorption/Desorption Studies (HADS) on Nd₁₆Fe₇₆B₈ and Nd₂Fe₁₄B. *Physica Scripta*, 1987, 435.
- ISNARD, O., YELON, W. B., MIRAGLIA, S. & FRUCHART, D. 1995. Neutron-diffraction study of the insertion scheme of hydrogen in Nd₂Fe₁₄B. *Journal of Applied Physics*, 78, 1892-1898.
- JACOBSON, J. & KIM, A. 1987. Oxidation behavior of Nd-Fe-B magnets. *Journal of Applied Physics*, 61, 3763-3765.
- JAVADIAN, S., GHARIBI, H. & FALLAH, H. T. 2010. Adsorption and Micellar Properties of Binary Ionic/Nonionic Surfactant Mixtures in Ethylene Glycol + Water. *Journal of Chemical & Engineering Data*, 55, 1122-1130.
- KAO, M. J., TIEN, D. C., JWO, C. S. & AND TSUNG, T. T. 2005. The study of hydrophilic characteristics of ethylene glycol. *Journal of Physics: Conference Series*, 13, 442.
- KIM, A. S., CAMP, F. E. & LIZZI, T. 1996. Hydrogen induced corrosion mechanism in NdFeB magnets. *Journal of Applied Physics*, 79, 4840-4842.
- KOGA, Y. 2003. Effect of Ethylene Glycol on the Molecular Organization of H₂O in Comparison with Methanol and Glycerol: A Calorimetric Study. *Journal of Solution Chemistry*, 32, 803-818.

- MATSUURA, Y. 2006. Recent development of Nd-Fe-B sintered magnets and their applications. *Journal of Magnetism and Magnetic Materials*, 303, 344-347.
- MOKAL, B. 1998. *The Production and Characterisation of PTFE-Bonded NdFeB Magnets*. Doctor of Philosophy PhD Thesis, University of Birmingham.
- NEW YORK UNIVERSITY. 2009. *Water and Ice* [Online]. New York, USA: New York University. Available: http://www.nyu.edu/pages/mathmol/textbook/info_water.html [Accessed 30/11/2010 2010].
- PARKER, J. L. & CLAEISSON, P. M. 1992. Direct measurements of the attraction between solvophobic surfaces in ethylene glycol and mixtures with water. *Langmuir*, 8, 757-759.
- PENNY, W. A. & SLATER, R. A. C. 1979. UK patent application 7903561.
- RODNIKOVA, M., CHUMAEVSKII, N., TROITSKII, V. & KAYUMOVA, D. 2006. Structure of liquid ethylene glycol. *Russian Journal of Physical Chemistry A, Focus on Chemistry*, 80, 826-830.
- SAIZ, L., PADRO, J. A. & GUARDIA, E. 2001. Structure of liquid ethylene glycol: A molecular dynamics simulation study with different force fields. *The Journal of Chemical Physics*, 114, 3187-3199.
- SOLES, C. L. & YEE, A. F. 2000. A discussion of the molecular mechanisms of moisture transport in epoxy resins. *Journal of Polymer Science Part B: Polymer Physics*, 38, 792-802.
- SONG, G. & STJOHN, D. 2004. Corrosion behaviour of magnesium in ethylene glycol. *Corrosion Science*, 46, 1381-1399.
- TATTAM, C. 1996. *The Processing and Properties of Bonded Nd-Fe-B Magnets*. Doctor of Philosophy PhD Thesis, University of Birmingham.
- TATTAM, C., WILLIAMS, A. J., HAY, J. N., HARRIS, I. R., TEDSTONE, S. F. & ASHRAF, M. M. 1994. The use of polytetrafluoroethylene in the production of high-density bonded Nd-Fe-B magnets. *Journal of Applied Physics*, 76, 6831-6833.
- TATTAM, C., WILLIAMS, A. J., HAY, J. N., HARRIS, I. R., TEDSTONE, S. F. & ASHRAF, M. M. 1996a. The corrosion behaviour of uncoated bonded Nd-Fe-B magnets in humid environments. *Journal of Magnetism and Magnetic Materials*, 152, L275-L278.

- TATTAM, C., WILLIAMS, A. J., HAY, J. N., HARRIS, I. R., TEDSTONE, S. F. & ASHRAF, M. M. 1996b. Improvement in the mechanical properties of PTFE bonded Nd-Fe-B magnets by heat treatment. *Journal of Magnetism and Magnetic Materials*, 154, 328-332.
- VIKING PUMP INC. 2011. *Mag Drive Pumps* [Online]. Co. Clare, Ireland: Viking Pump Inc. Available: <http://www.vikingpump.com/en/products/magdrivepump.html> [Accessed 12/02/2011 2011].
- VODYANKINA, O., KURINA, L. & IZATULINA, G. 1998. Surface interaction of ethylene glycol with silver. *Reaction Kinetics and Catalysis Letters*, 64, 103-107.
- WALTON, A., SPEIGHT, J. D., WILLIAMS, A. J. & HARRIS, I. R. 2000. A zinc coating method for Nd-Fe-B magnets. *Journal of Alloys and Compounds*, 306, 253-261.
- WILLEY, D. B., WILLIAMS, A. J. & HARRIS, I. R. 1997. Preparation and Properties of metal matrix hydride compacts via the rotary forging compaction route. *Journal of Alloys and Compounds*, 253-254, 698-703.
- YAN, G., WILLIAMS, A. J., FARR, J. P. G. & HARRIS, I. R. 1999. The effect of density on the corrosion of NdFeB magnets. *Journal of Alloys and Compounds*, 292, 266-274.
- ZAHARIEVA, J., MILANOVA, M., MITOV, M., LUTOV, L., MANEV, S. & TODOROVSKY, D. 2009. Corrosion of aluminium and aluminium alloy in ethylene glycol-water mixtures. *Journal of Alloys and Compounds*, 470, 397-403.
- ZHANG, J., ZHANG, P., MA, K., HAN, F., CHEN, G. & WEI, X. 2008. Hydrogen bonding interactions between ethylene glycol and water: density, excess molar volume, and spectral study. *Science in China Series B: Chemistry*, 51, 420-426.

Chapter 5: Results and Discussion:

Corrosion Behaviour of NdFeB Magnequench Particles (MQP)

This chapter is concerned with the corrosion behaviour of unbonded NdFeB Magnequench Particles (MQP) during exposure to the same aqueous environmental conditions as their bonded counterparts in the previous section i.e. fully submerged at 80°C in DI water, 50/50 (Dex-Cool/DI Water) solution or ‘pure’ Dex-Cool. The corrosion behaviour of the MQP will be characterised magnetically using the vibrating sample magnetometer (VSM). As with the previous section the focus will be upon the effect on H_{ci} values, thus enabling comparisons to be made easily between bonded and loose MQP corrosion behaviour.

In addition to this, hydrogen absorption/desorption studies (HADS) will be performed in an attempt to establish the link between induced H_{ci} losses as a result of aqueous corrosion and induced hydrogen uptake through exposure to elevated temperatures and hydrogen partial pressures. This will enable accurate identification of the phases present within the MQP involved in the hydrogen uptake from the disassociation of water through aqueous corrosion and resultant losses of H_{ci} .

Fig. 5.1 shows a plot of the aqueous corrosion behaviour of loose MQP, characterised using H_{ci} values of samples exposed to DI water.

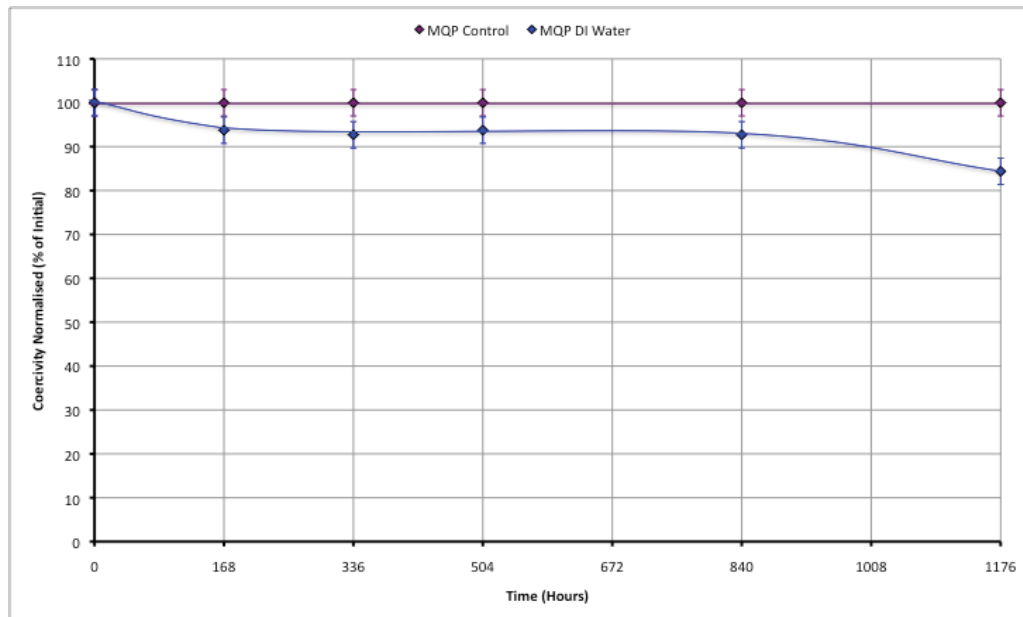


Fig. 5.1 Depicts normalised coercivity (%) against time for unbonded MQP exposed to an aqueous (DI water) environment at 80°C in the presence of varying concentrations of Dex-Cool.

It can be seen from Fig. 5.1 that the unbonded MQP suffer similar H_{ci} losses during exposure to aqueous environmental conditions. It is possible that this is the result of the same process as that seen in bonded samples. Although the H_{ci} losses experienced by the unbonded MQP are much less severe; after 1176 hours exposure the equivalent epoxy bonded sample fully submerged in DI water had suffered H_{ci} losses of approximately 50% of the initial value. The unbonded MQP after the same period of exposure to DI water had lost only 15% of the initial H_{ci} value.

This large discrepancy between the performance of bonded and unbonded MQP exposed to the same environmental conditions must be due to how the MQP are arranged during this exposure. Within this section the unbonded MQP were simply left in an undisturbed state i.e. allowed to settle at the bottom of the sample tube. With the benefit of hindsight it may have been prudent to agitate the MQP throughout the course of the experiment. The MQP

appeared to settle into a very compact uniform stacked arrangement. This highly uniform stacking arrangement is likely a result of the production methods utilised to manufacture the MQP i.e. melt spinning, the particles manufactured are very similar in shape. This shape is determined primarily by the curvature of the wheel upon which the molten alloy solidified upon during manufacturing. The relatively low variability in curvature of and size of particles promotes a very uniform stacking arrangement which is also aided by the smooth surface texture. Another factor which will promote the uniform stacking arrangement is the fact that although the MQP are in an unmagnetised state, there will exist areas of spontaneous magnetisation which will in turn attract particles to one another. This will greatly hinder the access for water to the MQP surface, effectively decreasing the surface area available for aqueous corrosion attack.

By contrast it would appear that within the structure of a bonded magnet, the MQP are effectively being held apart and separated by the bonding media. This is especially true for epoxy bonded samples which from the previous section has been shown to be permeable to water. This coupled with the individual particle encapsulation technique utilised to apply the epoxy resin coating ensures that there is minimal agglomeration of MQP resulting in uniformly spaced particles within the bonded samples and thus providing maximum available surface area for attack by aqueous corrosion.

It would be interesting to determine if the MQP were agitated over the duration of DI water exposure, if greater H_{ci} losses would result due to the availability of a larger surface area for aqueous corrosion attack. It would also be possible to use a smaller volume of MQP to prevent stacking. Although for the sake of continuity, this study utilised the same volume of MQP that was required to produce the bonded magnets of the same. It was

initially thought that this would enable more accurate comparisons to be made between the bonded and unbonded configurations. Unfortunately this did not prove to be the case.

5.1 Effect of Dex-Cool On Corrosion Behaviour of MQP

Fig. 5.2 is concerned with the effect of Dex-Cool additions to the aqueous environment and the effect this has on H_{ci} losses in MQP.

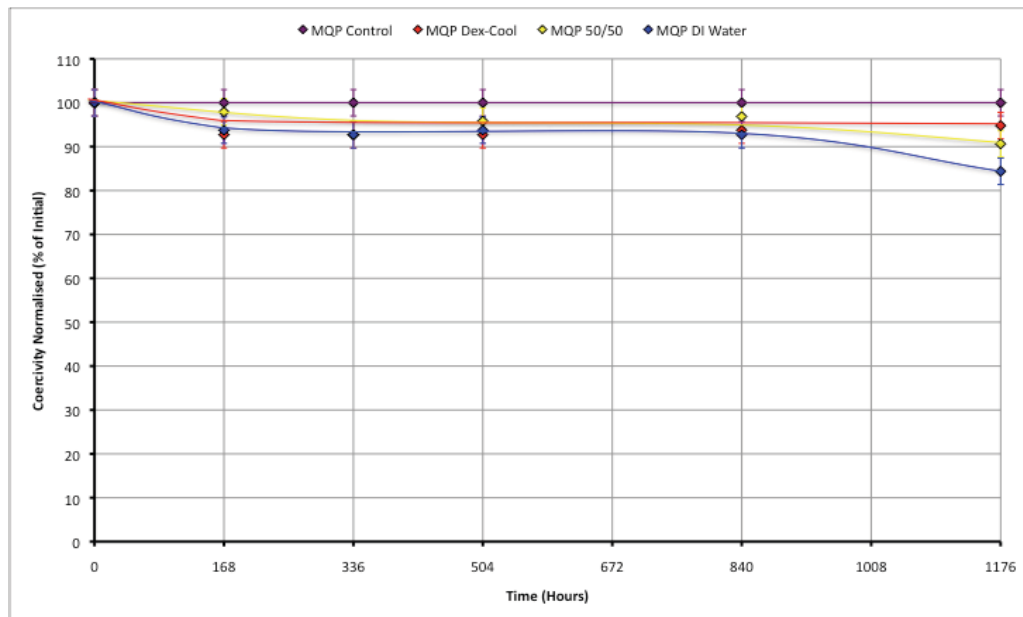


Fig. 5.2 Depicts normalised coercivity (%) against time for unbonded MQP exposed to an aqueous environment at 80°C in the presence of varying concentrations of Dex-Cool (DI water, 50/50 (Dex-Cool/DI water) solution, and ‘pure’ Dex-Cool).

From Fig. 5.2 it can be seen that additions of Dex-Cool did improve the aqueous corrosion performance of MQP in terms of H_{ci} preservation during exposure to the aqueous environment. The improvement in performance was not on the same scale as that seen for bonded samples although the degree of H_{ci} losses were not on the same scale either. It is likely that the lower aqueous corrosion rates of MQP compared to bonded magnets have masked some of the positive effects previously seen as a result of Dex-Cool additions.

It is worth noting that although the result of Dex-Cool additions were not as dramatic as when used in conjunction with bonded MQP the Dex-Cool and 50/50 (Dex-Cool/DI water) solution did retain approximately 95% and 90% of the initial H_{ci} value respectively, compared to the 85% that was observed for the sample exposed to DI water.

It is also interesting to note that the gap in performance between MQP exposed to 50/50 (Dex-Cool/DI water) solution compared to that of the 'pure' Dex-Cool appears to be much larger than for their PTFE bonded counterparts. This could possibly be due to the much larger surface area readily available for attack by aqueous corrosion compared to the available surface area in PTFE bonded magnets. It may be the case that due to the larger surface area a greater volume of Dex-Cool is required to provide protection for the MQP surface hence the reason why the 50/50 (Dex-Cool/DI water) was not so successful for the unbonded MQP as it was for the bonded samples.

5.2 Hydrogen Absorption/Desorption Studies (HADS) of MQP

This section of the study is centred upon the behaviour of the MQP in response to hydrogen absorption through aqueous corrosion or induced uptake. This behaviour will be characterised magnetically through measurements performed using the VSM focusing specifically on H_{ci} values. In conjunction with this, heat treatments were performed under vacuum across a range of temperatures to desorb any hydrogen present within the MQP. After each outgassing step the MQP was again characterised magnetically to determine the impact that the removal of absorbed hydrogen has upon H_{ci} values. This data should provide an accurate picture of the phases involved in the hydrogen absorption and the consequences in terms of H_{ci} losses as a result. This will also allow links to be made between the hydrogen absorption as a result of aqueous corrosion and associated effects upon magnetic properties.

5.2.1 Hydrogen Absorption in MQP

Fig. 5.3 shows a desorption trace plotted for a sample of MQP after hydriding at 200°C with a hydrogen partial pressure of 1.5 bar, cooling under a hydrogen atmosphere. The desorption was performed on the thermogravimetric analyser (TGA) with mass spectroscopy (MS) analysis of gasses evolved during heating.

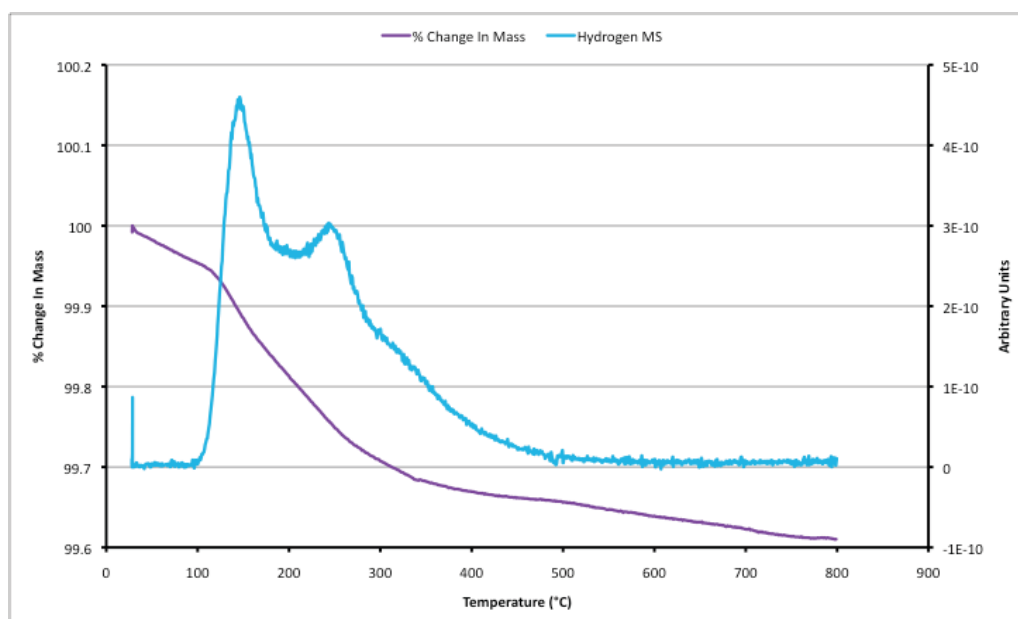


Fig. 5.3 Depicts the TGA/MS data of the hydrogen desorption trace for MQP after hydriding at 200°C and 1.5 bar hydrogen.

From the TGA/MS desorption trace above it can be seen that after the MQP sample has been exposed to the hydrogen atmosphere, hydrogen had been actively absorbed. This is supported by the decrease in sample mass and corresponding peaks depicting hydrogen desorption caused by the evolution of hydrogen gas during the heating cycle. This proves that hydrogen absorption will readily occur in MQP when exposed to favourable conditions.

The hydrogen desorption peaks that are present on the desorption trace in Fig. 5.3 correspond to hydrogen desorption peaks previously observed for the $\text{Nd}_2\text{Fe}_{14}\text{B}$ phase characterised by a sharp peak centered on 150 °C followed by a broad shoulder which indicates a peak centered on approximately 250 °C (Williams et al., 1991). It is important to highlight the absence of any high temperature desorption peaks which would be expected at approximately 600°C, where hydrogen would be expected to desorb from the Nd-rich phase (Williams et al., 1991). The absence of this high temperature hydrogen desorption peak confirms the presence of a relatively small volume of Nd-rich phase within the MQP.

To aid comparison, Fig. 5.4 shows the TGA/MS desorption trace for the same MQP sample before exposure to hydrogen atmosphere.

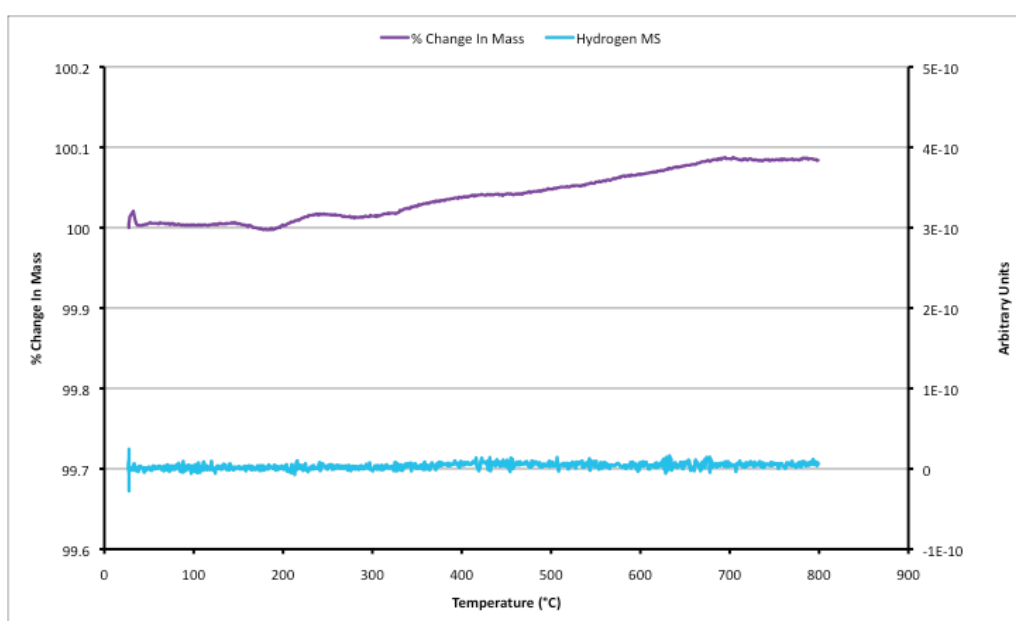


Fig. 5.4 Depicts the TGA/MS data of the hydrogen desorption trace for MQP before the hydriding step.

From the desorption trace in Fig. 5.4, it can be seen that before the sample was subject to hydrogen exposure, during the heating cycle in the TGA/MS there was no decrease in sample mass and the MS detected no hydrogen evolved during sample heating.

To magnetically characterise the effect of hydrogen absorption upon samples of MQP, hysteresis measurements were performed on the same sample before and after exposure to hydriding conditions. Fig. 5.5 shows the second quadrant demagnetisation curve of the MQP before and after hydrogen exposure.

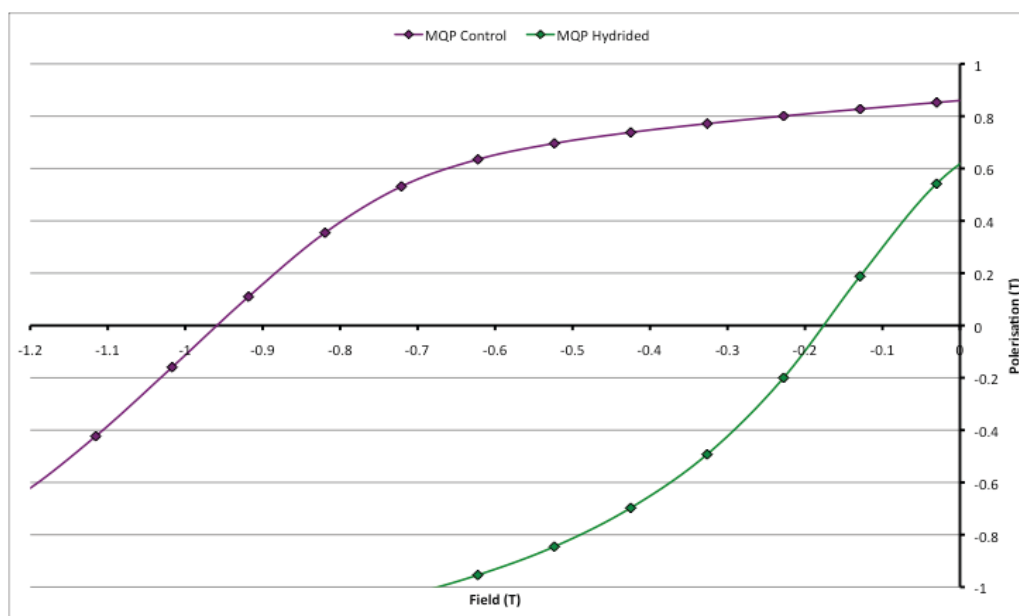


Fig. 5.5 Depicts the second quadrant demagnetisation curve taken from VSM data of the MQP sample before and after exposure to hydriding conditions.

The magnetic characterisation data in Fig. 5.5 shows the dramatic affect that exposure to and uptake of hydrogen by the $\text{Nd}_2\text{Fe}_{14}\text{B}$ phase can have upon the magnetic properties of the MQP. It can be seen that upon uptake of hydrogen the H_{ci} value is reduced to approximately 18% of the initial value.

Within the microstructure of MQP there exists a very small volume of the highly reactive Nd-rich phase compared with sintered magnets. This is predominantly due to the near stoichiometry of the starting alloy and also the rapid solidification technique employed to produce the alloy. This rapid solidification technique employed enables the alloy to be produced with fine polyhedral shaped $\text{Nd}_2\text{Fe}_{14}\text{B}$ grains approximately 30 nm in diameter. These grains are completely surrounded by a 2 nm thick layer of the paramagnetic Nd-rich phase (Herbst and Croat, 1991).

For MQP in the presence of hydrogen produced either during the aqueous corrosion process or exposure to a hydrogen atmosphere, in the absence of a significant volume of the highly reactive Nd-rich phase the next most reactive phase is the $\text{Nd}_2\text{Fe}_{14}\text{B}$ phase. This phase is ultimately responsible for the magnetic properties of the MQP and will also readily absorb hydrogen. Any hydrogen absorption involving this ferromagnetic phase will have serious implications for the magnetic properties in particular the H_{ci} , due to the crystal lattice expansion induced by the uptake of hydrogen (Oesterreicher and Oesterreicher, 1984), (Nikitin et al., 2003).

5.3 Intrinsic Coercivity (H_{ci}) Loss Due To Hydrogen Ingress

The similarities observed in the behaviour of the magnetic properties of MQP as a result of hydrogen ingress, from either hydrogen evolved from the disassociation of water during the aqueous corrosion process or, from exposure to a hydrogen atmosphere can be seen in Fig. 5.6.

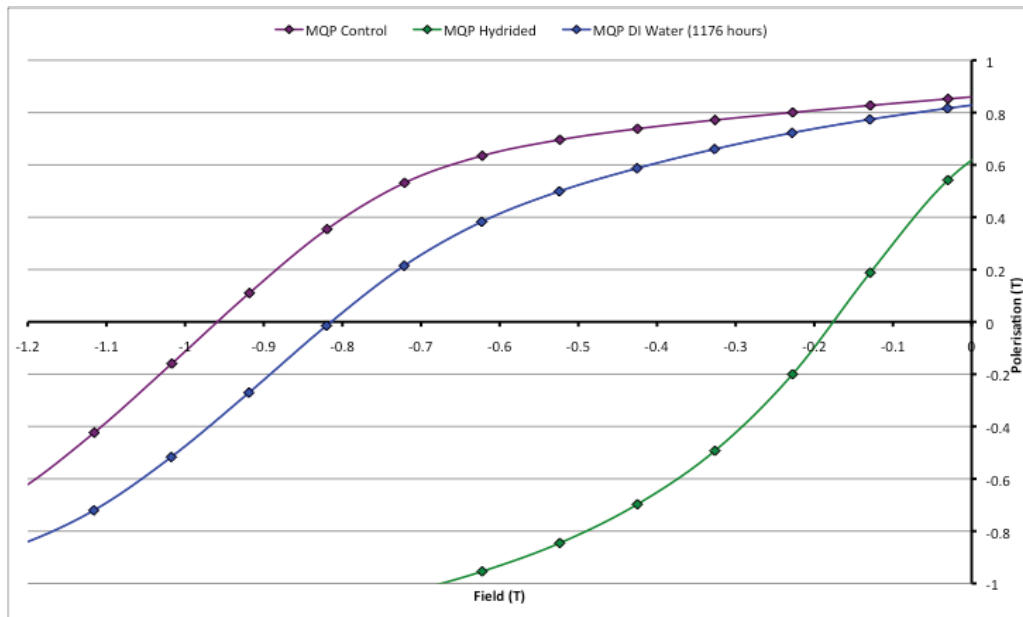


Fig. 5.6 Depicts the second quadrant demagnetisation curve taken from VSM data of the MQP sample after 1176 hours exposure to DI water (blue), before (purple) and after (green) exposure a hydriding conditions.

From Fig. 5.6 it can be seen that when a sample of MQP exposed to environmental conditions that facilitate the aqueous corrosion process, the effect can be characterised magnetically by a loss of H_{ci} . It can be seen that both samples of MQP display negative changes in magnetic properties as a result of the processes they are exposed to. Although in this case, uptake of hydrogen from exposure to a hydrogen atmosphere represents a much more severe demonstration of the detrimental effect that hydrogen absorption can have upon the magnetic properties of MQP.

5.4 Hydrogen Desorption and Effects Upon Magnetic Properties of MQP

This section of the chapter will attempt to magnetically characterise the effect of hydrogen absorption on unbonded MQP and establish the link between aqueous corrosion behaviour and hydrogen absorption (Kim et al., 1996). This was done with the aid of a sample of MQP subject to the same hydrogen atmosphere that induced hydrogen uptake by the alloy

and produced the desorption trace observed in Fig. 5.3. Magnetic measurements have been performed with the VSM in conjunction with heating cycles carried out under vacuum. After each heating/outgassing cycle a desorption trace has been performed with the TGA/MS to monitor hydrogen evolution from the sample during the heating cycle.

Fig. 5.7 shows a plot of the MQP H_{ci} before exposure to the hydrogen atmosphere, after exposure to the hydrogen atmosphere. The H_{ci} for each sample of MQP will be presented for each subsequent outgasing heat treatment.

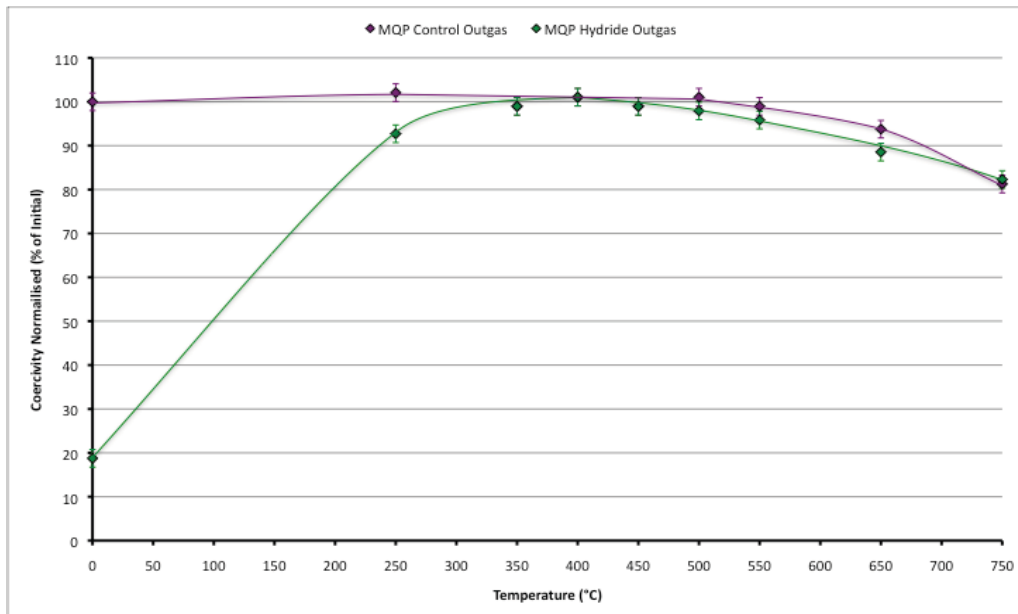


Fig. 5.7 Depicts the relationship between intrinsic coercivity (H_{ci}) and temperature of heat treatment performed to remove absorbed hydrogen on a control sample (purple) and a hydrided sample (green).

From Fig. 5.7 two traces can be seen. The purple line represents the MQP control trace, it was performed on a control sample to enable any affects upon H_{ci} , as a direct consequence of the heat treatments performed, to be accounted for. It can be seen that for this control sample, after the 250°C heat treatment was performed there was a small observed increase in the H_{ci} value. This is likely to be a result of the storage and handling of the alloy. As

MQP is much less susceptible to oxidation and corrosion processes due to the relatively small volume of Nd-rich phase, they are generally stored in air and at room temperature. This is generally accepted as the effects observed upon the magnetic properties tend to be negligible. It can be seen from the trace that an increase of approximately 2% of the initial H_{ci} value occurred. The H_{ci} losses suffered during this storage time are likely to be attributed to aqueous corrosion and subsequent uptake of hydrogen, as a result of contact with moisture contained within the air. It is also possible that this 250°C heating cycle may relieve any residual stresses induced during material production processes e.g. during the milling stage.

It can also be seen from the plot of the MQP control sample that the magnetic properties did not start to suffer the detrimental effects associated with the heat treatment until approximately 500 – 550°C. Even at these temperatures the effects could still be considered negligible. The H_{ci} losses observed at these temperatures could be due to oxidation of the $Nd_2Fe_{14}B$ phase as a result of the exposure to elevated temperatures and insufficient level of vacuum achieved within the vacuum furnace tube and not from desorbed hydrogen. However, it is more likely that subjecting the MQP to temperatures above 500°C for a sufficient period of time would encourage grain growth making nucleation and growth of reverse magnetic domains easier and thus giving a reduction in coercive force. To illustrate this point, Fig. 5.8 shows a hydrogen desorption trace for a hydrided sample heat treated at 750°C. This temperature would be sufficient to remove all absorbed hydrogen from any phases present in the MQP.

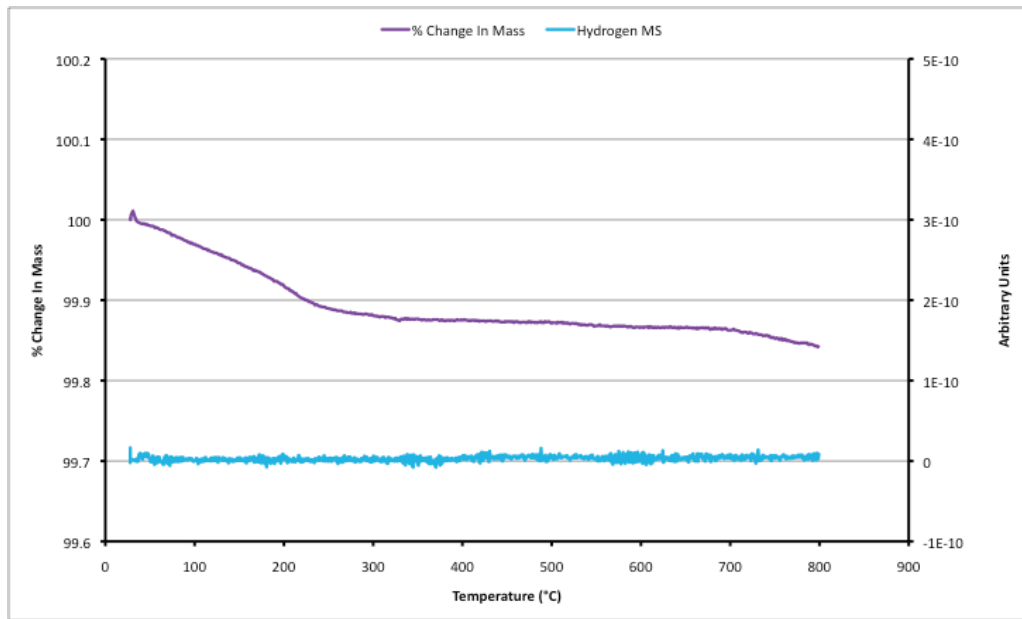


Fig. 5.8 Depicts the hydrogen desorption trace for the hydrided MQP sample after a 750°C heat treatment.

From the hydrogen desorption trace seen in Fig. 5.8 it is clear that after the hydrided sample has been subject to a heat treatment at 750°C there is no hydrogen desorbed during the heating cycle performed in the TGA/MS. This indicated that the H_{ci} losses observed in could be attributed to oxidation as a result of heating under insufficient vacuum levels and not from the presence of hydrogen and associated crystal lattice expansion effects.

It can be seen that after the 250°C heat treatment the H_{ci} has returned to approximately 93% of the initial value. Fig. 5.9 depicts the hydrogen desorption trace for the hydrided sample of MQP after it has been subject to a 250°C heat treatment.

The key information that can be derived using both Fig. 5.9 and Fig. 5.7 is the relationship between the removal of absorbed hydrogen (through outgassing heat treatments) and the improvement in magnetic properties, or more specifically increase in H_{ci} , as a result of this.

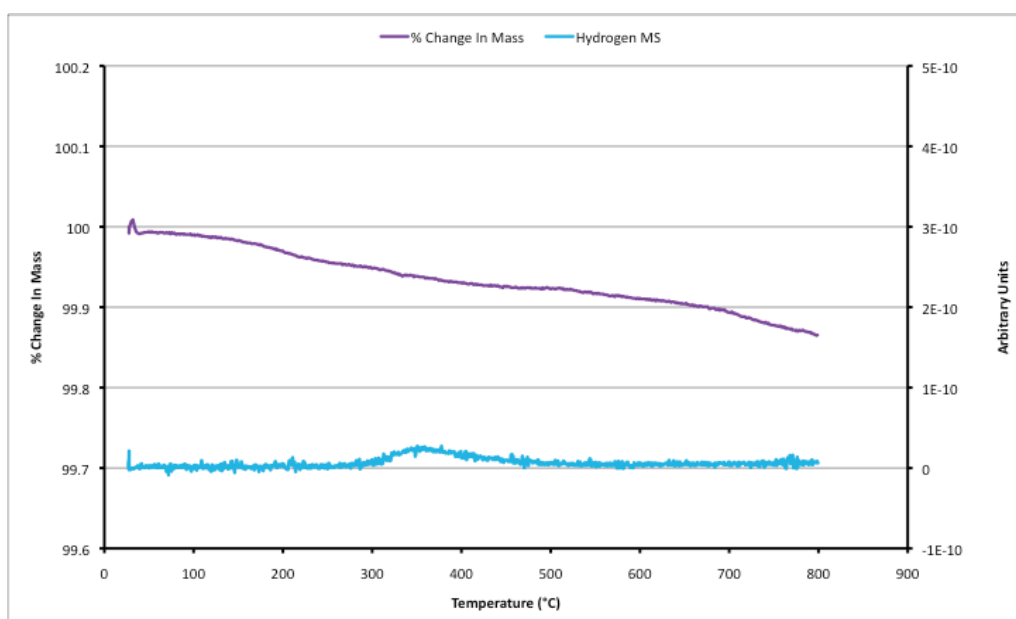


Fig. 5.9 Depicts the hydrogen desorption trace for the hydrided MQP sample after a 250°C heat treatment.

Fig. 5.9 clearly shows a hydrogen peak being desorbed from the sample between 300 – 500°C. This would suggest that the heat treatment performed at 250°C was too low to facilitate the desorption of all the hydrogen from the $\text{Nd}_2\text{Fe}_{14}\text{B}$ phase. On comparison with the hydrogen desorption trace shown for the same sample prior to the 250°C heat treatment in Fig. 5.3, this indicates that the majority of absorbed hydrogen had been removed. This is supported by the VSM data from Fig. 5.7 whereby, as the outgassing temperature is subsequently increased the H_{ci} value is returned closer to the initial value up until 400°C. This appears to be the optimum temperature at which to remove all absorbed hydrogen from the $\text{Nd}_2\text{Fe}_{14}\text{B}$ phase before degradation of magnetic properties.

The TGA/MS desorption trace for the hydrided MQP sample after the 350°C heat treatment can be seen in Fig. 5.10.

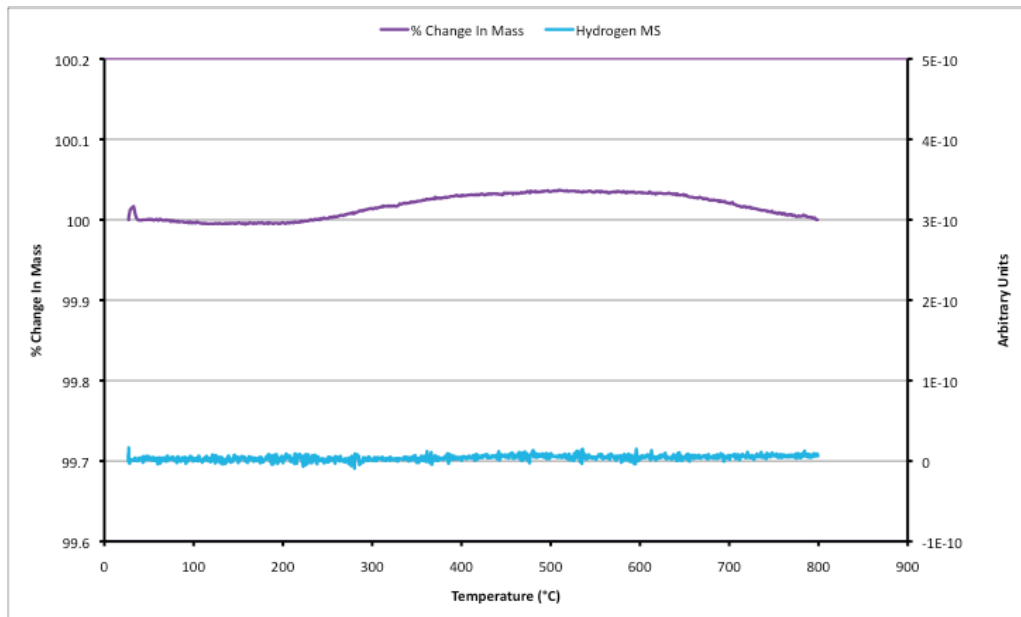


Fig. 5.10 Depicts the hydrogen desorption trace for the hydrided MQP sample after a 350°C heat treatment.

From the hydrogen desorption trace in Fig. 5.10 it can be seen that after the hydrided MQP had been subject to the 350°C heat treatment there was still a small hydrogen peak visible above the noise centred on 450°C. This indicates that the 350°C temperature was insufficient to desorb all of the hydrogen from within the $\text{Nd}_2\text{Fe}_{14}\text{B}$ phase. This data is supported by the VSM trace seen in Fig. 5.7, which shows that after the 350°C heat treatment the H_{ci} value is at approximately 98% of the initial value. Again indicating that full recovery of the initial H_{ci} value is due to absorbed hydrogen removal. The tiny sample mass change observed is likely due to contamination within the TGA system.

Below a TGA/MS desorption trace for the hydrided MQP sample after the 400°C heat treatment can be seen in Fig. 5.11.

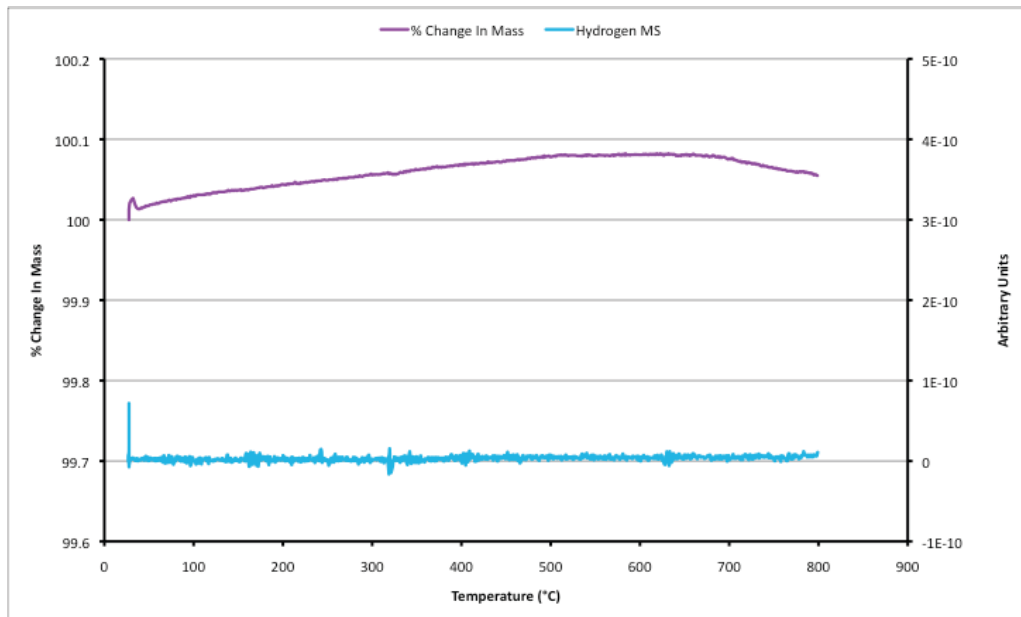


Fig. 5.11 Depicts the hydrogen desorption trace for the hydrided MQP sample after a 400°C heat treatment.

The hydrogen desorption trace in Fig. 5.11, performed on the hydrided sample after the 400°C heat treatment shows that the 400°C is sufficient to remove all of the desorbed hydrogen from the $\text{Nd}_2\text{Fe}_{14}\text{B}$ magnetic phase. This is supported by magnetic data from the VSM trace, which also indicates H_{ci} has returned to 101% of the initial value.

From Fig. 5.7 it can be seen that any heat treatments performed on the hydrided MQP at temperatures above 400°C results in degradation of the magnetic properties, which as previously discussed are likely due to the effects other than incomplete removal of absorbed hydrogen.

The H_{ci} of the hydrided sample never recovers to levels seen in the control sample upon heating past the 400°C point. This suggests that there is damage caused to the microstructure during the uptake of hydrogen that is irreversible even after desorption. It is possible that the application of heat to the MQP while in it's hydrided state enhanced the

diffusion process leading to accelerated grain growth. The expanded crystal lattices of the $\text{Nd}_2\text{Fe}_{14}\text{B}$ and Nd-rich phases, as a result of absorbed hydrogen located at interstitial sites, actively facilitates the diffusion of Nd and Fe atoms during thermal agitation effectively increasing the rate of diffusion and hence rate of grain growth.

A similar trend is noted in the MQP control sample whereby H_{ci} suffered degradation at temperatures above approximately 500°C . There is approximately a 100°C discrepancy between the temperature at which the H_{ci} of the hydrided sample begins to degrade compared to that of the control sample.

It seems clear from the results gathered in this section involving hydrogen absorption by MQP and subsequent TGA/MS analysis in conjunction with magnetic characterisation after each outgassing heat treatment, that the link between hydrogen absorption and H_{ci} has been clearly established.

5.4.1 Post Aqueous Corrosion Heat Treatment and Magnetic Properties

This section will relate the degradation of H_{ci} in an aqueous environment to the absorption of hydrogen. Fig. 5.12 shows the hydrogen desorption trace for a sample of MQP exposed to DI water over a 1176 hour period.

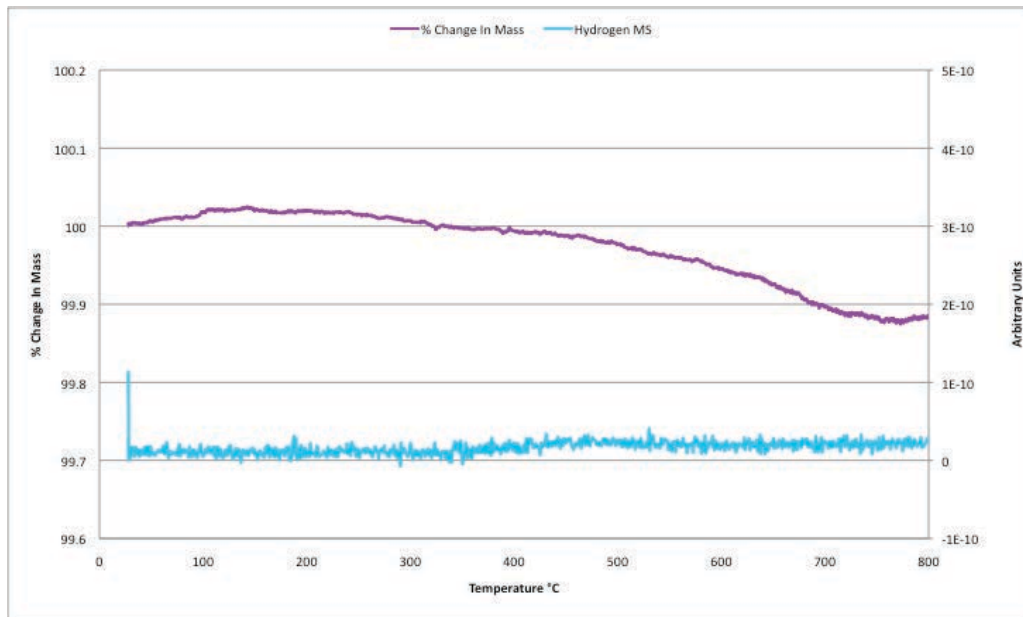


Fig. 5.12 Depicts the hydrogen desorption trace for the MQP sample exposed to DI water for 1176 hours.

It can be seen that during this time the sample had absorbed a small amount hydrogen. This can be seen by the small peak evident between 150 – 200°C. Although the absorption of hydrogen is not on the same scale as that for the MQP exposed to the hydrogen atmosphere (Fig. 5.3). This fits well as Fig. 5.13 will demonstrate the effect upon the magnetic properties are also not on the same scale as those for MQP exposed to the hydrogen atmosphere. The peak evident from approximately 400°C is possibly due to contamination within the TGA/MS system.

Fig. 5.13 shows a modified version of Fig. 5.7 including supplementary data relating to changes in H_{ci} relative to initial values for the sample of MQP exposed to DI water for 1176 hours. As before heat treatments were applied under vacuum to remove hydrogen that could have been absorbed as a result of the aqueous corrosion process.

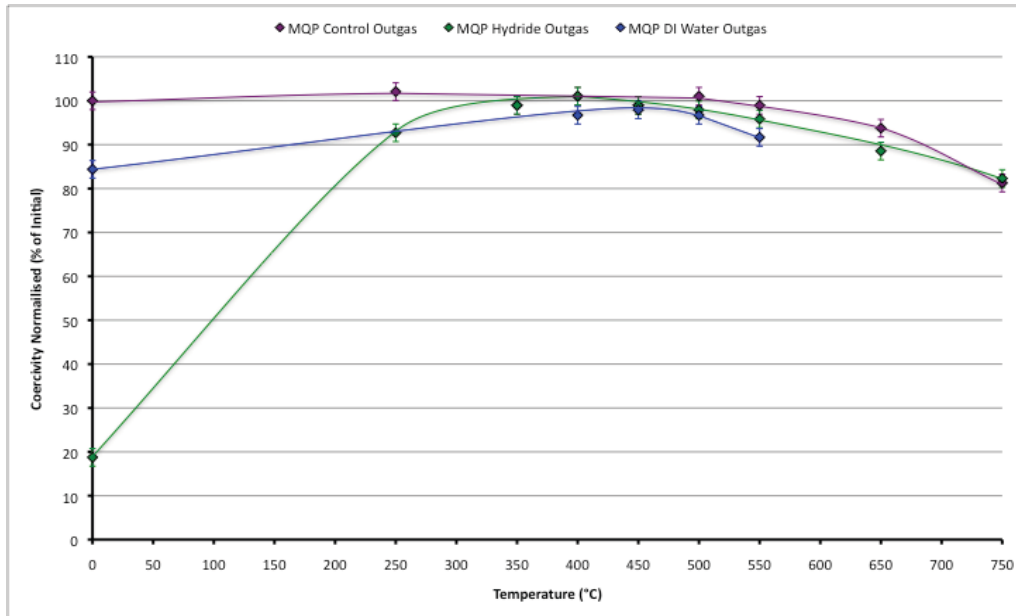


Fig. 5.13 Depicts the relationship between intrinsic coercivity (H_{ci}) and temperature of heat treatment performed to remove desorbed hydrogen on a control sample (purple), a hydrided sample (green) and a sample exposed to DI water for 1176 hours (blue).

It can be seen from Fig. 5.13 that the effect of 1176 hours exposure to DI water did not cause a reduction in H_{ci} as dramatic as that seen in the hydrided sample. After the 1176 hours exposure to DI water the H_{ci} was reduced to approximately 85% of the initial value. Following the same procedure as before outgassing techniques were performed within the temperature range that returned the H_{ci} of the hydrided sample i.e. centred on 400°C.

The sample exposed to DI water shows a partial recovery of H_{ci} upon heating under vacuum. The optimum outgas temperature for the sample exposed to DI water appears to be approximately 450°C, which is approximately 50°C higher than its control and hydrided sample counterparts. It should be noted that these differences are within expected margins of error. The 450°C outgas performed on the DI water exposure sample returned the H_{ci} to

approximately 98% of its initial value and are consistently lower than the control and hydrogen treated samples.

It is believed that hydrogen uptake plays a role in the aqueous corrosion process but is not the only mechanism of corrosion. During the aqueous corrosion process hydrogen is produced by the disassociation of water upon contact with the small volume of Nd-rich phase during the formation of $\text{Nd}(\text{OH})_3$ and possibly Nd_2O_3 . This process will undoubtedly cause some of the submicron-sized $\text{Nd}_2\text{Fe}_{14}\text{B}$ grains to lose adhesion with the bulk material of the MQP and may create free iron. These effects will be irreversible and unlike the effect of hydrogen absorption cannot be removed by vacuum annealing.

Apart from the disassociation of water that forms the hydrogen absorbed by the $\text{Nd}_2\text{Fe}_{14}\text{B}$ magnetic phase, the mechanisms responsible for H_{ci} losses are the same i.e. upon hydrogen absorption the $\text{Nd}_2\text{Fe}_{14}\text{B}$ phase suffers an expansion of the crystal lattice and reduction in exchange interactions between Fe – Fe and Nd – Fe atoms.

Fig. 5.14 shows the change in H_{ci} of samples exposed to ‘pure’ Dex-cool, 50/50 (Dex-Cool/DI water) solution and DI water for 1176 hours, after an outgassing heat treatment performed at 450°C.

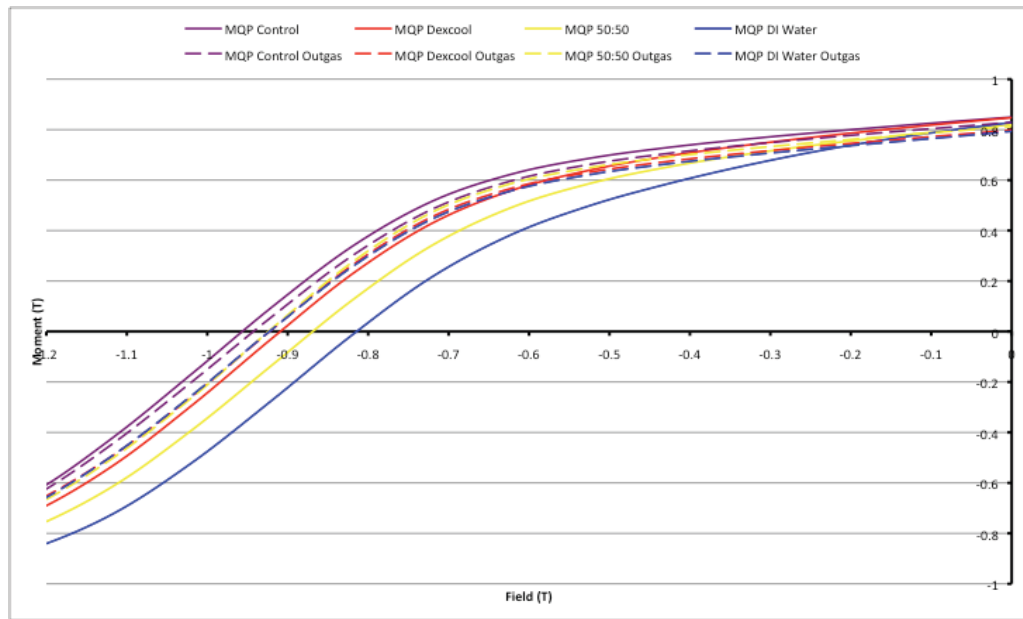


Fig. 5.14 Depicts the second quadrant demagnetisation curves for MQP samples exposed to ‘pure’ Dex-Cool (Red), 50/50 (yellow), DI water (blue) for 1176 hours and a control (purple) The corresponding dashed (- -) lines represent the magnetic properties after a 450°C outgas.

From Fig. 5.14 it can be seen that after the MQP had been exposed to the aqueous environment for 1176 all samples suffered losses in H_{ci} . Some more than others, which has previously been discussed within this chapter. After the samples had been subject to a 450°C outgassing treatment (denoted by - - -) it can be seen that all of the samples with the exception of one saw improvements in the H_{ci} values.

The sample that did not see any improvement in the H_{ci} was the control sample, it is possible that H_{ci} of this sample may have been affected by oxidation during heating. If this were the case, all the samples will have suffered the same fate, as the outgas was performed simultaneously on all samples. Another possibility is that the outgassing products from the corroded samples may have been absorbed by the control. It is possible that some of the positive effects in terms of H_{ci} recovery may have been masked as a result.

5.5 Influence of Dex-Cool On Hydrogen Absorption/Desorption Of MQP

This section will attempt to characterise the hydrogen absorption behaviour of MQP in the presence of a Dex-Cool “coating” with the use of TGA/MS. It is hoped that this will shed some light on the mechanism by which Dex-Cool actively preserves the H_{ci} of the alloy.

It has been demonstrated earlier within this section how readily a sample of MQP will absorb hydrogen under the correct conditions. Fig. 5.3 shows the TGA/MS hydrogen desorption trace of a hydrided sample of MQP.

The MQP was then treated with Dex-Cool by soaking for approximately 10 minutes. The MQP was then drained and allowed to dry under vacuum for approximately 12 hours. The Dex-Cool treated MQP was then subject to the same hydriding conditions as in the previous section.

Fig. 5.15 shows the hydrogen desorption trace of the Dex-Cool treated MQP after exposure to conditions known to induce hydrogen uptake.

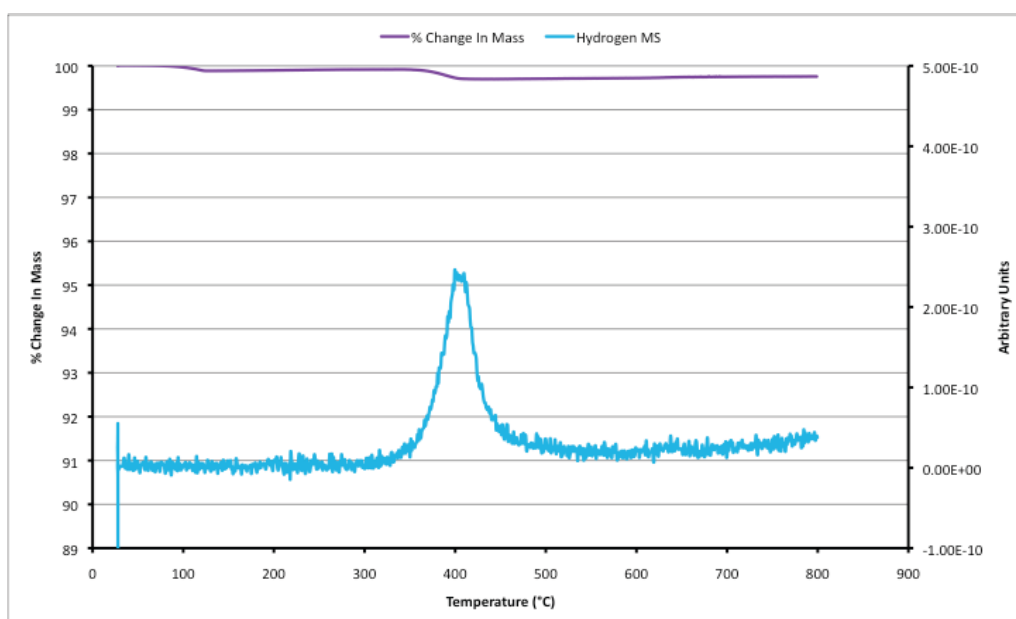


Fig. 5.15 Depicts the TGA/MS data of the hydrogen desorption trace for Dex-Cool treated MQP after hydriding at 200°C and 1.5 bar hydrogen.

From Fig. 5.15 it can be seen that there is one clear hydrogen desorption peak present. This peak is centred on approximately 400°C. It is apparent that there are no desorption events centred on 150°C or 250°C as in Fig. 5.3, which would correspond to the desorption of hydrogen from the $\text{Nd}_2\text{Fe}_{14}\text{B}$ phase in two stages. This would suggest that the Dex-Cool treatment has actively prevented the $\text{Nd}_2\text{Fe}_{14}\text{B}$ phase from absorbing hydrogen even under these extreme conditions. It is likely that this hydrogen desorption peak is the by-product of Dex-Cool decomposition during the heating cycle.

From the literature regarding use of EG on the oxide surfaces of metal catalysts, more specifically silver in this case. There is evidence to suggest from this unrelated study that the EG metal oxide surface interaction is characterised by the strength of the oxygen catalyst bond and the alcohol adsorption temperature (Vodyankina et al., 1998).

In the case of MQP the strength of the metal-oxide bond would be high due to the reactive nature of neodymium and the ease at which oxidation occurs, only requiring exposure to air at room temperature.

The other factor that Vodyankina et al. specify is critical to adsorption is the temperature at which this adsorption occurs. In the case of MQP it would appear that adsorption of EG onto the surface of MQP has occurred during the hydriding step. As previously stated the hydriding was performed at 200°C. It would appear that the heat applied for the purpose of activating the $\text{Nd}_2\text{Fe}_{14}\text{B}$ phase has actually aided the adsorption of EG onto the surface of the MQP.

The above study characterised the adsorption of EG using temperature-programmed reaction (TPR) spectra. The TPR spectra of an EG adsorption performed at 473K ($\sim 200^\circ\text{C}$) can be seen in Fig. 5.16.

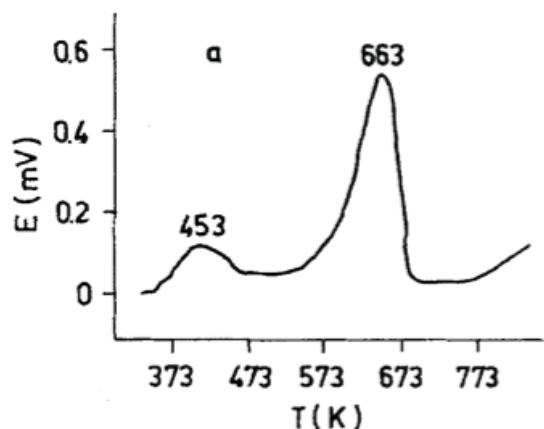


Fig. 5.16 Modified version of temperature-programmed reaction spectra on oxidised Ag surface at adsorption temperature of 473K (Vodyankina et al., 1998).

It can be seen that the TPR spectra contain two peaks. The first peak at 453K ($\sim 180^\circ\text{C}$) which the authors identify as the desorption of water. The second peak centred on 663K (\sim

390°C) which the authors related to the desorption of glyoxal, ethylene glycol and hydrogen (Vodyankina et al., 1998).

To allow an accurate comparison to be made with the data from Fig. 5.17, TGA/MS data was collected from a control sample of Dex-Cool treated MQP before exposure to hydrogen i.e. the Dex-Cool control was subject to the same heating cycle as the hydrided sample in the absence of hydrogen. This trace can be seen in Fig. 5.17.

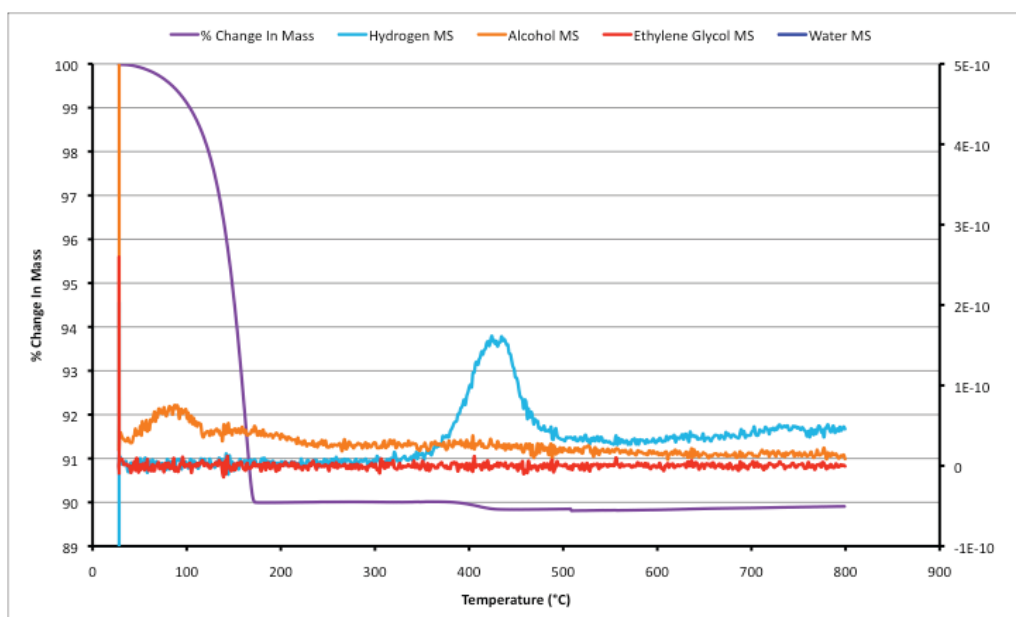


Fig. 5.17 Depicts the TGA/MS data of the desorption trace for Dex-Cool treated MQP post 200°C heat treatment prior to hydrogen exposure.

The peaks from the mass spec data are in strong agreement with the findings of Vodyankina et al. In that there is a hydrogen desorption event centred $\sim 400^{\circ}\text{C}$. This hydrogen desorption peak is in the same place as that observed for the Dex-Cool treated MQP exposed to hydrogen, seen in Fig. 5.17. This provides strong evidence that the hydrogen desorption peak seen in Fig. 5.17 is not a result of the evolution of hydrogen from any phase of the MQP alloy. It is likely that this is as a result of a similar desorption

event witnessed by Vodyankina et al. The desorption temperatures may be slightly different for MQP relative to AgO but this process could possibly be very similar.

To strengthen this argument if the above desorption trace is rescaled to show the desorption of water this is also within the range of water desorption described by Vodyankina et al. at approximately 453K (~ 180°C). This rescaled TGA/MS desorption trace can be seen in Fig. 5.18.

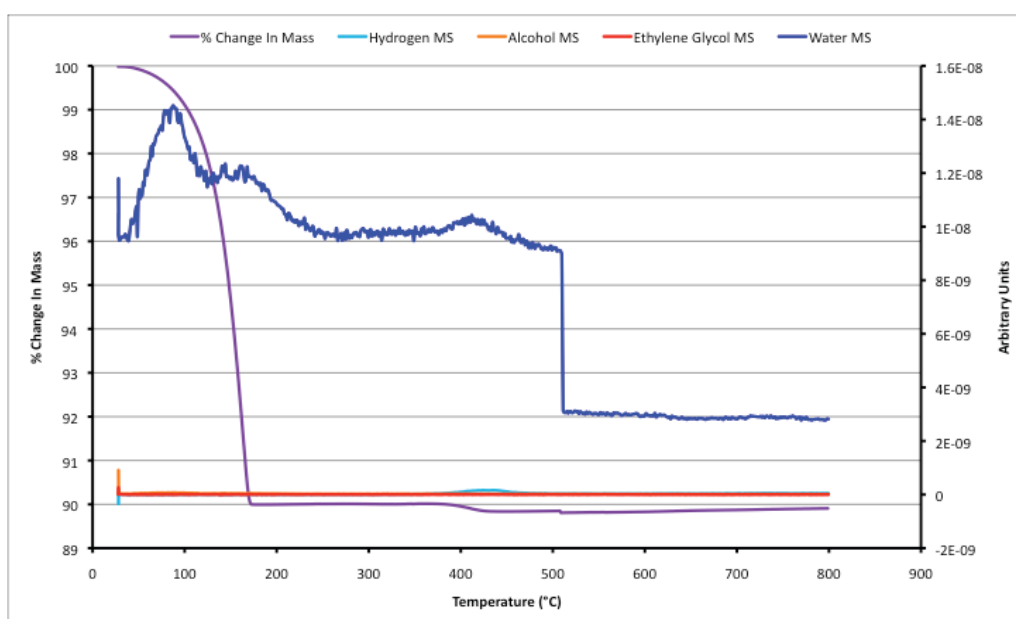


Fig. 5.18 Depicts the rescaled TGA/MS desorption trace from Fig. 5.17.

It can be seen from this rescaled TGA/MS desorption trace that there is a broad water desorption event below 100°C which is expected as any moisture from the surface of the sample evaporates. There is then another water desorption event centred approximately on 180°C which was also observed by Vodyankina et al from the surface of Ag. To give some idea of the change in scale the hydrogen desorption event centred on 400°C is just about visible.

Having established from the TGA/MS data it is likely that the formation of a Dex-Cool layer on the surface of the MQP has actively prevented hydrogen from entering the $\text{Nd}_2\text{Fe}_{14}\text{B}$ magnetic phase. Magnetic characterisation was performed on a Dex-Cool treated MQP sample exposed to hydriding conditions. This can be seen in Fig. 5.19.

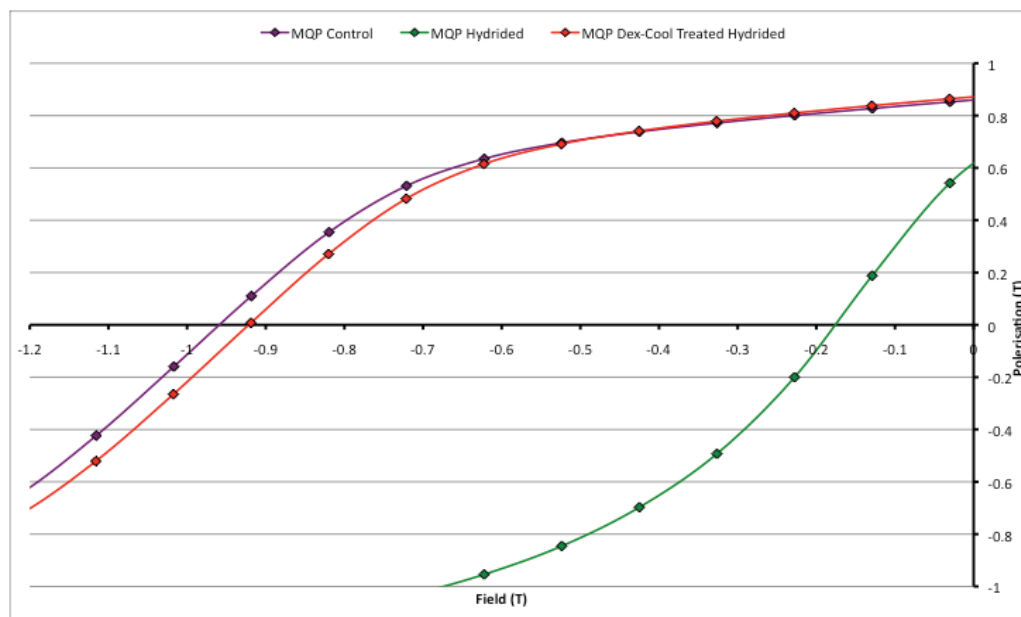


Fig. 5.19 Depicts the second quadrant demagnetisation curves taken from VSM data for a Dex-Cool treated sample of MQP before and after hydriding at 200°C and 1.5 bar hydrogen. For comparison MQP control (purple) and untreated MQP (green).

From Fig. 5.19 it can be seen that the effect of exposure to hydriding conditions on Dex-Cool treated MQP had very little effect upon the H_{ci} of the sample. This is apparent when compared to the effects of exposure on non-treated MQP (green).

It can be seen that exposure to hydriding conditions does have a detrimental effect upon the H_{ci} of the MQP even after treatment with Dex-Cool. It can be said with certainty that the “Dex-Cool treatment” does not totally prevent the ingress of hydrogen under these

extreme conditions. Although a dramatic improvement in the preservation of H_{ci} can be seen between the treated and non-treated samples.

To ascertain if the reduction of H_{ci} in the Dex-Cool treated MQP was due to the ingress of hydrogen during exposure to hydriding conditions an outgas was performed. The temperature selected was 400°C, this was deemed the optimum heat treatment temperature for the removal of absorbed hydrogen from Fig. 5.7. The second quadrant demagnetisation curves of the hydriding and outgassing heat treatment for Dex-Cool treated MQP can be seen in Fig. 5.20.

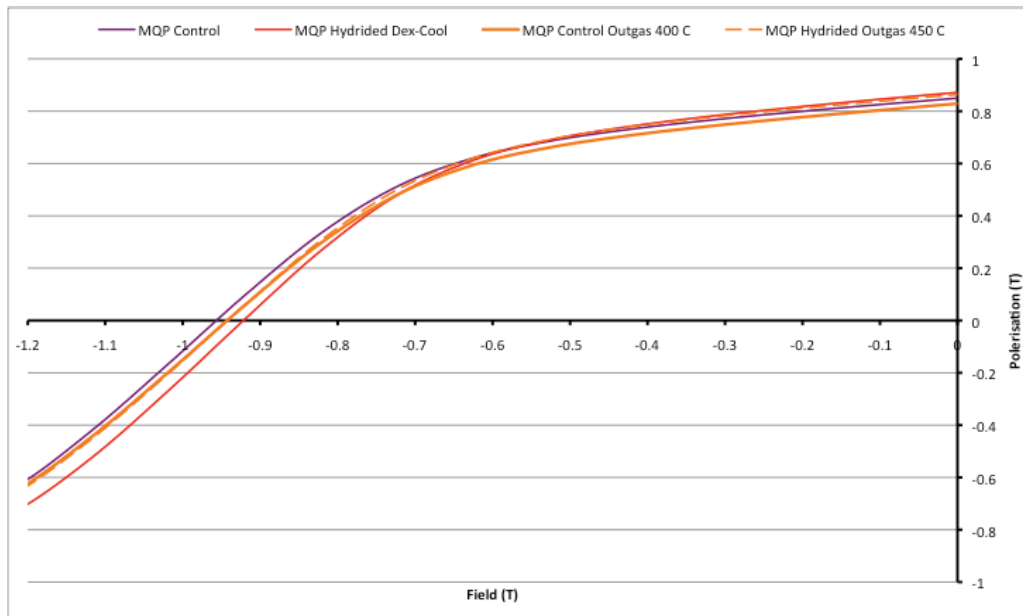


Fig. 5.20 Depicts the second quadrant demagnetisation curve taken from VSM data for an MQP control (purple) a Dex-Cool treated MQP subject to hydriding (red) and the subsequent outgas at 400°C for the hydrided and control samples (orange).

From Fig. 5.20 it can be seen that through the application of an outgassing heat treatment for the Dex-Cool treated MQP at 400°C some of the H_{ci} losses suffered after exposure to the hydriding conditions have been restored. This behaviour is very similar to that of MQP after hydrogen absorption. Although unlike the series of outgassing treatments performed

in Fig. 5.7 the full pre exposure H_{ci} value was not restored. It is likely that this is a result of oxidation due to an insufficient level of vacuum achieved during the heat treatment as the outgassed control sample behaved in the same way. This is the dashed (- - -) orange line just visible below the Dex-Cool treated MQP 400°C outgassed sample.

From this it can be summarised that although Dex-Cool treatment of MQP does prevent much of the hydrogen ingress due to exposure to known hydriding conditions, it does not totally prevent it and thus, associated H_{ci} losses are experienced by the MQP as a result. The hydriding conditions that the MQP was exposed to are severe when compared to effects seen upon H_{ci} as a result of aqueous corrosion. It could be speculated that the Dex-Cool treatment would be even more successful for use in protection against aqueous corrosion.

It can also be summarised from this section of the study that there is a form of bonding evident between the Dex-Cool and the surface of the MQP. It is likely that this involves the oxide surface layer on the MQP and the OH groups of EG, similar to the mechanisms seen in EG bonding with AgO (Vodyankina et al., 1998). This can be said with confidence due to the corresponding peaks of certain reactants evolved at particular temperatures i.e. water at 180°C and hydrogen at approximately 400°C.

References:

- HERBST, J. F. & CROAT, J. J. 1991. Neodymium-iron-boron permanent magnets. *Journal of Magnetism and Magnetic Materials*, 100, 57-78.
- KIM, A. S., CAMP, F. E. & LIZZI, T. 1996. Hydrogen induced corrosion mechanism in NdFeB magnets. *Journal of Applied Physics*, 79, 4840-4842.
- NIKITIN, S. A., TERESHINA, I. S., PANKRATOV, N. Y., PALEWSKI, T., DRULIS, H., MAKAROVA, M. V. & PASTUSHENKOV, Y. G. 2003. Effect of hydrogen on the magnetic characteristics of Nd₂Fe₁₄B single crystal. *physica status solidi (a)*, 196, 317-320.
- OESTERREICHER, K. & OESTERREICHER, H. 1984. Structure and Magnetic Properties of Nd₂Fe₁₄BH_{2.7}. *physica status solidi (a)*, 85, K61-K64.
- VODYANKINA, O., KURINA, L. & IZATULINA, G. 1998. Surface interaction of ethylene glycol with silver. *Reaction Kinetics and Catalysis Letters*, 64, 103-107.
- WILLIAMS, A. J., MCGUINNESS, P. J. & HARRIS, I. R. 1991. Mass spectrometer hydrogen desorption studies on some hydrided NdFeB-type alloys. *Journal of the Less Common Metals*, 171, 149-155.

Chapter 6: Conclusions

This chapter will summarise the findings of this study for; corrosion behaviour of NdFeB bonded magnets and corrosion behaviour of NdFeB MQP. The conclusions are as follows:

It has been shown that there is a direct correlation between the availability of moisture within a particular environment and the rate/severity of H_{ci} losses in MQP and MQI bonded magnets. This was demonstrated by the differing rates of H_{ci} loss dependant upon environmental conditions. As expected the most severe losses were observed in the aqueous environment followed by the high humidity environment, with no losses occurring in the dry environment.

The link between the aqueous corrosion process and subsequent reductions in H_{ci} as a result has been shown through exposure to moisture containing environments and magnetic characterisation at regular intervals.

Also through HADS and magnetic characterisation it has been shown that the absorption of hydrogen by MQP as a result of exposure to hydriding conditions similarly caused a reduction in H_{ci} , but several orders of magnitude greater. The desorption of hydrogen through the application of outgassing heat treatments saw the H_{ci} recover to pre exposure levels.

The same has also been shown to be true of MQP exposed to moisture containing environments. As a result of exposure H_{ci} losses occurred. Upon the application of an outgassing heat treatment at the same temperature as that for hydrided MQP, recovery of H_{ci} to near pre-exposure levels was achieved. It would be impossible to achieve pre-exposure levels of H_{ci} due to the irreversible damage caused to the alloy through the

aqueous corrosion process i.e. formation of corrosion products and loss of $\text{Nd}_2\text{Fe}_{14}\text{B}$ grains from the bulk material.

Hydrogen absorption by the $\text{Nd}_2\text{Fe}_{14}\text{B}$ magnetic phase has been clearly established as the route cause for H_{ci} reduction in MQP as a result of the associated crystal lattice expansion. The hydriding and aqueous corrosion processes differ in that the source of hydrogen as a result of the aqueous corrosion process is through the disassociation of water upon contact with neodymium.

Desirable barrier properties for bonding media have been shown to rely upon two primary factors. The permeability of the binder material to water and % volume of porosity incorporated into the structure of the bonding media. Permeability to water tends to be an inherent property of the material. Incorporation of porosity can differ depending upon the processing route utilised to produce the bonded magnet. The higher the degree of porosity incorporated into the bonded magnet, the more rapid the H_{ci} losses that will occur.

It has been shown that if the binder is permeable to water then its presence will actively facilitate the aqueous corrosion process. This phenomenon was observed through magnetic characterisation as unbonded MQP suffered from a fraction of the H_{ci} losses of its epoxy bonded counterpart as a result of exposure to the aqueous environment. It is thought that a permeable binder separates the MQP providing a much larger surface area for moisture to access resulting in aqueous corrosion attack.

Epoxy resin has been shown to be permeable to water through mass change data gathered and through magnetic characterisation in terms of H_{ci} losses experienced as a result of exposure to moisture.

It has been shown that PTFE outperforms epoxy resin as a binder in terms of preventing water ingress and preserving H_{ci} of the MQP. This can be attributed to the impermeability of PTFE to water and low % volume of porosity incorporated due to its excellent flow properties during pressing.

Zinc when utilised as a bonding medium has been shown to meet the criteria of being impermeable to water, although it seems to lack the ductility and desirable flow characteristics during uniaxial pressing to enable a bonded magnet to be produced with a density close to the theoretical maximum. The incorporation of a large degree of porosity into the bonded magnet structure is the primary obstacle preventing good aqueous corrosion performance in zinc bonded magnets. It should be noted that the LPPS zinc coating was relatively ineffective, although it had not been optimised for this application.

The majority of H_{ci} losses observed in PTFE bonded magnets occur very rapidly and are likely to be the result of a combination of the production method utilised and the physical properties of the binder material. MQP located at the surface of the bonded magnet are totally exposed to the environment and thus are vulnerable to attack by aqueous corrosion. This is in part due to the physical properties of PTFE as there is no form of intimate bonding between the PTFE and the MQP, also the fact that MQP and PTFE are blended as separate powders. Therefore, single particle encapsulation does not happen, unlike in epoxy resin bonded magnet production where the resin is introduced to the MQP in a liquid form.

The application of a spray on surface coating of PTFE to the PTFE bonded magnet after uniaxial pressing showed promise in terms of preventing H_{ci} losses, although this did not perform as well as the binder by comparison. It is thought that the powdery, spray-on nature of the surface coating applied and the absence of a pressing stage to aid

densification allowed the incorporation of a large volume of porosity and also did little to prevent MQP fall out as a result of thermal stresses induced by heat treating. This combination of incorporated porosity and loss of adhesion for MQP located at the surface of the bonded magnet, ultimately lead to the removal of complete particles of MQP damaging the spray on coating and leaving an exposed surface. This provided sufficient opportunity for water to access the underlying MQP effectively bypassing the surface coating.

The addition of Dex-Cool in two different concentrations (“pure” Dex-Cool and Dex-Cool/DI water (50/50 ratio)) saw an improvement in H_{ci} losses in all bonding media (epoxy resin, PTFE and zinc bonding media) although the H_{ci} preservation in the epoxy resin bonded magnets was far less pronounced than that observed in PTFE and zinc bonded magnets. It appears that for Dex-Cool to perform effectively as an H_{ci} loss inhibitor clean surfaces of MQP are required, as is seen in PTFE and zinc bonded magnets, where no intimate bonding takes place between the MQP and binder. This is not the case for epoxy resin bonded magnets where each MQP is coated utilising the single particle encapsulation method. It would suggest the intimate bonding of epoxy resin with the MQP surface is responsible for appreciably poorer performance in terms of H_{ci} retention, that is the epoxy acts as a barrier to the EG preventing it forming a protective coating on the MQP.

It seems that the H_{ci} preservation mechanism in the presence of Dex-Cool responsible for improved aqueous corrosion resistance in MQP cannot simply be attributed to the decreased availability of water within the solution as the performance of bonded magnets within “pure” Dex-Cool and the 50/50 (Dex-Cool/DI water) solution are relatively similar for all bonded magnets used within this study.

It is also apparent that the mechanism by which the Dex-Cool provides protection for the MQP against the effects of aqueous corrosion involves some form of adsorption/interaction with the surface of the MQP. This is supported by the requirement for a clean surface in order to receive the benefit of H_{ci} preservation by Dex-Cool from the effects of aqueous corrosion attack.

Chapter 7: Future Work

This future work chapter has been compiled as a result of findings that have been deemed to warrant further investigation that were outside the scope of this study, or as solutions to overcome problems that have presented themselves during the course of the compilation of the results and discussion chapter.

The poor performance of epoxy resin as a binder due to its permeability to water and the suggestion from the literature that the movement of water through nano-pores within the resin could be restricted through the availability of 'free' OH groups within these nano-pores. Further study is warranted on the ability to manipulate the availability of 'free' polar OH group within epoxy resin to limit flow of water through nano-pores. This could possibly be achieved through varying the mixing ratio of resin to hardener used to produce the epoxy resin. Through the production of epoxy resin bonded magnets with differing ratios of resin to hardener it will be possible to conduct a study to ascertain if this has any effect on the aqueous corrosion behaviour.

The use of PTFE as a binder was fairly successful in preventing aqueous corrosion, the major source of H_{ci} losses seem to be due to aqueous corrosion of the exposed surface MQP. The application of a PTFE coating saw a slight improvement in corrosion performance although this did not prevent surface MQP from breaking away during thermal stresses induced during heat treating. From its potential seen in use as a binder and surface coating it seems prudent to investigate the feasibility of producing a PTFE bonded magnet with a PTFE-rich outer layer to protect MQP located at the surface. This PTFE-rich layer could potentially be introduced through the application of a spray-on-type

coating on the inside of the die before pressing, or through lining the die with a pre-formed crucible of PTFE into which the blended MQP-PTFE mix would be loaded into.

This would allow the PTFE-rich layer to be subject to the pressing forces which are required for densification of the binder and hence to reduce the incorporated porosity of the surface coating. This PTFE-rich surface area would also address the problem of surface MQP losing adhesion during heat treating whilst protecting MQP which would have previously been located at the surface.

Amongst the most promising findings relating to corrosion prevention in magnetic materials are those of surface treatments, in particular Dex-Cool (ethylene glycol). These results are also the most difficult to explain in terms of a clear well defined mechanism of protection. For that reason alone further research is warranted to explain how ethylene glycol interacts in solution with water molecules, in terms of bonding and water molecule mobility. It is also important to ascertain how the ethylene glycol/water solution interacts with the surface of MQP to prevent the disassociation of water or the blocking of hydrogen absorption by the $\text{Nd}_2\text{Fe}_{14}\text{B}$ phase or a combination of the two.

It would have been interesting to investigate the effect of differing concentrations of Dex-Cool upon the aqueous corrosion behaviour of both bonded magnets and unbonded MQP. This could possibly provide useful information regarding the optimum concentration of Dex-Cool required within solution to preserve H_{ci} in bonded magnets.

It would be prudent to investigate the variables effecting the adsorption of Dex-Cool/EG on the surface of the MQP e.g. temperature. As Vodyankina et al. found different products were evolved during heating when the EG was adsorbed at different temperatures. This indicates that the surface interactions were temperature dependant. It would be useful to

employ temperature-programmed reaction (TPR) techniques similar to those used by Vodyankina et al. to allow accurate comparisons between EG adsorption on the surface of silver and the surface of MQP. Another technique that may produce more meaningful results than the TGA/MS utilised by this study is inelastic electron tunnelling spectroscopy which was also used by Bayman and Hansma to characterise the surface interactions between EG and aluminium oxide.

It would also be interesting to investigate the scope for application of this H_{ci} preservation mechanism within other areas e.g. sintered magnets, friable powder produced via the HD process. This could hold particular significance for use within rare earth magnet recycling, making handling of materials easier by reducing sensitivity to air/moisture.

To improve the ability to compare the aqueous corrosion behaviour of unbonded MQP with the same for bonded magnets, it would have been interesting to agitate the unbonded MQP throughout the duration of exposure to aqueous environments to see if H_{ci} losses similar to those seen in bonded magnets could be replicated.

It would also have been interesting to employ some HADS techniques on MQP exposed to the aqueous environment to confirm that the same $Nd_2Fe_{14}B$ phase was involved in hydrogen absorption during the aqueous corrosion process as that in exposure to known hydriding conditions.